UNIVERSITAT DE BARCELONA

Plastic Scintillation microspheres for radioactivity determination: synthesis, characterization and production

Luz Mary Santiago Santiago

Doctoral thesis

Plastic Scintillation microspheres for radioactivity determination: synthesis, characterization and production

Luz Mary Santiago Santiago

Department of Analytical Chemistry

Faculty of Chemistry

Universitat de Barcelona

Barcelona, September 2015

Programa de Doctorado:

Química Analítica del Medio Ambiente y la Polución

Plastic Scintillation microspheres for radioactivity determination: synthesis, characterization and production

Memoria presentada por:

Luz Mary Santiago Santiago

Para optar al título de Doctora por la Universitat de Barcelona

Barcelona, 21 de Septiembre de 2015

El Dr. Alex Tarancón Sanz y el Dr. José Francisco García, profesores del Departamento de Química Analítica de la Universitat de Barcelona

CERTIFICAN

Que el presente trabajo de investigación ha sido realizado por Luz Mary Santiago Santiago en el Departamento de Química Analítica de la Universitat de Barcelona bajo su dirección.

Barcelona, 21 de septiembre del 2015

Dr. Alex Tarancón Sanz
Profesor agregado interino del
Departamento de Química Analítica
de la Universitat de Barcelona

Dr. José Francisco García
Profesor titular del
Departamento de Química Analítica
de la Universitat de Barcelona

“A journey of a thousand miles begins with a single step”

Lao-Tsu

TABLE OF CONTENTS

ABSTRACT

Plastic scintillation microspheres (PSm) are a solid dispersion of one or more fluorescent solutes encapsulated within a polymeric matrix. They present spherical shape and their size varies in the micrometric range. PSm can be an alternative to liquid scintillation cocktails for most of the determinations of high and medium energy radionuclides and they are especially useful for those applications in which the use of the liquid scintillation cocktails presents some limitations, such as, the measurement of salty samples, measurements in continuous or as a medium to join measurement and separation steps (PSresins). Moreover, PSm are a polymerised material which possesses low reactivity, and this fact allows avoiding the production of mixed waste (composed by the mixture of radioactive and organic wastes) when measuring radionuclides contained in aqueous samples. However, PSm are not completely available in the market, since only a few providers are able to supply them at a high cost and with a limited range of sizes and compositions.

This thesis has been focused in two main objectives. The first one has been the evaluation of the feasibility of different methodologies to produce PSm, starting at laboratory scale and addressing their production at a higher scale and by employing automatic techniques. The second general objective has been to increase the knowledge about the energy transfer mechanism when PSm are employed for measuring alpha or beta emitters.

Polymeric microspheres can be produced through different methodologies, among them, the organic solvent extraction/evaporation (E/E), which has been evaluated in this thesis. This methodology is based on the formation of an emulsion by mixing both phases, the disperse (containing the polymer and fluorescent solutes dissolved in a proper organic solvent) and the continuous one (containing the surfactant dissolved in water). When both phases are in contact under constant stirring, microdroplets are formed, and the organic solvent contained within the microdroplets is slowly extracted by the continuous phase and simultaneously evaporated at the water/air interface, therefore causing the hardening of the microdroplet and its precipitation as a solid microsphere.

The feasibility of the methodology was evaluated to produce PSm, first at laboratory scale, by varying their composition and operational parameters, in order to

study their influence in the diameter of the microspheres. The methodology proved to be simple and highly feasible, with yields of 100% and has allowed us to produce PSm batches of different diameters and compositions, which are comparable to the commercial PSm. Through this methodology, it has been possible to evaluate the encapsulation of the fluorescent solutes (PPO, POPOP, pT and bis-MSB) and the naphthalene within the polymeric matrix (polystyrene) and the understanding of the dependence between the measurements of the radiometric capacities with regard to the PSm composition.

PSm containing increasing concentrations of naphthalene and a couple of scintillators (PPO/POPOP or pT/bis-MSB) were synthesised for evaluating the influence of naphthalene as a pulse delayer and therefore, as an enhancer of the PSm alpha/beta discrimination ability. The Quantulus 1220 and the Triathler liquid scintillation spectrometers were employed to determine the alpha/beta discrimination. The results showed that naphthalene enhances the ability of the PSm for discriminating particles, overcoming the limitations derived from the classical formulations that led to consider plastic scintillators as non capable for the alpha/beta discrimination due to their similar duration of both components, the fast (beta) and the slow one (alpha) in comparison with liquid scintillation cocktails. The results obtained by employing Quantulus 1220 showed high misclassification values (about 23%), since it classifies the signals into only two spectra and uses a parameter independent of the energy of the signal. However, values of misclassification lower than 5% were obtained when PSm containing PPO/POPOP were employed for measuring ^{241}Am and ^{90}Sr/^{90}Y in a Triathler detector, in which the 3D alpha/beta discrimination function permits a better selection of the counting window.

Influence of preparation parameters on the synthesis of plastic scintillation microspheres through organic solvent extraction/evaporation methodology have been also evaluated, in order to understand how the synthesis parameters influence the final size diameter, shape and morphology of the microspheres, which can be helpful to optimize the production of PSm according to the needs (desired diameter and composition). The temperature, polymer and surfactant concentration have been proved to be the parameters which have a major influence, whereas, stirring speed and organic/aqueous phase ratio showed a minor effect. Depending on the selected parameters, PSm from about 17 μm to 1 mm can be obtained. The maximum production

rate at the laboratory scale has been established in 40 g per synthesis. Substitution of naphthalene by 2,6-diisopropylnaphthalene (less toxic compound than naphthalene) has been also proved to be possible.

As an alternative to the organic solvent extraction/evaporation methodology, two techniques based on drying methods and using automatic equipment have been also evaluated for producing PSm. Specifically, the Supercritical Anti-solvent (SAS) technique performed at the "Laboratoire Mécanique, Modélisation et Procédés Propres" (M2P2) in the Aix-Marseille Universitè, and the Spray Drying (SD) technique, which was carried out at the facilities of the research and development department of Esteve Química by using a commercial equipment, the closed cycle Mobile Minor $^{(TM)}$.

The micronisation of the polystyrene trough SAS, consisted in the injection of the dispersed phase within a vessel containing CO_2 at supercritical conditions. The organic solution was nebulized through the capillary and the supercritical CO_2 dissolves the organic solvent contained within the droplets, thus causing the drying and the coprecipitation of the particles. The micronisation of scintillating particles was performed by evaluating the influence of some operational and formulation parameters, such as, polymer concentration, solvent/CO_2 molar ratio, injection velocity of the organic solution, capillary diameter. Ethyl acetate was employed to dissolve the polymer and the fluorescent solutes avoiding the use of dichloromethane. This methodology allowed us to obtain sub-micrometric polystyrene based scintillating particles with a yield of 90%. Scintillating solutes were proved to be successfully encapsulated from the organic solution containing the material to be micronised. However, radiometric capacities were very poor when comparing with those obtained for the PSm produced by the organic solvent extraction/evaporation methodology. Although the yield of production was high, the rate of production was very low, since the ability of the equipment to produce hundreds of grams is limited.

In the case the Spray Drying technique, the organic solution containing the polymer and the fluorescent solutes is nebulised to form the droplets and N_2 flowing in opposite direction at a determined temperature is used to extract the organic solvent from the nebulised droplet, therefore, the particles are formed before reaching the walls of the vessel. Some parameters like the feed flow rate, nozzle mass flow rate, feed concentration and the organic solvents (dichloromethane and the toluene) were

evaluated to optimize the PSm's quality and the yield of production. PSm of around 10 µm with similar features of those obtained through organic solvent extraction/evaporation methodology were obtained by using toluene, achieving a production rate of around 300 g per day in optimized conditions. However, the rate of production does not compensate the associated operational cost of production.

Taking into account that the best results for the production of the PSm were achieved through the organic solvent extraction/evaporation methodology, a proof of concept for producing PSm at higher scale (some kilograms per day) was performed at the facilities of an external company, Trastamo. The conditions of synthesis were extrapolated from those employed at laboratory scale. First attempt resulted in a production of 700 g of PSm of about 40 µm with acceptable cost. The PSm were able of detecting radioactivity; however future tests are necessary to enhance the yield, rate of production and the quality of the PSm.

The syntheses performed in this thesis allowed us to obtain PSm having a wide range of diameters, from submicron particles obtained through SAS, to PSm of a few micrometers obtained by using Spray Drying and organic solvent extraction/evaporation (E/E) methodology and also PSm in the millimetre scale also through E/E. This has represented an opportunity to make evident the dependence between the radiometric capacities of the scintillating particles with regard to their size and to confirm the effect of the particle and optical quenching when measuring radionuclide.

Particle quenching corresponds to the loose of the total or partial energy of a decaying particle before it reaches the scintillator (PSm), due to its interaction with the molecules of the medium. It can be evidenced by the decrease of detection efficiency. On the other hand, optical quenching is attributed to the inefficient transmission of the photons generated by the scintillator due to the change of media that they may pass through in their way to be collected by the PMT. It can be evidenced by a decrease on the detection efficiency and a shift on the spectrum position toward lower energies. The influence of both quenching phenomena is dependent on the diameter of the scintillating particle but in opposite direction, thus resulting radiometric capacities when a radionuclide is measured (especially the low energy ones) are a balance between particle and optical quenching.

Low values of detection efficiency and a shift of the spectrum toward higher energy position were observed when PSm of a few hundreds of micrometers were employed, confirming that higher PSm diameters favour the particle quenching but decrease the optical quenching. When PSm of a few micrometers were employed, detection efficiency values increased, as a result of the decreasing of the particle quenching. However, spectra position slightly shifted toward lower positions due to the presence of the optical quenching. Finally, when submicrometric scintillating particles were employed, values of detection efficiency were very low and the spectra shifted toward very low energies. The optical quenching caused a predominant influence making negligible the positive effect of decreasing the particle quenching. As an example, in the case of the measurement of ^{3}H, detection efficiency obtained when submicron scintillating particles were employed was 0.008(2)%, while employing PSm of ~22 µm it was 3.36(8)% and when the PSm diameter was around 145 µm, the detection efficiency obtained was 0.81(9)%.

Finally, in order to accomplish the study of the energy transfer mechanism in organic scintillators, a systematic study of the different quenching effects in various organic scintillators (liquid scintillation cocktail, gel scintillation cocktail, PSm of two different ranges of diameters) was performed. Quenching agents used were NaCl, $BaCl_2$, glycerine, nitromethane and methyl orange. The main remarks when increasing concentrations of salts and glycerine were added within the sample for measuring with PSm were a small decrease of the detection efficiency without significant variation of the external quenching parameter (SQP(E)) and spectra position, thus confirming the effect of the particle quenching. The addition of nitromethane and methyl orange caused a decrease of the detection efficiency, decrease of the SQP(E) and the shift of the spectra toward lower energies, as happens in a typical chemical and color quenching behaviour when liquid scintillators cocktails are employed with these two quenching agents.

List of publications

Publications from the thesis

Santiago, L.M., Bagán, H., Tarancón, A., García, J.F. Synthesis of plastic scintillation microspheres: Evaluation of scintillators. *Nuclear Instruments and Methods in Physics Research A* 698 (2013) 106-116.

Santiago, L.M., Bagán, H., Tarancón, A., García, J.F. Synthesis of plastic scintillation microspheres: Alpha/beta discrimination. *Applied Radiation and Isotopes* 93 (2014) 18-28.

Santiago, L.M., Tarancón, A., García, J.F. Influence of preparation parameters on the synthesis of plastic scintillation microspheres and evaluation of sample preparation. Sent to Advanced Powder Technology.

Santiago, L.M., Masmoudi, Y., Tarancón, A., Djerafi, R., Bagán, H., García, J.F., Badens, E. Polystyrene based sub-micron scintillating particles produced by supercritical anti-solvent precipitation. *Journal of Supercritical Fluids* 103 (2015) 18-27.

Santiago, L.M., Bagán, H., Tarancón, A., García, J.F. Production of polystyrene-based scintillation microspheres for the measurement of radioactivity by spray-drying. Accepted for publication in Journal of Radioanalytical and Nuclear Chemistry.

Santiago, L.M., Bagán, H., Tarancón, A., Rauret, G., García, J.F. Systematic study of particle quenching in organic scintillators. *Nuclear Instruments and Methods in Physics Research A* 698 (2013) 26-36.

Collaborations in other publications

Tarancón, A., Barrera, J., Santiago, L.M., Bagán, H., García, J.F. Application of the CIEMAT_NIST method to plastic scintillation microspheres. *Applied Radiation and Isotopes* 98 (2015) 13-22.

Stay Abroad

Organization: Aix-Marseille Université

Department: M2P2 Dr. Elisabeth Badens and Dr. Yasmine Masmoudi

City:	Aix-en-Provence	**Country:**	France
Length:	6 months	**Year:**	2013

List of abbreviations

ASES	Aerosol solvent extraction system
BBD	2,5-di-(4-biphenylyl)-1,3,4-oxadiazole
BBO	2,5-di(4-biphenylyl) oxazole
BBOT	2,5-bis-2-(5-t-butyl-benzoxazoyl) thiophene
Bis-MSB	1,4-bis(2-metilstiril) benzeno
Bq	Becquerel
Butyl-PBD	2-(4-tert-butylphenyl)-5-(4-phenylphenyl)-1,3,4-oxadiazole
cpm	Counts per minute
DCM	Dichloromethane
DIN	2,6-biisopropyl naphthalene
EAP	Ethoxylated alkylphenol
EC	Electron capture
E/E	Organic solvent extraction/evaporation
GAS	Gas anti-solvent
GSc	Gel scintillation cocktail
HBT	2-(2-hydroxyphenyl)-benzothiazole
HDEHP	Di-(2-ethylhexyl) phosphoric acid
IJ-SAS	Impinging jet
JE	Jet excitation
keV	Kiloelectron volt
LAB	Linear alkylbenzene
LS	Liquid scintillation
LSc	Liquid scintillation cocktail
MME	Microporous membranes of emulsification
M2P2	Laboratoire Mécanique, Modélisation et Procédés Propres
NPD	2-(1-naphthyl)-5-phenyl-1,3,4-oxadiazole
NPO	2-(1-naphthyl)-5-phenyloxazole
o/w	oil-in-water emulsion
PBBO	2-(4-biphenylyl)-6-phenylbenzoxazole
PBD	2-phenyl-5-(4-diphenyl)-1,3,4-oxadiazole
PBMA	poly(butyl methacrylate)
PDD	Pulse decay discriminator

PLA	Polylactic acid
PLGA	Poly(lactic-co-glycolic acid)
PMMA	Poly(methyl methacrylate)
PMP	1-phenyl-3-mesityl-2-pyrazoline
PMT	Photomultiplier
POPOP	1,4-di-(2-(4-methyl-5-phenyloxazolyl))-benzene (dimethyl)
PPF	Particle precision fabrication
PPO	2,5-diphenyloxazole
PSA	Pulse shape analysis
Ps	Plastic scintillation
PS	Polystyrene
PSm	Plastic scintillation microspheres
PSresins	Plastic scintillation resins
pT	p-terphenyl
PVA	Poly(vinyl alcohol)
PVT	Polyvinyltoluene
PXE	Phenylxylyl ethane
SAS	Supercritical anti-solvent
SD	Spray drying
SEDS	Supercritical enhanced dispersion solution
SOSS	Dioctilsulfocianato
SPA	Scintillation proximity assay
SPG	'Shirazu porous glass'
TBP	Tri butylphosphate
TEP	Triethylphosphate
W/O/W	Water/oil/water emulsion
3HF	Hydroxyflavone

Capítulo 1

Introducción

1. INTRODUCCIÓN

1.1. RADIOACTIVIDAD

La radioactividad se puede definir como una reacción nuclear de desintegración espontánea donde un núcleo inestable tiende a reorganizarse generando uno o más núcleos, con la subsecuente emisión de una partícula alfa (α) o beta (β) que puede ir acompañada de radiación gamma (ϒ) o de rayos X. Tanto los rayos x y la radiación gamma, como la emisión de las partículas α o β ionizan los materiales que atraviesan, motivo por el cual se les denomina radiaciones ionizantes. El proceso de desintegración que sufre un radionucleido podría llegar a formar una serie o familia radiactiva cuando el radionucleido hijo continúa desintegrándose hasta que finalmente se forma un radionucleido estable [L'Annunziata, 2013].

Las primeras observaciones sobre el fenómeno radiactivo fueron realizadas por Roentgen en el año 1885, cuando utilizaba un tubo de Crookes para estudiar sistemáticamente los rayos catódicos. Roentgen observó que al aplicar alta tensión al tubo, la hoja de papel recubierta de platinocianuro de bario producía luminiscencia. El estudio le condujo al descubrimiento de los rayos X [Ortega y Jorba, 1996].

Un año más tarde, en 1886, Henri Becquerel estudiaba los fenómenos de fluorescencia y fosforescencia y al colocar un cristal de Pechblenda (mineral que contiene uranio, de composición química UO_2) sobre una placa fotográfica sin exponerla al sol, observó lo mismo que Roentgen y dedujo que el elemento (uranio) contenido en la Pechblenda, emitía de forma natural [Lieser, 1997].

En 1898, Marie y Pierre Curie y de forma paralela e independiente, G. Schmidt, estudiaron en diferentes minerales el fenómeno observado por Becquerel y encontraron que el Torio también lo causaba. Al mismo tiempo, demostraron que la radioactividad no era el resultado de una reacción química, sino una propiedad propia del átomo y característica del núcleo de los átomos. Ese mismo año Marie y Piere Curie descubrieron el Radio y el Polonio.

En 1900, Paul Villard descubrió la existencia de una radiación altamente penetrante que no era desviable por un campo magnético externo y en el año 1903, Ernest Rutherford la nombró como radiación gamma.

Ya desde sus inicios, la radioactividad fue empleada en aplicaciones médicas junto con los rayos X, y con el tiempo, el número de aplicaciones se ha incrementado. Actualmente, la radioactividad se usa en la producción de energía y en aplicaciones médicas, específicamente en diagnóstico y terapia. Además, se emplea en el trazado de procesos químicos, fisiológicos y biológicos; en la esterilización de materiales quirúrgicos, productos químicos/biológicos, alimentos, obras de arte, entre otros. También posee aplicaciones industriales, tales como radiografías, control de espesor y de uniformidad de productos en forma de láminas, producción de pinturas luminiscentes, entre otros.

1.2. EMISIONES RADIOACTIVAS

La radioactividad se clasifica de acuerdo al tipo de emisión: alfa (α), beta (β) o radiación gamma (γ).

1.2.1. Partículas alfa (α)

Se conoce como partícula α a un fragmento compuesto por dos neutrones y dos protones, es decir, un núcleo de helio sin dos electrones. En el proceso radioactivo en el que se emite una partícula alfa, el número atómico del isótopo disminuye dos unidades y su masa en cuatro unidades, por lo que se convierte en un elemento diferente. Durante el proceso, los nucleones no cambian su identidad, ya que las sumas de los números másicos y de los números atómicos de los productos de desintegración son iguales al número másico y atómico, respectivamente, del nucleido padre [Ortega y Jorba, 1996]. La emisión de una partícula alfa se describe mediante la siguiente ecuación:

$$ {}^{A}_{Z}X \rightarrow {}^{A-4}_{Z-2}Y + {}^{4}_{2}He + K_T $$

Donde ${}^{A}_{Z}X$ representa el radionucleido padre de número atómico Z y masa A, ${}^{A-4}_{Z-2}Y$ es el radionucleido hijo de número atómico Z-2 y masa A-4, ${}^{4}_{2}He$ es la partícula alfa equivalente a un núcleo de Helio y K_T es la energía cinética total liberada en el decaimiento alfa.

Las partículas alfa son las más energéticas (en un rango que abarca desde 1 hasta los 10.5 MeV) y las más voluminosas, lo que hace que interaccionen fácilmente con el medio que atraviesan. Poseen una trayectoria corta y rectilínea en el aire, de unos 4 cm aproximadamente, y en sólidos y líquidos es mucho menor (50 µm en agua), dichas partículas pueden ser detenidas por una hoja de papel de seda. Estas características conllevan a que la partícula posea poco poder

de penetración y alta capacidad de ionización. Este tipo de radiación es común entre los elementos más pesados, tales como los isótopos de número atómico mayor a 150 (p. ej. uranio, polonio, radio, etc).

1.2.2. Partículas beta (β)

Las partículas **β** son electrones de alta energía que se producen durante la conversión en el núcleo de un neutrón a protón, dejándolo con una carga positiva y aumentando el número másico. Dichas partículas son emitidas junto con un neutrino, el cual es muy difícil de detectar, y que posee una capacidad de penetración muy elevada. La suma de las energías del neutrino y la partícula beta es una constante para cada isótopo y define la energía máxima ($E_{máx}$) observada para cualquier partícula emitida por el isótopo. Exiten tres tipos de procesos de emisiones de partículas beta:

$$proceso\ \beta^-: {}^{A}_{Z}X \rightarrow {}_{Z+1}{}^{A}Y + e^- + \tilde{\nu} + K_t$$

En el proceso β^-, el nucleido padre emite un electrón y un antineutrino ($\tilde{\nu}$) para transformarse en un isóbaro que posee un número atómico una unidad mayor.

$$proceso\ \beta^+: {}^{A}_{Z}X \rightarrow {}_{Z-1}{}^{A}Y' + e^+ + \nu + K_t$$

En el proceso β^+, el nucleido padre emite un positrón y un neutrino (ν) para transformase en un isóbaro que posee un número atómico con una unidad menor.

$$Captura\ electrónica\ (CE): {}^{A}_{Z}X + e^- \rightarrow {}_{Z-1}{}^{A}Y' + \nu + K_t$$

La captura electrónica no resulta en la emisión de ninguna partícula. Ocurre cuando el núcleo inestable captura un electrón de las capas internas para transformar un protón en neutrón con la subsecuente emisión de un neutrino. El hueco dejado en la capa electrónica produce la emisión de rayos X o de electrones Auger para la reorganización de las capas electrónicas.

Por otro lado, un proceso asociado a la desintegración beta, es la emisión de radiación electromagnética conocida como efecto Cherenkov, el cual se produce cuando las partículas cargadas que poseen suficiente energía pueden viajar a través de un medio transparente a una velocidad mayor que la velocidad de la luz en ese medio [L'Annunziata, 2013].

Las partículas beta son emitidas en un amplio espectro de energía, que va desde energía cercana a 0 hasta un valor de $E_{\beta máx}$ característico para cada substancia emisora, la cual puede variar desde los 18 keV para el ^{3}H hasta 13 MeV para el ^{12}B, aunque en general no suelen

superar los 5 MeV [Ortega y Jorba, 1996]. En general, las partículas beta poseen una masa mucho menor que la de las partículas alfa y son capaces de viajar a velocidades mayores que las de una partícula alfa de energía equivalente. Debido a su poca masa, gran velocidad y poca carga, la ionización específica producida por la partícula beta en aire es mucho menor que la generada por las partículas alfa. La distancia recorrida por las partículas beta puede llegar a ser de unos varios metros en el aire, unos cuantos centímetros en el tejido corporal o varios milímetros en el metal o plástico. Se necesitan alrededor de 1,5 mm de plomo para detener las partículas beta.

1.2.3. Radiación gamma (ϒ)

La radiación gamma se produce debido a la pérdida de energía de excitación de un núcleo mediante la emisión de radiación electromagnética por un proceso de conversión interna. Este tipo de radiación acompaña, en la mayoría de los casos, la emisión de partículas alfa o beta. La radiación gamma difiere de la radiación alfa o beta por el hecho de que se trata de radiación electromagnética y no de partículas y se describe de la siguiente manera:

$${}^{A}_{Z}X^{*} \rightarrow {}^{A}_{Z}X + \gamma$$

La radiación gamma es un tipo de radiación ionizante que al poseer longitudes de onda muy cortas (menores a una décima de nanómetro) presenta una capacidad de penetración superior en comparación con la de las partículas alfa y beta. Constituye la forma de radiación electromagnética más energética, ya que varía en un rango que va desde unos 100 keV hasta los 10 MeV, puede recorrer varios metros en el aire y varios centímetros en el cuerpo humano. Se requieren entre unos 5-25 cm de plomo y hasta 3 m de hormigón para construir un blindaje óptimo.

Un fenómeno asociado a la radiación gamma es el denomidado efecto Compton, el cual sucede cuando un electrón del orbital atómico absorbe parte de la energía de la radiación ϒ, pasa a un estado excitado y escapa del átomo en forma de partícula beta generando electrones secundarios equivalentes a los emitidos.

1.3. TÉCNICAS DE DETECCIÓN DE LA RADIOACTIVIDAD

Las radiaciones ionizantes pueden ser detectadas mediante diferentes técnicas, las cuales se clasifican de acuerdo al material que interacciona con la partícula emitida o radiación gamma. Entre las principales técnicas se encuentran las de ionización gaseosa, las de centelleo, las basadas en semiconductores, las de termoluminiscenia y las basadas en la detección de la radiación Cherenkov.

1.3.1. Detectores de ionización gaseosa

Su fundamento físico se basa en la colección de la carga liberada cuando la radiación ionizante interacciona con el gas del detector creando pares ión-electrón mediante el empleo de dos electrodos entre los que se establece una diferencia de potencial que permite la generación de un impulso eléctrico de detección.

Se han desarrollado diferentes tipos de detectores de ionización gaseosa, tales como las cámaras de ionización gaseosa, los contadores proporcionales y los contadores Geiger-Müller. Dichos detectores se diferencian entre ellos principalmente por la zona de polarización donde se aplica el voltaje (Figura 1).

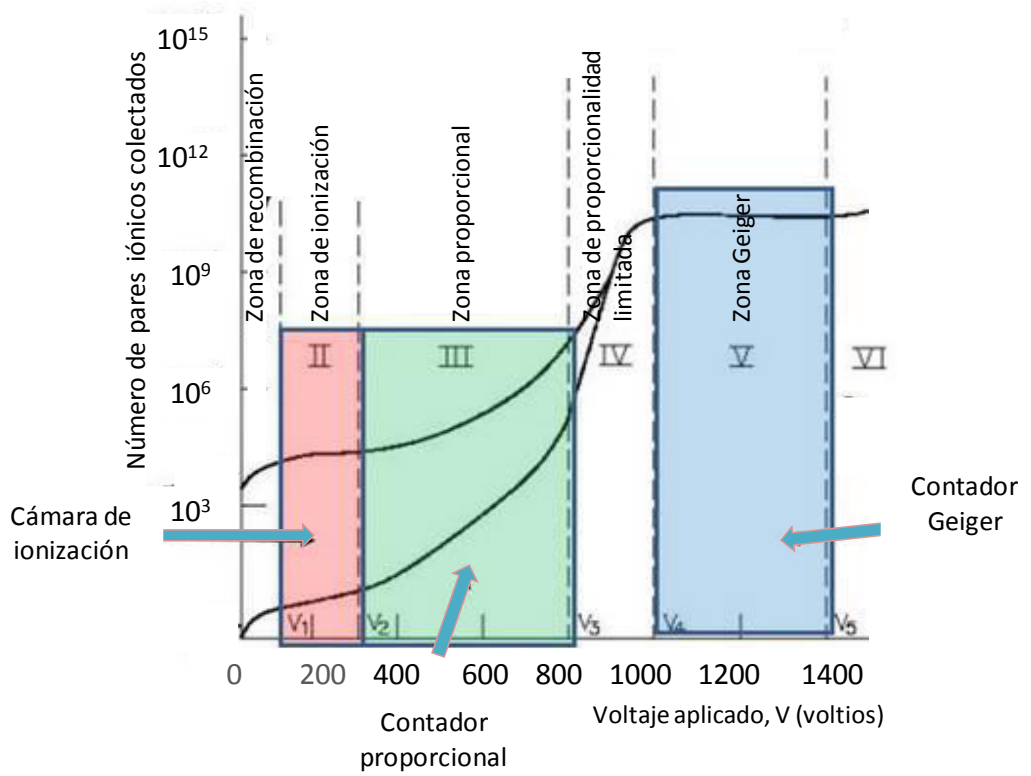

Figura 1. Zonas de polarización de las diferentes técnicas de detección de radioactividad

Para los tres sistemas mencionados, el detector está constituido por dos electrodos metálicos aislados eléctricamente y contenidos en un recinto relleno con gases no conductores. La muestra a medir puede ser un gas o un material que se sitúa en el interior de la cámara o en el exterior de ésta, separada por una ventana de espesor variable.

- **Cámaras de ionización**

Este tipo de detectores trabajan polarizadas en la zona de ionización y pueden emplear electrodos en forma cilíndrica o esférica. Se mide la intensidad de la radiación y se considera una técnica muy apropiada para el recuento de partículas muy ionizantes, tales como las partículas alfa u otros iones pesados que producen impulsos anchos, ya que no aprovecha el efecto multiplicador de la carga eléctrica [Ortega y Jorba, 1996]. Se puede emplear también para medir partículas beta o radiación gamma, si se desea conocer la intensidad de la radiación mas no la energía individual de cada partícula.

- **Contadores proporcionales**

Los contadores proporcionales son similares a las cámaras de ionización gaseosa, con la principal diferencia de que poseen un ánodo en forma de hilo metálico, se aplica un potencial mayor y además trabajan polarizados en la zona proporcional para aprovechar el efecto multiplicador del campo eléctrico. Este tipo de contador distingue entre partículas de diferente naturaleza debido a la amplitud de los impulsos de detección. Se emplea para la detección de partículas alfa y beta y también en la detección de rayos X de baja energía y de radiación gamma.

- **Contadores Geiger-Müller**

Su geometría es similar a la de los contadores proporcionales, sin embargo difieren en el tipo de gas que contienen en el recinto interior, en que el electrodo central suele ser más grueso y en que trabajan polarizados en la zona Geiger. Generalmente, el potencial aplicado para este tipo de detectores es muy alto, lo cual genera grandes amplificaciones para la producción en cadena de mayor cantidad de pares iónicos. Dichos detectores, se consideran adecuados para el control de niveles altos de radioactividad, en la detección de partículas alfa, partículas beta de media y alta energía y de radiación gamma. Los impulsos que suministran los contadores Geiger-Müller no guardan una relación directa con el tipo y la energía de las partículas emisoras.

1.3.2. Detectores de centelleo

Se basan en el fenómeno de luminiscencia inducida en algunos materiales por la transferencia de energía desde una partícula radioactiva hasta moléculas fluorescentes. Las moléculas excitadas emiten fotones en el proceso de desexcitación que son detectados por un fotomultiplicador, para luego convertirlos en impulsos eléctricos. Los detectores de centelleo constan principalmente de un material fluorescente asociado a un sistema fotoeléctrico y a una cadena electrónica.

Los materiales centelleadores pueden ser de naturaleza orgánica e inorgánica. Deben ser transparentes a su propia emisión para permitir que los fotones generados alcancen el fotomultiplicador. El espectro de fluorescencia del centelleador se debe corresponder con el intervalo de frecuencia al que es sensible el fotomultiplicador y el destello producido por una interacción debe tener un período de decaimiento suficientemente corto para que no se superpongan los impulsos generados por desintegraciones sucesivas.

- **Centelleadores inorgánicos**

Los centelleadores inorgánicos están compuestos generalmente por un cristal, según Lempicki, 1995 y Bizarri, 2010 el proceso de centelleo se basa principalmente en las siguientes etapas:

1. La creación de pares electrón-hueco por un fotón absorbido de rayos X o radiación gamma.
2. La transferencia de energía después de la propagación del par electrón-hueco hacia un centro luminiscente.
3. La emisión de fotones desde el centro luminiscente.

La detección de dichos fotones emitidos permite la observación de las diferentes desintegraciones radioactivas. Entre los centelleadores inorgánicos más utilizados, se encuentran el de Ioduro de Sodio dopado con Talio (NAI(Tl)), el de Ioduro de Cesio dopado con Talio o Sodio (CsI(Na)), los de Sulfuro de Zinc dopados con Plata (ZnS(Ag)) y algunos desarrollados en las últimas décadas tales como los compuestos por BaF_2, CsF y el CaF_2, entre otros. Su principal uso se basa en la detección de rayos gamma.

- **Centelleadores orgánicos**

Pueden ser sólidos o líquidos y están compuestos principalmente por un disolvente orgánico que actúa como medio para absorber la energía de la partícula radioactiva y como matriz para contener uno o varios solutos fluorescentes, los cuales actúan como una eficiente fuente de fotones después de aceptar la energía cedida por las moléculas excitadas de disolvente. Este tipo de centelleadores son empleados con frecuencia en la determinación de emisores beta, aunque también se usan para la detección de partículas alfa y con menor frecuencia para la detección de radiación gamma.

1.3.3. Semiconductores

Los detectores semiconductores funcionan de manera similar a los detectores de ionización gaseosa, con la diferencia de que se trata de un detector en estado sólido. Cuando un emisor atraviesa el cristal semiconductor, crea pares electrón-hueco de forma directa o indirecta. Lo hace de forma directa cuando la partícula a lo largo de su trayectoria cede parte de su energía a electrones de la banda de valencia que pasan a ocupar un lugar en la banda de conducción con la consecuente creación de un hueco en la banda de valencia, hasta que dicha partícula cede toda su energía. La producción de pares electrón-hueco de forma indirecta se da cuando la partícula emisora produce electrones altamente energéticos, los cuales pierden su energía produciendo pares electrón-hueco.

Se distinguen dos tipos de semiconductores, los intrínsecos y los extrínsecos. Los primeros, conducen la corriente eléctrica debido a su estructura atómica y entre los más conocidos se encuentran el germanio y el silicio. Mientras que los segundos, son el resultado de agregar cantidades muy pequeñas de un elemento de valencia cinco (p.ej. Antimonio, Fósforo, Litio, étc.) a un semiconductor intrínseco para incrementar su conductividad.

Los detectores semiconductores en diferentes configuraciones se caracterizan porque poseen alta densidad del medio ionizado y por tanto, alta eficiencia de detección y porque la movilidad de los electrones y huecos es elevada y el volumen del medio detector es reducido, permitiendo que el tiempo de recolección de cargas pueda ser del orden de los nanosegundos. Sin embargo, debido a su conductividad intrínseca, el detector produce altos niveles de ruido que podrían enmascarar la señal respecto a emisiones de muy baja energía.

Los detectores semiconductores son utilizados en la determinación de partículas α, gamma y rayos X y son capaces de diferenciar partículas o radiaciones de energías muy similares. Para la medida de emisores α se emplean a menudo los de Silicio, mientras que para la cuantificación de mezclas de emisores gamma se emplean los semiconductores de Germanio de alta pureza.

1.3.4. Termoluminiscencia

Este tipo de detectores se basan en el fenómeno de la luminiscencia. Debido a defectos del cristal o a la presencia de impurezas, los materiales se excitan al absorber la energía depositada y al calentarse a elevadas temperaturas se relajan con una consecuente emisión de fotones. Sus componentes básicos son el sistema de calentamiento controlado y el sistema de detección de los fotones emitidos y su conversión a señal eléctrica.

Existen diferentes tipos de dosímetros termoluminiscentes, entre ellos los de LiF:Mg y LiF:Ti, CaF_2:Mn y CaF_2:Dy, $CaSO_4$(Dy), $Li_2B_4O_7$, BeO, siendo los dos primeros los que se emplean con mayor frecuencia. Se usan para evaluar dosis producidas por radiación gamma, por partículas cargadas o por neutrones.

Los detectores de termoluminiscencia poseen pequeñas dimensiones, por lo que pueden ser utilizados en lugares donde otro detector no puede acceder por el tamaño y en aplicaciones como la dosimetría retrospectiva por su capacidad de detectar fotones de baja energía y partículas beta [El-Faramawy et al., 2014]. Se pueden usar para la medición de la mayoría de los tipos de radiación, con la posibilidad de emplearse para la discriminación de la radiación beta-gamma o neutrón-gamma.

1.4. CENTELLEO ORGÁNICO

A finales de los años 40 se comenzaron a desarrollar los centelleadores orgánicos para ser usados en la detección de emisores radioactivos mediante la conversión de la energía cinética de un evento de desintegración en fotones y su detección mediante el uso de un fotomultiplicador, el cual los convierte en pulsos eléctricos [Steinberg, 1959; L'Annunziata, 2013].

Dentro de los diferentes tipos de centelleadores orgánicos, el primero en desarrollarse fue el centelleo líquido. Su origen como técnica para la cuantificación de la radioactividad se atribuye a las primeras investigaciones de Kallmann y Reynolds [Kallmann, 1950; Reynolds et al., 1950], alrededor de los años 50. Durante los siguientes años los estudios se enfocaron en la formulación, el desarrollo y el establecimiento de las propiedades y los mecanismos de

transferencia de energía de los nuevos centelleadores orgánicos, así como también en la construcción y mejora de la instrumentación empleada para la detección de los fotones. Los avances realizados condujeron a la mejora del rendimiento de contaje, incrementar la sensibilidad de los equipos, reducir el tiempo de medida y mejorar las condiciones operatorias en cuanto a la manipulación de las muestras y de los datos.

En general, los centelleadores orgánicos se componen de una matriz orgánica y uno o un par de solutos fluorescente disueltos en dicha matriz, excepto los centelleadores orgánicos en forma de cristal que se componen sólo de un compuesto puro. Hoy día existe una gran variedad en la composición de los centelleadores orgánicos, lo cual los hacen útiles para distintos tipos de muestras y aplicaciones.

Entre los centelleadores orgánicos, se encuentran los centelleadores líquidos (en forma de cóctel de centelleador líquido o gel) y los centelleadores sólidos, que pueden ser cristales o centelleadores plásticos.

1.4.1. Componentes

La formulación de un centelleador orgánico debe asegurar la máxima absorción de la radiación, una eficiente transferencia de energía y un óptimo rendimiento de centelleo. También, debe en lo posible garantizar que el centelleador posea un alto punto de inflamabilidad, baja o nula toxicidad, establidad y que no genere altos costes de almacenamiento o gestión de los residuos.

El centelleador orgánico absorbe la energía emitida por el radioisótopo y la re-emite en forma de fotones. Para llevar a cabo la absorción y re-emisión, los centelleadores orgánicos poseen dos componentes básicos, el disolvente orgánico y los solutos fluorescentes.

Los centelleadores orgánicos, generalmente se preparan de acuerdo al tipo de emisor, a la muestra que se desee medir y a sus requerimientos específicos. Todos sus componentes deben poseer la más alta pureza para evitar interferencias en el proceso de transferencia de energía para la producción de fotones y de su detección, ya que dichas interferencias pueden ser causadas incluso por trazas de impurezas [Gibson y Lally, 1971]. Los cócteles de centelleador líquido además del solvente orgánico y los solutos fluorescentes, también pueden contener algunos aditivos, tales como surfactantes o estabilizadores, mientras que los centelleadores plásticos

pueden contener compuestos o elementos que mejoran sus propiedades para aplicaciones específicas, tales como metales (p.ej. Boro, Gadolinio, Cadmio, étc) [Bertrand et al., 2014].

1.4.1.1. Disolvente orgánico

Es el componente que se encuentra en mayor proporción en los centelleadores orgánicos y sirve como medio para contener la muestra y para disolver los solutos fluorescentes y aditivos. Los compuestos orgánicos aromáticos se consideran como los disolventes más adecuados para formular un centelleador orgánico, ya que debido a su estructura electrónica presentan una mayor capacidad para recoger en forma de excitación parte de la energía de la partícula radioactiva con la que interacciona.

Generalmente, los centelleadores orgánicos formados por cristales son preparados a partir de compuestos puros tales como antraceno, estilbeno o naftaleno (Figura 2), los cuales poseen tiempos de decaimiento en el orden de los nanosegundos, por lo que resultan poseer una alta capacidad para absorber la radiación incidente y transformarla en fotones. El antraceno es el compuesto que posee un mayor rendimiento lumínico entre los centelleadores orgánicos, por lo que se usa como referencia.

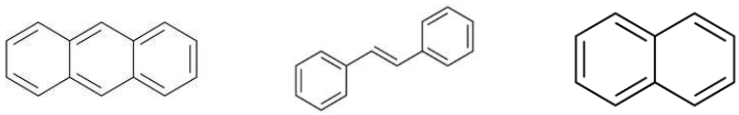

Antraceno Estilbeno Naftaleno

Figura 2. Diferentes compuestos que se emplean para la fabricación de centelleadores cristal

Respecto a la formulación de los cócteles de centelleador líquido, los disolventes orgánicos más empleados desde los comienzos han sido los alquilbencenos y los éteres alifáticos, tales como el tolueno, el p -xileno y el 1,4-dioxano respectivamente (Figura 3).

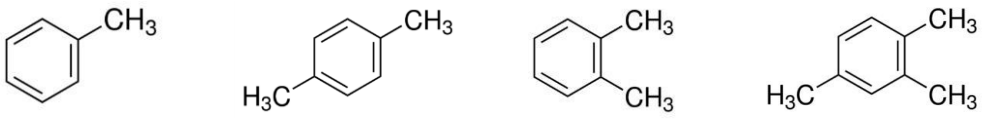

Tolueno p-xileno o-xileno pseudocumene

Figura 3. Solventes comunes en la formulación de los cócteles de centelleador líquido.

Sin embargo, en los últimos años se han empleado disolventes orgánicos tales como el 2,6-diisopropilnaftaleno (DIN), el fenilxililetano (PXE) y los alquilbencenos lineales (LAB), los cuales se consideran menos tóxicos y más seguros por poseer baja presión de vapor y un alto punto de inflamabilidad (sobre los 140 ºC) (Figura 4).

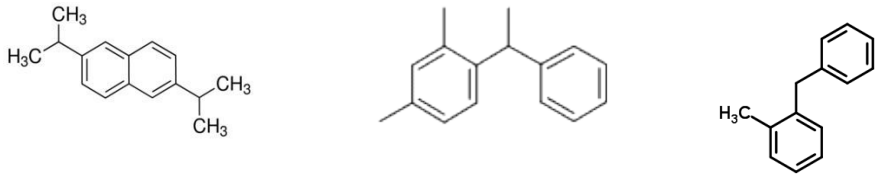

2,6-diisopropilnaftaleno (DIN) fenilxililetano (PXE) benciltolueno

Figura 4. Disolventes orgánicos de última generación empleados en la formulación de cócteles de centelleo líquido.

Finalmente, en la formulación de los centelleadores plásticos los disolventes orgánicos empleados como matriz polimérica más comunes son el poliestireno (PS), el poliviniltolueno (PVT), el polimetilmetacrilato (PMMA), polibencil metacrilato (PBMA) (Figura 5). Sin embargo, de acuerdo a los requerimientos de formulación y de sus aplicaciones, también se pueden emplear otras matrices poliméricas tales como los polixiloxanos, las resinas epoxi, los poliésteres y las poliamidas, entre otros.

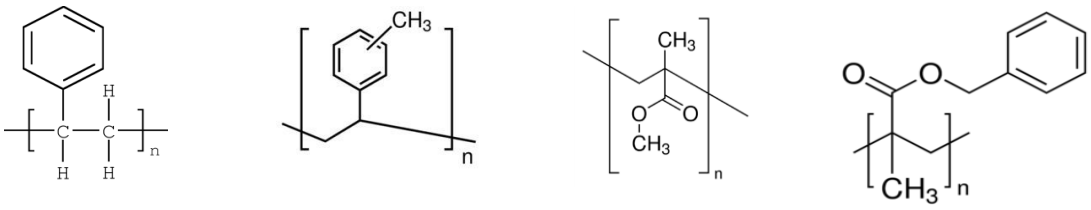

Poliestireno (**PS**) Poliviniltolueno (**PVT**) Polimetilmetacrilato (**PMMA**) Polibencil metacrilato (**PBMA**)

Figura 5. Principales matrices poliméricas empleadas en la formulación de los centelleadores plásticos.

1.4.1.2. Solutos fluorescentes

Se distinguen dos tipos de solutos fluorescentes, los primarios y los secundarios. Los solutos fluorescentes primarios (Figura 6) permiten la conversión de la energía capturada por el disolvente orgánico para emitirla en forma de fotones a una longitud de onda superior a la de

éste, alrededor de 270 nm. Según se describe en la bibliografía las moléculas de soluto fluorescente inducen un momento dipolar en su capa de solvatación, permitiendo la transferencia directa de energía entre las moléculas excitadas de disolvente orgánico y el soluto fluorescente. Algunos de los solutos fluorescentes primarios empleados en la formulación de centelleadores orgánicos líquidos o plásticos se presentan a continuación.

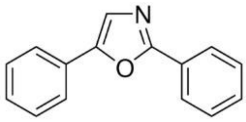

2,5-difeniloxazol (PPO)

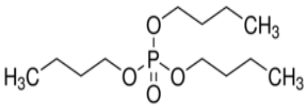

Fosfato de tributilo (TBP)

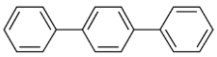

p-terfenil (tP)

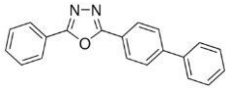

2-fenil-5-(4-difenil)-1,3,4-oxadiazol (PBD)

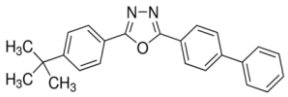

2–(4'-t-butilfenil)–5–(4"-bifenilil)–1,3,4-oxadiazol (Butyl-PBD)

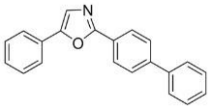

2-(bifenil-4-il)-5-feniloxazol (PBO)

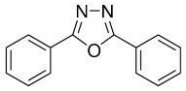

2,5-difenil-1,3,4-oxadiazol (PPD)

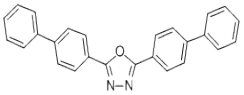

2,5-di-(bifenil-4-il)-1,3,4-oxadiazol (BBD)

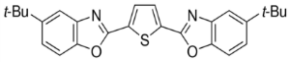

2,5-bis-(5-tert-butil-benzoxazol-2-il) tiofeno (BBOT)

Figura 6. Solutos fluorescentes primarios más utilizados en la formulación de los centelleadores orgánicos

Los solutos fluorescentes primarios deben ser capaces de ser excitados por moléculas excitadas de disolvente y además, deben ser solubles en el disolvente a una concentración adecuada para permitir una óptima emisión de fotones, alrededor de 10 g L^{-1} [Horrocks, 1974].

Por otro lado, los solutos fluorescentes secundarios (Figura 7) aceptan la energía del soluto fluorescente primario y la re-emiten a una longitud de onda mayor (415-430 nm) [Merino et at. 2005], ya que la mayoría de los solutos fluorescentes primarios emiten los fotones por debajo de los 408 nm, la cual se considera una longitud de onda de emisión inapropiada para ser captada por el fotomultiplicador. Aunque los fototubos modernos son capaces de detectar los fotones

emitidos por el soluto fluorescente primario, la adición del soluto fluorescente secundario, agregado en un intervalo de concentración entre 0.01-0.5% para evitar la autoabsorción, permite incrementar la eficiencia de detección de forma significativa. Algunos de los solutos secundarios usados con más frecuencia en la formulación de los centelleadores orgánicos son:

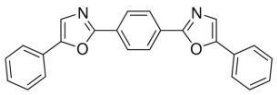

1,4-bis-(2-(5-fenoxiloxazolil) benceno (POPOP)

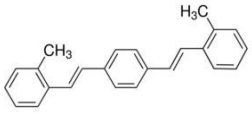

1,4-bis(2-metilstiril) benceno (Bis-MSB)

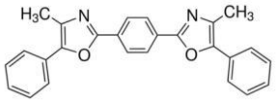

1,4-bis-2-(4-metil-5-feniloxazolil)-benceno (dimetil-POPOP)

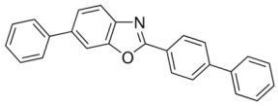

2-(bifenil-4-il)-6-fenilbenzoxazol (PBBO)

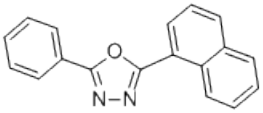

2-(1-naftil)-5-fenil-1,3,4-oxadiazol (NPD)

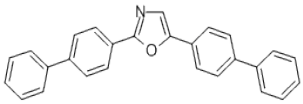

2,5-di(4-bifenil-4-il)oxazol (BBO)

Figura 7. Solutos fluorescentes secundarios más usados en el centelleo orgánico

Algunos solutos fluorescentes desarrollados en las últimas décadas, tales como la 3-hidroxiflavona (3HF), el 2-(2'-hidroxifenil) benzotiazol (HBT), la 1-fenil-3-mesitil-2-pirazolina (PMP) (Figura 8) suprimen la necesidad de adicionar un soluto fluorescente secundario debido a sus excelentes propiedades fluorescentes, ya que emiten a longitudes de onda mayores a 400 nm, poseen un alto rendimiento lumínico y un tiempo corto de decaimiento de fluorescencia [Güsten y Mirsky, 1991].

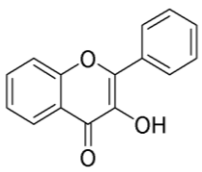

3-hidroxiflavona (3-HF)

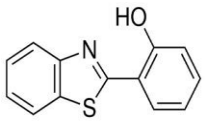

2-(2'-hidroxifenil) benzotiazol (HBT)

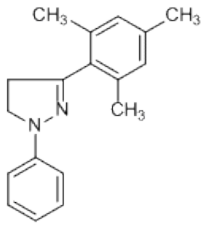

1-fenil-3-mesitil-2-pirazolina (PMP)

Figura 8. Solutos fluorescentes de última generación.

Los solutos fluorescentes deben ser solubles en el disolvente orgánico a temperaturas de trabajo y no deben precipitar con el tiempo ni al mezclarlo con la muestra a medir, la cual generalmente es acuosa.

1.4.1.3. Otros aditivos

La formulación de los centelleadores orgánicos puede incluir compuestos adicionales a los anteriormente mencionados, con la finalidad de ampliar sus aplicaciones.

En el caso de los centelleadores líquidos, los agentes extractantes, tales como el bis-(2-etilhexil) fosfato (HDEHP) aseguran la homogeneidad y estabilidad de la muestra mediante la formación de complejos o la formación de emulsiones uniformes de micelas muy pequeñas.

La adición de un surfactante es necesaria cuando se desean medir muestras hidrofílicas usando un centelleador orgánico líquido, por ejemplo el Tritón-X100, ya que permiten emulsificar la muestra dentro del disolvente orgánico creando micelas de tamaño nanométrico, manteniendo así la transparencia de la emulsión. Se pueden adicionar surfactantes tipo aniónico (p. ej. dioctilsulfocianato (SOSS)) o no-iónico (p. ej. alquilfenol etoxilado (EAP), trietil fosfato (TEP) o sales alifáticas de polioxietilensorbitano (TWEEN)) [Merino y Los, 2005]. Debido a la presencia de múltiples componentes, a los centelleadores líquidos se les conoce comúnmente como cócteles de centelleador líquido.

Por otro lado, las matrices poliméricas pueden ser químicamente modificadas para adaptarlas a determinadas aplicaciones (adición de metales, metales pesados, solutos fluorescentes fluorados, polímeros reticulados, étc). Por ejemplo, la adición de metales, tales como el litio, cadmio, boro o gadolinio dentro de la composición de los centelleadores plásticos permite modificar el material centelleador para incrementar su densidad y de esta forma, aumentar la interacción con la radiación gamma o para hacer el material centelleador más selectivo a nucleos que poseen una mayor sección eficaz hacia un tipo de radiación específica [Bertrand et al., 2014].

1.4.2. Equipos

Existen diferentes configuraciones de los contadores de centelleo, sin embargo estos se basan principalemente en:

- Una cámara de medida en la que se sitúa el vial y el centelleador orgánico.

- Un conjunto de 1, 2 ó 3 fotomultiplicadores en coincidencia que detectan los fotones emitidos.
- Una cadena electrónica que permite la amplificación y la clasificación de los impulsos eléctricos generados por los fotomultiplicadores.

La cámara de medida se encuentra habitualmente incluida dentro de un sistema de blindaje que permite reducir la señal de fondo producida por la radiación cósmica, dichos blindajes suelen ser de plomo. La reducción del fondo también se consigue mediante la utilización de dos fotomultiplicadores en coincidencia instalados en la cámara de medida. Esta configuración permite que sólo sean señales coincidentes reales aquellas que son observadas simultáneamente por los dos fotomultiplicadores, siendo el resto descartadas. Existen diferentes casas comerciales que suministran detectores con este tipo de configuración.

1.4.3. Mecanismo de detección en centelleo orgánico

El fundamente físico de la detección mediante el centelleo líquido, es el que se ha estudiado más ampliamente y se puede considerar extrapolable a los demás tipos de centelleadores orgánicos (Figura 9). Se basa principalmente, en que una partícula emisora al entrar en contacto con el cóctel de centelleo, cede su energía a las moléculas de disolvente orgánico, las cuales se excitan y posteriormente transfieren la energía a las moléculas de solutos fluorescentes, que al desexcitarse producen fotones de una longitud de onda característica de éstos. La energía de la partícula emitida determinará su alcance en el centelleador y a su vez el número de fotones que se generan, el cual será proporcional a dicha energía.

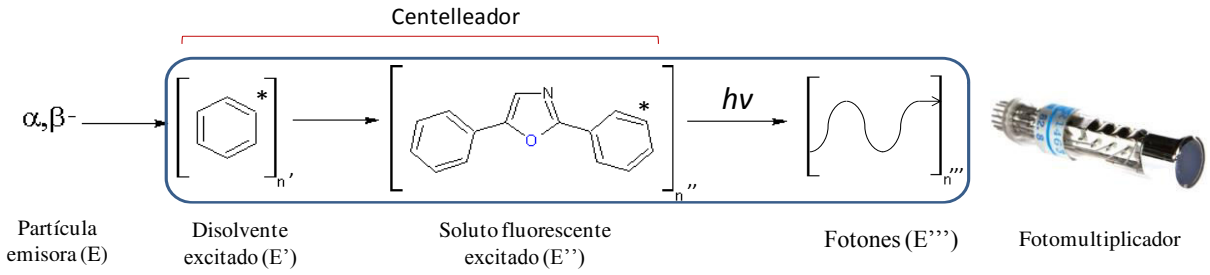

Figura 9. Mecanismo de transferencia de energía para la producción de fotones

1.4.4. Eficiencia de detección y espectro

La eficiencia de detección o eficiencia de contaje se refiere al porcentaje de desintegraciones que producen un pulso detectable de fotones y se calcula de acuerdo a la ecuación 1. La eficiencia de detección depende del isótopo, composición de muestra y del equipo empleado para la medida. Eficiencias de detección muy bajas pueden ser causadas por la baja energía del emisor y la consecuente baja producción de fotones. La disminución en la eficiencia de detección puede producirse por diferentes interferencias en las distintas etapas de conversión de energía en fotones o la disminución en la detección de los fotones producidos. Este conjunto de fenómenos es conocido como quenching.

$$\text{Eficiencia de detección} = \frac{\text{Nº de eventos detectados}}{\text{Nº de desintegraciones}} \qquad \text{(Ec. 1)}$$

La clasificación de los pulsos detectados en función del número de fotones de cada pulso, es decir su energía, permite construir un espectro de energías, tal como se muestra en la Figura 10, que depende del espectro inicial del emisor, del sistema de detección y de los fenómenos de quenching.

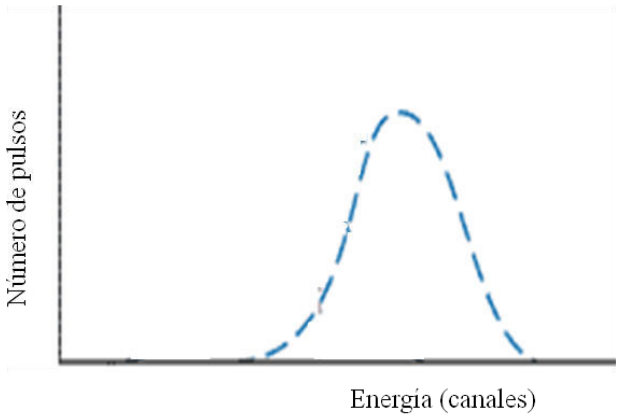

Figura 10. Espectro de eficiencia de detección de un radionucleido

1.4.5. Quenching

El quenching se define como cualquier factor que causa una disminución de la energía o interfiere en el proceso de su transferencia desde que la partícula es emitida hasta que los fotones son detectados por el fotomultiplicador (PMT). El fenómeno de quenching, en la mayoría de los casos que se emplea el centelleo líquido, se aprecia mediante el desplazamiento del espectro hacia energías más bajas y una consecuente reducción de la eficiencia de detección (Figura 11).

Sin embargo, su comportamiento depende del tipo de interferencia que lo produce, del tipo de centelleador y de la muestra.

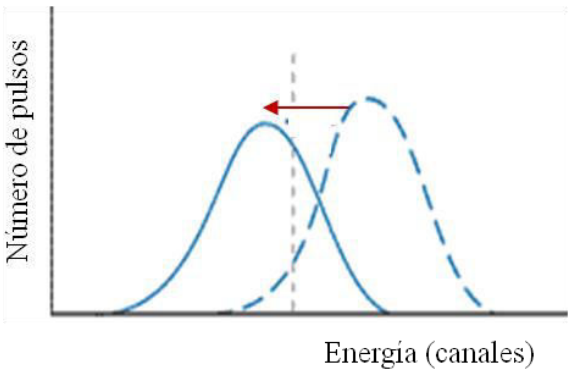

Figura 11. Efecto del quenching sobre la eficiencia de detección

Los tipos de quenching más conocidos cuando se emplean cócteles de centelleo líquido son el químico, el de color y el de ionización (Figura 12). Por otro lado, en otros centelleadores orgánicos plásticos, también se definen el quenching de partícula y el quenching óptico.

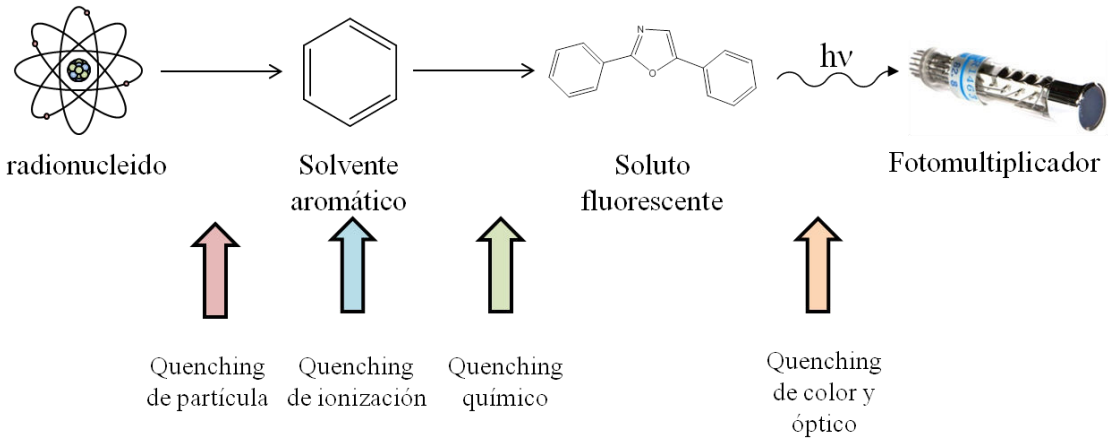

Figura 12. Diferentes tipos de quenching que afectan el centelleo orgánico (líquido y sólido).

A continuación se describen los principales tipos de quenching que afectan las medidas con centelleador orgánico:

El *Quenching de ionización* Se manifiesta mediante la reducción de la producción de fotones debido a la disminución del número de procesos de excitación primaria del disolvente producto de la alta densidad de las moléculas ionizadas. Este tipo de quenching es dependiente del centelleador, del tipo de partícula emitida (alfa o beta) y de su energía, por lo que se

considera constante en unas condiciones de medida constantes (centelleador) y para un determinado isótopo [Birks, 1964].

El *quenching químico* causa la disminución de los fotones producidos en el proceso de centelleo debido a la presencia de substancias químicas en la muestra, que interfieren en la transferencia de energía entre el disolvente aromático y los solutos fluorescentes. Algunos ejemplos de agentes que producen quenching químico son: el nitrometano, la acetona, el tetracloruro de carbono.

El *quenching de color* causa la disminución de los fotones detectados respecto a los emitidos como consecuencia de la presencia de substancias coloreadas en la muestra, las cuales absorben los fotones producidos.

El *quenching de partícula* corresponde a la reducción de la eficiencia de detección y a cambios en la distribución del espectro debido a que las partículas emitidas pierden total o parcialmente su energía al interaccionar con moléculas del medio antes de alcanzar el centelleador. Se considera como el tipo de quenching más importante en las medidas con microesferas de centelleador plástico, en las que la solución de la muestra y el polímero centelleador constituyen fases diferentes. Este tipo de quenching es importante principalmente para los emisores de baja y media energía.

El *quenching óptico* corresponde al debilitamiento de la señal debido a la pérdida o ineficiente transmisión de fotones a lo largo de su trayectoria desde el punto donde son emitidos hasta el fotocátodo del fotomultiplicador debido a los sucesivos cambios de fase (solución acuosa-centelleador) con índice de refracción diferente.

1.4.6. Otros fenómenos

Además de los tipos de quenching descritos, durante el proceso de centelleo pueden ocurrir otros fenómenos que alteran o debilitan la producción o detección de fotones y por lo tanto las capacidades radiométricas de la medida. Entre estos, se pueden mencionar:

- Quimioluminiscencia: producida por reacciones químicas que ocurren entre los componentes del coctel o debidas a la misma muestra, y que generan una emisión adicional de fotones con duraciones muy variables.
- Fosforescencia: producida por algunos compuestos que poseen una fotoluminiscencia duradera.

- Microprecipitación: puede darse como resultado de la incompatibilidad entre el coctel de centelleo y la muestra a medir.
- Adsorción: posiblemente debida a la afinidad entre los iones contenidos en la muestra radioactiva y los centros activos de la superficie interna del vial.

1.4.7. Parámetros de quenching

El grado de quenching de una muestra, puede ser determinado mediante dos procedimientos. El primero, relacionado con la posición del espectro de la muestra y el segundo, con la posición del espectro generado cuando la muestra es irradiada con una fuente externa gamma (p.ej. ^{152}Eu). La interacción de los rayos gamma con los átomos de la solución de muestra genera mediante el efecto Compton un gran número de electrones que finalmente son convertidos en fotones medidos por el detector. El espectro generado, se denomina espectro Compton y tiende a desplazarse a valores de energía más bajos cuando las muestras son afectadas por efectos del quenching. El procedimiento habitual es el segundo y el parámetro de quenching asociado en el detector depende de la casa comercial que lo fabrique, en el caso del Quantulus (Perkin Elmer), se emplea el SQP(E), el cual corresponde al espectro generado por la fuente gamma externa donde el área cumulativa es 99,75% del área total [L'Annunziata, 2013].

1.4.8. Capacidad de los centelleadores orgánicos para discriminar partículas (α/β)

Los centelleadores orgánicos de acuerdo a su composición pueden ser empleados para la discriminación de partículas alfa y beta o de radiación gamma y neutrones empleando un parámetro de discriminación, el cual se establece en cada equipo comercial mediante la medida del tiempo de los pulsos individuales y su comparación con un parámetro propio para cada instrumento (p.ej. *Pulse Decay Discriminator* (PDD) para Packard, *Pulse Shape Analysis* (PSA) para el Quantulus, entre otros).

El mecanismo de discriminación de partículas fue propuesto por Parker y Hatchard [Parker y Hatchard, 1961] y posteriormente desarrollado por Laustritat [Laustriat, 1968]. La metodología ha sido desarrollada en los últimos 50 años [Brooks, 1959; Roush et al., 1964] y ha sido implementada en distintas aplicaciones. Actualmente es la base de los métodos para la determinación del índice alfa/beta en análisis de rutina [Montaña et al., 2013] y la determinación de neutrones y fotones [Polack et al., 2015].

En centelleo orgánico los eventos alfa y beta se pueden discriminar a partir de la diferencia en la duración de sus pulsos electrónicos producidos en el ánodo del tubo fotomultiplicador, originados por los diferentes mecanismos de de-excitacion del medio centelleante para partículas de baja ionización (electrones) y partículas altamente ionizantes, tales como las partículas alfa.

Los pulsos producidos en la medida de centelleo constan de dos componentes, el rápido y el lento. Dichos pulsos ocurren en diferentes proporciones para cada tipo de emisor. El componente rápido viene dado por la de-excitación de los estados singuletes, que pierden su energía vía procesos de fluorescencia conllevando a una rápida emisión de fotones. Mientras que el componente lento se da cuando dos estados tripletes interactúan y forman dos estados singuletes con al menos uno de ellos excitado. El proceso es llamado aniquilación de tripletes, y resulta en la emisión de un fotón con una duración más larga de algunos cientos de nanosegundos [King y Voltz, 1966].

El paso de partículas cargadas a través de un medio centelleador formado por compuestos aromáticos conlleva a la excitación y a la ionización de sus moléculas [Kreslo et al., 2011] y está directamente relacionado con la transferencia linear de energía, la cual es la cantidad de energía depositada por la carga de la partícula por unidad de longitud en el trayecto. En el rango de energía de 0,1 a 10 MeV, la transferencia linear de energía para partículas alfa es de algunos órdenes de magnitud mayores que para electrones ligeros (beta) [Kreslo et al., 2011]. La mayor ionización específica de las partículas alfa conduce a una mayor proporción de moléculas excitadas en estados tripletes, lo que finalmente se traduce en una duración más larga de los pulsos [L'Annunziata, 2013] con respecto a las partículas beta, en la que se producen más singuletes y por tanto domina la componente rápida.

El cóctel de centelleador líquido ha sido exitosamente empleado para la discriminación de partículas α/β. Por otro lado, la bibliografía describe que en los centelleadores plásticos la discriminación es difícil debido a la similitud de la duración de los pulsos para los dos tipos de partículas, ya que los componentes de pulso rápido y lento son muy similares [Normand et al., 2002].

Aunque la interacción de las partículas en las medidas con centelleadores plásticos sigue un mecanismo similar al de centelleo líquido, éste no se encuentra bien establecido, ya que la interacción dipolo-dipolo es el único mecanismo activo no-radiativo para la transferencia de energía en el plástico [Brooks et al., 1979; Birks, 1964]. En las moléculas de centelleador plástico, la probabilidad de tripletes excitados coincidentes es menor que en las moléculas de

centelleador líquido ya que la difusión de energía a través de la cadena es muy rápida, por lo que el componente de pulso retrasado también es de menor importancia [Bagán et al., 2010].

1.4.9. Técnica de centelleo líquido y Cherenkov

Dentro de las diferentes formas de centelleo orgánico, el centelleo líquido (LS) es la técnica más estudiada y consolidada hasta la presente. Se considera como la metodología estándar de rutina en los laboratorios para cuantificar la radioactividad en los emisores beta, debido a sus prestaciones desde el punto de vista analítico y a que el proceso de preparación de muestras de medida es simple. Generalmente, la muestra a medir se mezcla con el cóctel de centelleador adecuado dentro de un vial de centelleo, el cual se introduce dentro de la cámara de medida donde se encuentran los fotomultiplicadores. La alta sensibilidad de los fotomultiplicadores aunado al blindaje del equipo permiten detectar niveles de radioactividad muy bajos.

El centelleo líquido ha sido muy útil para las medidas de radioactividad debido a su alta eficiencia [Fox, 1976; Birks, 1964; Horrocks, 1974] especialmente en la determinación de un amplio rango de emisores beta de baja y media energía, entre los cuales se encuentran ^{3}H ($E_{\beta máx}$=18 keV), ^{14}C ($E_{\beta máx}$=156 keV), ^{35}S ($E_{\beta máx}$=167 keV), ^{63}Ni ($E_{\beta máx}$=67 keV). Si bien, también se utiliza en la determinación de emisores beta de alta energía, emisores alfa, radionucleidos de captura electrónica y radiación gamma. Además, ofrece la posibilidad de discriminar partículas tales como las alfas de las betas mediante el uso de un cóctel de composición adecuada y el tratamiento electrónico de los pulsos. Esto permite que el centelelador líquido sea una técnica alternativa a los contadores proporcionales en muestras de interés medioambiental.

El centelleo líquido provee una óptima eficiencia de detección, en el caso de las partículas beta ésta depende de la energía original de su desintegración, por lo que para partículas que poseen una energía de desintegración sobre los 100 keV la eficiencia de detección es del 80-100%, mientras que para las partículas con energía de desintegración menor como es el caso del ^{3}H, la eficiencia de detección puede variar entre 10-60% dependiendo también de otros factores, tal como la presencia de interferentes [L'Annunziata, 2013].

La medida por centelleo líquido es muy apropiada para muestras acuosas, las cuales se mezclan con el cóctel de centelleo para crear una emulsión. Uno de los componentes del cóctel de centelleador líquido es el emulsificante, éste permite la formación de micelas de la muestra,

generalmente acuosa, rodeadas por centelleador orgánico. El tamaño de las micelas es del orden de los nanómetros, lo que asegura que la distancia entre el lugar donde ocurre la desintegración hasta que la partícula emitida o radiación encuentra la molécula de disolvente para depositar su energía sea de ese orden y de que la probabilidad de interacción sea alta, resultando en valores de eficiencia de detección altos incluso para emisores de media energía y valores óptimos para los emisores de baja energía.

Sin embargo, la eficiencia de detección del radionucleido en la muestra es variable ya que se ve influenciada por el grado de quenching, el cual es ocasionado por interferentes presentes en la muestra. Adicionalmente, la metodología posee limitada selectividad cuando se mide simultáneamente más de un radionucleido en la muestra, resultando en un espectro de señales superpuestas, por lo que se requieren pasos previos de separación química y por tanto mayor tiempo de preparación.

Aunque en los últimos años algunos cócteles de centelleador líquido se han formulado para que sean biodegradables, su tratamiento por parte de los laboratorios después de la medida sigue resultando complejo debido a la cantidad de residuo generado. Este aspecto se complica cuando se ha de medir con un cóctel de centelleador líquido no biodegradable, ya que al mezclar la muestra radioactiva con el cóctel se produce un residuo mixto que se caracteriza por ser tóxico y radioactivo [Tahmassian et al., 1991; Kalbhem y Tarkanen, 1984], y como consecuencia, difícil de almacenar debido a sus propias características [McCormick, 1991] y a las regulaciones establecidas para la disposición de residuos nucleares y peligrosos [Einsenbud, 1987].

Alternativamente al centelleo líquido, las partículas beta de energía superior a 263 keV pueden ser detectadas y cuantificadas en un espectrómetro de centelleo líquido mediante la técnica de Cherenkov sin la necesidad de emplear el cóctel de centelleo [Horrocks, 1974]. Tal como se mencionó anteriormente, cuando la partícula beta de alta energía viaja por un medio, normalmente acuoso, a una velocidad mayor a la velocidad de la luz, sufre un proceso de frenado y se emite radiación Cherenkov en forma de fotones que pueden ir desde longitudes de onda en el intervalo del ultravioleta hasta el visible (Figura 13).

La metodología Cherencov permite la determinación de algunos radioisótopos, tales como el ^{32}P ($E_{máx}$= 1710 keV), ^{90}Sr (^{90}Y $E_{máx}$= 2280 keV), ^{86}Rb ($E_{máx}$= 1770 keV), ^{89}Sr ($E_{máx}$= 1490 keV). El proceso no se ve afectado por debilitamientos de señal causados por quenching químico. Sin embargo la eficiencia de detección de los emisores beta en agua es aproximadamente 35-70% y dependiente de si se ve o no afectada por la pérdida de la detección

de fotones en el fotmomultiplicador debido a quenching de color [Horrocks, 1974; L'Annunziata, 2013].

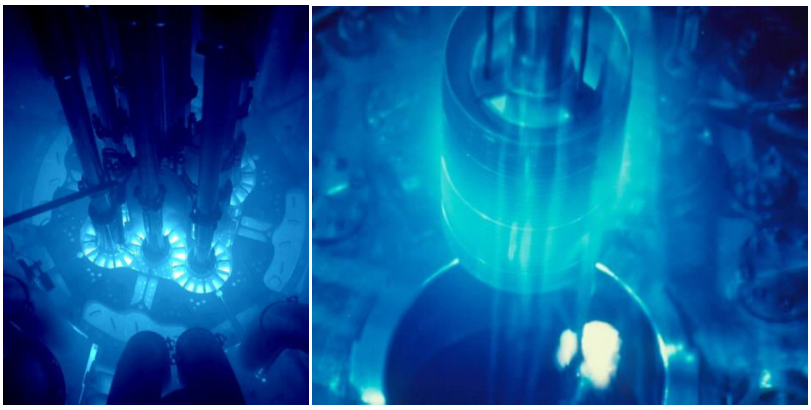

Figure 13. Luz producida por la radiación Cherenkov en un reactor.

1.4.10. Medida con centelleadores plásticos

El desarrollo y la producción de centelleadores plásticos (PSs) se inició posteriormente a la aparición del centelleador líquido, a finales de los años 50 [Rapkin et al., 1962], cuando se demostró que diferentes formas de estos materiales se podían obtener a partir de distintos polímeros [Schorr y Torney, 1950], por lo que se consideró como una alternativa muy versátil ante las técnicas clásicas de centelleo (inorgánico y líquido). Sin embargo, los resultados obtenidos en las primeras aplicaciones analíticas no fueron muy exitosos, y esto impidió que los centelleadores plásticos se emplearan ampliamente para la determinación de emisores beta en medidas de rutina.

El centelleador plástico se compone de uno o un par de solutos fluorescentes encapsulados en una matriz polimérica. El material resultante es capaz de producir fotones cuando interactúa con una fuente radioactiva [Bertrand et al., 2014]. Sus componentes al igual que en el cóctel de centelleo líquido son de alta pureza para garantizar una óptima transferencia de energía y producción de fotones.

Los centelleadores plásticos también pueden contener un disolvente aromático secundario, tal como el naftaleno, el antraceno, el 2,6-diisopropilnaftaleno, entre otros. Dichos compuestos mejoran la transferencia de energía entre el disolvente y el soluto y en ciertas ocasiones influye en la duración de los pulsos, mejorando sus capacidades en cuanto a la discriminación de partículas.

Los centelleadores plásticos se pueden encontrar en distintas formas (Figura 14), entre las más conocidas:

- Barras, bloques o láminas que es como se preparaban desde sus inicios.
- Fibras de centelleador plástico, las cuales fueron desarrolladas a partir de los años 1989 por Saint-Gobain, y consisten generalmente en un núcleo polimérico que contiene los solutos fluorescentes disueltos y un recubrimiento polimérico de índice de refracción diferente al interior para mejorar la transmisión de la señal óptica.
- Microesferas de centelleador plástico (PSm por sus siglas en inglés, *Plastic Scintillation microspheres*), las cuales han sido el objeto de estudio en esta tesis doctoral.

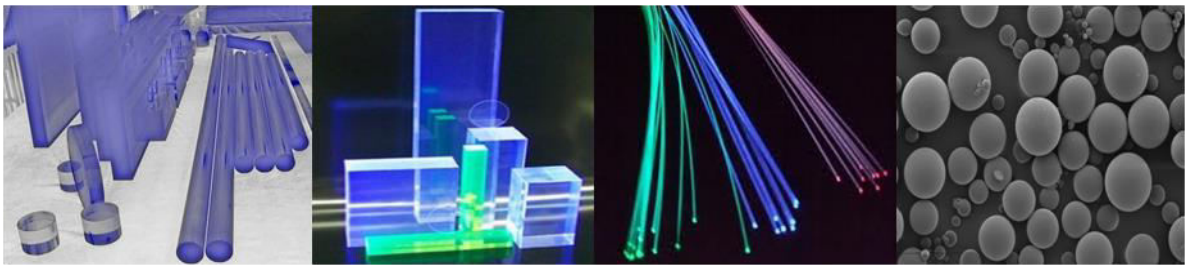

Figura 14. Distintas formas de presentación de los centelleadores plásticos.

Algunas de las características más importantes que hacen de los centelleadores plásticos un material interesante para la determinación de los radionucleidos se mencionan a continuación:

- Se pueden preparar en grandes cantidades, formas y dimensiones. Además se pueden preparar en base a distintas formulaciones, de acuerdo a la aplicación para la que se requieran.
- Pueden ser manipulados sin especificaciones especiales.
- Poseen una estructura rígida que permite una respuesta de centelleo más rápida que la de los cócteles de centelleador líquido.
- Al estar completamente polimerizados poseen una reactividad muy baja por lo que no generan problemas para ser almacenados y además, no generan residuos mixtos, ya que no se mezclan con la muestra acuosa permitiendo la posible recuperación de ambos.

Los centelleadores plásticos en forma de bloque o láminas son utilizados en un amplio rango de aplicaciones, entre las cuales se encuentran:

- Detectores de elevado volumen para la determinación total de las radiaciones gamma con energías mayores a los 100 keV, rayos-X, partículas cargadas y neutrones.

- Control de seguridad como monitores de portales, para escanear cargas y para realizar calibraciones a nivel industrial.
- Blindaje activo en los sistemas de detección de fondo de equipos comerciales.
- Microplacas contadoras de centelleador sólido.
- Dosimetría y simulaciones dosimétricas [Beddart et al., 1992].

1.5. MICROESFERAS DE CENTELLEADOR PLÁSTICO (PSm).

1.5.1. Generalidades

El uso de los centelleadores plásticos en distintas aplicaciones se deriva de su habilidad para ser producidos en diferentes formas y composiciones. Las microesferas de centelleador plástico son una mezcla sólida de forma esférica de un polímero que funciona como disolvente orgánico matriz para encapsular las moléculas de solutos fluorescentes. Las PSm pueden tener tamaños que varían desde las pocas decenas hasta los cientos de micrómetros.

Las medidas con PSm se realizan mezclando una cantidad de microesferas junto con la muestra acuosa a analizar en un vial de polietileno sin la necesidad de agregar surfactante, puesto que la mezcla, al ser heterogénea, no requiere que se forme una emulsión (Figura 15). Los eventos de decaimiento se miden empleando el mismo equipo que se usa para la medida por centelleo líquido.

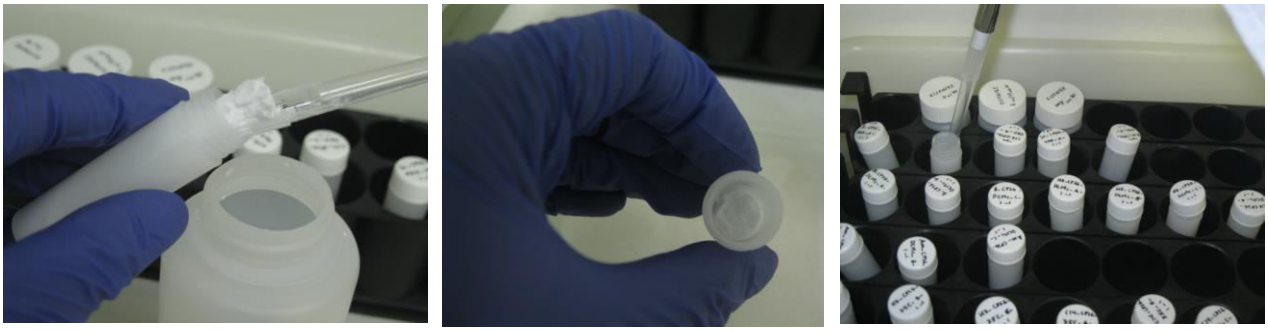

Figura 15. Medida empleando PSm, preparación de los viales.

El mecanismo de transferencia de energía y la detección de fotones por parte del fotomultiplicador es muy similar al de centelleo líquido. Las partículas emitidas como consecuencia del decaimiento radioactivo se desplazan a través del medio hasta alcanzar la superficie de la PSm donde comienza el proceso de transferencia de energía hasta que los fotones son producidos y detectados por el fotomultiplicador [Tarancón et al., 2003]. Sin embargo, la

diferencia más importante entre ambas metodologías respecto al mecanismo de transferencia de energía se basa en que al tratarse de microesferas sólidas, la distancia que debe desplazarse una partícula emitida que se encuentra en el seno de la disolución acuosa hasta alcanzar la superficie de la PSm podría ser del orden micrométrico, mientras que en el caso de centelleo líquido, se crea una emulsión donde las moléculas tienen un contacto cercano ya que la trayectoria queda reducida al orden de los nanómetros (Figura 16).

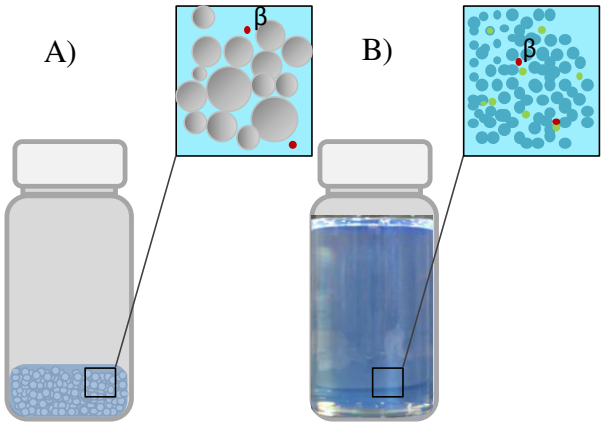

Figura 16. Diferencia entre un vial que contiene A) la muestra y las PSm, B) la muestra y el cóctel de centelleo líquido.

Las medidas con PSm presentan buenos parámetros de detección en la medida de emisores beta de altas energías resultando en altas eficiencias de detección, por lo que hace de la metodología una alternativa óptima al uso del centelleo líquido y de la técnica de Cherenkov [Tarancón, et al., 2002a; DeVol et al., 2001a]. Por lo que respecta a la detección de partículas beta de energía baja o partículas alfa, su eficiencia es inferior debido al quenching de partícula.

Las PSm abren las posibilidades de desarrollar nuevas aplicaciones en base a las prestaciones que proveen su forma sólida y polimérica. Así, debido a que las PSm se encuentran completamente polimerizadas no reaccionan, no son inflamables ni tóxicas y después de la medida, éstas y la muestra radioactiva pueden ser segregadas mediante filtración o tratadas como un residuo plástico [Tarancón et al., 2002b], evitando de este modo la producción de residuo mixto [Tahmassian et al., 1991; McCormick, 1991].

Las PSm junto con las fibras de centelleador plástico [Tarancón et al., 2005; Headrick et al., 2000] se emplean como material de detección de emisores beta, especialmente de media y alta energía, en las celdas de sistemas de flujo continuo [DeVol et al., 2001b; Hofstetter, 1995] y en remoto [DeVol et al., 2001b, Perkins et al., 1995]. Las PSm se consideran adecuadas para

construir el receptor de un sensor en continuo ya que se pueden alojar en el interior de la celda de medida y la muestra puede pasar a través de ellas. También porque son sensibles a los diferentes tipos de partículas emitidas y además, a su habilidad para operar sin consumir otros reactivos para producir la señal [Tarancón et al., 2002a; Tarancón et al., 2002b; Tarancón et al., 2004; Tarancón et al., 2003; McCormick, 1991; Birks, 1964].

Las PSm son útiles en la cuantificación de la actividad de emisores en soluciones salinas y de algunas muestras de origen biológico, las cuales no se pueden llevar a cabo mediante el uso de centelleador líquido ya que al mezclar una solución salina con el cóctel de centelleo puede resultar una emulsión inestable y la aparición de separación de fases en el vial de medida y como consecuencia, errores en la calibración de la eficiencia de detección [Bagán et al., 2009].

Otra de las aplicaciones en la que las PSm resultan de utilidad es la de el ensayo de centelleo por proximidad (SPA) [Bosworth et al., 1989]. En esta técnica el centelleador se recubre con una molécula receptora y el ligando se marca con el isótopo de medida. La microesfera centelleadora emite fotones cuando detecta la partícula radioactiva del ligando el cual está unido a la molécula receptora. Los fotones generados se detectan mediante un fotomultiplicador. La técnica se emplea principalmente con emisores de baja energía tales como el ^{3}H o el ^{125}I, los cuales no son detectados si no están en la superficie de la esfera.

En los últimos años, las PSm se han empleado como resinas mediante la inmovilización de extractante selectivo sobre la superficie centelleadora (PS resins), permitiendo de esta manera la separación y pre-concentración en un vial-columna que puede ser medido luego sin pasos adicionales de elución y preparación de muestra [Bagán et al., 2011; Bagán et al., 2012; DeVol et al., 2001a]. Esta metodología, proporciona la ventaja de poder medir directamente el vial conteniendo el radionucleido inmovilizado en la superficie de las PSm, y por lo tanto aumentar el volumen de la disolución acuosa analizada y así alcanzar los limites de detección deseados [Bagán et al., 2011], reducir la cantidad de residuos generados y reducir el tiempo de análisis.

1.5.2. Estado actual

Las PSm son un material relativamente nuevo y poco evaluado para determinaciones radiométricas. Actualmente se conocen sólo dos proveedores comerciales, Saint-Gobain y Detec Rad, los cuales producen mayormente centelleadores plásticos en formas de láminas o fibras y restringen su producción de microesferas sólo a algunos tamaños y composiciones específicas por demanda. Así, todas las aplicaciones descritas anteriormente encuentran su restricción en la

baja disponibilidad de PSm comerciales, lo cual afecta en el coste y en la posibilidad de disponer de PSm de composición y tamaño variable. El desarrollo de métodos de producción tanto a escala de laboratorio como a escala industrial favorecería el desarrollo de estas aplicaciones.

Por otro lado, la implementación y optimización de procedimientos para la producción de PSm podría ser de interés no sólo para disminuir su coste, sino para permitir disponer de ellas en diferentes tamaños y composiciones para emplearlas en el desarrollo de nuevas aplicaciones en el campo de la detección de la radioactividad, así como también poder emplearlas para el estudio del mecanismo de transferencia de energía cuando se mide un radionucleido.

1.6. PRODUCCIÓN DE MICROESFERAS POLIMÉRICAS

La producción de microesferas poliméricas puede llevarse a cabo mediante diferentes técnicas. Resulta difícil realizar una estricta clasificación de las técnicas empleadas para producir microesferas, ya que algunas pueden ser híbridos de dos o más metodologías o pueden emplear diferentes mecanismos de producción de micropartículas al mismo tiempo [Tran et al., 2011]. A continuación, se muestra una clasificación de algunas de las técnicas existentes basada en la reactividad de los componentes a micronizar, el mecanismo por el cual se forman las microgotas y el tipo de mecanismo por el cual se elimina el disolvente de las microgotas (Figura 17).

En general, el potencial de la técnica para producir microesferas depende de su habilidad para formar microgotas a partir de la disolución que contiene el polímero o el monómero y los solutos a encapsular y de la capacidad de secar o evaporar el disolvente orgánico contenido en dichas microgotas. La selección de la técnica depende de diversos factores, tales como la necesidad de emplear equipos específicos, la capacidad que proporciona para producir microesferas de determinados diámetros, distribución de tamaños y morfologías, la naturaleza hidrofílica o no del compuesto que se emplea como matriz polimérica y los compuestos que se desean encapsular en ella, el tipo de secado de las microesferas y el rendimiento de producción deseado.

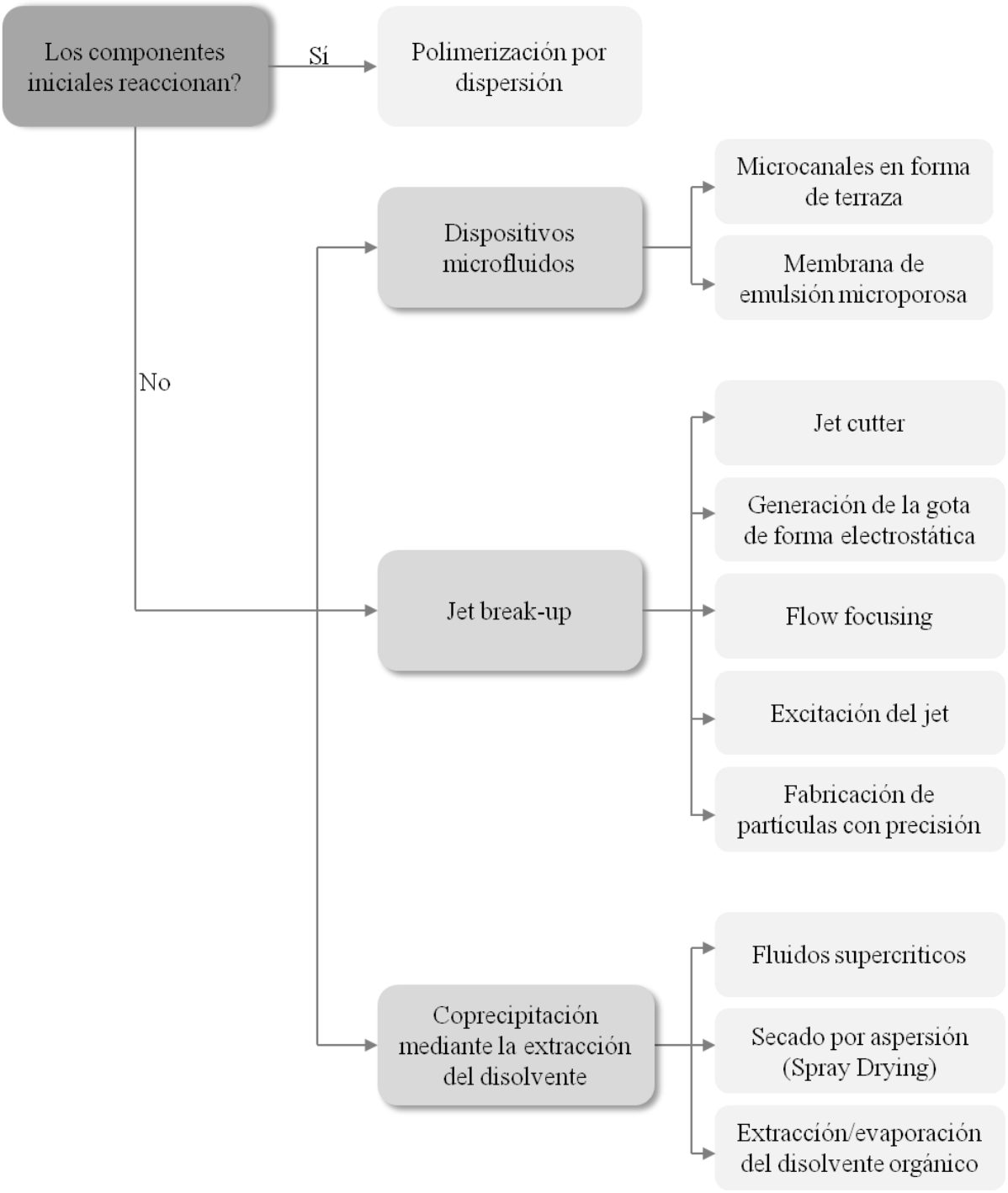

Figura 17. Diagrama de clasificación de algunas de las técnicas de producción de microesferas poliméricas

1.6.1. Polimerización por dispersión

Es un proceso de polimerización heterogéneo que se lleva a cabo en un medio homogéneo que contiene un estabilizador estérico disuelto en un disolvente orgánico, un monómero y un iniciador radical. El disolvente seleccionado como medio de reacción disuelve el monómero y el iniciador, pero no el polímero.

El polímero que se forma es insoluble y por lo tanto precipita para formar una dispersión coloidal que contiene en su seno el estabilizador polimérico, el cual previene la floculación y la agregación de las partículas que se van formando [Lok y Ober, 1985]. Según Hong et al., 2007 el proceso comienza a partir de una fase homogénea y la separación de fase ocurre cuando las cadenas oligoméricas de propagación precipitan para formar partículas poliméricas. Bajo condiciones favorables, se pueden obtener partículas monodispersas de diámetros muy reducidos.

La naturaleza y la cantidad de monómero agregada y la habilidad del estabilizador para mantener la estabilidad coloidal de las partículas crecientes es lo que principalmente determina el tamaño final de la partícula, su distribución de tamaños y el peso molecular del polímero obtenido. Otros parámetros que también influyen en la formación de las partículas poliméricas son la concentración del iniciador, la temperatura, la cual influye directamente en la velocidad de polimerización y la viscosidad del medio de polimerización [Barrett, 1973; Lok y Ober, 1985].

Mediante esta metodología se pueden producir microesferas de distintas composiciones y diámetros partiendo de diferentes monómeros y componentes. Se considera que la polimerización por dispersión es muy adecuada para la producción de microesferas monodispersas entre 1-10 µm [Hong et al., 2007].

Jinhua et al., 2014, obtuvieron microesferas de poliestireno a partir de estireno, etanol/2-metoxietanol como disolventes, azobisisobutironitrilo como iniciador y polivinil- pirrolidona como estabilizador. Por otro lado, Lok y Ober, 1985, evaluaron la producción de microesferas de poliestireno usando diferentes disolventes y obtuvieron microesferas de unos 12 µm de diámetro, al mismo tiempo que comprobaron que el tamaño y la distribución de tamaños poseían una alta dependencia con el sistema monómero/disolvente/iniciador.

La principal ventaja de esta técnica es que permite producir partículas poliméricas monodispersas en un proceso de un paso único. Sin embargo, el tamaño de las microesferas es del orden submicrométrico o de los pocos micrómetros, la producción a gran escala no es

factible en muchos casos, se hace difícil poseer un control físico del proceso y la encapsulación de los solutos es muy dependiente de la naturaleza de los componentes de la reacción.

1.6.2. Dispositivos de microfluidos

La metodología en general fue desarrollada por Amsdem, 1999 y consiste en la inyección de la fase dispersa a través de un microcanal con la finalidad de crear un microgoteo uniforme a consecuencia de la gravedad. Dependiendo de la técnica, el microgoteo, puede ir o no cubierto por un flujo perpendicular de fase contínua que contiene el surfactante. Las metodologías basadas en dispositivos de microfluidos son aquellas que emplean sistemas de microcanales en forma de terraza y membranas microporosas de emulsificación.

1.6.2.1. Microcanales en forma de terraza

La producción de microesferas se realiza mediante la generación de gotas uniformes a través del rompimiento inducido o espontáneo de la fase dispersa. Según Van Dijke et al., 2008 el proceso de formación de la gota se divide en dos etapas principales: la primera que consiste en la dilatación de la fase dispersa que sale del microcanal, y la segunda basada en el desprendimiento de la gota hasta que ésta cae dentro de la fase continua que contiene el surfactante y su consecuente solidificación manteniendo la forma esférica. Durante la dilatación de la fase dispersa, ésta se ve forzada a crear una forma de disco en la terraza, la cual al alcanzar el borde y debido a la tensión superficial [Sugiura et al. 2002a] cae transformándose espontáneamente en una esfera, considerada como la forma más estable desde el punto de vista termodinámico (Figura 18).

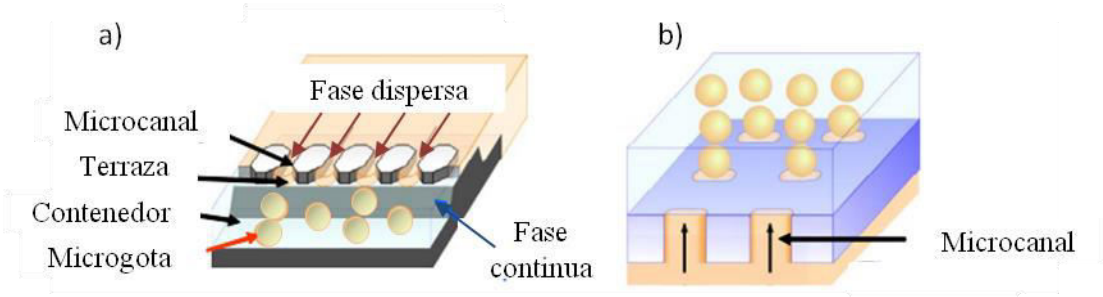

Figura 18. Ilustración esquemática de la generación de la microgota mediante los microcanales. A) Formación indirecta; B) Formación directa.

Mediante esta metodología se han obtenido microesferas, por ejemplo, de ácido poli(láctico-co-glicólico) (PLGA) en diclorometano (DCM) utilizando una fase continua de

polivinil alcohol (PVA), resultando en microesferas de un intervalo de diámetros entre 70-300 µm con un coeficiente de variación del 5 al 35% [Tran et al., 2011]. Chuah et al., 2010 emplearon esta técnica para producir microesferas monodispersas de gelatina y alginato. Por otro lado Ikkai et al., 2005 obtuvieron microesferas que tenían un tamaño de diámetro de unos pocos micrómetros hasta 100 µm con una desviación estándar de un 5%.

El tamaño de la microesfera es dependiente de la geometría de la placa. Para incrementar el tamaño de las microesferas se han de emplear microcanales con terrazas más largas y más profundas. Una de las ventajas de la metodología es que las condiciones operatorias se consideran relativamente sencillas, ya que no se requieren fuerzas adicionales para el rompimiento de la gota. Sin embargo, el hecho de que el tamaño de la gota dependa de las caracteristicas físicas de la terraza, constituye una limitación para la obtención de microesferas de diámetros mayores a 100 µm ya que la fabricación de microcanales de una profundidad mayor a los 16 µm y terrazas de longitud mayor a 240 µm por medio de sistemas de impresión no es factible [Sugiura et al. 2002b]. Por otro lado, el rendimiento de producción se ve condicionado por la velocidad de flujo de la fase dispersa, por lo que, una fase dispersa de baja viscosidad es un requisito indispensable.

1.6.2.2. Membranas microporosas de emulsificación

La metodología fue en principio propuesta por Nagashima and Shimizu [Kandori et al., 1995] y luego desarrollada por Omi, 1996 y Ma et al., 1999. Consiste en la generación de gotas monodispersas en la superficie de una membrana porosa aplicando presión para hacer pasar la fase dispersa a través de dicha membrana hacia una fase continua que contiene el surfactante [Tran et al., 2011] y permite la extracción del disolvente orgánico y la solidificación de las microesferas (Figura 19).

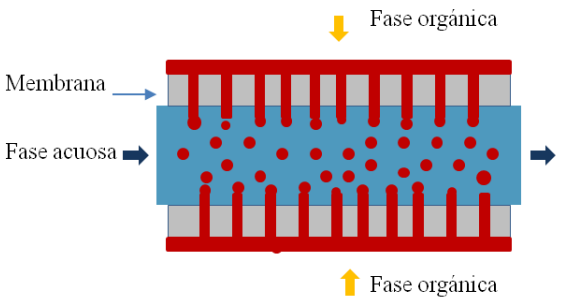

Figura 19. Representación gráfica de la producción de microesferas empleando una membrana microposora de emulsificación.

La membrana porosa utilizada con mayor frecuencia es la *'Shirazu Porous Glass'* (SPG), la cual está formada por poros de tamaño uniforme dispuestos en una placa de Al_2O_3-SiO_2 [Omi, 1996] y que al ser hidrofílica resulta muy adecuada para las emulsiones O/W (*oil/water*). Además, antes de comenzar el proceso de la producción de microesferas es posible modificar químicamente la superficie de la membrana de forma que se pueda trabajar con un tipo específico de emulsión.

El tamaño de diámetro del poro [Lambrich y Schubert, 2005] y la tensión interfacial entre la fase dispersa, la fase continua y la superficie de la membrana [Makino et al., 2004] son algunas de las variables que influyen mayormente en el diámetro final de las microesferas. En todos los casos, el uso de agentes emulsificantes es adecuado para evitar la coalescencia.

Mediante el uso de la membrana porosa, se pueden obtener microesferas poliméricas que van desde los 10 a los 100 µm [Shiga et al, 1996; Gasparini et al., 2007]. Por otro lado, mediante el empleo de un tratamiento de pre-mezclado de la disolución orgánica, se pueden llegar a obtener tamaños de 1-2 µm y distribuciones de tamaños más estrechas que con otras metodologías cuando dicha disolución se hace pasar varias veces a través de la membrana porosa [Doan et al., 2009].

La mayor ventaja que ofrece esta técnica es la obtención de microgotas de tamaño uniforme y una estrecha distribución de su tamaño de diámetro, además de que el consumo de energía es menor porque no se han de usar flujos de fase dispersa que impliquen el uso de sistemas de alta energía para producir la gota. Sin embargo, una de sus limitaciones más importante es que la velocidad de flujo de la fase dispersa a través de los poros es lenta, por lo que el rendimiento de producción no es alto.

1.6.3. Procesos de *jet break-up*

En este tipo de procesos, la disolución que contiene el polímero disuelto es inyectada a flujo constante a través de un capilar para formar un flujo laminar de fase dispersa en forma chorro, el cual es cortado mediante diferentes técnicas para producir gotas monodispersas. A continuación se describen algunas de las metodologías más empleadas que implican procesos de rompimiento del flujo de fase disersa.

1.6.3.1. *Jet-cutter*

La metodología se desarrolló con la finalidad de producir esferas uniformes de tamaños menores a 1 mm mediante la inyección de una disolución polimérica de alta viscosidad a través de un capilar para formar un flujo de fase dispersa, el cual es cortado en segmentos cilíndricos uniformes por medio de una herramienta de corte rotatoria o un conjunto de hilos [Prüsse et al., 1998a] (Figura 20).

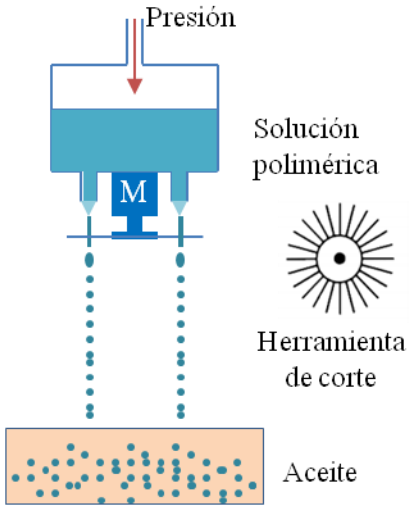

Figura 20. Esquema de la metodología Jet-Cutting (M= motor)

Las variables que ejercen mayor influencia en la formación y el tamaño de las gotas son: la tensión superficial, ya que transforma los segmentos cilíndricos en microgotas que al caer son solidificadas en un baño de fase continua [Prüsse et al., 1998a]; el número de hilos de corte; la frecuencia de rotación de la herramienta de corte y la velocidad de flujo de la fase dispersa a través del capilar [Prüsse et al., 2000].

De acuerdo a Prüsse et al., 2000, la técnica se ha empleado exitosamente en la producción de micropartículas biodegradables a partir de pectina, quitosano, alginato y gelatina.

La mayor ventaja de la técnica, es que es posible emplear disoluciones dispersas de alta viscosidad (> 500 mPas) con una alta velocidad de flujo (10-30 m s^{-1}) para obtener altos valores de rendimiento de microesferas monodispersas con una estrecha distribución de tamaños de diámetros. Sin embargo, la metodología posee algunas limitaciones, entre estas, que durante el proceso de corte se produce una pérdida de fase orgánica (menor al 5%), la cual es proporcional al tamaño de diámetro del hilo de corte [Prüsse et al., 1998b]. Por otro lado, la metodología es

óptima sólo para la producción de microesferas de tamaños de diámetros menores a 100 µm y la posibilidad de llevarlo a producción industrial es inviable [Garti y McClements, 2012].

1.6.3.2. Generación de la gota de forma electrostática

La técnica se basa en fuerzas electrostáticas que se emplean para perturbar una superficie líquida y así formar una fuente cargada de pequeñas gotas [Bugarski et al., 1994]. La metodología emplea un equipo sencillo y fácil de manejar y también ofrece la posibilidad de trabajar con capilares de diámetros milimétricos que disminuyen el riesgo de bloqueo durante la inyección de la fase dispersa.

La generación de la gota se puede llevar a cabo mediante dos modos operativos: el modo de chorro y el modo de goteo. En el primer modo, la disolución dispersa se inyecta a través del capilar a altas velocidades para crear un chorro uniforme y estable, por lo que para romperlo en pequeñas gotas se requiere aplicar una corriente eléctrica alta. Por otro lado, mediante el modo de goteo, la inyección de la fase dispersa igualmente se realiza a través del capilar, pero en este caso, de manera más lenta y suave sin la necesidad de crear un flujo de fase dispersa. Una corriente eléctrica pequeña (hasta unos 4 kV) es aplicada para crear las gotas debido a la fuerza electrostática [Moghadam et al., 2008].

El tamaño de diámetro de las microesferas resultantes y la distribución de tamaños dependen de distintas variables, entre las más importantes, el diámetro del capilar, la geometría y separación del electrodo [Bugarski et al., 1994], el voltaje aplicado, la velocidad de flujo de la solución polimérica, la tensión superficial, la densidad y la viscosidad [Poncelet et al., 1999].

Ding et al., 2005 y Lee et al., 2010 sugieren la posibilidad de obtener microesferas poliméricas monodispersas menores a 15 µm mediante el modo de chorro. Mientras que Bugarski et al., 1994 presentaron la producción de microesferas de tres intervalos de tamaños, las primeras, de unos 170 µm de diámetro, las segundas de 50 µm, preparadas ajustando las condiciones de trabajo y finalmente un tercer lote de microesferas de unos 400 ± 150 µm obtenidas mediante un sistema de inyección multicapilar.

La metodología es reproducible, controlable y en condiciones óptimas puede producir microesferas uniformes. Sin embargo, normalmente se requiere aplicar un alto campo eléctrico y el tamaño y distribución de tamaños de las microesferas es muy dependiente de la variación de los parámetros empleados.

1.6.3.3. Flow focusing

El proceso fue desarrollado por Gañán-Calvo et al., 1998 y se basa en inyectar una disolución orgánica a través de un capilar central para formar un flujo de fase dispersa en forma de chorro e inyectar alrededor de éste, una solución gaseosa o acuosa, la cual es inmiscible con la fase dispersa (Figura 21).

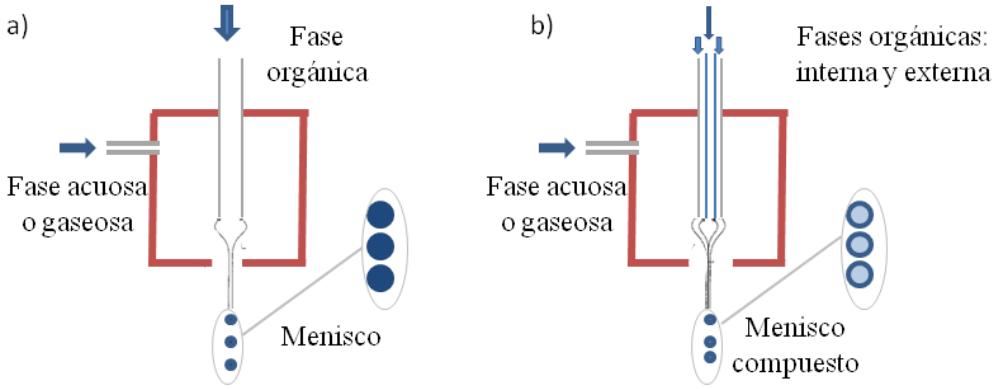

Figure 21. Esquema de la formación de la gota mediante *Flow-focusing* A) Simple; B) Compuesto (dos capilares concéntricos).

Dependiendo de la naturaleza de la disolución externa (acuosa o gaseosa), el proceso puede ser hidrodinámico o aerodinámico. Según Schneider et al., 2008, normalmente la fase externa actúa como fase continua y contiene algún surfactante como el polivinilalcohol y su velocidad de flujo es mayor que la de la fase dispersa, lo que lleva a la formación de un delgado chorro de fase dispersa y a su rompimiento en forma de gotas monodispersas de menor tamaño que el diámetro del agujero del capilar.

El diámetro, la distribución de tamaños y la morfología de las microesferas se ven influenciados por diferentes variables, tales como la concentración del polímero y la densidad de la disolución polimérica, la velocidad de flujo de las diferentes fases y el tamaño del capilar. Normalmente, las microesferas producidas son de un tamaño menor al del orificio del capilar empleado en su producción [Martín-Banderas et al., 2006].

La técnica se considera adecuada para producir micro y nanoesferas poliméricas de tamaños uniformes. Por otro lado, también se considera óptima para la encapsulación de compuestos lábiles, tales como proteínas, células, entre otros. Debido a su especial geometría, el flujo generador de partículas no está sometido a estrés por la tensión de rompimiento.

Entre las mayores ventajas de la técnica destacan su sencillez para ser empleada y el bajo coste para producir las microesferas [Schneider et al., 2008]. Las microesferas se pueden obtener en un solo paso sin la necesidad de usar una fuente de excitación externa y pasos adicionales de purificación. El proceso puede ser escalable, teniendo en cuenta que la técnica ofrecería altas tasas de producción al diseñar una configuración de capilares en paralelo para multiplicar la producción de partículas. Además de esto, la metodología puede ser empleada para producir microesferas multicapas o de diferentes morfologías, tales como, barras monodispersas y partículas en formas de discos [Xu et al., 2005], étc.

Sin embargo, la metodología permite la producción de nanopartículas o micropartículas monodispersas menores a 10 µm [Martín-Banderas et al., 2011] y se describe como inadecuada para la producción de tamaños mayores. Además de que el rendimiento es muy bajo cuando no se cuenta con un arreglo de múltiples capilares en paralelo [Xu et al., 2009].

1.6.3.4. Excitación del Jet

Las microesferas se forman a partir de la aplicación de una vibración de frecuencia constante a un fluido líquido laminar, el cual por el efecto de la vibración se divide en gotas monodispersas [Mazzitelli et al., 2008]. Este fenómeno fue originalmente estudiado por Lord Rayleigh a finales del siglo XIX [Rayleigh, 1878] y establece que una oscilación longitudinal impuesta a una corriente líquida causa una inestabilidad periódica en la superficie, la cual hace que el líquido se rompa formando una cadena de gotas uniformes.

Según Koch et al., 2003 y Seifert y Phillips, 1997 la longitud de onda de disrupción adecuada que se debe emplear para controlar el tamaño de las microgotas, se puede predecir a partir de la teoría de inestabilidad del fluido viscoso, en la cual Weber evaluó el efecto de la viscosidad en la producción de las microesferas. Para evitar la formación gotas satélites y por consecuencia, de aglomerados, la frecuencia de vibración se ha de mantener tan baja como sea posible cuando se emplean diámetros de capilares pequeños [Del Gaudio et al., 2009].

Al emplear la metodología de excitación del jet, se han de tener en cuenta varios parámetros que influyen en la morfología, tamaño y distribución de tamaños de las microesferas, algunos de ellos son: la frecuencia de vibración del capilar de inyección; la amplitud de vibración del capilar; la velocidad de bombeo de la fase orgánica [Zvonar et al., 2009]; la distancia entre el capilar y el baño de contiene la fase continua [Mazzitelli et al. 2008], entre

otros. Según Berkland et al., 2001 y Mazzitelli et al., 2008, cuando se incrementa la concentración del polímero y la velocidad de flujo, se incrementa el tamaño de la gota.

La técnica de excitación del jet se emplea para la producción de partículas de tamaños nano y micrométricos [Seifert y Phillips, 1997; Zvonar et al., 2009]. Es una de las metodologías más reconocidas en la producción de microesferas de alginato. Seifert y Phillips, 1997 produjeron exitosamente microesferas de este componente, que comprendían un intervalo de tamaños entre los 0.5 y 1 mm con una desviación estándar menor al 10%.

La técnica permite la obtención de una amplia variedad de productos micrométricos a partir de disolventes orgánicos y/o acuosos con una alta productividad y una estrecha distribución de tamaños [Zvonar et al., 2009]. Además de que el proceso es altamente reproducible, puede llevarse a cabo en condiciones suaves y puede ser escalado por medio del uso de dispositivos de múltiples capilares, sin embargo uno de los mayores inconvenientes es que el equipo es complejo.

1.6.3.5. Fabricación de partículas con precisión

En esta metodología, la fase dispersa que contiene el polímero y los compuestos a encapsular, es inyectada a través de un pequeño capilar de vidrio para formar un flujo uniforme de fase dispersa, mientras que un transductor ultrasónico controlado por un generador de frecuencias interrumpe la corriente de fase dispersa de manera que la rompe uniformemente para formar una cadena de gotas monodispersas. Al mismo tiempo, una corriente de disolución continua bombeada a mayor velocidad que la fase dispersa mediante una segunda bomba de inyección, la rodea protegiendo las micro o nanogotas de la coalescencia.

El rompimiento del flujo de fase dispersa se atribuye a la excitación causada por un generador de frecuencia, tal como la excitación acústica. Los flujos de fase dispersa en forma de chorro, tienden a romperse naturalmente en gotas no uniformes, por lo que la frecuencia aplicada por el transductor, genera inestabilidades periódicas uniformes que causan rompimientos monodispersos [Staymates et al., 2010].

Algunos de los parámetros que influyen en el tamaño de las partículas son: la concentración de polímero en la fase dispersa, la proporción entre la velocidad de flujo y la frecuencia de excitación acústica, la cual debe ser establecida para la obtención de partículas de un tamaño deseado [Berkland et al., 2001]. Según Staymates et al. 2010, al aumentar la frecuencia de excitación acústica el diámetro de la gota disminuye.

Mediante esta metodología, Berkland et al. 2001 produjeron microesferas uniformes que van desde 1 µm hasta unos 500 µm de diámetro. Choy et al., 2007 fabricaron microsferas hidrogel de quitosan y alginato en un intervalo de tamaños comprendido entre unos 50 y 200 µm a partir de un capilar con un diámetro de 250 µm.

Generalmente, la técnica produce micropartículas o microcápsulas uniformes con estrecha distribución de tamaños, además de ofrecer un control preciso sobre la morfología de la partícula. Esta metodología representa una optimización de las técnicas que emplean capilares ultrasónicos, ya que la intensidad de la onda acústica es más baja y es posible ajustar su frecuencia respecto a la velocidad de inyección de la disolución para controlar el tamaño de diámetro de las partículas [Berkland et al. 2001]. El proceso puede ser escalable hasta obtener cientos de gramos por minuto. Sin embargo, la mayor limitación de la metodología es la complejidad del equipo y la posible obturación del capilar durante el proceso de formación de las partículas.

1.6.4. Secado del disolvente mediante extracción

1.6.4.1. Fluidos supercríticos (SCF)

La técnica de los fluidos supercríticos es de gran interés para la producción de micro [Jung y Perrut, 2001] o nanopartículas [Reverchon et al., 2007] con características controladas. Permite modular y ajustar las propiedades fisicoquímicas de los componentes desde el estado gaseoso al estado líquido para emplearlos en un determinado proceso. Los fluidos supercríticos poseen varias aplicaciones en diferentes campos, tales como, los de la química, la petroquímica, el medio ambiente, la agroalimentaria, la perfumería, la farmacia, entre otros.

Uno de los compuestos que se emplea con mayor frecuencia como fluido supercrítico es el CO_2, lo cual supone una ventaja ya que éste se encuentra en estado gaseoso a temperatura ambiente, no es inflamable, ni tóxico, posee una temperatura crítica baja, se puede separar del producto final mediante la despresurización del sistema y es económico [Beckman et al., 2004].

La producción de partículas poliméricas usando fluidos supercriticos puede ser llevada a cabo usando el fluido supercritico como disolvente, como anti-solvente o como soluto, dependiendo de la naturaleza química y del peso molecular del compuesto a ser precipitado. En en el caso del poliestireno, al ser insoluble en CO_2, la metodología mas apropiada es la del anti-disolvente supercrítico (SAS).

Su mayor uso en lo que respecta a la tecnología de polímeros se ha venido desarrollando a partir de los años 80 [Rey y Cansell, 1998], ya que se pueden emplear como medio de reacción para las polimerizaciones, en la impregnación y recristalización de polímeros, etc.

- **Técnica del anti-disolvente supercrítico.**

La micronización de partículas mediante esta técnica se basa en la baja solubilidad que posee el compuesto a ser precipitado en el fluido supercrítico, el cual en este caso se comporta como anti-disolvente. Se requiere el uso de un disolvente orgánico para disolver previamente el polímero y los compuestos a encapsular [Boutin et al. 2004] creando una disolución orgánica, la cual se inyecta en la autoclave a través de un capilar, que contiene el fluido supercrítico y una cantidad de disolvente orgánico en condiciones de presión y temperaturas supercríticas.

El disolvente orgánico contenido en la disolución orgánica se difunde en la fase de fluido supercrítico, mientras que el fluido supercritico se difunde simultáneamente dentro de la disolución líquida para dar lugar a su sobresaturación y por ende, a la coprecipitación del polímero y los demás solutos a ser encapsulados, mediante un proceso semi-continuo [Lesoin et al., 2011] en el que las partículas poliméricas micronizadas se acumulan dentro de un filtro colocado en el fondo de la autoclave. La configuración de equipo se esquematiza en la Figura 22.

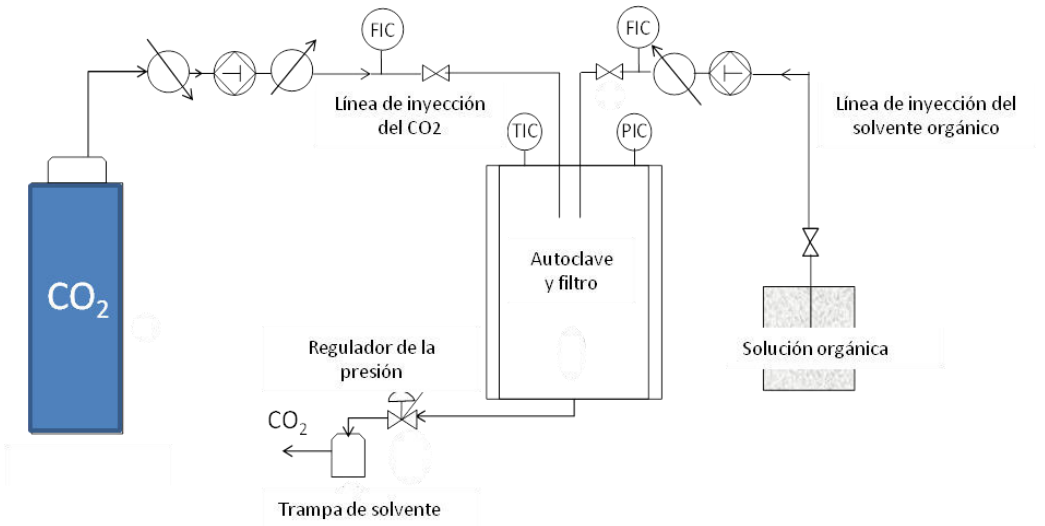

Figura 22. Esquema del equipo empleado en la técnica de micronización mediante el anti-disolvente supercrítico

Se han desarrollado diferentes variaciones de la técnica SAS, entre las cuales se pueden mencionar: *impinging jet* (IJ-SAS) [Careno et al., 2012], *Supercritical Enhanced Dispersion Solution* (SEDS), *Gas Anti-Solvent* (GAS), *Aerosol Solvent Extraction System* (ASES) [Yeo y

Kiran, 2005]. Cada una de las diferentes configuraciones se diferencia entre sí principalmente por el modo de inyección de la fase dispersa. La metodología de micronización mediante anti-disolvente supercrítico es una de la más adecuadas cuando se desean obtener partículas a partir de polímeros como el poliestireno, el cual no es soluble en CO_2.

Los principales fenómenos físico-químicos que influyen en la precipitación de las partículas su tamaño, morfología y polimorfismo mediante la técnica del anti-disolvente supercrítico son el comportamiento hidrodinámico de las fases, las condiciones de la mezcla, la cinética de la transferencia de masa, la cinética de nucleación y crecimiento de partícula. Mientras que los parámetros operatorios y/o de formulación que ejercen más influencia en la forma y tamaño de las partículas micronizadas son la concentración de polímero en la disolución orgánica, la fracción molar entre el disolvente orgánico respecto al fluido supercrítico, el diámetro de capilar y la velocidad de inyección de la solución orgánica.

La técnica permite la obtención de micro [Jung y Perrut, 2001] y nanopartículas [Reverchon et al., 2007] de características controladas [Reverchon et al., 2003]. Se ha empleado para la micronización [Fages et al., 2004] y para la obtención de micro o nanocompuestos a partir de polímeros, bio-polímeros, moléculas farmacéuticas, materiales orgánicos e inorgánicos (p.ej. colorantes, catalizadores, precursores de superconductores, etc.), explosivos, entre otros. En los pocos trabajos descritos donde se microniza el poliestireno, se emplea como disolvente orgánico el diclorometano [Jeong et al., 2008] o el tolueno [Dixon y Johnston, 1993]. Este disolvente tiene alta capacidad para disolver los polímeros, sin embargo también es conocido por su alta toxicidad.

Otra de las ventajas de trabajar con el CO_2 es que debido a la naturaleza del proceso y a que las partículas obtenidas se lavan con el disolvente supercrítico, las cantidades residuales de disolvente orgánico son mínimas. Sin embargo, el equipo no es sencillo, requiere mucha atención del operador porque se suele trabajar con presiones altas, y la producción de grandes cantidades de microesferas requiere instalaciones industriales.

1.6.4.2. Técnica de secado por aspersión *(Spray-Drying)*.

Al igual que en la técnica anterior, en el Spray Drying, la disolución orgánica que contiene el polímero y los compuestos a encapsular se inyecta en la autoclave a través de un capilar, el cual se encuentra acondicionado con una membrana que permite la producción de gotas individuales mediante la nebulización de la disolución a la vez que el disolvente se evapora por

efecto de un gas (tal como el N_2) acondicionado a elevadas temperaturas que fluye en sentido contrario a la caída de las gotas [Paudel et al. 2013]. La alta proporción entre volumen y superficie de la microgota favorece un secado rápido y eficiente de las gotas y como consecuencia, la formación de microesferas. El disolvente empleado puede ser acuoso u orgánico en función del tipo de compuesto que se desee coprecipitar.

Según Paudel et al. 2013, el proceso de Spray Drying consiste básicamente en cuatro etapas: la nebulización de la disolución que contiene el material a ser micronizado para que se formen microgotas; la mezcla de las microgotas con el gas de secado; la evaporación del disolvente contenido en las microgotas y finalmente la separación de las partículas secas. La Figura 23 esquematiza el proceso de extracción del disolvente orgánico contenido en la microgota.

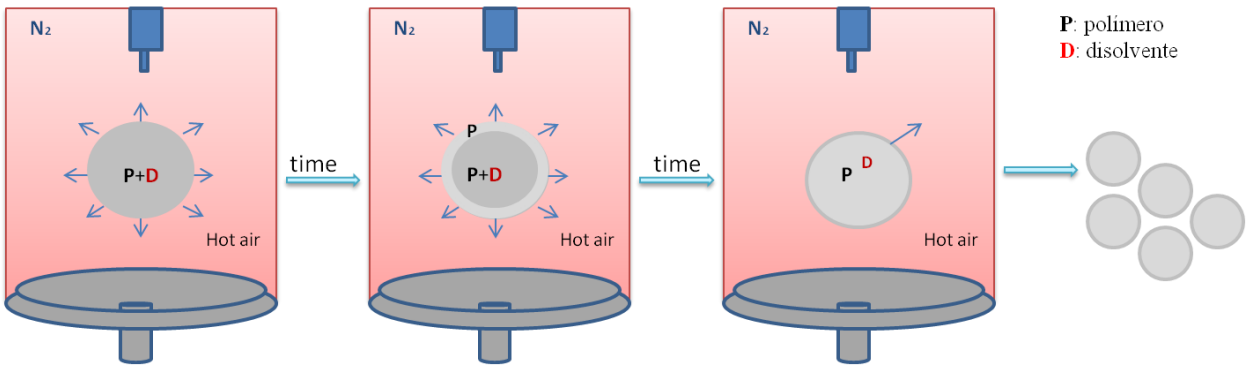

Figura 23. Secado de la micropartícula dentro del autoclave del Mobile Minor

La formación de las micro o nanopartículas de distintas formas y tamaños, la dispersión de tamaños y el rendimiento de producción dependen de varios parámetros tales como la temperatura de entrada de la disolución, la velocidad con la que se inyecta la fase dispersa [Conte et al., 1994], la velocidad de flujo del gas de nebulización [Maa et al., 1997], la velocidad rotatoria del disco en el atomizador, la composición de la disolución que se desea micronizar, los sólidos que están contenidos en la disolución, el tipo de disolvente, la viscosidad y finalmente la tensión superficial de la solución de secado [Paudel et al., 2013]. Sin embargo, el parámetro clave es el tamaño del autoclave, el cual puede variar en varios órdenes de magnitud y limitar el nivel de producción y el tamaño de las partículas.

La técnica de *Spray Drying* es ampliamente utilizada para la producción a gran escala de polvos secos, gránulos, aglomerados y macropartículas [Patel et al., 2008] generalmente a partir de disoluciones, emulsiones o suspensiones de polímeros hidrofóbicos o hidrofílicos,

biodegradables [Bodmeier y Chen, 1998] o no y que incluyen compuestos a encapsular solubles o insolubles en agua [Mu y Feng, 2001], debido a que proporciona un mejor secado del disolvente orgánico en comparación con otras técnicas.

Algunas de las principales fortalezas de la técnica según Giunchedi et al. 2001, se basan en que permite un óptimo control de los parámetros operatorios y en que consiste en un proceso de un paso y es fácilmente escalable. Además, Paudel et al., 2013 sugieren que la evaporación del disolvente es muy rápida, lo que hace la técnica muy interesante para la preparación de dispersiones sólidas amorfas. Sin embargo, parámetros como la temperatura a la que se debe acondicionar la autoclave para llevar a cabo el proceso podría no ser conveniente para determinados polímeros y, especialmente, cuando se deseen encapsular compuestos que puedan verse afectados. Además, según Johansen et al., 2000 el control de tamaño de partícula es difícil y los rendimientos para lotes pequeños es moderado.

Existen diferentes configuraciones de equipos de Spray Drying en el mercado. El equipo adecuado para un proceso se selecciona de acuerdo a los requerimientos de dicho proceso, los materiales de partida que se emplean, las características del producto final deseado y la relación entre el coste y el rendimiento de producción. Los equipos varían en su configuración de acuerdo a la casa que los comercializa. Los procesos más relevantes en los que se emplean los equipos de Spray Drying son mencionados a continuación: obtención de productos químicos, productos de alimentación, cosmética, farmacéuticos y plantas piloto a pequeña escala empleadas para la investigación.

1.6.4.3. Metodología de extracción/evaporación del disolvente orgánico

La obtención de microesferas por medio de la metodología extracción/evaporación del disolvente orgánico se basa en cuatro pasos claves, de acuerdo a O'Donell et al., 1997 (Figura 24). El primero consiste en preparar la fase dispersa que contiene el polímero y los compuestos a encapsular, disueltos homogéneamente en un disolvente adecuado (inmiscible en agua), el cual generalmente suele ser orgánico. El segundo consiste en crear una emulsión, mediante la adición de la fase dispersa a la fase continua inmiscible, la cual contiene el surfactante y se encuentra en constante agitación para formar las microgotas discretas. Una vez las microgotas están formadas, el disolvente orgánico que está contenido en su matriz es extraído, se difunde en la fase continua y se evapora en la interface agua/aire, lo cual permite el endurecimiento de las microesferas.

Finalmente, después de varias horas de agitación, las microesferas endurecidas se filtran y se secan.

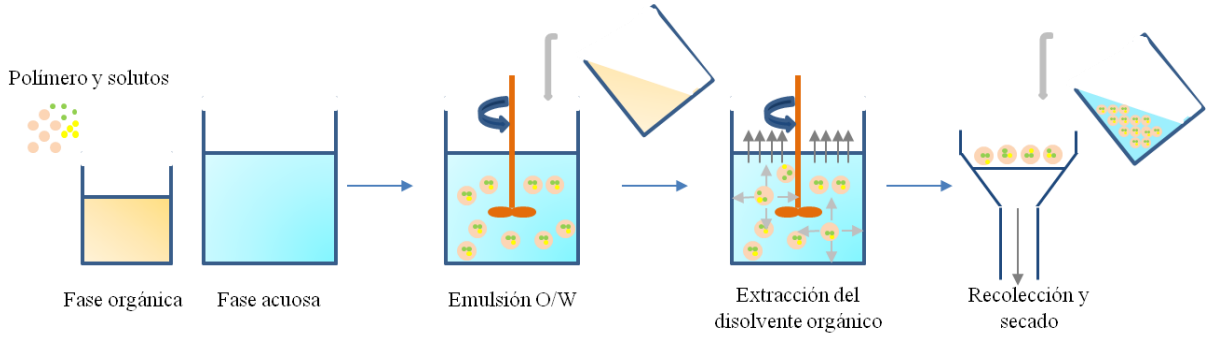

Figura 24. Esquema de la formación de microesferas mediante la extracción/evaporación del disolvente orgánico.

La metodología de evaporación del disolvente orgánico es una técnica muy popular para la encapsulación de diferentes tipos de compuestos. Existen variaciones de la técnica, la más adecuada se selecciona teniendo en cuenta si el compuesto a encapsular es hidrófilo o no [Li et al., 2008]. En general, el método más simple empleado para la producción de microesferas con compuestos a encapsular insolubles o muy poco solubles en agua es el de *'oil-in-water'* (O/W).

Las características de las microesferas resultantes dependen de la formulación empleada, es decir de la cantidad y la naturaleza de los materiales de partida y de los parámetros operatorios empleados durante su producción. Por lo tanto las variables que ejercen mayor influencia en el tamaño final, la distribución de tamaños y la morfología de las microesferas son: el tipo de polímero matriz, los compuestos a ser encapsulados, el tipo de disolvente orgánico usado para formar la fase dispersa, la cantidad y tipo de surfactante empleado en la fase continua, la proporción entre fase dispersa y continua, la velocidad de agitación y la temperatura a la que se forma la dispersión.

La técnica de evaporación/extracción del disolvente se ha empleado para la encapsulación de compuestos poco solubles en agua en matrices poliméricas, tales como el ácido poli(láctico-co-glicólico); el ácido poli-láctico (PLA); el polietilenglicol. Por otro lado, los compuestos altamente hidrofílicos, que no se disuelven en el disolvente orgánico y además podrían difundirse en la fase continua durante la emulsión dando lugar a pérdidas [Li et al., 2008], son encapsulados mediante la producción de microesferas con metodologías alternativas derivadas de la 'O/W', tales como: la emulsión doble o múltiple (W/O/W), el método del co-disolvente (O/W), el método de dispersión (O/W) y el método evaporación/extracción no acuosa.

Dalpiaz et al., 2001 prepararon microesferas a partir de la formación de una emulsión entre la fase dispersa que contenía ácido poli-lactico disuelto en diclorometano y una fase acuosa compuesta por agua desionizada, para evaluar la encapsulación y posterior liberación controlada de la N^6-ciclopentiladenosina. Las microesferas resultantes tenían de un tamaño de diámetro de unos 21 ± 9 μm, presentaron una superficie lisa y uniforme y un porcentaje de encapsulación de alrededor de 1.1%. Por otro lado, Mao et al., 2008 prepararon microesferas de PLGA usando diclorometano como disolvente orgánico y una fase continua formada por agua desionizada y polivinilalcohol. Se encapsuló un compuesto hidrofóbico (ABT627) en la matriz polimérica y se variaron diferentes parámetros operatorios para estudiar su influencia en la producción de las microesferas y en el rendimiento de encapsulación. Según sus estudios, los parámetros más determinantes resultaron ser la proporción entre la fase continua y la fase dispersa, la concentración del polímero y la concentración del surfactante.

Según Freitas et al., 2005 la metodología de evaporación/extracción del disolvente orgánico se considera como una de las más apropiadas para la obtención de microesferas debido a que resulta económica, simple, no requiere el empleo de equipos sofisticados, de elevadas temperaturas y tampoco de agentes inductores de separación de fases, y además porque permite controlar la morfología y el tamaño de diámetro de las microesferas. Otro de los aspectos positivos de la metodología mencionado por Li et al., 1995 es que no implica reacciones químicas complejas. Sin embargo, no es posible obtener un estricto control sobre la uniformidad de la distribución de tamaños de las microesferas y además, la metodología es altamente dependiente de la naturaleza del disolvente orgánico que se emplea para crear la fase dispersa.

Valorando los aspectos positivos de la metodología, y en vista de que no requiere de equipos ni instalaciones complejas, se ha seleccionado como la metodología de preferencia para ser empleada de forma mayoritaria en el presente trabajo.

1.7. METODOLOGÍA DE EVAPORACIÓN/EXTRACCIÓN DEL DISOLVENTE ORGÁNICO

1.7.1. Generalidades

La sencillez, eficiencia, rapidez, el coste económico y la posibilidad de utilizar la metodología a escala de laboratorio usando un vaso de precipitado y sin la necesidad de emplear equipos complejos, hacen de la evaporación/extracción una técnica muy adecuada para el ensayo de la producción de microesferas poliméricas de diferentes diámetros y composiciones.

La metodología sirve como apoyo a muchas de las descritas anteriormente, en las cuales la técnica principal aporta la forma en que las gotas se crean y por lo tanto su monodispersidad y distribución de tamaño. En algunas de estas metodologías la fase dispersa es preparada e inyectada a través de un capilar o un microcanal, formando las gotas uniformes bien sea por disrupciones mecánicas (p.ej. rompimiento del flujo de fase dispersa), eléctricas (p.ej. generación de la gota de forma electrostática), aplicando vibraciones de una frecuencia similar (p.ej. excitación del flujo de fase dispersa), ultrasonidos (p.ej. producción de partículas con precisión), por la tensión superficial (p.ej. sistemas de canales en forma de microterraza) o por presión (p.ej. membranas de microemulsión). Sin embargo, al final las gotas formadas caen en un recipiente que contiene la fase continua con el surfactante y es donde ocurre la extracción y la evaporación del disolvente orgánico y el subsecuente endurecimiento de las microesferas.

Lo que simplifica la metodología de extracción/evaporación del disolvente orgánico es que la formación de la gota de fase dispersa se produce debido a la agitación aplicada al momento de formar la emulsión sin la necesidad se añadir componentes adicionales al equipo. Además de las variables ya mencionadas que influyen en el proceso de formación de la microesfera, otros factores como la viscosidad de las fases continua y dispersa, la tensión interfacial entre las dos fases, el tamaño del recipiente que contiene la emulsión y el tamaño de los agitadores son factores que también han de tenerse en cuenta.

Una vez las microgotas están formadas, el siguiente paso es la extracción del disolvente orgánico y su subsecuente evaporación, la cual se facilita cuando el disolvente orgánico es ligeramente soluble en la fase continua, permitiendo de esta manera la precipitación de la matriz polimérica.

La velocidad de extracción del disolvente orgánico depende de una serie de factores, tales como su naturaleza (solubilidad y temperatura de ebullición), el tipo de matriz polimérica empleada, el tipo de compuesto encapsulado, entre otros. La evaporación del disolvente orgánico para la formación de la microsfera ocurre ya que la fase continua tiene suficiente capacidad de disolver lentamente el disolvente de la fase dispersa, éste es extraído de la microgota y al alcanzar la superficie de la emulsión y entrar en contacto con el aire, se evapora. La temperatura por tanto es otro de los parámetros más influyentes en la velocidad de extracción del disolvente orgánico de las microesferas en el proceso de solidificación ya que a temperaturas más altas la evaporación del disolvente orgánico presente en la fase continua es más rápida.

1.7.2. El disolvente orgánico

El tipo de disolvente orgánico empleado representa un factor determinante en la formación de las microesferas, en que el proceso se lleve a cabo con éxito, en su rendimiento y en la morfología y características de las partículas finales. Según Li et al., 2008 para obtener resultados óptimos en la producción de microesferas mediante la metodología, el disolvente debe poseer ciertas condiciones, tales como:

- Capacidad para disolver el polímero seleccionado como matriz.
- Escasa solubilidad en la fase continua.
- Bajo punto de ebullición y alta volatilidad.
- Baja toxicidad.

Anteriormente el cloroformo era el disolvente orgánico mayormente utilizado, sin embargo debido a su alta toxicidad y baja presión de vapor ha sido reemplazado por el diclorometano. Según Sah, 2000 el diclorometano se convirtió en el disolvente orgánico más frecuentemente utilizado para formar la fase dispersa debido a que posee:

- Muy baja solubilidad en agua (13 g L^{-1} a 20 ºC), cumpliendo así con el criterio de que una emulsión debería estar compuesta de dos líquidos inmiscibles.
- Bajo punto de ebullición (39.8 ºC) y alta presión de vapor, por lo que las moléculas de disolvente extraídas de la microgotas a la fase acuosa se evaporan fácilmente permitiendo el endurecimiento de las microesferas.
- Alta volatilidad, por lo tanto facilita la eliminación del disolvente residual en las microesferas durante el secado.

Sin embargo, el diclorometano está catalogado como un compuesto carcinógeno [Li et al., 2008] y es una de las 38 substancias que se encuentra en la lista de substancias peligrosas [Sah, 2000]. Por lo que se trabaja en la búsqueda de solventes orgánicos menos tóxicos.

El acetato de etilo, por otro lado, es un disolvente orgánico de menor toxicidad y parece ser de utilidad en la producción de las microesferas. Sin embargo, debido a que es parcialmente miscible con el agua (4.5 veces más que el diclorometano) las microesferas no se pueden formar si la fase dispersa es introducida directamente en la fase continua. De acuerdo a Freytag et al., 2000 la repentina extracción de gran cantidad de acetato de etilo desde la fase dispersa ocasiona

la precipitación del polímero en aglomerados en forma de fibras. Para resolver este problema creado por la miscibilidad del solvente con el agua, se plantea el uso de tres métodos:
(1) Pre-saturar la solución acuosa con solvente [Bahl y Sah, 2000].
(2) Emulsificar primero la fase dispersa en una pequeña cantidad de solución acuosa y una vez que las gotas se han formado, la emulsión se transvasa en una cantidad mayor de agua [Freytag et al., 2000].
(3) Emulsificar la fase dispersa en una pequeña cantidad de solución acuosa y posteriormente agitarla hasta que el solvente orgánico se evapore permitiendo de esta manera la solidificación de las microesferas [Sah et al., 1997].

Si bien, mediante estas tres metodologías propuestas es posible producir microesferas usando el acetato de etilo, según Herrmann y Bodmeier, 1998 las partículas obtenidas usando el diclorometano son esféricas y mas uniformes mientras que las obtenidas usando el acetato de etilo tienden a ser amorfas, además de que la eficiencia de encapsulación y el rendimiento de producción es significativamente menor.

Otro disolvente orgánico que resulta de interés para la producción de microesferas mediante la metodología de extracción/evaporación es el formiato de etilo. Sah et al., 2000 sintetizaron microesferas de PLGA usando este disolvente. Se observó que la velocidad de evaporación del formiato de etilo en agua era 2.1 veces más rápida que la del diclorometano, a pesar de que el formiato de etilo posee una menor presión de vapor y un punto de ebullición más alto. El fenómeno se explica por el hecho de que más moléculas de formiato de etilo son expuestas a la interface liquido-aire gracias a su alta solubilidad en agua.

Diferentes disolventes orgánicos menos tóxicos han sido evaluados, sin embargo, no hay resultados suficientes para comparar la calidad de las microesferas preparadas. El diclorometano, es hasta la presente, el disolvente orgánico más utilizado por su rápida evaporación, su alta eficiencia de encapsulamiento y porque produce las microesferas mas uniformes y más esféricas.

1.7.3. El surfactante

El surfactante se emplea para estabilizar la emulsión y para evitar la coalescencia y aglomeración de las gotas de la fase dispersa recién formadas, ya que cubre la superficie de las gotas con su parte hidrofóbica dejando expuesta al agua la parte hidrofílica, además de que reduce la tensión superficial de la fase continua.

Un surfactante adecuado contribuye a mejorar la morfología de la microesferas, a que se formen de un tamaño regular y a que la distribución de tamaños sea más estrecha. Hay diferentes

tipos de surfactantes y se clasifican de acuerdo a la naturaleza de la parte hidrofilica de la molécula: aniónicos, catiónicos, anfotéricos y non-ionicos (Figura 25).

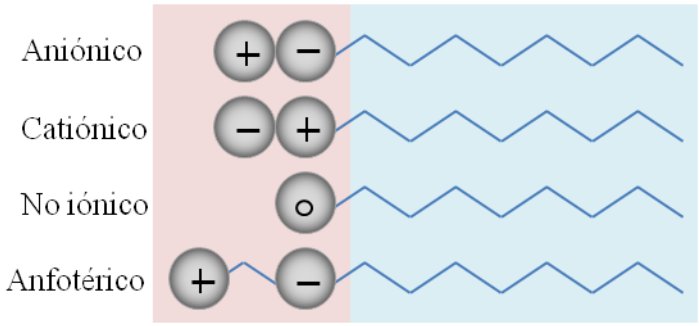

Figura 25. Diferentes tipos de surfactantes.

Según Li et al., 2008 los surfactantes más típicos empleados en la formación de la emulsión de diclorometano/H_2O, son el polivinilalcohol, la metilcelulosa, el tween, el span (no-iónicos); el dodecilsulfato de sodio (aniónico); el bromuro de hexadeciltrimetilamonio (catiónico).

El incremento de la concentración de surfactante en la formulación de la fase continua tiende a reducir el tamaño de las microesferas [Jeffery et al. 1993; Carrio et al., 1995] debido a que disminuye la tensión superficial permitiendo así la formación de microgotas más pequeñas. De acuerdo a Li et al., 2008 cuando la tensión superficial ha disminuido al máximo, la cantidad extra de surfactante no causa ningún efecto en el tamaño de las gotas, sino que tiende a quedarse en forma de micelas.

1.7.4. Recolección y secado de las microesferas poliméricas

Una vez que las microesferas se han solidificado debido a la extracción del solvente orgánico, se recolectan de forma sencilla mediante filtración o centrifugación en el caso de que sean muy pequeñas o de que se hayan empleado altas concentraciones de surfactante y la viscosidad de la fase acuosa haya aumentado.

Las microesferas obtenidas pueden contener residuos de disolvente orgánico, surfactante o compuesto no encapsulado en su superficie, por lo que se deben lavar con agua y algún compuesto que funcione como extractante. El lavado puede contribuir en la eliminación del disolvente orgánico residual que pudo haber quedado retenido dentro de las microesferas como una impureza volátil. Finalmente, las microesferas se secan a temperatura ambiente o en una

estufa a una temperatura adecuada, o por medio de la liofilización. Alguna perdida de tamaño debida al secado no se descarta, sin embargo se considera muy baja [Berkland et al., 2001].

1.8. Referencias

Amsden, B. The production of uniformly sized polymer microspheres. Pharmaceutical Research 16 (1999) 1140-1143.

Bahl, Y., Sah, H. Dynamic changes in the size distribution of emulsion droplets during ethyl acetate-based microencapsulation process. AAPS Pharmaceutical Science Technology 1 (1) (2000) 41-49.

Bagán, H., Hartvig, S., Tarancón, A., Rauret, G., García, J.F. Plastic vs. liquid scintillation for ^{14}C radiotracers determination in high salt matrices. Analytica Chimica Acta 631 (2009) 229-236.

Bagán, H., Tarancón, A., Rauret, G., García, J.F. Alpha/beta pulse shape discrimination in plastic scintillation using commercial scintillation detectors. Analytica Chimica Acta 670 (2010) 11–17.

Bagán, H., Tarancón, A., Rauret, G., García, J.F. Radiostrontium separation and measurement in a single step using plastic scintillators plus selective extractants. Application to aqueous sample analysis. Analytica Chimica Acta 686 (2011) 50-56.

Bagán, H., Tarancón, A., Stavsetra, L., Rauret, G., García, J.F. Determination of oil reservoir radiotracer ($S^{14}CN^{-}$) in a single step using a plastic scintillator extractive resin. Analytica Chimica Acta 736 (2012) 30-35.

Barrett, K.E.J. Dispersion Polymerization in Organic Media. British Polymer Journal 5 (1973) 259-271.

Beckman, E. Supercritical and near-critical CO_2 in green chemical synthesis and processing. Journal of Supercritical Fluids 28 (2004) 121–191

Beddart, A.S., Mackie, T.R., Attix, F.H. Water-equivalent plastic scintillation detectors for high energy beam dosimetry: I. Physical characteristics and theoretical considerations. Physics in Medicine and Biology, 37 (10) (1992) 1883-1900.

Berkland, C., Kim, K., Pack, W. Fabrication of PLG microspheres with precisely controlled and monodisperse size distributions. Journal of Controlled Release 73 (2001) 59–74.

Bertrand, G., Hamel, M., Sguerra, F. Current status on plastic scintillators modifications. Chemistry European Journal 20 (2014) 15660-15685.

Birks J.B. The theory and practice of liquid scintillation counting. Pergamon Press, Oxford. 1964 Bodmeier, R. and Chen, H.G. Preparation of biodegradable poly(+/-) lactide microparticles using a spray drying technique. Journal of Pharmacy and Pharmacology 40 (1988) 754.

Bizarri, G. Scintillation mechanisms of inorganic materials: from crystal characteristics to scintillation properties. Journal of Crystal Growth 312 (2010) 1213-1215.

Bosworth, N., Towers, P. Scintillation proximity assay. Nature 341 (1989) 167-168.

Boutin, O., Badens, E., Carretier, E., Charbit, G. Co-precipitation of a herbicide and biodegradable materials by the supercritical anti-solvent technique. Journal of Supercritical Fluids 31 (2004) 89-99.

Bugarski, B., Li, Q., Goosen, M.F.A., Poncelet, D., Neufeld, R., Vunjak, G. Electrostatic droplet generation: mechanism of polymer droplet formation. Materials, Interfaces and Electrochemical Phenomena 40 (1994) 1026–1031.

Brooks, F.D. A scintillator counter with neutron and gamma-ray discriminators. Nuclear Instruments and Methods 4 (1959) 151-163.

Brooks, F.D. Development of organic scintillators. Nuclear Instruments and Methods 162 (1979) 477.

Careno, S., Boutin, O., Badens, E. Drug recrystallization using Supercritical Anti-Solvent (SAS) process with impinging jets: effect of process parameters. Journal of Crystal Growth, 342 (2012), 34-41.

Carrio, A., Schwach, G., Coudane, J., Vert, M. Preparation and degradation of surfactant-free PLAGA microspheres, Journal of Control Release 37 (1995) 113 – 121.

Choy, Y.B., Choi, H., Kim, K. Uniform Biodegradable Hydrogel Microspheres Fabricated by a Surfactant-Free Electric-Field-Assisted Method. Macromolecular Bioscience 7 (2007) 423-428.

Chuah, A.M., Kuroiwa, T., Kobayashi, I., Zhang, X. Nakajima, M. Preparation of uniformly sized alginate microsphers using the novel combined methods of microchannel emulsification and external gelatin. Colloids Surfaces A 351 (2010) 9-17.

Conte, U., Conti, B., Guinchedi, P., Maggi, L. Spray dried polylactide microsphere preparation: influence of the technological parameters. Drug Development and Industrial Pharmacy 20 (1994) 235-258.

Dalpiaz, A., Scatturin A., Pavan, B., Biondi, C., Vandelli, M.A., Forni, F. Poly(lactic acid) microspheres for the sustained release of a selective A_1 receptor agonist. Journal of Controlled Release 73 (2001) 303–313

Del Gaudio, P., Russo, P., Lauro, M.R., Colombo, P., Aquino, R.P. Encapsulation of Ketoprofen and Ketoprofen Lysinate by Prilling for Controlled Drug Release AAPS Pharmaceutical Science Technology 10 (2009) 1178-1185

DeVol, T.A., Egorov, O.B., Roane, J.E., Paulenova, A., Grate, J.W. Extractive Scintillating Resin for ^{99}Tc Quantification in Aqueous Solutions. Journal of Radioanalytical and Nuclear Chemistry 249 (2001a) 181-189.

DeVol, T.A., Duiffey, J.M., Paulenova, A. Combined extraction chromatography and scintillation detection for off-line and on-line monitoring of strontium in aqueous samples. Journal of Radioanalytical and Nuclear Chemistry 249 (2001b) 295-301.

Ding, L., Lee, T., Wang, C.H. Fabrication of monodispersed taxol-loaded particles using electrohydrodynamic atomization. Journal of Controlled Release 102 (2005) 395–413.

Dixon, D., Johnston, P. Polymeric materials formed by precipitation with a compressed fluid antisolvent. Materials, Interfaces and Electrochemical Phenomena 39 (1993) 127-139.

Doan, T.V.P., Olivier, J.C. Preparation of rifampicin-loaded PLGA microspheres for lung delivery as aerosol by premix membrane homogenization. International Journal of Pharmaceutics 382 (2009) 61–66.

Einsenbud, M. Environmental Radioactivity, Academic Press, New York, United States (1987)

El-Faramawy, N.A., Göksu, H.Y., Panzer, W. Thermoluminescence dosimetric properties of a new thin beta detector (LiF:Mg, Cu, P; GR-200F) in comparison with highly sensitive Al_2O_3:C beta dosimeters. Journal of Radiological Protection 3 (2004) 273-82.

Fages, J., Lochard, H., Letourneau, J., Sauceau, M., Rodier, E. Particle generation for pharmaceutical applications using supercritical fluid technology. Powder Technology 141 (2004) 219 – 226.

Fox, B.W. Techniques of sample preparation for liquid scintillation counting, in: Work T.S. and Work E., Laboratory Techniques in Biochemistry and Molecular Biology. North Holland Publ. Co., Amsterdam, 5 (1976).

Freitas, S., Merkle, H.P., Gander, B. Microencapsulation by solvent extraction/evaporation: reviewing the state of the art of microsphere preparation process technology. Journal of Controlled Release 102 (2005) 313 – 332.

Freytag, T., Dashevsky, A., Tillman, L., Hardee, G.E., Bodmeier, R. Improvement of the encapsulation efficiency of oligonucleotide-containing biodegradable microspheres. Journal of Controlled Release 69 (2000) 197-207.

Ganán-Calvo, A.M. Generation of steady liquid microthreads and micron-sized monodisperse sprays in gas streams. Physical Review Letters 80 (1998) 285–288.

Garti, N., McClements, J. Encapsulation technologies and delivery systems for food ingredients and nutraceuticals. Woodhead Publishing, Cambrigde, United Kingdom (2012) pp. 561.

Gasparini, G., Kosvintsev, S.R., Stillwell, M.T., Holdich, R.G. Preparation and characterization of PLGA particles for subcutaneous controlled drug release by membrane emulsification. Colloids and Surfaces B: Biointerfaces B 61 (2007) 199–207.

Gibson, J.A.B., Lally, A.E. Liquid scintillation counting as an analytical tool. The Analyst 96 (1971) 1147.

Giunchedi, P., Conti, B., Genta, Ida., Conte, U., Plugisi, G. Emulsion Spray-Drying for the preparation of albumin loaded PLGA microspheres. Drug Development and Industrial Pharmacy 27 (2001) 745-750.

Güsten, H., Mirsky, J. Chapter I. PMP, a novel scintillation solute whith a large stoke shift, in: Ross, H., Noakes, J.E., Spaulding, J.D, Liquid scintillation counting and organic scintillators, Lewis Publishers, Michigan (1991) pp. 1-7.

Headrick, J., Sepaniak, M., Alexandratos, S., Datskos, P. Chelating scintillation fibers for measurements of ^{137}Cs. Analytical Chemistry 72 (9) (2000) 1994-2000.

Herrmann, J., Bodmeier, R. Biodegradable somatostatin acetate containing microspheres prepared by various aqueous and non-aqueous solvent evaporation methods. European Journal of Pharmaceutics and Biopharmaceutics 45 (1) (1998) 75-82.

Hofstetter, K.J. Continuous aqueous tritium monitoring. Fusion Technology 28, (1995) 1527–1531

Hong, J., Hong, C.K., Shim, S.E. Synthesis of polystyrene microspheres by dispersion polymerization using poly(vinyl alcohol) as a steric stabilizer in aqueous alcohol media. Colloids and Surfaces A: Physicochemical Engineering Aspects 302 (2007) 225–233

Horrocks, D.L. Applications of Liquid Scintillation Counting, Academic Press, New York-San Francisco- London, (1974) pp. 12-257.

Ikkai, F., Iwamoto, S., Adachi, E., Nakajima, M. New method of producing mono-sized polymer gel particles using microchannel emulsification and UV irradiation. Colloid and Polymer Science 283 (2005) 1149–1153

Jeffery, H., Davis, S.S., O'Hagan, D.T. The preparation and characterization of poly(lactide-co-glycolide) microparticles: II. The entrapment of a model protein using a (water-in-oil)-in water emulsion solvent evaporation technique. Pharmaceutical Research 10 (1993) 417–423

Jeong, H., Yoo, K., Lim, J. Preparation of polystyrene submicron particles using ASES process in supercritical carbon dioxide. Journal of Industrial and Engineering Chemistry 14 (2008) 77-83.

Jinhua, L., Guangyuan, Z. Polystyrene microbeads by dispersion polymerization: Effect of Solvent on Particle Morphology. International Journal of Polymer Science 2014 (2014), 1-4.

Johansen, H.P., Merkle, B., Gander, B. Technological considerations related to the up-scaling of protein encapsulation by spray-drying. European Journal Pharm Biopharm 50 (2000) 413-417.

Jung, J., Perrut, M. Particle design using supercritical fluids: literature and patent survey. Journal of Supercritical Fluids 20 (2001) 179–219.

Kalbhem, D., Tarkanen, V.J. Review on the evolution of safety, ecology and economical aspects in liquid scintillation counting materials and techniques. In: Advances in Scintillation Counting. McQuarrie, S.A., Ediss, C., Wiebe, L.I., Edmonton, Alberta, Canadá (1984) pp.66–71

Kallmann, H. Scintillation counting with solutions. Physical Reviews 78 (5) (1950) 621-622.

Kandori, K., Kishi, K., Ishikawa, T. Preparation of monodispersed W/O emulsions by Shirasu-porous-glass filter emulsification technique. Colloids and Surfaces 55 (1991) 73-78.

King, T.A., Voltz, R. The time dependence of scintillation intensity in aromatic materials. Proceedings of the Royal Society of London A 289 (1966) 424-439.

Koch, S., Schwinger, C., Kressler, J., Heinzen, C., Rainov, N.G. Alginate encapsulation of genetically engineered mammalian cells: comparison of production devices, methods and microcapsule characteristics. Journal of Microencapsulation 20 (2003) 303–316

Kreslo, I., Badhrees, I., Delaquis, S., Ereditato, A., Janos, S., Messina, M., Moser, U., Rossi, B., Zeller, M. Pulse-shape discrimination of scintillation from alpha and beta particles with liquid scintillator and Geiger-mode multipixel avalanche diodes. Journal of Instrumentation 6 (2011) 1-10.

Lambrich, U., Schubert, H. Emulsification using microporous systems. Journal of Membrane Science 257, (2005) 76–84.

L'Annunziata, M.F. Handbook of radioactivity analysis. Academin Press, third edition, San Diego, United States (2013).

Laustriat, G. The luminiscence decay of organic scintillators. Molecular Crystals 4 (1968) 127.

Lee, Y.H., Mei, F., Bai, M.Y., Zhao, S., Chen, D.R. Release profile characteristics of biodegradable-polymer-coated drug particles fabricated by dual-capillary electrospray. Journal of Controlled Release 145 (2010) 58–65.

Lempicki, A. The physics of inorganic scintillators. Journal of Applied Spectroscpy 62(1995) 209-231.

Lesoin, L., Crampon, C., Boutin, O., Badens, E. Preparation of liposomes using the supercritical anti-solvent (SAS) process and comparison with a conventional method. Journal of Supercritical Fluids 57 (2011) 162–174.

Li, W., Anderson, K.W., DeLuca, P.P. Kinetic and thermodynamic modelling of the formation of polymeric microspheres using solvent extraction/evaporation method. Journal of Controlled Release 37 (1995) 187-198.

Li, M., Rouaud, O., Poncelet, D. Microencapsulation by solvent evaporation: State of the art for process engineering approaches. International Journal of Pharmaceutics 363 (2008) 26–39.

Lieser, K.H. Nuclear and radioachemistry, fundamentals and applications. Wiley-VCH, second edition, Berlin- Germany (2007).

Lok, K.P., Ober, C.K. Particle size control in dispersion polymerization of polystyrene. Canadian Journal of Chemistry 63 (1985) 209-216.

Ma, G.H., Nagai, M., Omi, S. Study on preparation and morphology of uniform artificial polystyrene–poly(methyl methacrylate) composite microspheres by employing the SPG (Shirasu Porous Glass) membrane emulsification technique. Journal of Colloid and Interface Science 214 (1999) 264-282.

Maa, Y.F., Contantino, H.R., Nguyen, P.A., Hsu, C.C. The effect of operating and formulation variables on the morphology of spray-dried protein particles. Pharmaceutical Development and Technology 2 (1997) 213-223.

Makino, K., Nakajima, T., Shikamura, M., Ito, F., Ando, S., Kochi, C., Inagawa, H., Soma, G.-I., Terada, H. Efficient intracellular delivery of rifampicin to alveolar macrophages using rifampicin-loaded PLGA microspheres: Effects of molecular weight and composition of PLGA on release of rifampicin. Colloids and Surfaces B: Biointerfaces 36(2004) 35-42.

Mao, S., Shi, Y., Li, L., Xu, J., Schaper, A., Kissel, T. Effects of process and formulation parameters on characteristics and internal morphology of poly(D,L-lactide-co-glycolide) microspheres formed by the solvent evaporation method. European Journal of Pharmaceutics and Biopharmaceutics 68, 2 (2008) 214–223.

Martín-Banderas, L., Rodriguez-Gil, A., Cebolla, A., Chavez, S., Berdun-Alverez, T., Fernandez Garcia, J.M., Flores-Mosquera, M., Ganán-Calvo, A.M. Towards high-throughput production of uniformly encoded microparticles. Advanced Materials 18 (2006) 559–564.

Martín-Banderas, L., González-Prieto, R., Rodrıguez-Gil, A., Fernandez-Arévalo, M., Flores-Mosquera, M., Chávez, S., Gañán-Calvo, A.M. Application of flow focusing to the break-up of a magnetite suspension jet for the production of paramagnetic microparticles. Journal of Nanomaterials 2011 (2011) 1-10.

Mazzitelli, S., Tosi, A., Balestra C., Nastruzzi, C. Production and characterization of alginate microcapsules produced by a vibrational encapsulation device. Journal of Biomaterials Applications 23 (2008) 123- 145

McCormick, J.W. Liquid Scintillation Counting and Organic Scintillators. Lewis Publishers Inc., Michigan-United States, (1991) pp. 561–571

Merino, A., Los, J.M., Rodríguez, L. "Cocktail composition for liquid scintillation measurements". Centro de Investigaciones Energéticas, Medioambientales y Tecnológicas CIEMAT. Spanish patent EP1555546 A2, 28 octubre 2005.

Moghadam, H., Samimi, M., Samimi, A., Khorram, M. Electro-spray of high viscous liquids for producing mono-sized spherical alginate beads. Particuology 6 (2008) 271–275.

Montaña, M., Fons, J., Corbacho, J.A., Camacho, A., Zapata-García, D., Guillén, J., Serrano, I., Tent, J., Baeza, A., Llauradó, M., Vallés, I. A comparative experimental study of gross alpha methods in natural waters. Journal of Environmental Radioactivity 118 (2013) 1-8.

Mu, L., Feng, S.S. Fabrication, characterization and in vitro release of paclitaxel (Taxol®) loaded poly (lactic-co-glycolic acid) microspheres prepared by Spray Drying technique with lipid/cholesterol emulsifiers. Journal of Controlled Release 76 (2001) 239 –254

Normand, S., Mouanda, B., Hann, S., Louvel, M. Discrimination methods between neutron and gamma rays for boron loaded plastic scintillators. Nuclear Instruments and Methods in Physics Research A 484 (2002) 342-350.

O'Donnell, P.B.; McGinity, J.W. Preparation of microspheres by the solvent evaporation technique. Advanced Drug Delivery Reviews 28 (1997) 25–42

Omi, S. Preparation of monodisperse microspheres using the Shirasu porous glass emulsification technique. Colloids and Surfaces A: Physicochemical and Engineering Aspects 109 (1996) 97-107.

Ortega, X., Jorba, J. Radiaciones Ionizantes. Politext Edicions UPC, segunda edición (1996) pp. 75-352

Patel, P., Mundargi, R.C., Babu, V.R., Jain, D., Rangaswamy, V.; Aminabhavi, T.M. Microencapsulation of doxycycline into poly(lactide-*co*-glycolide) by spray drying technique: Effect of polymer molecular weight on process parameters. Journal of Applied Polymer Science 108 (2008) 4038-4046.

Paudel, A., Worku, Z.A., Meeus, Joke., Guns, S., Van den Mooter, G. Manufacturing of solid dispersions of poorly water soluble durgs by spray drying: Formulation and process considerations. International Journal of Pharmaceutics 453 (2013) 253.

Parker, C.A., Hatchard, C.G. Triplet-singlet emission in fluid solutions. Transactions of the Faraday Society 57 (1961) 1894-1904.

Perkins, R.W., Schilk, A.J., Wagner, R.A., Wogman, N.A. "Apparatus for field determinations of concentrations of radioactive constituents in a medium". US Patent 5442180, 15th august 1995.

Polack, J.K., Flaska, M., Enqvist, A., Sosa, C.S., Lawrence, C.C., Pozzi, S.A. An algorithm for charge-integration, pulse-shape discrimination and estimation of neutron/photon misclassification in organic scintillators. Nuclear Instruments and Methods in Physics Research A 795 (2015) 253–267

Poncelet, D., Babak, V., Neufeld, R.J., Goosen, M.F.A., Bugarski, B. Theory of electrostatic dispersion of polymer solution in the production of microgel beds containing biocatalyst. Advances in Colloid and Interface Sciences 79 (1999) 213–28.

Prüße, U., Fox, B., Kirchhoff, M., Bruske, F., Breford, J., Vorlop, K-D. New process (jet cutting method) for the production of spherical beads from highly viscous polymer solutions. Chemical Engineering and Technology 21 (1998a) 29–33.

Prüße, U., Fox, B., Kirchhoff, M., Bruske, F., Breford, J., Vorlop, K-D. The jet cutting method as a new immobilization technique. Biotechnology Techniques 12 (1998b) 105–108.

Prüße, U., Dalluhn, J., Breford, J., Vorlop, K-D. Production of spherical beads by jet cutting. Chemical Engineering and Technology 23 (2000) 1105–1110.

Rapkin, E., Gibbs, J.A. A System for continuous measurement of radioactivity in flowing streams. Nature 194 (1962) 34-36

Rayleigh, L. On the stability of jets. Proceedings of London Mathematical Society 10 (1878) 4–13.

Reverchón, E. Cleofe, M., Caputo, G. Supercritical fluid processing of polymers: composite particles and porous materials elaboration. Current Opinion in Solid State and Materials Science 7 (2003) 391-397.

Reverchon, E., De Marco, I., Torino, E. Nanoparticles production by supercritical antisolvent precipitation: A general interpretation. Journal of Supercritical Fluids 43 (2007) 126–138.

Rey, S., Cansell, F. Universal supercritical binary mixture for polymer fractionation. Polymer Journal 30 (1998) 863-867.

Reynolds, G.T., Harrison, F.B., Salvini, B. Liquid scintillation counters. Phyical Reviews 78 (4) (1950) 488.

Roush, M.L., Wilson, M.A., Hornyak, W.F. Pulse shape discrimination. Nuclear Instruments and Methods 31 (1964) 112.

Sah, H. Microencapsulation techniques using ethyl acetate as a dispersed solvent: effects of its extraction rate on the characteristics of PLGA microspheres. Journal of Controlled Release 47 (1997) 233-245.

Sah, H. Ethyl formate - alternative dispersed solvent useful in preparing PLGA microspheres. International Journal of Pharmaceutics 195 (2000) 103–113.

Seifert D.B., Phillips, J.A. Production of Small, Monodispersed Alginate Beads for Cell Immobilization. Biotechnology Progress 13 (1997) 562-568.

Schneider, T., Zhao, H., Jackson, J.K., Chapman, G.H., Dykes, J., Häfeli, U.O. Use of hydrodynamic flow focusing for the generationn of biodegradable camptothecin loaded polymer microspheres. Journal of Pharmaceutical Sciences 97 (2008) 4943–4954.

Schorr, M.G., Torney, F.L. Solid non-crystalline scintillation phosphors. Physics Reviews 80 (1950) 474-479.

Shiga, K., Muramatsu, N., Kondo, T. Preparation of poly(d,l-lactide) and copoly(lactide-glycolide) microspheres of uniform size. Journal of Pharmacy and Pharmacology 48 (1996) 891–895.

Staymates, M., Fletcher, R., Staymates, J., Greg G., Berkland, C. Production and characterization of polymer microspheres containing trace explosives using precision particle fabrication technology. Journal of Microencapsulation 27 (5) (2010) 426–435.

Steinberg, D. Radioassay of Aqueous Solutions mixed with Solid Crystalline Fluors. Nature 183 (1959) 1253-1254.

Sugiura, S., Nakajima, M., Seki, M. Preparation of monodispersed polymeric microspheres over 50 μm employing microchannel emulsification. Industrial and Engineering Chemical Research 41 (2002a) 4043–4047.

Sugiura, S., Nakajima, M., Seki, M. Preparation of monodispersed emulsion with large droplets using microchannel emulsification. Journal of the American Oil's Chemists Society 79 (2002b) 515-519.

Tahmassian, A., Eveloff J., Tisdale, H. Liquid scintillation waste. In: Liquid Scintillation Counting and Organic Scintillators. Ross, H. Lewis Publishers Inc., Michigan, United States, 1991 pp.573–575.

Tarancón, A., García, J.F., Rauret, G. Mixed waste reduction in radioactivity determination by using plastic scintillators. Analytica Chimica Acta 463 (2002a) 125-134.

Tarancón, A., Alonso, E., García, J.F., Rauret, G. Comparative study of quenching correction procedures for $^{90}Sr/^{90}Y$ determination by Cerenkov, liquid scintillation and plastic scintillation techniques. Analytica Chimica Acta 471 (1) (2002b) 135–143.

Tarancón, A., Garcia, J.F., Rauret, G. Reusability of plastic scintillators used in beta emitter activity determination. Applied Radiation and Isotopes 59 (2003) 373-376.

Tarancón, A., Garcia, J.F., Rauret, G. Determination of beta emitters (^{90}Sr, ^{14}C and ^{3}H) in routine measurements using plastic scintillation beads. Nuclear Instruments and Methods in Physics Research Section A: Accelerators, Spectrometers, Detectors and Associated Equipment 516 (2–3) (2004) 602–609.

Tarancón, A., Padro, A., Garcıa, J.F., Rauret, G. Development of a radiochemical sensor, Part 2: Application to liquid effluents. Analytica Chimica Acta 538 (2005) 241–249

Tran, V-T., Benoît, J-P., Vernier-Julienne, M-C. Why and how to prepare biodegradable, monodispersed polymeric microparticles in the field of pharmacy?. International Journal of Pharmaceutics 407 (2011) 1-11.

Van Dijke, K.C., Schroën, K., Boom, R.M. Microchannel emulsification: From computational fluid dynamics to predictive analytical model. Langmuir 24 (2008) 10107-10115

Xu, S., Nie, Z., Seo, M., Lewis, P., Kumacheva, E., Stone, H., Garstecki, P., Weibel, D., Gitlin, I., Whitesides, G. Generation of monodisperse particles by using microfluidics: control over size, shape, and composition. Angewandte Chemie International Edition 44 (2005) 724–728

Xu, Q., Hashimoto, M., Dang, T.T., Hoare, T., Kohane, D.S., Whitesides, G.M., Langer, R., Anderson, D.G. Preparation of monodisperse biodegradable polymer microparticles using a microfluidic flow-focusing device for controlled drug delivery. Small 5 (2009) 1575–1581

Yeo, S., Kiran, E. Formation of polymer particles with supercritical fluids: A review. Journal of Supercritical Fluids 34 (2005) 287–308.

Zvonar A., Kristl J., Kerc J.; Grabnar P.A. High celecoxib-loaded nanoparticles prepared by a vibrating nozzle device. Journal of Microencapsulation 26 (8) (2009) 748–759.

Chapter 2

Objectives

2. GENERAL OBJECTIVES

- To evaluate different methodologies which allow producing plastic scintillation microspheres (PSm) of different diameters and compositions under laboratory conditions with the aim of overtaking the dependence on commercial suppliers and spreading their use in new applications.
- To explore the energy transfer mechanism for radioactivity measurements employing plastic scintillation microspheres.

2.1. Specific objectives

- To evaluate the feasibility of the organic solvent extraction/evaporation methodology to produce plastic scintillation microspheres.
- To produce plastic scintillation microspheres of several diameters and compositions through the organic solvent extraction/evaporation methodology.
- To produce plastic scintillation microspheres able to discriminate alpha/beta particles.
- To produce plastic scintillation particles employing supercritical fluid technique.
- To produce plastic scintillation microspheres through Spray Drying methodology using a closed cycle Mobile Minor.
- To test the production of plastic scintillation microspheres at a large scale by employing the organic solvent extraction/evaporation methodology.
- To evaluate the effect of the plastic scintillating particles diameter and different quenching agents on the radiometric capacities of some radionuclides.

Chapter 3

Results

Chapter 3.1

Synthesis of plastic scintillation microspheres through the organic solvent extraction/evaporation methodology

---

3.1.1. Synthesis of plastic scintillation microspheres: Evaluation of Scintillators.

3.1.2. Synthesis of plastic scintillation microspheres: Alpha/beta discrimination.

3.1.3. Influence of preparation parameters on the synthesis of plastic scintillation microspheres and evaluation of sample preparation.

Nuclear Instruments and Methods in Physics Research A 698 (2013) 106–116

Contents lists available at SciVerse ScienceDirect

Nuclear Instruments and Methods in Physics Research A

journal homepage: www.elsevier.com/locate/nima

Synthesis of plastic scintillation microspheres: Evaluation of scintillators

L.M. Santiago, H. Bagán, A. Tarancón *, J.F. Garcia

Department of Analytical Chemistry of the University of Barcelona, Diagonal 645, E-08028 Barcelona, Spain

ARTICLE INFO

Article history:
Received 16 April 2012
Received in revised form
10 September 2012
Accepted 17 September 2012
Available online 26 September 2012

Keywords:
Plastic scintillation
Mixed waste
Microspheres
Microparticle synthesis
Radioactivity

ABSTRACT

The use of plastic scintillation microspheres (PSm) appear to be an alternative to liquid scintillation for the quantification of alpha and beta emitters because it does not generate mixed wastes after the measurement (organic and radioactive). In addition to routine radionuclide determinations, PSm can be used for further applications, e.g. for usage in a continuous monitoring equipment, for measurements of samples with a high salt concentration and for an extractive scintillation support which permits the separation, pre-concentration and measurement of the radionuclides without additional steps of elution and sample preparation. However, only a few manufacturers provide PSm, and the low number of regular suppliers reduces its availability and restricts the compositions and sizes available.

In this article, a synthesis method based on the extraction/evaporation methodology has been developed and successfully used for the synthesis of plastic scintillation microspheres. Seven different compositions of plastic scintillation microspheres have been synthesised; PSm1 with polystyrene, PSm2 with 2,5-Diphenyloxazol(PPO), PSm3 with p-terphenyl (pT), PSm4 with PPO and 1,4-bis (5-phenyloxazol-2-yl) (POPOP), PSm5 pT and (1,4-bis [2-methylstyryl] benzene) (Bis-MSB), PSm6 with PPO, POPOP and naphthalene and PSm7 with pT, Bis-MSB and naphthalene.

The synthesised plastic scintillation microspheres have been characterised in terms of their morphology, detection capabilities and alpha/beta separation capacity. The microspheres had a median diameter of approximately 130 μm. Maximum detection efficiency values were obtained for the PSm4 composition as follows 1.18% for ^{3}H, 51.2% for ^{14}C, 180.6% for ^{90}Sr/^{90}Y and 76.7% for ^{241}Am. Values of the *SQP*(*E*) parameter were approximately 790 for PSm4 and PSm5. These values show that the synthesised PSm exhibit good scintillation properties and that the spectra are at channel numbers higher than in commercial PSm. Finally, the addition of naphthalene modifies the shape of the pulses produced by alpha and beta particles leading to better alpha/beta separation.

1. Introduction

Liquid scintillation counting (LSC) [1,2] is the most often used technique for the measurement of beta and alpha emitters in environmental samples [3] and in highly active samples [4] that are produced by nuclear power plants, in research centres, or in hospitals. LSC is a simple and very well established technique; however, the use of LSC in some specific applications such as continuous measurements or measuring of samples with high salinity is problematic. Moreover, the measurements with liquid scintillators generate a mixed waste that has both radioactive and organic properties [5] and a special regulation is devoted to their disposal [6]. This regulation causes special difficulties for the centres in which large amounts of mixed waste are generated [7–9].

The use of plastic scintillation microspheres (PSm) appears to be an alternative to liquid scintillation to solve some of the problems associated with its use. PSm are a solid solution of fluorescent solutes in a polymeric solvent and have a diameter that can vary from tens of micrometres to a few millimetres. Since the polymer is completely polymerised, PSm have no reactivity and are neither flammable nor toxic. Moreover, as they are solid, PSm can be separated from the radioactive sample by filtration after the measurement and no mixed waste is produced [10,11]. Since the composition of PSm is similar to that of liquid scintillators, the scintillation mechanism is also similar. However, considerable differences are observed for weak beta emitters (e.g. ^{3}H) and alpha emitters (when microspheres of high diameter are used) since the particles lose energy in the aqueous phase before reaching the scintillator [12].

In addition to the routine determination of radionuclides, specific applications of PSm, which take advantage from its characteristics, are continuous monitoring of radionuclides in fluid streams [13,14]; measurement of samples with a high salt content that can produce instability (phase separation) when

* Corresponding author. Tel.: +34 9340 21281; fax: +34 9340 21233.
E-mail address: alex.tarancon@ub.edu (A. Tarancón).

0168-9002/$ - see front matter © 2012 Elsevier B.V. All rights reserved.
http://dx.doi.org/10.1016/j.nima.2012.09.028

measured by LSC [15]; usage as a selective extractant scintillation support (PSm resin) in which the radionuclides can be separated and pre-concentrated in a column-vial that can be measured later without additional steps of elution and sample preparation [16–19].

PSm are a relatively new material, and there are only a few manufacturers providing them [20,21]. However, due to the low number of regular suppliers, it is difficult to purchase PSm and only a few compositions and diameters of the microspheres are available. For this reason, the development of procedures for the synthesis of PSm could be of interest not only to regularly provide PSm for the different applications but also to synthesise PSm with new compositions which can be used to solve important radioanalytical challenges.

Among the different procedures described in the literature for the synthesis of polymeric microspheres [22–24], the most important are drop disruption using microwaves [25,26], polymerisation [27–29] and evaporation/extraction [30,31]. The advantage of evaporation/extraction is that it can be easily implemented in a laboratory and that there are no reactions during the synthesis. Therefore, the components in the PSm are known, which avoids possible quenching effects. In addition, this technique is well described in the literature and is commonly used in the pharmaceutical industry to produce formulations in which the active compound is encapsulated within a biodegradable polymeric matrix. This method is based on the mixture of an organic solution, in which the polymer and the active compounds are dissolved, with a large volume of an aqueous solution with an emulsifier dissolved. After mixing both solutions, microdroplets of the organic solvent are formed in the aqueous solution and are stabilised by the presence of the emulsifier. Then, the aqueous solution extracts slowly the organic solvent of the droplets and at the same time the extracted organic solvent is evaporated from the aqueous solution (which is in contact with the air). After a period of time, the organic solvent is completely extracted from the droplets, and the polymer, with the active compound encapsulated, becomes solid in form of a microspheres and precipitates.

The first objective of this work was to adapt the evaporation/extraction method for the preparation of PSm by using polystyrene as the polymeric solvent and a series of scintillation fluorescent solutes as the active compounds. The scintillation solutes considered in this paper are a selection of those that are commonly described in the literature [32]. p-Terphenyl (pT) and 2,5-diphenyloxazol(PPO) were used as primary solutes and were combined with 1,4-bis(5-phenyloxazol-2-yl) (POPOP) and (1,4-bis [2-methylstyryl] benzene) (Bis-MSB) as secondary solutes [4]. Naphthalene was also evaluated as a secondary solvent, since it has been described in the literature as a component that is capable of enhancing alpha/beta discrimination capabilities of organic scintillators [33–34]. The second objective was to evaluate the capabilities of the differently synthesised PSm and the influence of each component (primary solute, secondary solute, primary solvent and secondary solvent).

2. Experimental

2.1. Reagents

Polystyrene (molecular weight of 250000 g/mol) was purchased from Acros Organics (Geel, Belgium). Fully hydrolysed polyvinylalcohol was obtained from Merck (Schuchardt OHG, Germany). Naphthalene (synthesis reagent), 2,5-diphenylozaxol (scintillation reagent) and dichloromethane (liquid chromatography solvent, 99.9% purity) were purchased from Merck (Darmstadt, Germany). p-Terphenyl and 1,4-bis(2-methylstyryl) benzene (both of scintillation grade) were supplied by Fluka Analytical (Buchs, Switzerland). 1,4-bis(5-phenyloxazol-2-yl)benzene (scintillation grade) was supplied by the Montedison Group, Division Chimica (Milan, Italy).

The radioactive samples were prepared in 6 mL Pico Prias polyethylene vials (PerkinElmer) from the following active stock solutions: A ^{3}H solution ($^{3}H_2O$) with a concentration of 3941(138) Bq/g prepared from a standard of 69.84(244) kBq/g provided by Eckert–Ziegler (Berlin, Germany) in deionised water; a ^{14}C solution (in form of labelled glucose) of 114.6(29) Bq/g prepared from a standard of 44.70(112) kBq/g from Amersham International (Buckinghamshire, UK) in a carrier solution containing 50 μg/g of glucose and 1 mg/g of formaldehyde in deionised water; a $^{90}Sr/^{90}Y$ active stock solution (Sr^{2+} and Y^{3+}) of 37.22(28) Bq/g prepared from a standard of 4.071(31) kBq/g from Amersham International in 0.1 HCl as carrier solution; a ^{241}Am solution (Am^{3+}) of 185.5(19) Bq/g prepared from a standard of 55.44(55) kBq/g supplied by Amersham International in 0.5 M HCl deionised water solution.

2.2. Instruments

The samples were centrifuged using an AJ2-HS centrifuge (Beckman-Coulter Inc., Brea, USA) and sonicated using an Ultrasons-P ultrasonic bath of 40 kHz (JP Selecta, Abrera, Spain).

The radioactive samples were measured using a 1220 QUANTULUS liquid scintillation spectrometer (PerkinElmer) equipped with logarithmic amplification, a multichannel analyser (4096 channels distributed into four segments of 1024 channels), alpha/beta discrimination and background reduction by means of an active guard detector.

The size distribution of the plastic scintillation microspheres was determined using an LS 13 320 single-wavelength laser diffraction particle size analyser (Beckman-Coulter Inc., Brea, USA).

Secondary-electron images were obtained using a Stereoscan S-360 scanning electron microscope.

2.3. Synthesis procedure

PSm were synthesised using the evaporation/extraction method. This synthesis method was adapted to our purposes as follows: 100 mL of dichloromethane containing 10 g of polymer and the corresponding amount of the fluorescent solutes and naphthalene were carefully poured into a 3 L glass that contained 2 L of an aqueous solution of 20 g of polyvinylalcohol in deionised water. The organic/aqueous mixture was continuously stirred with a magnetic stirrer at 16.7 Hz to ensure the formation of a heterogeneous mixture of organic droplets in an aqueous solvent. The mixture was stirred for 5 h to allow the extraction and evaporation of the organic solvent. After this period, the microspheres were separated by filtration and then washed with ethanol and deionised water. Finally, the PSm were dried in an oven at about 40 °C.

Seven different compositions of PSm (from PSm1 to PSm7) were synthesised to evaluate the influence of each component in the scintillator. Table 1 summarises the amount of fluorescent solute and naphthalene added in each synthesis. Each synthesis was performed in triplicate.

In cases of PSm1, PSm2, PSm3, PSm4 and PSm5, the microspheres were mixed in a plastic container and homogenised by shaking. In cases of PSm6 and PSm7, the obtained microspheres from each synthesis were stored separately to evaluate the reproducibility of the synthesis method. After determining the particle size and measuring a tritium sample, the PSm6 and PSm7 were homogenised using the same procedure.

Table 1
Composition of the organic phase of the different syntheses.

PSm1	10 g of polystyrene in 100 mL of dichloromethane
PSm2	10 g of polystyrene and 0.2 g of PPO in 100 mL of dichloromethane
PSm3	10 g of polystyrene and 0.2 g of pT in 100 mL of dichloromethane
PSm4	10 g of polystyrene, 0.2 g of PPO and 0.005 g of POPOP in 100 mL of dichloromethane
PSm5	10 g of polystyrene, 0.2 g of pT and 0.005 g of Bis-MSB in 100 mL of dichloromethane
PSm6	10 g of polystyrene, 1.2 g of naphthalene, 0.2 g of PPO and 0.005 g of POPOP in 100 mL of dichloromethane
PSm7	10 g of polystyrene, 1.2 g of naphthalene, 0.2 g of pT and 0.005 g of Bis-MSB in 100 mL of dichloromethane

2.4. Radioactivity measurements

2.4.1. Sample preparation

The radioactive samples were prepared by adding 1.5 g of the PSm and 0.75 mL of the corresponding counting solution (active or blank solution) to a 6 mL polyethylene vial. After that the vials were sonicated with ultrasounds for 2 min and centrifuged for 10 min at 83.3 Hz to ensure homogenisation.

The active counting solutions were prepared by diluting a known quantity of an active stock solution of the respective radionuclide (^{3}H, ^{14}C, ^{90}Sr/^{90}Y or ^{241}Am) in a carrier solution of known volume. The activity in the measurement samples was approximately 450 Bq for ^{3}H, 35.8 Bq for ^{14}C, 3.92 Bq for ^{90}Sr/ ^{90}Y and 31.7 Bq for ^{241}Am samples. A blank was prepared for each active measurement sample by adding carrier solution rather than active stock solution.

For all of the PSm, three replicates of each isotope were prepared and measured using homogenised PSm. In case of PSm6 and PSm7, a sample containing ^{3}H was previously measured with the microspheres obtained from the three replicate syntheses.

All solutions and samples were prepared by weighing.

2.4.2. Measurement

The measurements were performed using a "low" coincident bias and a "^{14}C" multichannel analyser (MCA) configuration. The coincident bias is a default setting of the Quantulus which determines the amplitude threshold level (low or high) for summing pulses obtained in each photomultiplier and is used to prevent the sum of non symmetric background pulses. High coincident bias setting removes part of the signals detected in the first 300 channels, reducing the background but also the ^{3}H detection efficiency. MCA default configurations are ^{3}H (low energy), ^{14}C (medium and high energy), alpha/beta (for alpha/beta discrimination) and free setup (free configuration). When ^{14}C configuration is used no correction for chemiluminescence is applied [35].

The counting times for the blank, ^{3}H, ^{14}C and ^{241}Am samples were 60 min each. The ^{90}Sr/^{90}Y samples were measured for 90 min and the duration for the measurement with external gamma-ray source (^{152}Eu) was adjusted to 10 min.

While evaluating the capability of the PSm for separation between alpha and beta particles, the alpha/beta MCA configuration default setting of the Quantulus detector was selected. In this configuration pulses are classified as alpha (in the alpha part of the multichannel analyser) or beta (in the beta part of the multichannel analyser). The discrimination is done by comparing the relationship between two areas of each pulse (i.e., the total area of the pulse and the area of the pulse tail) with respect to the PSA value. The PSA value can be selected by the user and can be varied from 10 to 250. PSA determines the threshold level to classify a pulse as alpha or beta. The measurements were performed for PSA values that varied from 10 to 180 for PSm1, PSm2, PSm3, PSm4 and PSm5, and from 10 to 250 for PSm6 and PSm7.

2.4.3. Data analysis

The obtained spectrum from each measurement was smoothed using a Savitzky–Golay algorithm [36] included in the Matlab® software (Mathworks, Natwick, United States). The net spectrum of an active sample was obtained by subtracting the corresponding spectrum of the blank solution from the active sample spectrum. The detection efficiency was calculated as the ratio between the net counts in the entire spectrum and the activity that was added to the measurement vial. The uncertainty associated to the count rate and to the detection efficiency values correspond to the higher value between the experimental standard deviation between replicates and the combined standard uncertainty considering the canonical values of the main uncertainty sources (weighting, count rate of the active and background sample).

The misclassification, in percentage, was calculated from the counts of the corresponding isotope in the wrong part of the multichannel analyser (alpha part of the MCA for ^{90}Sr/^{90}Y samples and the beta part of the MCA for ^{241}Am samples) with respect to the total number of counts (alpha and beta part of the MCA).

The quenching indicator $SQP(E)$ was calculated by the detector for each sample; it corresponds to the end-point channel that limits 99.75% of the total counts of the spectrum which was generated by the external gamma-ray source [35].

3. Results and discussion

Seven different compositions of plastic scintillation microspheres (from PSm1 to PSm7) were synthesised in triplicate. In all cases, the masses of the microspheres were close to the sum of the masses of the polymer and solutes, which implies that the synthesis yields were 100%.

The performances of the PSm were evaluated by considering the following aspects:

- Morphology was evaluated by visual analysis of the scanning electron microscopy images, and through analysis of the particle size distribution of the microspheres.
- Radiometric capabilities:
  - The detection capability was determined by examining the detection efficiency of a weak energy beta emitter (^{3}H, E_{max}=18.6 keV), a medium energy beta emitter (^{14}C, E_{max}=156.5 keV), a high energy beta emitter (^{90}Sr/^{90}Y, E_{max}=545.9 keV and, E_{max}=2279.8 keV respectively) and an alpha emitter (^{241}Am).
  - The scintillation photon production was evaluated by examining the spectrum obtained in the measurement of each radionuclide and the spectrum generated by the external gamma-ray source.
- The capability to distinguish between alpha and beta particles was evaluated by determining the misclassification of alpha

and beta events when measuring a high energy beta emitter (^{90}Sr/^{90}Y) and an alpha emitter (^{241}Am), respectively.

3.1. Synthesis reproducibility

The most important aspects of the evaporation/extraction method for obtaining polymeric microspheres are the formation of stable organic droplets in the aqueous phase when the phases are mixed and the evolution of these droplets during the continuous process of extraction and evaporation of the organic solvent. The form and size of the droplets, which determines the shape and size of the resulting microspheres, depend on several variables, such as the speed and type of agitation, the mixing of the aqueous and organic phases, the composition and proportion of the components in both phases (specifically the proportion of emulsifier), and the temperature of the aqueous/organic mixture.

For this reason, the first step was to evaluate the reproducibility of the PSm that was obtained using the adapted evaporation/extraction method. The reproducibility was evaluated by measuring ^{3}H samples with the PSm6 and PSm7 microspheres obtained in three replicate syntheses, and by determining the particle size distribution. The results are compared to those obtained when the microspheres of the replicate syntheses are mixed and homogenised.

The results show that the uncertainty associated to the ^{3}H detection efficiency drastically decreases when homogenised microspheres are used (PSm6: 1.027(15)% (relative standard deviation, RSD, of 1.5%) and PSm7: 0.819(9)% (RSD of 1.1%)) compared to that obtained when microspheres from the individual synthesis are used (PSm6: 1.033(33)% (RSD of 3.2%) and PSm7: 0.752(73)% (RSD of 9.7%)). Moreover, when using homogenised PSm, the uncertainty on the detection efficiency between replicated samples is similar to the combined standard uncertainty (0.014 and 0.012 for PSm6 and PSm7, respectively) associated to the mean value.

The lack of reproducibility between syntheses is confirmed by the dispersion in the particle size (Fig. 1). The particle size distribution is represented in form of boxes. In this type of representation, the horizontal line inside the box corresponds to the median value of the diameter distribution. The bottom and top values of the box correspond to the diameter values in which we find the 25th and 75th percentiles of the microspheres diameter population (50% of all PSm). Finally, the lower and upper whiskers determine the diameter values where 10th and 90th percentiles of the microspheres diameter distribution are found (80% of all PSm). Fig. 1 shows that the distribution is similar in three replicate measurements when homogenisation was carried out (lower and upper whiskers, bottom and top of the box and median have similar values), whereas differences can be observed in the distribution between microspheres obtained in replicate synthesis without homogenisation.

As previously described in the literature [37], the ^{3}H detection efficiency in measurements with PSm (as well as other low and medium energy beta emitters and alpha emitters) is greatly dependant on the PSm diameter because the diameter determines the distance that a particle (alpha or beta) has to travel in the solution before interacting with the scintillator microspheres and being detected. When the diameter of PSm increases, the mean path length in the aqueous phase increases, and hence, the counting efficiency decreases. Therefore, differences in the diameter between microspheres with the same composition can be the origin of significant differences in the determined detection efficiencies measured.

The homogenisation of microspheres obtained in different syntheses causes a diameter distribution that is more reproducible between replicate preparations and, as consequence, the component of the uncertainty due to differences in the diameter distribution between replicate measurements is reduced.

3.2. Morphology

The scanning electron microscopy images, Fig. 2, shows that most of the microspheres are spherical and only a small proportion are broken or have an amorphous shape. This indicates that the stirring speed is adequate and that the extraction of the organic solvent is gradual and not instantaneous. Based on the images, most of the microspheres have a diameter larger than 100 micrometres, although a significant portion of them have a very small diameter (tens of micrometres). Finally, the microspheres that contain only polystyrene or PPO as the primary solute (PSm1, PSm2, PSm4 and PSm6) have a smooth surface, whereas a portion of the microspheres that contain pT as the primary solute exhibit a rough surface, especially those containing naphthalene.

Particle size distribution analysis for the PSm1–PSm7 microspheres in form of box plot are shown in Fig. 3. The PSm that contain PPO as the primary solute (PSm2, PSm4 and PSm6) exhibit a sharp distribution of diameters, with a median diameter of approximately 125 μm. 50% of the microspheres (between bottom and top of the box) had diameters between 90 and 160 μm and 80% of the microspheres (between lower and upper whisker) had diameters within the range of 70–195 μm. In all cases, the diameters of the microspheres are symmetrically distributed around the median value.

This homogeneous behaviour contrasts with the distribution found for the microspheres that contained pT as the primary solute (PSm3, PSm5 and PSm7) since spread and non-symmetrical distributions are observed. The median value is slightly higher than in the PPO microspheres (approximately 135 μm), whereas 50% of the microspheres had diameters between 90 and 200 μm and 80% of the population had diameters in a range of 400 μm. These large diameter intervals (large boxes and large distance between whiskers) are due to the presence of agglomerations of the microspheres, which have very large diameters.

The microspheres that contain only polystyrene (PSm1) exhibit a broader and less homogeneous distribution than the PPO microspheres. The broadest distribution is observed for the microspheres containing pT, with a medium value of 170 μm that is higher than that obtained for the other microspheres.

3.3. Radiometric capabilities

3.3.1. Background

Background values for the different PSm (Table 2) are similar, although a small increase is observed for PSm with secondary solute and secondary solvent. As all of the compounds used are organic and contain hydrogen, oxygen and carbon atoms, the increase in the count rate cannot be attributed to an increase in the density of the material, to an increase of the scintillation properties of the scintillator or to an increase on the activity within the used components.

3.3.2. ^{3}H

^{3}H is a very low energy beta emitter. Its measurement using organic scintillators is highly influenced by any process that modifies the energy of the beta particles or the energy that is transmitted through the scintillator, which could lead finally to the non-detection of the particles (quenching effect). In the case of ^{3}H measurements by means of PSm, the most important quenching effect is particle quenching, which can be understood

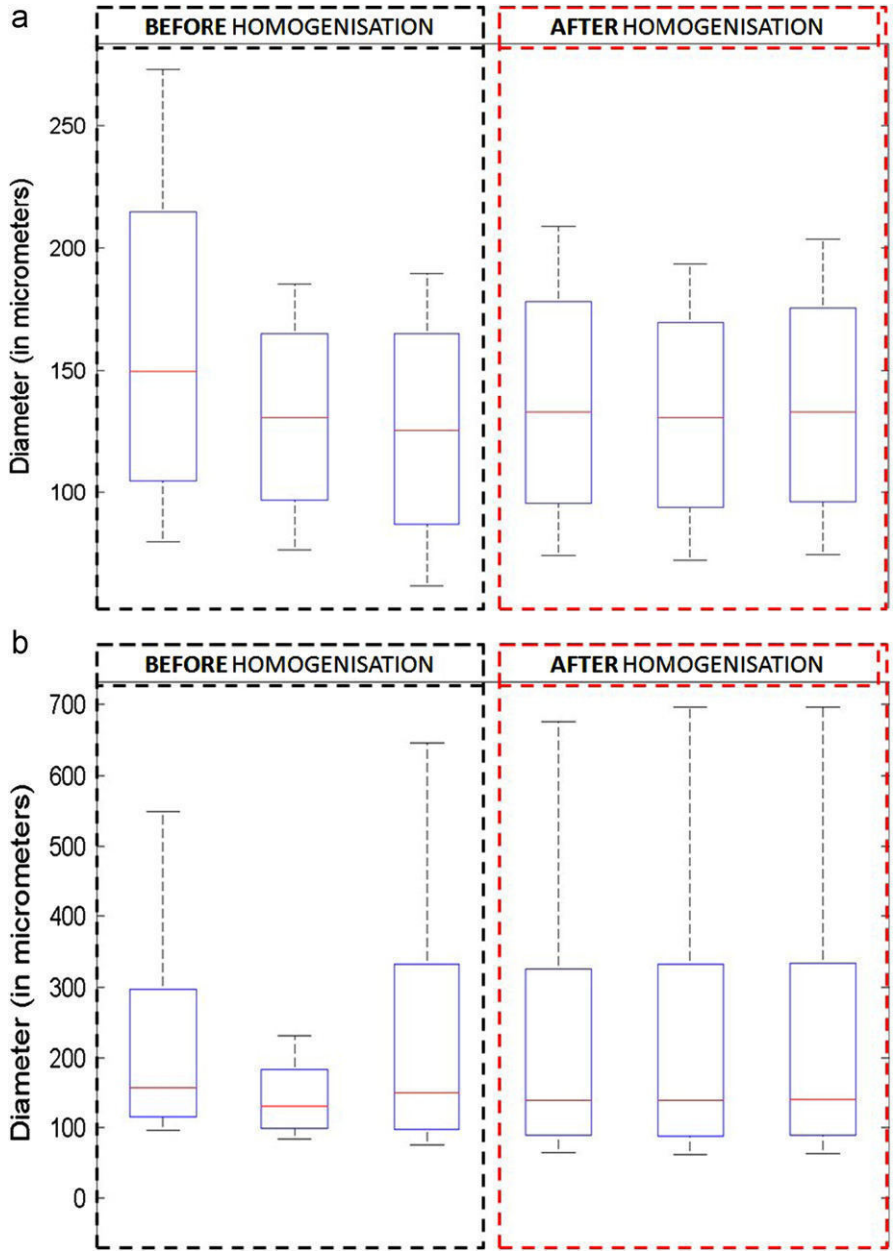

Fig. 1. Box plot of the particle size distribution for PSm6 and PSm7 before and after being homogenised (the horizontal red line into the box represents the median (50th percentile) of the population, top and bottom of the boxes 25th and 75th percentile respectively and lower and upper whisker 10th and 90th percentile).

as the probability of a particle (alpha or beta) interacting with the molecules of the aqueous media before the particle arrives to a microsphere. Because of the low energy of the beta particles that are emitted by ^{3}H, most of the beta particles are stopped before reaching the PSm; therefore, the detection efficiency is highly dependent on the distance travelled by the particle, and thus, on the diameter of the microsphere. In addition, other quenching effects such as ionisation, chemical or colour quenching also have important effects on the detection efficiency of ^{3}H, since the reduction of the energy transmitted due to any of these effects could lead, with high probability, to the non-detection of the disintegration.

Detection efficiency values obtained in the measurement of ^{3}H samples are shown in Table 2. PSm1 is capable to detect ^{3}H, which demonstrates that this polymer is able to convert the energy of the low-energy beta particle into scintillation photons. However, the detection efficiency is very low due to particle quenching but also to the low quantum efficiency of the photomultipliers [38] at the wavelength of emission of polystyrene [39]. The quantum efficiency of the photomultipliers is wavelength-dependent and have a maximum at 400 nm which is very far from the wavelength of emission of the polystyrene of PSm1 (270 nm).

When a primary solute is added (PSm2 and PSm3), the detection efficiency increases because the energy deposited into the polystyrene is transmitted to the primary solute, which emits photons at a wavelength (maximum emission is at 354 nm for PPO and 337 nm for pT) at which the PMT have a higher quantum efficiency. The value of the detection efficiency in both cases is similar to that described in the literature when using commercial PSm [11,12,37]. When a secondary solute is added (PSm4 and PSm5), the efficiency is again improved because the energy is transmitted from the primary to the secondary solute, which emits scintillation photons at a wavelength (maximum emission is at 407 nm for POPOP and 418 nm for Bis-MSB)

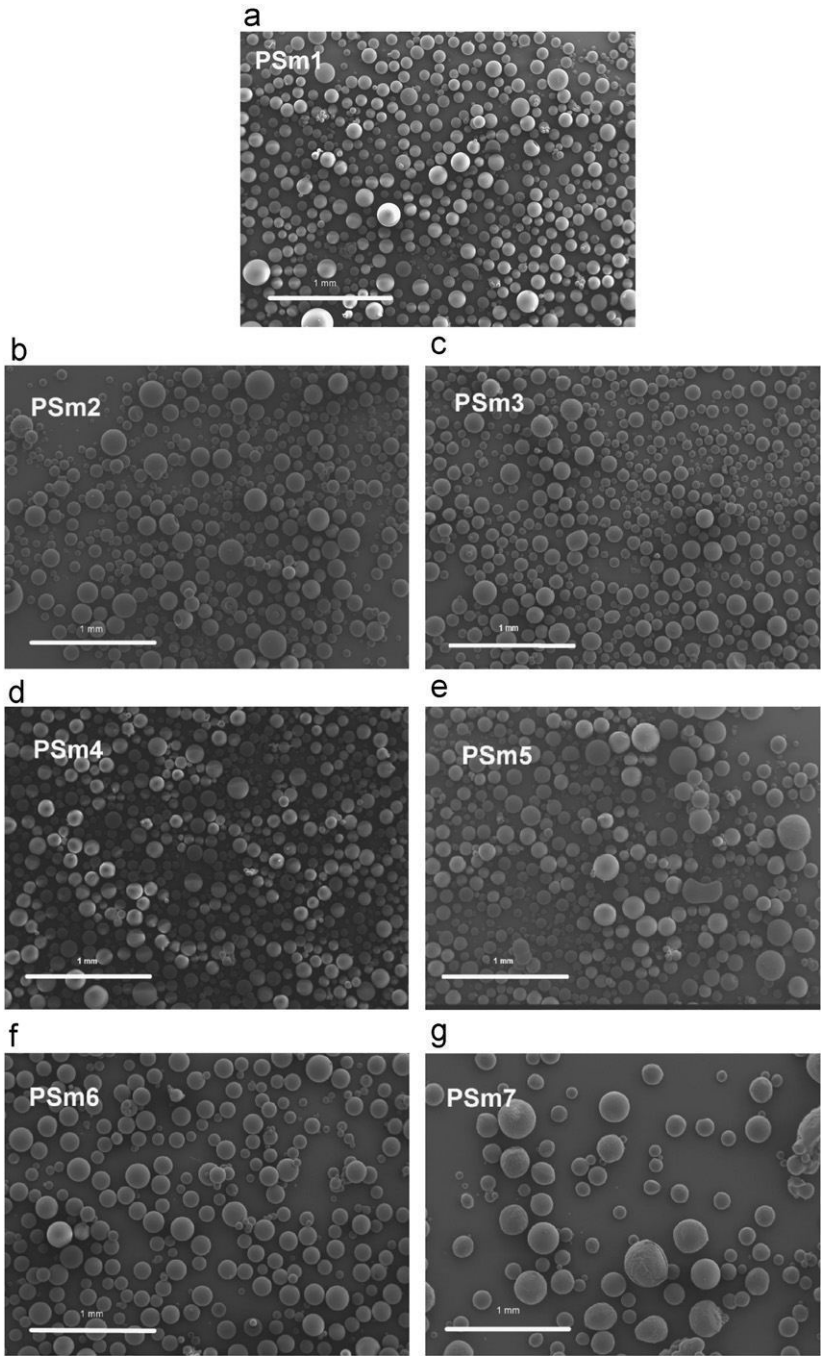

Fig. 2. Scanning electron microscopy image of the synthesised PSm.

that matches the wavelength of maximum quantum efficiency of the PMT.

Finally, the addition of naphthalene (PSm6 and PSm7) results in a small reduction of the detection efficiency, which is likely due to the addition of a new step in the energy transfer process that causes the loss of energy transferred to the scintillator, and thus, a reduction of the detection efficiency.

If we compare the behaviour of the different scintillators, the PSm that contain PPO as a primary solute always have higher efficiencies than the respective PSm that contain pT as a primary solute (PSm2 vs. PSm3, PSm4 vs. PSm5 and PSm6 vs. PSm7). This can be attributed to a higher yield of PPO but also to the small diameter of the microspheres that contain PPO.

3.3.3. ^{14}C

^{14}C is a medium energy beta emitter whose measurement with PSm is still affected by the distance that the beta particle has to travel before it reaches a microsphere. The detection efficiency of ^{14}C is approximately half the efficiency observed when using liquid scintillation counting. For this radionuclide, the detection efficiency is relatively less affected by other quenching effects than ^{3}H, as the energy deposited per disintegration, and therefore, the number of scintillation photons emitted, is higher.

As observed for ^{3}H, PSm1 is capable to detect ^{14}C, but with a very low efficiency, whereas the addition of scintillation solutes results in an increase of the efficiency to a value that is close to 50%. The differences between the PSm microspheres that have

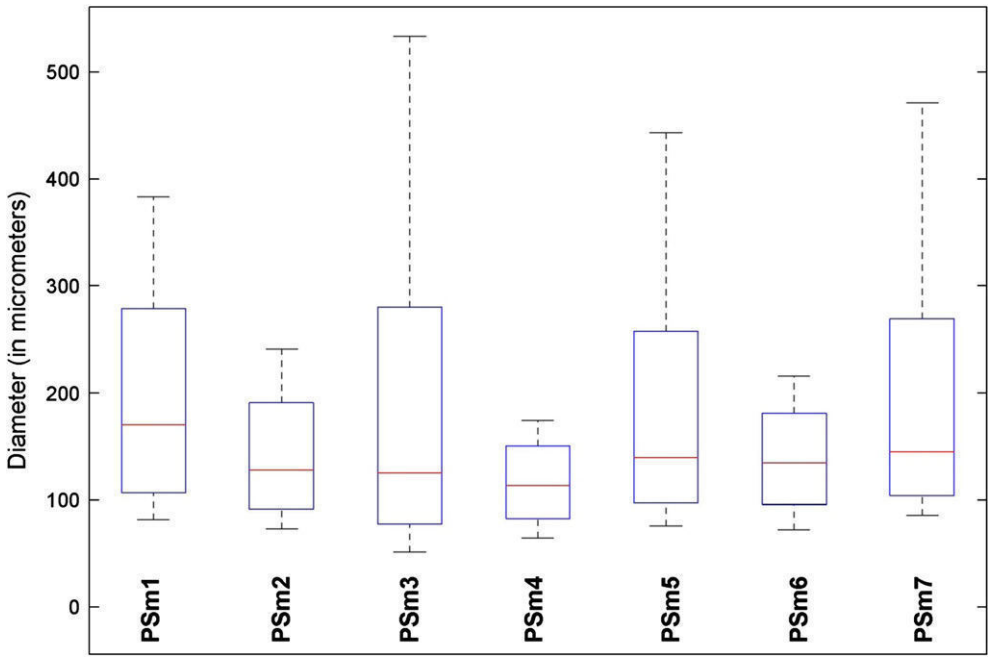

Fig. 3. Box plot of the particle size distribution of the homogenised microspheres that were obtained from the different syntheses.

Table 2
Values of background, ^{3}H, ^{14}C, ^{90}Sr/^{90}Y, ^{241}Am detection efficiencies and *SQP*(*E*) for the different PSm.

	Background (counts per minute)	^{3}H (%)	^{14}C (%)	^{90}Sr/^{90}Y (%)	^{241}Am (%)	*SQP*(*E*)
PSm1	0.95(13)	0.014(1)	8.6(15)	134.9(35)	52.9(11)	428(5)
PSm2	1.01(13)	0.829(26)	48.6(9)	182.4(27)	74.4(21)	732(6)
PSm3	0.92(18)	0.650(12)	45.7(7)	180.3(27)	72.3(17)	694(6)
PSm4	1.10(18)	1.185(18)	51.2(8)	180.6(27)	76.7(11)	782(5)
PSm5	1.16(14)	1.135(29)	49.8(7)	178.7(27)	73.2(14)	783(4)
PSm6	1.10(13)	1.025(15)	48.7(16)	180.9(27)	74.9(29)	791(4)
PSm7	1.28(21)	0.819(12)	45.9(17)	178.1(27)	70.9(39)	790(5)

only a primary solute and those that have both solutes, primary and secondary, are reduced in terms of detection efficiency, but differences are still present. With regard to the differences between scintillators, better results are always obtained for the PSm that contains PPO.

3.3.4. ^{90}Sr/^{90}Y

The energy of the beta particles released by ^{90}Sr/^{90}Y is so high that the detection efficiency depends less on the diameter. On the other hand the diameter of the microspheres has a similar influence to the detection efficiency as other quenching effects that are related to the measured solution or the scintillation process.

The detection efficiency is approximately 180% in all cases (considering the sum of ^{90}Sr and ^{90}Y), except for PSm1 where a significant amount of the emitted scintillation photons were not detected by the PMTs. In this case, the addition of the secondary solute or naphthalene does not produce significant changes in the detection efficiency. The microspheres that contain PPO have detection efficiencies higher than those of the pT microspheres, although the differences are not significant.

3.3.5. ^{241}Am

The measurement of alpha particles using PSm exhibits a different behaviour compared with that observed for the measurement of beta particles. Alpha particles have higher energies than beta particles and their capability to induce ionisation processes is higher, too. On the other hand the range of alpha particles in aqueous media is lower, around 100 μm. Therefore, the probability that an alpha particle is not detected is not negligible when the measurements are performed using PSm.

The ^{241}Am detection efficiency values obtained are around 75% in most cases, with the exception of PSm1. The differences related to the addition of the primary or the primary and the secondary solute are not significant, and plastic scintillation microspheres that contain PPO have the highest detection efficiency. As with ^{90}Sr/^{90}Y, these differences are too small to be attributed to differences in diameter or to different yields of the scintillator.

3.3.6. Spectra and SQP(E)

While information about the detection capabilities can be evaluated using the detection efficiency, information about the transformation of the energy of the particles into scintillation photons, can be obtained from the spectrum acquired (Figs. 4a–e), or from any parameter that is related to the spectrum distribution. This is the case for the quenching indicator *SQP*(*E*), obtained from the spectrum generated by the Compton electrons originated when the sample is irradiated by the external gamma-ray source (Table 2).

In the case of PSm1, the spectra are located at low channel numbers for all of the radionuclides (^{3}H, ^{14}C, ^{90}Sr/^{90}Y and ^{241}Am) and the *SQP*(*E*) values are the lowest for the evaluated compositions. This can be attributed to two factors: a poor scintillation yield of polystyrene and the inefficient detection of scintillation photons of low wavelength that are emitted by polystyrene.

When the primary solute is added (pT or PPO) to the PSm, the spectra move to higher channel numbers and the *SQP*(*E*) values also increase. This movement is more pronounced for PPO, likely because the wavelength of maximum intensity of PPO is closer to the wavelength of maximum detection of the photomultipliers.

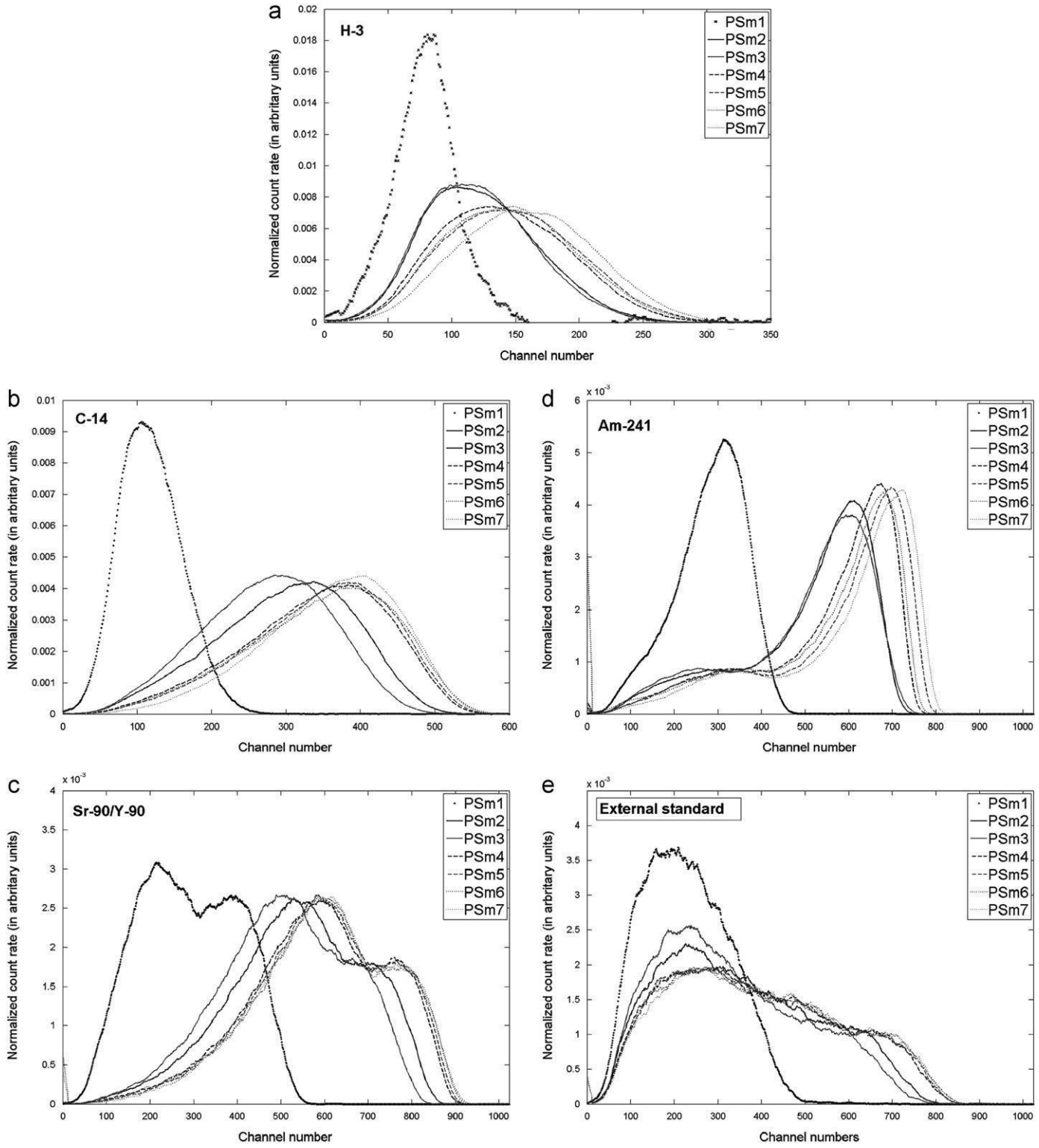

Fig. 4. Normalised count rate spectra obtained in the measurement of ^{3}H(a), ^{14}C(b), ^{90}Sr/^{90}Y(c), ^{241}Am(d) with the synthesised PSm. Spectra obtained when the microspheres are irradiated with an external gamma source (e).

When a secondary solute is added (POPOP or Bis-MSB), the situation improves again for both, the spectrum position and the *SQP*(*E*). In this case, there are no significant differences between the scintillators. For low and medium energy beta emitters, the spectra shift is correlated with an increase of detection efficiency.

Finally, the addition of naphthalene also produces an increase of the number of scintillation photons that are detected per disintegration, as seen from the increase in the *SQP*(*E*) and the movement of all the spectra to higher channel numbers. However, this shift to higher energies is not correlated with an increase of the detection efficiency which, on the contrary, decreases.

One special case is the spectrum of the alpha emitter, ^{241}Am, that was obtained with PSm3 (pT). This spectrum appears at the same position as the spectrum from PSm2 (PPO), whereas the

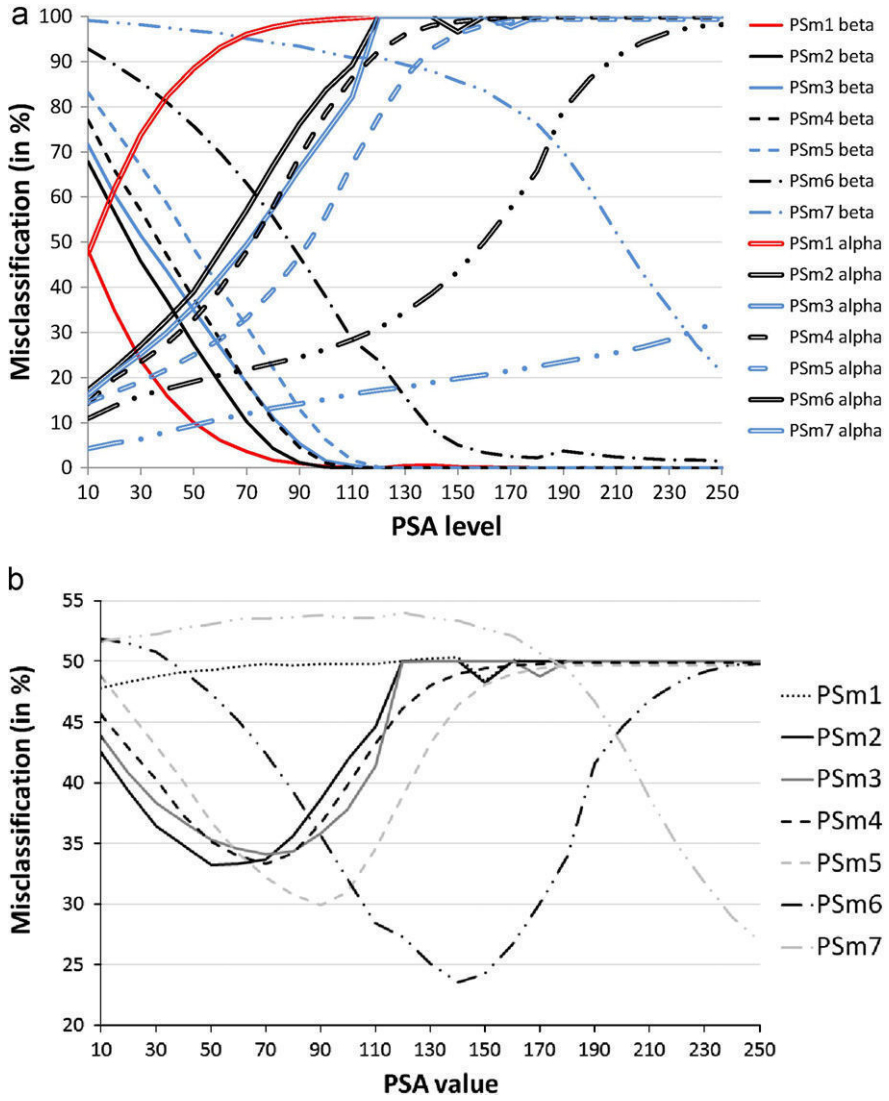

Fig. 5. Alpha and Beta misclassification for different PSA values (Fig. 5a). Mean misclassification at different PSA values (Fig. 5b).

spectra obtained with the other PSm that contain pT (PSm5 and PSm7) appear at higher channel numbers than those for PSm that contain PPO (PSm4 and PSm6). This difference can be attributed to the mechanism for deposition of the alpha particle energy in the scintillator and how this energy is transmitted within the scintillator components. In general, an alpha particle originates a higher density of ionisations and excitations in the scintillator than a beta particle. This behaviour leads to the formation of a higher proportion of triplet states and consequently, to a delay in the production of scintillation photons, which is the basis of discrimination between alpha and beta signals in organic scintillators (liquid, gel or plastic). In this case, the results suggest that the fluorescent solutes have an important role in the transfer processes of the energy that an alpha particle deposits in the scintillator.

3.4. Alpha/beta discrimination

The last evaluated property was the capability of the PSm to separate between signals produced by alpha and beta particles using the principle that beta pulses are faster than alpha pulses in organic scintillators. To evaluate the discrimination between alpha and beta particles, $^{90}Sr/^{90}Y$ and ^{241}Am solutions were measured in a commercial detector with pulse shape discrimination (Quantulus) using the PSm synthesised.

Fig. 5(a) shows the alpha and beta misclassifications obtained when using different PSA values whereas Fig. 5(b) shows the value of misclassification as the mean for alpha and beta particles. PSm1 was not capable to distinguish between alpha and beta particles, since alpha particles are usually misclassified. This can be due to the low number of scintillation photons that were emitted by PSm1 (the pulse tail may be very short) but may also be due to a very prompt emission by the polymer. As a result, the minimum mean error, 47.8%, is obtained at the lowest PSA value of 10.

When the primary solute is added, the discrimination improves slightly for alpha particles, and as a result, the misclassification of alpha particles at low PSA values decreases. However, an increase in the misclassification of beta particles at the same PSA values also occurs. It can be said that the addition of primary solute results in a higher production of scintillation photons, and also results in a delay of their temporal distribution (improving the alpha classification). However, the errors are still high with mean values of 33.2% and 34.1% for PSA values of 50 and 70 for PSm2 and P2m3, respectively.

The addition of POPOP as a secondary solute (PSm4) does not result in a significant improvement in the discrimination between

alpha and beta particles, although it seems that more pulses are classified as alpha. A minimum error of 33.3% at a PSA value of 70 is obtained. Better results are obtained using Bis-MSB since the misclassification curve moves significantly to the right because of an increasing delay in the pulses. The mean errors also improve; a minimum value of 29.9% at a PSA value of 90 is obtained.

Finally, the results for PSm6 and PSm7 show the influence of the addition of naphthalene to the microspheres. Naphthalene can act as a primary solute (maximum emission at 322 nm) or as a secondary solvent (due to its high concentration and to its electronic structure similar to that of an aromatic solvent), which delays the electronic energy transfer process between the primary solvent and the primary solute. As a result, the use of naphthalene is described for the enhancement of alpha and beta discrimination. In our case, the addition of naphthalene is translated in a movement of the misclassification curve to higher PSA values, which means that pulses are longer. In the case of PSm6, the errors decrease and a value of 24.3% is obtained at a PSA value of 150. In the case the PSm7, the beta particles are misclassified, whereas alpha particles are classified correctly. As a consequence, the lowest error, 27.0%, is obtained at the highest PSA value, 250.

In comparing the different solutes used, the pT/Bis-MSB pair induces a higher effect on the pulse delay and as a consequence, better results are obtained than with the use of the PPO/POPOP pair. This difference is enhanced when naphthalene is included, but in this case the effect is too excessive for the pT/Bis-MSB pair, and better results are obtained for the PPO/POPOP pair.

It must be noted that even after the improvement achieved by the addition of naphthalene, the errors still remain high in comparison with liquid scintillators. In this sense, it has also been documented that plastic scintillators present a light emission faster than the liquid scintillators, making more difficult the discrimination in the former. The characteristic of the detector, which is designed for measurements using liquid scintillators, with a discrimination parameter that is constant for all energies reduces the possibilities of an exhaustive analysis of the obtained signals. Moreover, ^{241}Am is not a pure alpha emitter and also emits conversion electrons and gamma-rays which could transfer energy to secondary electrons via Compton scattering and the photoelectric effect. If the alpha particle loses all its energy in the aqueous phase and does not reach the PSm, the electrons still may reach the scintillator and a beta signal is created. Thus, it is unlikely that all ^{241}Am disintegrations are classified as alpha when using PSm.

However, improvements of the discrimination between alpha and beta particles could be achieved using PSm with wider range of naphthalene concentrations, alpha emitters with a low probability of emission of conversion electrons and gamma-rays and electronic equipment with variable discrimination settings in function of energy.

4. Conclusions

A synthesis method based on the extraction/evaporation method has been successfully used to synthesise plastic scintillation microspheres. The full synthesis is performed in a period of one day, and the homogenisation of the microspheres results in a homogeneous mixture of spherical and smooth plastic scintillation microspheres that have a median diameter of approximately 130 μm. The composition of the microspheres depends on the polymeric solvent, the primary solute, the secondary solute and other additives that are added to the organic phase during the synthesis.

Among the microspheres that were synthesised with different compositions, PSm1 presented the worst results because of the emission of scintillation photons with a wavelength out of the optimal response range of the photomultipliers. Despite this fact, PSm1 is capable to detect even the low energy beta particles emitted by ^{3}H. The addition of a primary scintillation solute (PPO and pT) in PSm2 and PSm3 and a secondary solute (POPOP and Bis-MSB) in PSm4 and PSm5, respectively, lead to a significant increase of the detection efficiency and a shift of the spectra to higher channel numbers. The detection efficiency values obtained for ^{3}H, ^{14}C, ^{90}Sr/^{90}Y and ^{241}Am using these PSm are better than those obtained using commercial plastic scintillation microspheres. Moreover, the position of the spectra and the values of the parameter related with the position of the spectra induced by the external gamma-ray source (*SQP*(*E*)) reveal that the energy transfer (once the particle arrives to the microsphere) in the synthesised scintillators is better than in the commercial ones. The detection efficiencies of low-energy beta emitters are still much lower than in liquid scintillation counting but for high energy emitters the values are comparable.

The addition of naphthalene to the microspheres results in a small decrease in the detection efficiency, but in an improvement in the energy transmission, since the spectra move to higher channel numbers and the *SQP*(*E*) values are higher. Moreover, naphthalene produces a significant delay in the pulse duration, which is important for PSm6 and very important for PSm7. This delay enhances the capabilities of alpha/beta discrimination, although the obtained errors are still higher than 20%. In this sense, the evaluation of new compositions (different naphthalene quantities) and the analysis using more powerful electronic equipment will permit a more exhaustive analysis of the alpha/beta discrimination capabilities of the plastic scintillation microspheres.

Acknowledgments

The authors thank the Ministerio de Ciencia e Innovación (Spain) (MICINN) for financial support under CTM2008-01147 and CTM2011-27211 and Grant for research (CTM2008-01147), and Dr. Gemma Rauret for her support and years of participation on PSm development.

References

[1] R. Broda, P. Cassette, K. Kossert, Metrologia 44 (2007) S36.
[2] D.L. Horrocks, Applications of Liquid Scintillation Counting, Academic Press, New York San Francisco London, 1974.
[3] F. Schoenhofer, Science of the Total Environment 173/174 (1995) 29.
[4] M.F. L'Annunziata, Handbook of Radioactivity Análisis, 2nd ed., Academic Press, San Diego, 2003.
[5] EPA/Radiation Protection Program/Mixed Waste, 〈http://www.epa.gov/radiation/mixed-waste/〉 2011.
[6] Environmental Protection Agency (EPA), 40 CFR Part 266, Storage, Treatment, Transportation, and Disposal of Mixed Waste, Federal Register 66 95 2001.
[7] J. Hsu, J.K. Krieger, Liquid scintillation counting and organic scintillators. in: Proceedings of the International Conference on New Trends in Liquid Scintillation Counting and Organic Scintillators in 1989, Lewis Publishers, Chelsea, 1991, 557–600.
[8] A. Tahnassian, J. Eveloff, H. Tisdale, Liquid scintillation counting and organic scintillators. in: Proceedings of the International Conference on New Trends in Liquid Scintillation Counting and Organic Scintillators in 1989. Lewis Publishers, Chelsea, 1991, 573–575.
[9] D.A. Kalbhen, V.J. Tarkkanen, Proceedings of the International Conference on Advances in Scintillation Counting, Alberta, Canada, May 15–18, 1983, University of Alberta, 66–70.
[10] A. Tarancon, E. Alonso, J.F. Garcia, G. Rauret, Analytica Chimica Acta 471 (2002) 135.
[11] A. Tarancon, J.F. García, G. Rauret, Analytica Chimica Acta 463 (2002) 125.
[12] L. Santiago, A. Tarancón, H. Bagán, G. Rauret, J.F. Garcia, Nuclear Instruments and Methods http://dx.doi.org/10.1016/j.nima.2012.09.041, in press.
[13] A. Tarancon, A. Padro, J.F. Garcia, G. Rauret, Analytica Chimica Acta 538 (2005) 241.
[14] J.W. Grate, O.B. Egorov, M.J. O'Hara, T.A. DeVol, Chemical Reviews 108 (2008) 543.

[15] H. Bagán, S. Hartvig, A. Tarancón, G. Rauret, J.F. García, Analytica Chimica Acta 631 (2009) 229.
[16] H. Bagán, A. Tarancón, L. Stavsetra, G. Rauret, J.F. García, Analytica Chimica Acta 736 (2012) 30.
[17] H. Bagán, A. Tarancón, G. Rauret, J.F. García, Analytica Chimica Acta 686 (2011) 50.
[18] T.A. DeVol, O.B. Egorov, J.E. Roane, A. Paulenova, J.W. Grate, Journal of Radioanalytical and Nuclear Chemistry 249 (2001) 181.
[19] O.B. Egorov, M.J. O'Hara, J.W. Grate, Analytical Chemistry 78 (2006) 5480.
[20] Saint-Gobain Organic Scintillators, 〈http://www.detectors.saint.gobain.com/Organic-scintillators.apsx〉 2012.
[21] Detec-Rad Scintillators, 〈http://www.detec-rad.com/wiki/index.php/Scintillators〉 2008.
[22] S. Freiberg, X.X. Zhu, International Journal of Pharmaceutics 282 (2004) 1.
[23] C. Pinto Reis, R.J. Neufeld, J. Ribeiro António, F. Veiga, Nanomedicine: Nanotechnology, Biology and Medicine 2 (2006) 8.
[24] J.P. Rao, K.E. Geckeler, Progress in Polymer Science 36 (2011) 887.
[25] C. Berkland, K. Kim, D.W. Pack, Journal of Controlled Release 73 (2001) 59.
[26] M.J. Fulwyler, J.D. Perrings, L.S. Cram, Review of Scientific Instruments 44(2) (1973) 204.
[27] I. Tsagkatakis, S. Peper, R. Retter, M. Bell, E. Bakker, Analytical Chemistry 73 (2001) 6083.
[28] Y. Jin, M. Jiang, Y. Shi, Y. Lin, Y. Peng, K. Dai, B. Lu, Analytica Chimica Acta 612 (2008) 105.
[29] X. Hou, B. Liu, X. Deng, B. Zhang, J. Yan, Journal of Biomedical Materials Research Part A 83A (2007) 280.
[30] S. Freitas, H.P. Merkle, B. Gander, Journal of Controlled Release 102 (2005) 313.
[31] P.B. O'Donnell, J.W. McGinity, Advanced Drug Delivery Reviews 28 (1997) 25.
[32] J.B. Birks, The Theory and Practice of Scintillation Counting, Pergamon Press, Oxford, 1964.
[33] J.M. Pates, G.T. Cook, A.B. MacKenzie, C.J. Passo, Analyst 123 (1998) 2201.
[34] F.D. Brooks, R.W. Pringle, B.L. Funt, IEEE Transactions on Nuclear Science NS-7 (1960) 35.
[35] Quantulus™ Instrument Manual, PerkinElmer Life Sciences.
[36] A. Savitzky, J.M.E. Golay, Analytical Chemistry 36 (8) (1964) 1627.
[37] A. Tarancon, G. Rauret, J.F García, Analytica Chimica Acta 590 (2) (2007) 232.
[38] Hamamatsu Photonics, Photomultiplier Tubes: Basics and Applications, 3rd ed., 2007.
[39] B.P. Wittmershaus, T.T. Baseler, G.T. Beaumont, Y. Zhang, Journal of Luminescence 96 (2002) 107.

Chapter 3.1

Synthesis of plastic scintillation microspheres through the organic solvent extraction/evaporation methodology

---

3.1.1. Synthesis of plastic scintillation microspheres: Evaluation of Scintillators.

3.1.2. Synthesis of plastic scintillation microspheres: Alpha/beta discrimination.

3.1.3. Influence of preparation parameters on the synthesis of plastic scintillation microspheres and evaluation of sample preparation.

Applied Radiation and Isotopes 93 (2014) 18–28

Contents lists available at ScienceDirect

Applied Radiation and Isotopes

journal homepage: www.elsevier.com/locate/apradiso

Synthesis of plastic scintillation microspheres: Alpha/beta discrimination

L.M. Santiago, H. Bagán, A. Tarancón*, J.F. Garcia

Department of Analytical Chemistry of the University of Barcelona, Diagonal 645, E-08028 Barcelona, Spain

HIGHLIGHTS

- Plastic scintillation microspheres for α/β discrimination have been synthesised.
- The energy transfer process in PSm with different compositions has been investigated.
- The α/β discrimination capabilities of two commercial detectors have been evaluated.
- 2% and 0.5% of misclassifications for β and α radionuclides have been achieved respectively.

ARTICLE INFO

Available online 24 April 2014

Keywords:
Plastic scintillation
Mixed waste
Microspheres
Microparticle synthesis
Radioactivity
α/β discrimination

ABSTRACT

Plastic scintillation microspheres (PSm) have been developed as an alternative for liquid scintillation cocktails due to their ability to avoid the mixed waste, besides other strengths in which the possibility for alpha/beta discrimination is included. The aim of this work was to evaluate the capability of PSm containing two combinations of fluorescence solutes (PPO/POPOP and pT/Bis-MSB) and variable amounts of a second organic solvent (naphthalene) to enhance the alpha/beta discrimination. Two commercial detectors with different Pulse Shape Discrimination performances (Quantulus and Triathler) were used to evaluate the alpha/beta discrimination. An optimal discrimination of alpha/beta particles was reached, with very low misclassification values (2% for beta particles and 0.5% for alpha particles), when PSm containing PPO/POPOP and between 0.6 and 2.0 g of naphthalene were evaluated using Triathler and the appropriate programme for data processing.

1. Introduction

The accurate and precise determination of the activity of samples in which alpha and beta type signals are mixed currently represents a challenge in the field of radiation detection. This challenge exists for the detection of neutron and gamma activities (Flaska and Pozzi, 2007; Gamage et al., 2011; Klein and Neumann, 2002; Zaitseva et al., 2012) and for the quantification of mixtures of alpha- and beta-emitting radionuclides in different types of samples from natural or artificial origins and from different fields (Dávila Rangel et al., 2002; Happel et al., 2004; Kleinschmidt, 2004; McKlveen and McDowell, 1984; Pates et al., 1998; Salonen, 1993, 1997; Sanchez-Cabeza and Pujol, 1995; Wierczinski et al., 1996). In all these cases, the solution proposed for the determination is the use of organic scintillators combined with the discrimination between the signals generated based on the different temporal distribution of pulses (i.e. pulse shape discrimination (PSD)) because in this way, complex separations can be avoided (Bagán et al., 2011).

When measured with organic scintillators, the signals generated by alpha and high-energy beta particles appear in the same energy region of a multichannel analyser even though the energy of alpha particles is approximately five times higher than that of the beta particles. This signal overlap is because the alpha particles have higher linear energy transfer than the beta particles; therefore, the passage of the alpha particles through the scintillator leads to a greater specific ionisation of solvent molecules; this ionisation does not ultimately result in the production of photons. Moreover, the proportion of excited triplet states is also higher for the alpha particles than for the beta particles, in which the proportion of singlet excitations is higher. The recombination of two triplet states leads to the relaxation of states and the emission of photons. This process is delayed in time relative to the relaxation of singlet excited states. The measurement of the delayed component of the photon emission of alpha particles is the basis for the pulse shape discrimination technique described by various authors (Birks, 1964; Brooks, 1979; L'Annunziata, 2013; McDowell and McDowell, 1991; Moebius and Moebius, 2012) and implemented in commercial detectors. In commercial detectors, the energy and

* Corresponding author. Tel.: +34 934021281; fax: +34 934021233.
E-mail address: alex.tarancon@ub.edu (A. Tarancón).

http://dx.doi.org/10.1016/j.apradiso.2014.04.002
0969-8043/

amplitude of each pulse are measured. Depending on the electronics implemented, the signals can be classified with regard to a discrimination parameter as alpha or beta in two dimensional spectra of counts as a function of energy (Quantulus or Tricarb detectors), or the signals can be classified with regard to their energy and duration in a three-dimensional spectrum (Triathler and Hidex SL300 detectors).

The use of liquid scintillators (LSs) combined with pulse shape discrimination has been widely applied to the quantification of mixtures of alpha and beta radionuclides and demonstrates low misclassifications if the appropriate scintillator is used, if the calibration process is realistic and if the electronic setup is optimised correctly. However, measurement with liquid scintillators presents an important drawback, which is the generation of mixed waste (Hsu and Krieger, 1991; Tahnassian et al., 1991); this type of waste deserves special regulations for its disposal because of its characteristics, radioactive and hazardous (EPA, 2001, 2006). The use of plastic scintillation microspheres (PSm), among other configurations that use plastic scintillators (sheets or containers), can be considered to overcome this drawback. PSm are a solid solution of fluorescent solutes in a polymeric solvent and can have a diameter in the range of tens or hundreds of micrometres. Because the polymer is completely polymerised, PSm have no reactivity; thus, PSm are neither flammable nor toxic, and because the PSm are solid, the sample and the scintillator microspheres can be segregated by filtration after the measurement (Tarancon et al., 2002, 2004). Concerning the measurements with PSm, they are very similar to that of liquid scintillators (i.e. preparation, sample volume, vials and detector). PSm are mixed with an aqueous sample to yield a heterogeneous mixture. In this heterogeneous mixture, a particle emitted by a radionuclide must travel through the sample medium until it reaches the surface of the microsphere in which is detected. The detection efficiency for measurements with PSm depends on the diameter of the microspheres and the energy of the radioactive particle. Therefore the detection efficiency is lower to that of liquid scintillation for low-energy beta emitters, slightly lower for alpha and medium-energy beta emitters and similar for high-energy beta emitters (Sanz and Kossert, 2011; Santiago et al., 2013b).

From the perspective of the mechanism, because the composition of PSm is similar to that of LSs, it can be expected that the energy transfer mechanism should be similar. However, the rigid structure of the solid scintillator may affect the relaxation process for the triplet states of the solvent. For example, previous tests have shown that discrimination between beta and alpha particles is possible with commercial PSm (with a commercial detector), but with higher misclassifications than with LSs. However, the limited information about the energy transfer process in organic scintillators, the limited availability of commercial PSm and the limited setup options or commercial detection equipment hide the reasons for the high rate of misclassifications. The objective of this study is to obtain information about the energy transfer process in PSm though the evaluation of the alpha/beta discrimination obtained when using PSm of different compositions.

To this end, PSm of different compositions have been synthesised through an evaporation/extraction method (Santiago et al., 2013a). The synthesised PSm are composed of polystyrene (PS) as the polymeric organic solvent; 2,5-diphenyloxazol (PPO) and *p*-terphenyl (pT) as primary solutes; and 1,4-bis(5-phenyloxazol-2-yl) (POPOP) and 1,4-bis[2-methylstyryl] benzene (Bis-MSB) as secondary solutes. To improve the pulse shape discrimination, various amounts of second organic solvent were added in each synthesis. Of the different compounds described in the literature, naphthalene is well known to be a secondary solvent capable of enhancing discrimination between alpha and beta signals in organic scintillators because naphthalene has a long decay time (i.e. 96 ns) (Hallam and Birks, 1978; Rodriguez Barquero and Grau Carles, 1998; Yang et al., 1990). The addition of naphthalene to the scintillator enhances the formation of excited triplet states; this enhancement leads to an increase in the delayed component of the scintillation pulse. As described above, this increase leads to a greater increase in the pulse duration of alpha signals than beta signals and consequently leads to a better separation of alpha and beta disintegration events. Measurements with PSm of different compositions (i.e. with variable capabilities for alpha/beta discrimination) in commercial detectors with different pulse shape discrimination performances (Quantulus and Triathler) can be used to define some of the aspects that cause the high misclassification in PSm.

2. Experimental

2.1. Reagents

All the reagents used were of analytical or scintillation grade. Polystyrene (PS) (MW 250,000 g/mol) was provided by Acros Organics (Geel, Belgium). Fully hydrolysed poly(vinyl alcohol) (PVA) was purchased from Merck (Schuchardt OHG, Germany). Dichloromethane, naphthalene and 2,5-diphenyloxazol were supplied by Merck (Darmstadt, Germany). 1,4-bis(2-methylstyryl)-benzene and *p*-terphenyl were purchased from Fluka Analytical (Buchs, Switzerland). 1,4-bis(5-phenyloxazol-2-yl)benzene was supplied by the Montedison Group, Division Chimica (Milan, Italy).

Radioactive samples were prepared in 6 mL Pico Prias polyethylene vials (PerkinElmer, USA) from the following active stock solutions: a ^{3}H solution (HTO) with a concentration of 3.94(14) kBq/g in deionised water prepared from a standard of 69.8(24) kBq/g provided by Eckert-Ziegler (Berlin, Germany); a ^{14}C solution (labelled glucose) of 114.6(29) Bq/g prepared from a standard of 44.7(11) kBq/g from Amersham International (Buckinghamshire, UK) in a carrier solution of 50 µg/g of glucose and 1 mg/g of formaldehyde in deionised water; a $^{90}Sr/^{90}Y$ active stock solution (Sr^{2+} and Y^{3+}) of 37.22(28) Bq/g prepared from a standard of 4.071(31) kBq/g from Amersham International in 0.1 M HCl; and finally, a ^{241}Am solution (Am^{3+}) of 185.5(19) Bq/g prepared from a standard of 55.44(55) kBq/g supplied by Amersham International in 0.5 M HCl in deionised water.

2.2. Equipment

An AJ2-HS centrifuge (from Beckman-Coulter Inc., Brea, USA) was used to centrifuge the measurement vials and an Ultrasons-P ultrasonic bath (from JP Selecta, Abrera, Spain) was used to sonicate the vials (40 kHz).

The measurements of radioactive samples were performed with a 1220 Quantulus detector and with a Triathler detector. The 1220 Quantulus liquid scintillation spectrometer (from PerkinElmer, USA) is equipped with logarithmic amplification, a multichannel analyser with 4096 channels distributed into four segments of 1024 channels (four spectra), and it is capable of alpha–beta discrimination. Background reduction is achieved by a combination of passive shielding and active shielding based on a guard detector. The Triathler liquid scintillation spectrometer (from Hidex, Turku, Finland) is a single-sample detector equipped with one photomultiplier, a multichannel analyser with 2048 channels (one spectrum of 64 energy channels and 32 time channels) and has alpha–beta discrimination capabilities.

A LS 13 320 single-wavelength laser diffraction particle size analyser (from Beckman-Coulter Inc., Brea, USA) was used to determine the size distribution of plastic scintillation microspheres.

Secondary-electron images of the PSm were obtained with a Stereoscan S-360 scanning electron microscope.

2.3. Synthesis procedure.

Two series of plastic scintillation microspheres (seven different compositions with PPO/POPOP and eight compositions with pT/Bis-MSB as primary and secondary fluorescent solutes, respectively) were synthesised with increasing quantities of naphthalene (the compositions are summarised in Tables 1 and 2) (Santiago et al., 2013a). All the syntheses were performed under the same conditions, including the temperature of the aqueous/organic mixture, type and speed of agitation, organic/aqueous phase proportion and proportions of the components in both phases. Only the quantity of naphthalene was changed between syntheses.

2.4. Radioactivity measurements

2.4.1. Sample preparation

The measurement vials were prepared by adding 1.5 g of the synthesised PSm and 0.75 mL of the counting solution (active or blank solution) into a 6 mL polyethylene scintillation vial. After preparation, the vials were shaken ultrasonically for 2 min, and then they were centrifuged for 10 min at 16.7 Hz to ensure homogenisation and to improve the efficiency and reproducibility of the measurement.

The counting solutions were prepared by diluting a known quantity of active stock solution (^{3}H, ^{14}C, ^{90}Sr/^{90}Y and ^{241}Am) in a known volume of carrier solution to obtain the desired activity in the measurement sample. The activities in the measurement samples were approximately 450 Bq for ^{3}H, 35 Bq for ^{14}C, 4 Bq for ^{90}Sr/^{90}Y and 32 Bq for ^{241}Am. A blank counting solution was prepared for each active measurement sample by the addition of carrier solution instead of active stock solution. All the solutions were prepared by weight.

2.4.2. Measurements

The measurements with the Quantulus detector were performed with the "low" coincident bias and multichannel analyser (MCA) in the "C14" configuration. The counting times were 60 min for the blank, ^{3}H, ^{14}C and ^{241}Am samples and 90 min for the ^{90}Sr/^{90}Y samples. The spectrum produced by an external standard gamma source (^{152}Eu) was obtained by measuring for 10 min. The alpha/beta discrimination capabilities were evaluated by the measurement of the background, ^{90}Sr/^{90}Y and ^{241}Am samples for 20 min for each vial and for each value of the PSA parameter (ranging from 10 to 250 in intervals of 10 units). The PSA is a parameter of Quantulus detector that can vary from 10 to 250 (in a unity interval). The user defines the PSA value before counting and then the alpha/beta discrimination is performed through the comparison between this value and the ratio between the total area of the pulse to the area of the tail of the pulse. If the ratio is higher or lower than the value of the PSA parameter, the event is classified as beta (in the first half of the first MCA) or as alpha (in the second half of the first MCA). As a result, two spectra (i.e. beta and alpha) are obtained. In all cases, the measurement vials were stored in the dark for 2 h before counting.

The background, ^{90}Sr/^{90}Y and ^{241}Am samples were also measured with the Triathler detector for 120 min for each vial with the predefined ^{222}Rn protocol.

Table 1
Components of the PSm containing PPO and POPOP.

10 g PS, 0.2 g PPO, 0.005 g POPOP
10 g PS, 0.6 g naphthalene, 0.2 g PPO, 0.005 g POPOP
10 g PS, 0.8 g naphthalene, 0.2 g PPO, 0.005 g POPOP
10 g PS, 1.2 g naphthalene, 0.2 g PPO, 0.005 g POPOP
10 g PS, 2.0 g naphthalene, 0.2 g PPO, 0.005 g POPOP
10 g PS, 2.5 g naphthalene, 0.2 g PPO, 0.005 g POPOP
10 g PS, 3.0 g naphthalene, 0.2 g PPO, 0.005 g POPOP

Table 2
Components of the PSm containing pT and Bis-MSB.

10 g PS, 0.2 g pT, 0.005 g Bis-MSB
10 g PS, 0.01 g naphthalene, 0.2 g pT, 0.005 g Bis-MSB
10 g PS, 0.05 g naphthalene, 0.2 g pT, 0.005 g Bis-MSB
10 g PS, 0.1 g naphthalene, 0.2 g pT, 0.005 g Bis-MSB
10 g PS, 0.3 g naphthalene, 0.2 g pT, 0.005 g Bis-MSB
10 g PS, 0.5 g naphthalene, 0.2 g pT, 0.005 g Bis-MSB
10 g PS, 0.8 g naphthalene, 0.2 g pT, 0.005 g Bis-MSB
10 g PS, 1.2 g naphthalene, 0.2 g pT, 0.005 g Bis-MSB

2.4.3. Data treatment

The spectrum obtained in each measurement was smoothed with a Savitzky–Golay algorithm (Savitzky and Golay, 1964). The net spectrum was obtained by subtracting the spectrum of the corresponding blank solution. The detection efficiency was calculated from the ratio between the net counts over the whole spectrum and the activity added to the measurement vial.

The SPQ(E) parameter was calculated by the detector for each sample and corresponds to the end-point channel that limits the 99.75% of the total counts of the spectrum generated by the external gamma source.

If signals were classified as alpha or beta, the misclassification was calculated to evaluate the capability to discriminate between alpha and beta events. The misclassification of alpha events was defined to be the efficiency for alpha particles relative to the sum of the efficiencies for alpha and beta particles in the beta spectrum. The misclassification of beta events was defined to be the efficiency for beta particles relative to the sum of the efficiencies for alpha and beta particles in the alpha spectrum.

3. Results and discussion

The synthesised PSm were evaluated with regard to their morphologies, radiometric performances and alpha/beta discrimination capabilities.

The morphologies were evaluated through analysis of the scanning electron microscopy images of the PSm and through analysis of the particle size distribution with a particle size analyser.

The radiometric performances were evaluated through measurements of samples containing a weak beta emitter (^{3}H, E_{max}=18.6 keV), a medium-energy beta emitter (^{14}C, E_{max}=156.5 keV), a high-energy beta emitter (^{90}Sr/^{90}Y, E_{max}=2279.8 keV) and an alpha emitter (^{241}Am, E_{max}=5637.82 keV). The evaluation comprises analysis of the detection efficiency for all the radionuclides and analysis of the yield for light emission from the position of the spectrum and the position of the spectrum generated by the external gamma-ray source (the SQP(E) parameter of the Quantulus detector).

The capability to discriminate between alpha and beta particles was evaluated by determining the misclassification of alpha and beta events for measurements of a high-energy beta emitter (^{90}Sr/^{90}Y) and an alpha emitter (^{241}Am) with the Quantulus and in the Triathler detector.

3.1. Morphology and particle size analysis

The images obtained by scanning electron microscopy show that the PSm containing PPO/POPOP or PT/Bis-MSB as fluorescent solutes are spherical and smooth in most cases (Fig. 1). With the

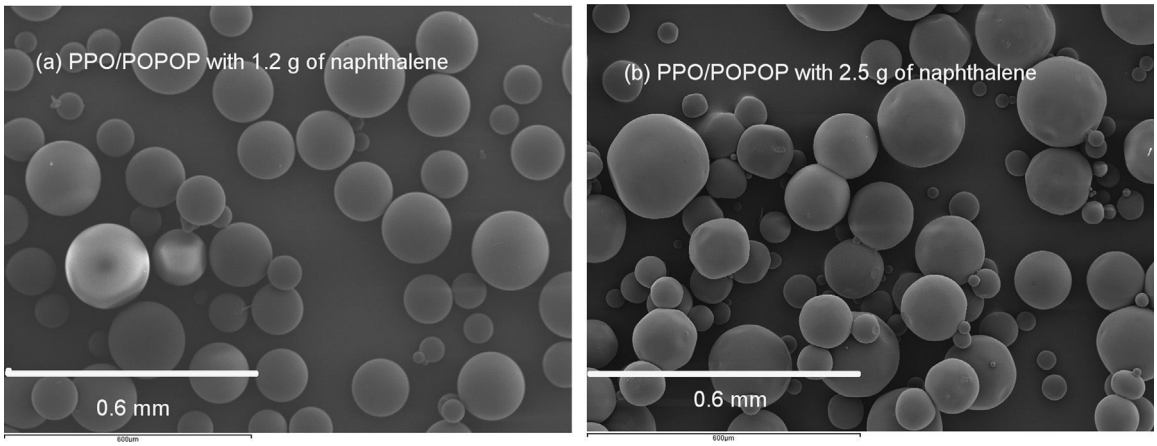

Fig. 1. Plastic scintillation microspheres containing polystyrene, PPO, POPOP and 1.2 g (a) and 2.5 g (b) of naphthalene.

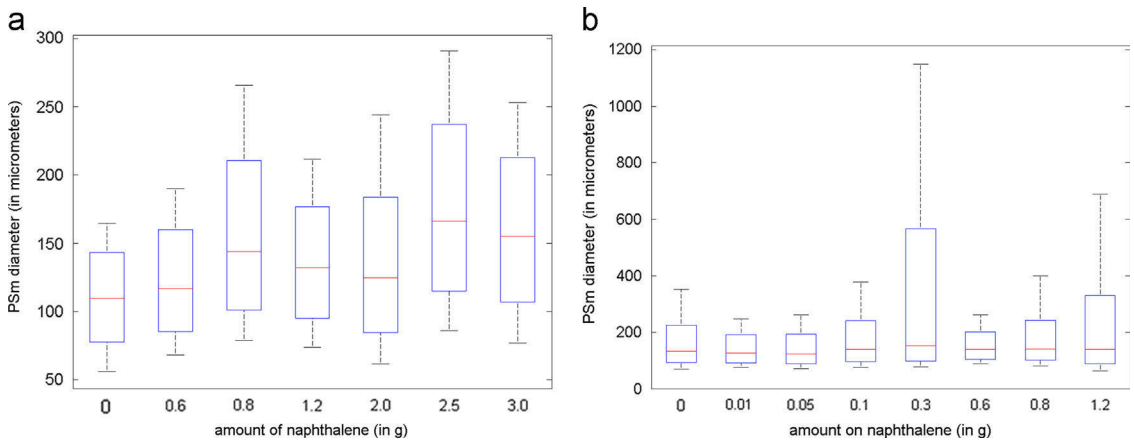

Fig. 2. Boxplots of the particle size distribution of the synthesised PSm: (a) PSm containing PPO and POPOP; and (b) PSm containing pT and Bis-MSB.

exception of PSm containing more than 2.5 g of naphthalene, the addition of increasing quantities of naphthalene apparently did not cause any significant change in the morphology of the microspheres. In the exceptions, the particles are flatter; this flatness may result from the slow extraction of the organic solvent. The slow extraction causes the microspheres to spend a longer time in an embryonic state and to have more collisions with other microspheres throughout the agitation.

Although SEM images make possible to obtain an indication of the size uniformity of the PSm, this variability is better evaluated by the particle size analysis performed with the size analyser. The values for the particle size distributions of all the synthesised PSm are shown in Fig. 2 and are presented in a boxplot.

It can be observed that PSm synthesised with PPO/POPOP have a median diameter between 110 and 160 μm and have a small increase in diameter when the amount of naphthalene added increases. The amplitudes of the distributions are similar in all cases with 90% of the microspheres having diameters between 60 and 250 μm. The microspheres with a sharper diameter distribution are those that having less amount of naphthalene. For the PSm containing pT and Bis-MSB, the median diameters are independent of the amount of naphthalene and are approximately 150 μm. However, the diameter distribution generally presents non-homogenous behaviour because the PSm with 0.01, 0.05 and 0.6 g of naphthalene have diameter distribution similar to that of PPO/POPOP microspheres whereas the PSm with 0, 0.1 and 0.8 g of naphthalene have wider distributions, including PSm with diameters of approximately 400 μm. Finally, large agglomerations appear for PSm with 0.3 g and 1.2 g of naphthalene.

3.2. Radiometric capabilities

3.2.1. Background

The background values do not seem to be affected by the addition of naphthalene (Tables 3 and 4). Mean values of 1.23(21) cpm for the PSm containing PPO/POPOP and 1.10(16) cpm for the PSm containing pT/Bis-MSB were obtained.

3.2.2. ^{3}H detection efficiency

Tables 3 and 4 show the values obtained for the detection efficiency when ^{3}H samples were measured with the synthesised PSm, i.e. PSm containing PPO/POPOP or pT/Bis-MSB, respectively, and increasing quantities of naphthalene.

For the PSm synthesised with PPO and POPOP as fluorescent solutes, the highest detection efficiency is obtained for the PSm without naphthalene whereas the lowest detection efficiencies correspond to the PSm with higher amounts of naphthalene (2.5 and 3.0 g). Moreover, the PSm with lower mean diameter (i.e. 0, 0.6, 1.2 and 2.0 g of naphthalene) have detection efficiencies larger than 1% whereas the PSm synthesised with higher mean diameters (i.e. 0.8, 2.5 and 3.0 g of naphthalene) have detection efficiencies smaller than 1%.

For the PSm containing pT and Bis-MSB, an important decrease can be observed in the detection efficiency when naphthalene is added. A constant ^{3}H detection efficiency of 0.77(2)% is obtained for PSm with 0.05 g or more of naphthalene and this behaviour does not seem to be correlated with the size of microspheres.

Table 3
Values for the background, ^{3}H, ^{14}C, $^{90}Sr/^{90}Y$, and ^{241}Am detection efficiencies and the SQP(E) for the PSm containing PPO and POPOP in a Quantulus detector.

Naphthalene (g)	BKG (cpm)	^{3}H (%)	^{14}C (%)	$^{90}Sr/^{90}Y$ (%)	^{241}Am (%)	SQP (E)
0	1.10 (5)	1.19 (7)	51.2 (4)	180.6 (9)	76.7 (6)	782 (5)
0.6	1.36 (8)	1.10 (2)	49.6 (6)	185.6 (25)	76.2 (9)	781 (2)
0.8	0.97 (15)	0.96 (1)	47.3 (6)	174.9 (23)	72.4 (9)	791 (5)
1.2	1.10 (13)	1.03 (2)	48.7 (6)	180.9 (27)	74.9 (29)	791 (4)
2.0	1.09 (16)	1.12 (2)	51.1 (6)	180.7 (24)	77.3 (9)	796 (4)
2.5	1.50 (18)	0.64 (1)	39.9 (5)	191.2 (25)	74.3 (9)	767 (7)
3.0	1.46 (18)	0.72 (2)	44.0 (6)	194.1 (26)	64.3 (9)	776 (0)

Table 4
Values for the background, ^{3}H, ^{14}C, $^{90}Sr/^{90}Y$, and ^{241}Am detection efficiencies and the SQP(E) for the PSm containing pT and Bis-MSB in a Quantulus detector.

Naphthalene (g)	BKG (cpm)	^{3}H (%)	^{14}C (%)	$^{90}Sr/^{90}Y$ (%)	^{241}Am (%)	SQP (E)
0	1.16 (14)	1.14 (3)	49.8 (3)	178.7 (26)	73.2 (14)	783 (4)
0.01	1.18 (16)	0.90 (2)	48.9 (6)	–	75.5 (9)	781 (2)
0.05	1.19 (16)	0.78 (1)	48.7 (6)	–	76.4 (9)	771 (5)
0.1	1.21 (16)	0.74 (1)	46.4 (6)	187.8 (25)	72.6 (9)	747 (9)
0.3	1.09 (16)	0.77 (11)	45.9 (6)	178.7 (24)	72.8 (9)	761 (2)
0.6	0.89 (14)	0.79 (12)	44.4 (6)	181.6 (24)	70.9 (9)	791 (9)
0.8	0.81 (13)	0.75 (1)	45.3 (6)	182.8 (24)	69.0 (8)	782 (4)
1.2	1.28 (21)	0.82 (1)	45.9 (17)	178.1 (30)	70.9 (39)	790 (5)

From the results obtained for both types of PSm, it can be concluded that the presence of naphthalene causes a small decrease in the ^{3}H detection efficiency. This effect is more relevant for the microspheres containing pT and Bis-MSB, likely because naphthalene modifies the energy transfer process between the polystyrene and the *p*-terphenyl molecules. However, this effect is small, and it appears to be combined with the efficiency variations caused by changes in the diameters of the PSm and therefore in the probability that a beta particle interacts with the medium and does not reach the surface of the microsphere (i.e. particle quenching).

3.2.3. ^{14}C detection efficiency

^{14}C detection efficiencies shown in Tables 3 and 4 exhibit similar behaviours to those obtained for ^{3}H; however, in this case, the decrease in the detection efficiency with the addition of naphthalene is much smaller and can also be attributed to particle quenching due to changes in the diameters of the PSm or in the packaging of microspheres.

In this sense, in the PSm containing PPO and POPOP, the detection efficiencies seem to be slightly correlated with the sizes of the PSm. The higher detection efficiencies 51.2(4)%, 49.6(6)%, 48.7(16)% and 51.1(6)% are obtained for the synthesis with 0, 0.6, 1.2 and 2.0 g of naphthalene, respectively, and correspond to the PSm with smaller diameters. In contrast, the PSm containing 0.8, 2.5 and 3.0 g of naphthalene exhibit lower detection efficiencies (47.3(6)%, 39.9(5)% and 44.0(6)%, respectively) and show the highest diameters. In this sense, the PSm with 2.5 g of naphthalene exhibit the largest median diameter (165 μm) and the lowest detection efficiency (39.9(5)%); however, these values do not correspond to the PSm with a higher amount of naphthalene (i.e. 3.0 g)

For the PSm containing pT and Bis-MSB, the addition of small quantities of naphthalene (i.e. less than 0.05 g) causes an important decrease in the detection efficiency; however, for higher quantities of naphthalene, the detection efficiency becomes constant.

3.2.4. $^{90}Sr/^{90}Y$ detection efficiency

For $^{90}Sr/^{90}Y$, the detection efficiencies are approximately 180%, and the observed variation does not seem to be associated with the diameters of the microspheres or with the amount of naphthalene. This result is most likely because the beta particles emitted by ^{90}Sr and ^{90}Y are too energetic to be affected by a small variation in the diameter of the PSm or by slight changes in the electronic transfer process and are most likely to be affected by variations in the sample preparation (i.e. degree of packaging).

3.2.5. ^{241}Am

As for $^{90}Sr/^{90}Y$, the detection efficiencies for ^{241}Am remain constant with the increase in naphthalene (approximately 72% in both types of PSm) and are not correlated with the variation in the diameters of the PSm.

3.2.6. Light emission: spectrum and SQP(E)

The yield for light production by the PSm can be evaluated from two experimental parameters obtained during the measurements of the active samples: the position and shape of the spectrum for each radionuclide and the SQP(E) parameter derived from the spectrum of the Compton electrons generated when the sample is irradiated by the external gamma source. In both parameters the relative position of the spectrum gives information on the number of photons that emerge from the measurement vial. A shift of the spectrum of the radionuclide to lower energies or a decrease in the SPQ(E) parameter is caused by a quenching effect (chemical, colour or optical). The spectra obtained in the measurements of ^{3}H, ^{14}C, $^{90}Sr/^{90}Y$ and ^{241}Am samples are shown in Fig. 3 (for PPO/POPOP PSm as an example) whereas the SQP(E) values are shown in Tables 3 and 4.

The obtained results show that an increase in the concentration of naphthalene in the synthesised PSm does not produce a significant shift in the spectra to higher or lower energies. In the same way, the variations in the value of the SPQ(E) for the evaluated PSm have no correlation with the quantity of naphthalene added in each synthesis. It can be concluded that the small variations observed in the spectral positions and in the SQP (E) values can be attributed to other quenching factors (most likely, optical quenching because of variations in the packaging in the sample preparation step).

In the $^{90}Sr/^{90}Am$ and ^{241}Am spectra, a peak can be observed in the very first channels for both types of PSm. The intensities of these signals increase with the amount of naphthalene added and are higher for alpha emitters than for beta emitters. These signals could be related to a luminescence effect or to events that were not classified correctly in the multichannel analyser (MCA) because of the shape of the pulse.

3.3. α/β discrimination

Two different commercial detectors (Quantulus and Triathler) have been used to evaluate the capabilities of the PSm to discriminate between alpha and beta signals as a function of the composition of the PSm. In both cases, the separation is based on an analysis of the temporal pulse distribution produced by alpha and beta particles in the scintillator.

3.3.1. Alpha/beta discrimination with Quantulus

To evaluate the behaviours of the two different types of synthesised PSm with increasing quantities of naphthalene, a background sample, an $^{90}Sr/^{90}Y$ (beta emitter) sample and an ^{241}Am (alpha emitter) sample were measured for different values of the PSA parameter (from 10 to 250). Once the measurements were performed, the proportion of correctly classified beta and

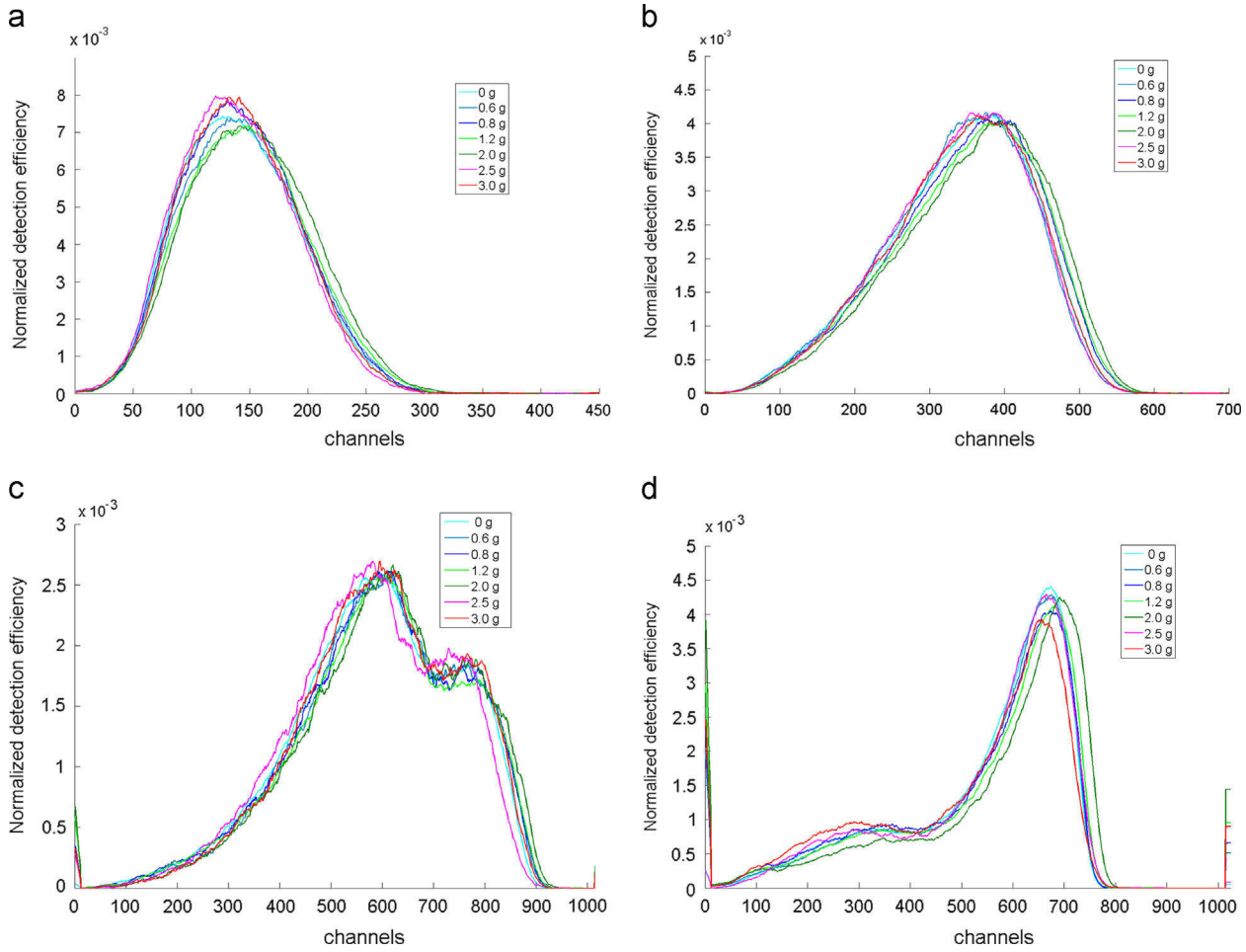

Fig. 3. Normalised spectra of ^{3}H(a), ^{14}C(b), ^{90}Sr/^{90}Y(c) and ^{241}Am (d) samples measured with PSm containing PPO and POPOP and increasing amounts of naphthalene in the Quantulus detector.

alpha signals were determined. Fig. 4 shows these results for the amount of misclassification for beta and alpha particles. The general trend for the PSm containing PPO and POPOP is that for a define value of the PSA parameter, the misclassification of beta particles increases and the misclassification of alpha particles decreases as the amount of naphthalene increases.

For beta particles, when no naphthalene is added, the classification is completely correct for PSA values larger than 100. When naphthalene is added, the number of beta particles that are misclassified increases and even in the case with the highest amount of naphthalene (i.e. 3 g) there is a small proportion of beta particles that are always wrong classified. This misclassification is because the addition of naphthalene causes a delay in the photon emission and consequently, more pulses are classified as alpha.

In contrast, when no naphthalene is added, the classification of alpha particles is incorrect, and even at very low PSA values, there is a relevant proportion of alpha particles that are always misclassified. As for beta particles, the addition of naphthalene causes a delay in the pulses, and consequently, the proportion of misclassified alpha particles decreases. However, even under the best conditions, there is still a proportion of alpha particles that are always misclassified (approximately 10% when 3 g of naphthalene is added and the PSA value is 10). Most likely, these signals are those at the tail of the spectrum of the alpha emitter. This tail corresponds to the conversion electrons and gamma-rays also emitted by ^{241}Am and detected when the concomitantly emitted alpha particle does not achieve a PSm. Note that in measurements with PSm of these diameters (larger than 50 μm) there is a probability that an alpha particle interacts with the medium before reaching the surface of a PSm and does not produce a scintillating signal. This probability is the reason why the detection efficiency for alpha emitter is less than 100%.

The behaviour observed for the PSm containing pT and Bis-MSB was similar; however, in this case, the misclassification of beta particles was higher whereas the misclassification of alpha particles was improved relative to the PPO/POPOP microspheres. Under closer examination of results, it can be seen that when no naphthalene is added, the beta particles are correctly classified for PSA values larger than 120. Moreover, there is a misclassification of at least 20% for the alpha particles at the lowest value of the PSA parameter (i.e. 10) and this value increases until the alpha particles are completely misclassified for values of the PSA parameter larger than 120. This situation changes significantly when even small amounts of naphthalene are added. For the beta emitters, the number of wrongly classified beta particles increases, and even at very high values of the PSA parameter, the misclassification is significant (e.g. the misclassification when 1.2 g of naphthalene is added is approximately 20% at the maximum PSA value). As with the PPO/POPOP microspheres, the situation is reversed for the alpha emitter because the particle classification improves due to the delay of pulses. In this case, it can be observed that at worst conditions for alpha particle classification, the highest values of the PSA parameter, there are a significant number of signals that are correctly classified. However, at the lowest PSA value, there is a proportion (approximately 10%) that is still classified as beta; most likely, this classification is because this

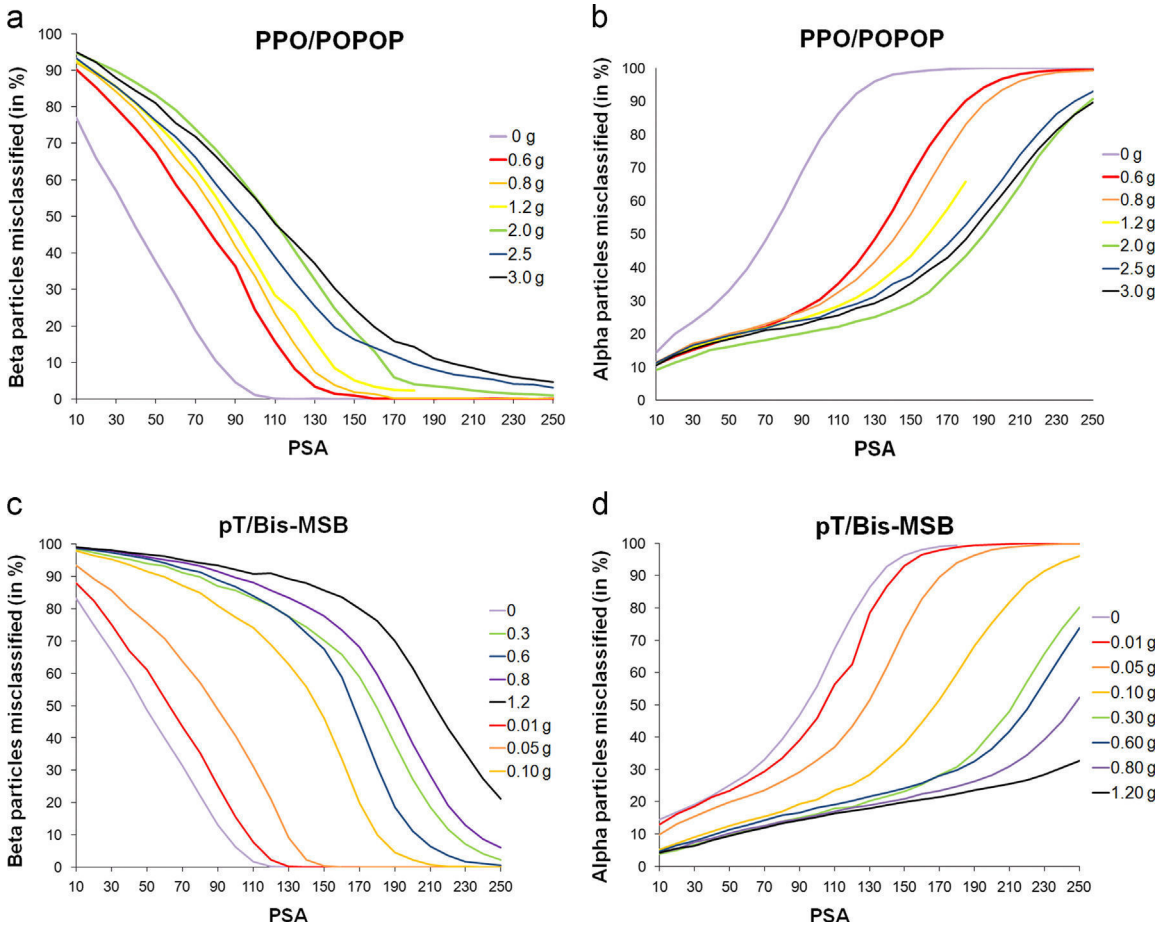

Fig. 4. Misclassification with the Quantulus detector: (a) beta particles with PPO/POPOP, (b) alpha particles with PPO/POPOP, (c) beta particles with pT/Bis-MSB and (d) alpha particles with pT/Bis-MSB.

signal is not from alpha particles but is from beta particles (i.e. Compton electrons from the gamma-rays also emitted by ^{241}Am).

It can be concluded that the effect of naphthalene in the pT/Bis-MSB PSm is higher than in the PPO/POPOP PSm; the higher effect is most likely because the energy transfer between naphthalene and *p*-terphenyl is less probable than the transfer between naphthalene and PPO. When the amount of naphthalene is increased, this probability is reduced; therefore, the delay of the pulses is higher, and the classification of the particles changes accordingly.

To identify which conditions (i.e. pair of solutes, amount of naphthalene and PSA value) are the most appropriate for the alpha/beta discrimination, the mean misclassification has been calculated for each PSA value (Fig. 5). It can be observed that when the quantity of naphthalene in the PSm increases, the lowest value of mean misclassification is found at higher values of the PSA parameter. This behaviour is more significant for the PSm containing pT/Bis-MSB because at the maximum naphthalene quantity (i.e. 1.2 g) and the highest PSA value (i.e. 250) the lowest mean misclassification value is not reached. This change in the position of the minimum value means the misclassification value is combined with a decrease in this minimum value. However, in both cases (PPO/POPOP and pT/Bis-MSB), there is a naphthalene content (2.0 and 0.6 g, respectively) above which the benefit obtained in the delay of the alpha signals is not balanced by the worsening in the classification of beta signals. Therefore, an increase in the minimum value for the mean misclassification is observed.

In the comparison between both types of PSm, lower mean errors are obtained with the PPO/POPOP pair (less than 20% for 2.0 g of naphthalene); however, there is a significant proportion of signals that are not correctly classified. The possible reasons for this misclassification include the proportion of alpha emissions that are detected through the noncoincident detection of the conversion electrons and gamma rays (which behave as beta particles), the intrinsic characteristics of the plastic scintillators (i.e. the fast decay time of the scintillators based on polymers) and the discrimination capabilities of the detector used (i.e. classifying the signals into only two spectra and by a parameter that is independent of the energy of the signal).

3.3.2. *Alpha/beta discrimination with Triathler*

For detection with the Triathler, the result of the measurement is a three-dimensional plot in which each pulse is classified by the length of the pulse (in 32 channels) and the energy of the pulse (in 64 channels). The pulses can be classified as beta or alpha after the measurement by integrating the area defined by the Pulse Length Index (PLI) and the energy limits (lower and upper). Based on these integrations, the alpha part of the spectrum is above the PLI whereas the beta part of the spectrum is below the PLI.

The contours of the spectra obtained when ^{90}Sr/^{90}Y and ^{241}Am samples are measured with PSm of different compositions (i.e. different amounts of naphthalene) are shown in Fig. 6. For the PSm containing PPO/POPOP, the addition of naphthalene corresponds to the movement of the spectrum to longer time durations (*y* axis

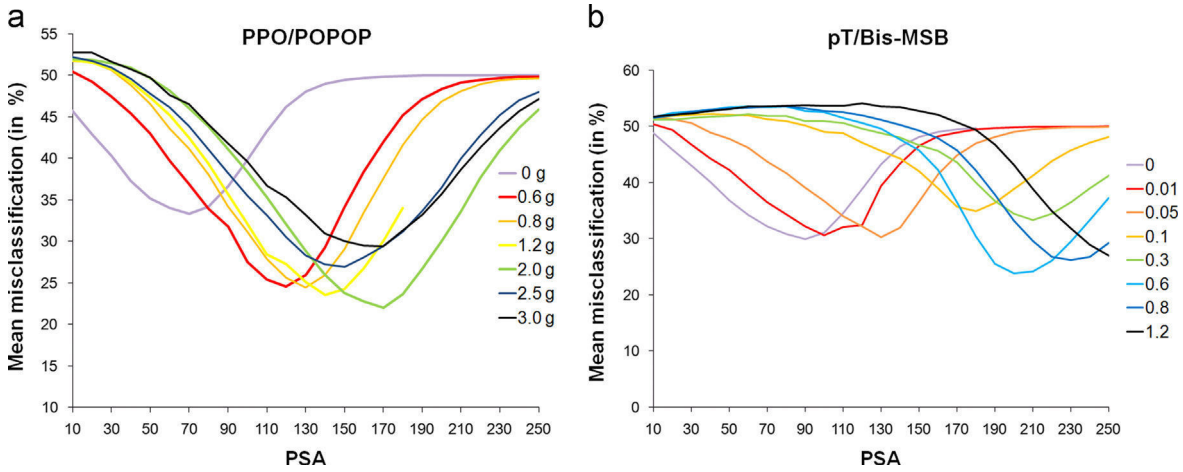

Fig. 5. Misclassification with the Quantulus detector: (a) PSm with PPO/POPOP and (b) PSm with pT/Bis-MSB.

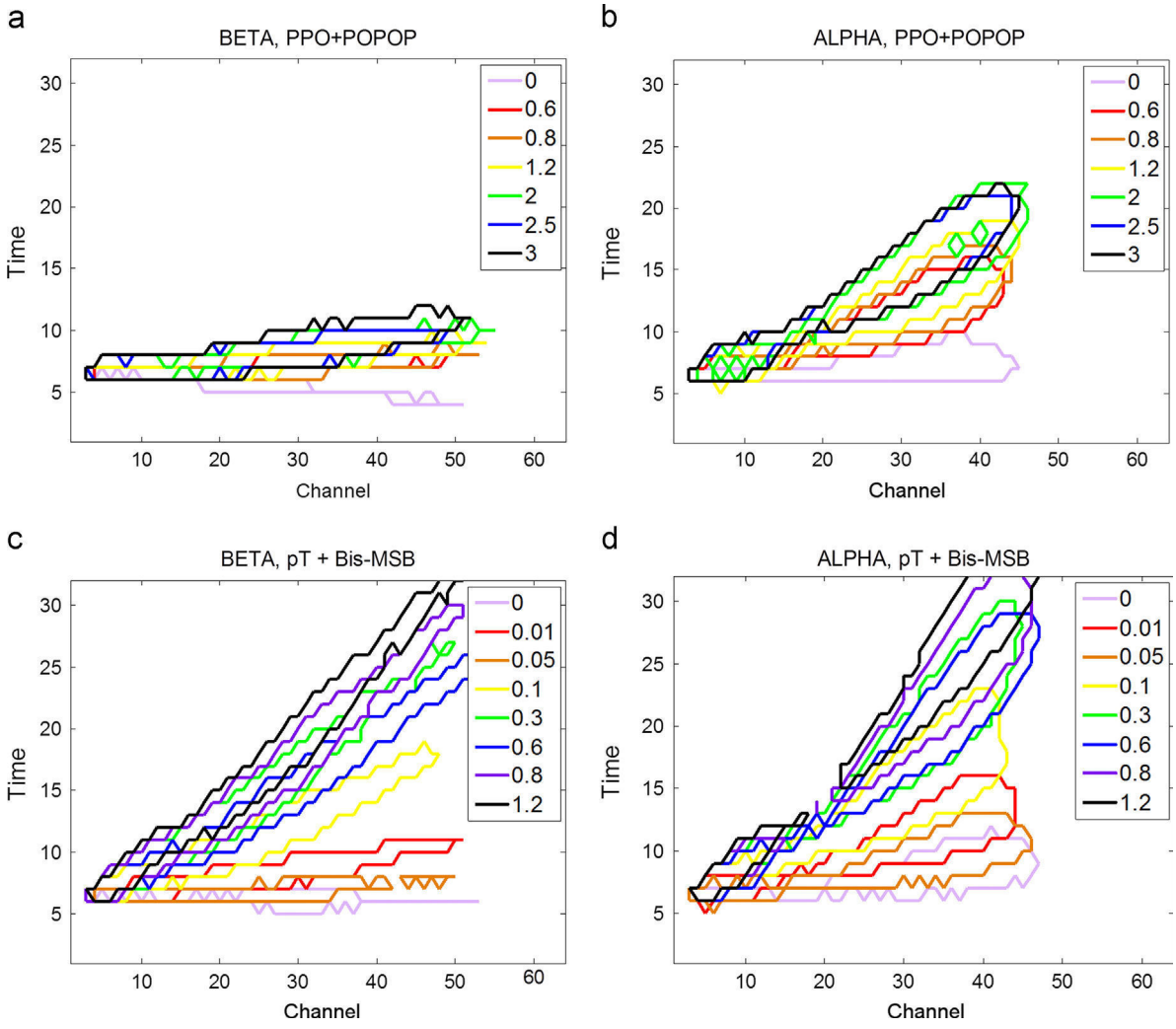

Fig. 6. Contours of the spectra obtained with the Triathler detector: (a) beta particles with PPO/POPOP, (b) alpha particles with PPO/POPOP, (c) beta particles with pT/Bis-MSB and (d) alpha particles with pT/Bis-MSB.

of the plot) because of the delay of pulses. This movement is more prominent for alpha particles than for the beta particles and is well correlated with the amount of naphthalene present in the evaluated PSm (from 0 to 3.0 g). It is important to highlight that because the beta particle spectrum remains in the same position, the discrimination between beta and alpha signals is enhanced when naphthalene is added. Therefore, it can deduced that for PSm containing PPO and POPOP, the addition of naphthalene only affects electronic transfer from the solvent in the triplet state (the state caused by the interaction of the polymer with the alpha

particles) to the primary fluorescent solute whereas the transfer from the singlet state (produced by the betas) to the primary fluorescent solute remains unchanged.

For the results obtained with PSm containing pT and Bis-MSB, it can be seen that the addition of small amounts of naphthalene causes an increase in the delayed component of the pulse; therefore, the spectrum is shifted to longer times (y axis). This shift happens for both the alpha and beta signals; thus, both spectra continue to be overlapped. As with the Quantulus measurements, the PSm containing pT and Bis-MSB have worst alpha/beta discrimination capabilities. As described previously it can be deduced that the addition of naphthalene causes a delay in the electronic transfer from the solvent, regardless of whether the solvent is in the singlet state or in the triplet state, to the primary fluorescent solute. Therefore, the introduced delay affects the beta signals (i.e. excitation to singlet) and alpha signals (i.e. excitation to triplet) equally.

As stated previously, by considering the positions of the obtained spectra, it is possible to define regions in which the integration should be performed to determine the alpha and beta emitters with the lowest amount of misclassification.

These regions are defined by the low-energy and high-energy limits and the pulse length index. However, these integration windows (rectangular in shape and perpendicular to the axis) usually do not perfectly fit the shape of the obtained spectra, and high misclassification values are consequently obtained.

With the goal of defining a better integration region for measurements with the Triathler, a computation method has been developed that selects those regions in which the misclassified events are minimised. In this method, the proportion of alpha signals relative to the sum of alpha and beta signals (i.e. the alpha proportion) and the proportion of beta signals relative to the sum of beta and alpha signals (i.e. the beta proportion) are calculated for each region of the spectrum with a 3×3 dimension. If the beta or alpha proportions are lower than a predefined threshold (5% is used in these experiments), the central point of the 3×3 matrix is defined to be an alpha region (i.e. a point of the spectrum with a low beta contribution) or as a beta region (i.e. a point of the spectrum with a low alpha contribution). To compensate for the possible differences in the count rates or the activities of the alpha and beta samples, the calculations are performed with the efficiency spectrum (net count rate divided by the activity of the measured standard).

Through this approximation, the regions of the spectrum with lower alpha and beta contributions (i.e. low misclassification) can be obtained. Fig. 7 shows the perimeter of the regions (beta and alpha) defined when a sample with ^{241}Am and a sample with ^{90}Sr/^{90}Y are measured with PSm containing PPO and POPOP and 2 g of naphthalene.

Finally, Fig. 8 shows the misclassifications (i.e. the proportion of alpha and beta signals that are wrongly classified) and detection efficiencies when samples of ^{90}Sr/^{90}Y and ^{241}Am are measured with both types of PSm with increasing amounts of naphthalene and with the optimised integration regions.

For the PSm containing PPO and POPOP, very good discrimination is achieved and for PSm with lower than 2 g of naphthalene, we obtained a misclassification for beta particles of less than 2% whereas there is practically no contribution from the alpha particles in the beta window (less than 0.5%). In the integration regions selected for each type of PSm, the detection efficiency for the alpha emitter is approximately 25% whereas for the beta, it is approximately 90%. We should highlight the important reduction achieved in this way for the background in the alpha window (approximately 80 cpm in the full area, 0.5 cpm in the alpha window and 20 cpm in the beta region) because most of the background noise is classified as beta. This reduction makes the limit of detection under the measurement conditions (i.e. a counting time of 120 min and a volume of 0.75 mL) approximately 20 Bq/L for alpha particles and approximately 80 Bq/L for the beta radionuclides. These values, especially the value for the alpha emitter, can be considered to be low if we consider the volume of the sample, the counting time and the fact that the Triathler is a detector with a very high background because it has only one photomultiplier and a low amount of lead shielding from cosmic radiation.

For the PSm containing pT and Bis-MSB, the addition of small amounts of naphthalene (less than 0.5 g) causes an improvement in the situation whereas for higher amounts, the delay in the signals from the beta particles is too large, and the region with good discrimination is too small. Consequently, the detection efficiency for the alpha and beta particles is too low, and the low detection efficiency causes an increase in the limit of detection. As with the Quantulus detector, the PSm with pT and Bis-MSB present worse results than the PSm with PPO and POPOP.

4. Conclusions

Plastic scintillation microspheres containing PPO and POPOP or pT and Bis-MSB and naphthalene as a secondary solvent have been synthesised through the evaporation/extraction method. The addition of naphthalene to the PSm does not significantly change either the radiometric capabilities or the shape or diameter of the PSm. A slight decrease in the detection efficiency for low-energy

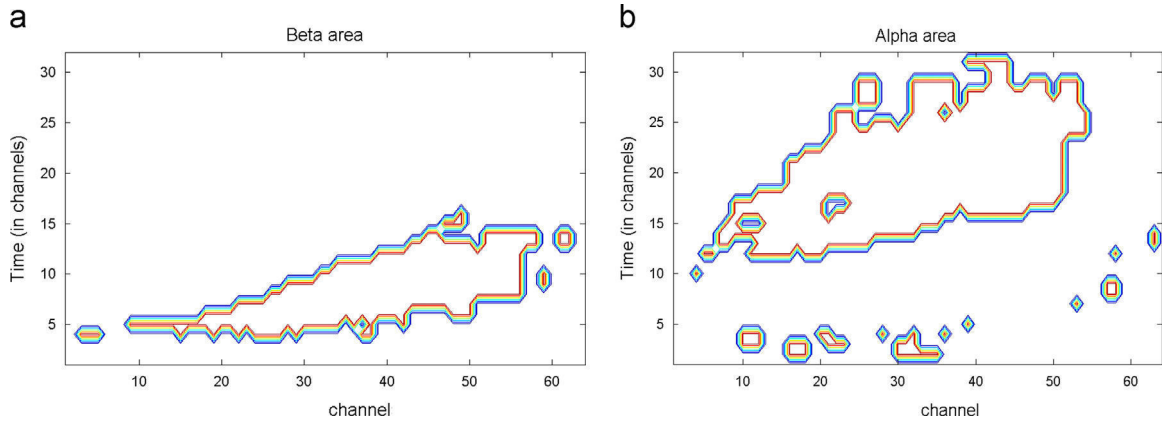

Fig. 7. Perimeter of the alpha and beta regions defined for PSm containing 2.0 g of naphthalene and PPO and POPOP.

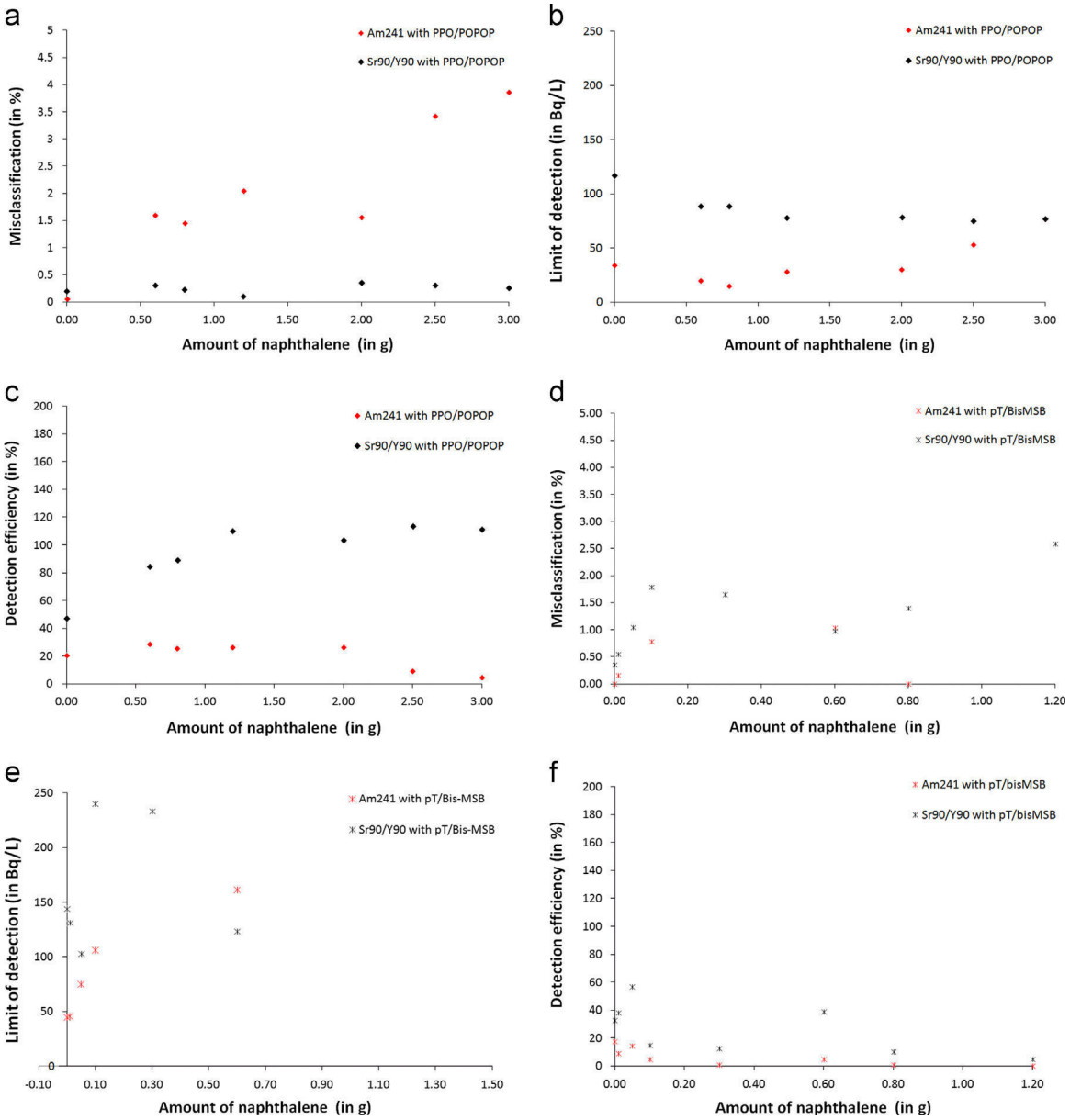

Fig. 8. Results obtained for the $^{90}Sr/^{90}Y$ and ^{241}Am samples measured with PSm with the Triathler detector with optimised integration regions: (a) misclassification with PPO/POPOP, (b) misclassification with pT/Bis-MSB, (c) limit of detection with PPO/POPOP, (d) limit of detection with pT/Bis-MSB, (e) detection efficiency with PPO/POPOP and (f) misclassification with pT/Bis-MSB.

beta emitters has been observed; however, these variations are on the same order of magnitude as those attributed to the change in the median diameter of the microspheres, to the different degrees of packaging or to variations in the optical conditions of the samples.

With regard to alpha/beta discrimination, the addition of naphthalene causes a delay in the pulses, and this delay can be used to improve the discrimination capabilities of PSm. For the PSm containing PPO and POPOP, the alpha signals are delayed more than the beta signals, and this increased delay leads to a significant improvement in the discrimination capability. This improvement is more evident for detectors in which the pulses are classified by the duration and energy of each event in a three dimensional plot, such as the Triathler, than in those detectors, such as the Quantulus, in which the pulses are classified as alpha or beta in two-dimensional spectra (of energy as a function of number of counts) after comparison of the duration of the pulse with a discrimination parameter.

For the Triathler detector, correct discrimination of alpha and beta particles can be performed after proper selection of the alpha and beta integration regions. In this way and with PSm containing PPO and POPOP and between 0.6 and 2 g of naphthalene, the analysis of alpha and beta radionuclides can be performed with very low misclassifications (i.e. 2% for the beta particles and 0.5% for the alpha particles), high detection efficiencies (i.e. approximately 25% for alpha particles and 80% for beta particles) and low detection limits (i.e. 20 Bq/L for the alpha particles and 80 Bq/L for the beta particles) in 120 min of measurement and 0.75 mL of sample.

For the PSm containing pT and Bis-MSB, the addition of naphthalene causes a very significant delay in the alpha and beta signals; therefore, the discrimination is not significantly improved relative to the PSm without naphthalene.

The improvement caused by the use of naphthalene as a delayer of pulses opens new possibilities toward the definition of new analytical applications for plastic scintillation microspheres.

To this end, the replacement of naphthalene with other less toxic products, such as 2,6-diisopropylnaphthalene (Pujol and Sanchez-Cabeza, 1997) or others (Salimgareeva and Kolesov, 2005), should be considered.

Acknowledgements

The authors thank the Ministerio de Ciencia e Innovación (Spain) (MICINN) for financial support under CTM2008-01147 and CTM2011-27211 and a grant for research (CTM2008-01147).

References

Bagán, H., Tarancón, A., Rauret, G., García, J.F., 2011. Mixture quantification using PLS in plastic scintillation measurements. Appl. Radiat. Isot. 69 (6), 898–903.

Birks, J.B., 1964. The Theory and Practice of Scintillation Counting. Pergamon Press, Oxford.

Brooks, F.D., 1979. Development of organic scintillators. Nucl. Instrum. Methods 162 (1–3), 477–505.

Dávila Rangel, J.I., López del Río, H., García, F.M., Torres, L.L.Q., Villalba, M.L., et al., 2002. Radioactivity in bottled waters sold in mexico. Appl. Radiat. Isot. 56 (6), 931–936.

EPA, 2001. Mixed-waste rule:40 CFR 266: storage, treatment, transportation, and disposal of mixed-waste. Fed. Regist. 66, 95.

EPA, 2006. EPA's mixed waste program. ⟨http://www.epa.gov/rpdweb00/mixed-waste/⟩.

Flaska, M., Pozzi, S.A., 2007. Identification of shielded neutron sources with the liquid scintillator BC-501A using a digital pulse shape discrimination method. Nucl. Instrum. Methods Phys. Res. Sect. A 577 (3), 654–663.

Gamage, K.A.A., Joyce, M.J., Hawkes, N.P., 2011. A comparison of four different digital algorithms for pulse-shape discrimination in fast scintillators. Nucl. Instrum. Methods Phys. Res. Sect. A 642 (1), 78–83.

Hallam, A., Birks, J.B., 1978. Energy transfer in organic systems XIII. Plastic scintillators. J. Phys. B 11 (18), 3273.

Happel, S., Letessier, P., Ensinger, W., Eikenberg, J.H., Thakkar, A.H., et al., 2004. Gross alpha determination in drinking water using a highly specific resin and LSC. Appl. Radiat. Isot. 61 (2–3), 339–344.

Hsu, J., Krieger, J.K., 1991. Mixed waste: a review from a generators perspective. Liquid scintillation counting and organic scintillators. In: Proceedings of the International Conference on New Trends in Liquid Scintillation Counting and Organic Scintillator (1989). Lewis Publishers, Chelsea, Michigan, pp. 557–600.

Klein, H., Neumann, S., 2002. Neutron and photon spectrometry with liquid scintillation detectors in mixed fields. Nucl. Instrum. Methods Phys. Res. Sect. A 476 (1–2), 132–142.

Kleinschmidt, R.I., 2004. Gross alpha and beta activity analysis in water – a routine laboratory method using liquid scintillation analysis. Appl. Radiat. Isot. 61 (2–3), 333–338.

L'Annunziata, M.F., 2013. Handbook of Radioactivity Análisis, 3rd ed. Academic Press, San Diego.

McDowell, W.J., McDowell, B.L., 1991. Liquid scintillation alpha spectrometry: a method for today and tomorrow. Liquid scintillation counting and organic scintillators. In: Proceedings of the International Conference on New Trends in Liquid Scintillation Counting and Organic Scintillator (1989), Lewis Publishers, Chelsea, Michigan, pp. 105–121.

McKlveen, J.W., McDowell, W.J., 1984. Liquid scintillation alpha spectrometry techniques. Nucl. Instrum. Methods Phys. Res. 223 (2–3), 372–376.

Moebius, S.S., Moebius, T.L., 2012. Handbook of Liquid Scintillation Spectrometry, 1st ed. Karlsruhe Institute of Technology, Karlsruhe.

Pates, J.M., Cook, G.T., MacKenzie, A.B., Passo, C.J., 1998. Implications of beta energy and quench level for alpha/beta liquid scintillation spectrometry calibration. Analyst 123, 2201–2207.

Pujol, L., Sanchez-Cabeza, J.A., 1997. Role of quenching on alpha/beta separation in liquid scintillation counting for several high capacity cocktails. Analyst 122, 383–385.

Rodriguez Barquero, L., Grau Carles, A., 1998. The influence of the primary solute on alpha/beta discrimination. Appl. Radiat. Isot. 49 (9–11), 1065–1068.

Salimgareeva, V.N., Kolesov, S.V., 2005. Plastic scintillators based on polymethyl methacrylate: a review. Instrum. Exp. Tech. 48 (3), 273–282.

Salonen, L., 1993. A rapid method for monitoring of uranium and radium in drinking water. Sci. Total Environ. 130–131, 23–35.

Salonen, L., Hukkanen, H., 1997. Advantages of low background liquid scintillation alpha-spectrometry and pulse shape analysis in measuring ^{222}Rn, uranium and ^{226}Ra in groundwater samples. J. Radioanal. Nucl. Chem. 226 (1–2), 67–74.

Sanchez-Cabeza, J.A., Pujol, L., 1995. A rapid method for the simultaneous determination of gross alpha and beta activities in water samples using a low background liquid scintillation counter. Health Phys. 68 (5), 674–682.

Santiago, L.M., Bagán, H., Tarancón, A., Garcia, J.F., 2013a. Synthesis of plastic scintillation microspheres: evaluation of scintillators. Nucl. Instrum. Methods Phys. Res. Sect. A 698, 106–116.

Santiago, L.M., Bagán, H., Tarancón, A., Rauret, G., Garcia, J.F., 2013b. Systematic study of particle quenching in organic scintillators. Nucl. Instrum. Methods Phys. Res. Sect. A 698, 26–36.

Sanz, A.T., Kossert, K., 2011. Application of a free parameter model to plastic scintillation samples. Nucl. Instrum. Methods Phys. Res. Sect. A 648 (1), 124–131.

Savitzky, A., Golay, M.J.E., 1964. Smoothing and differentiation of data by simplified least squares procedures. Anal. Chem. 36 (8), 1627–1639.

Tahnassian, A., Eveloff, J., Tisdale, H., 1991. Liquid scintillation waste. Liquid scintillation counting and organic scintillators. In: Proceedings of the International Conference on New Trends in Liquid Scintillation Counting and Organic Scintillator (1989), Lewis Publishers, Chelsea, Michigan, pp. 573–575.

Tarancon, A., García, J.F., Rauret, G., 2002. Mixed waste reduction in radioactivity determination by using plastic scintillators. Anal. Chim. Acta 463, 125–134.

Tarancón, A., García, J.F., Rauret, G., 2004. Determination of beta emitters (^{90}Sr, ^{14}C and ^{3}H) in routine measurements using plastic scintillation beads. Nucl. Instrum. Methods Phys. Res. Sect. A 516 (2–3), 602–609.

Wierczinski, B., Eberhardt, K., Hermann, G., Kratz, J.V., Mendel, M., et al., 1996. Liquid-scintillation spectroscopy of α-particle emitters and detection of spontaneous fission events for on-line studies of actinide and transactinide elements. Nucl. Instrum. Methods Phys. Res. Sect. A 370 (2–3), 532–538.

Yang, D., Zhu, Y., Mobius, S., Keller, C., 1990. Simultaneous determination of alpha and beta-emitting nuclides by liquid scintillation counting. J. Radioanal. Nucl. Chem. 144 (1), 63–71.

Zaitseva, N., Rupert, B.L., Pawełczak, I., Glenn, A., Martinez, H.P., et al., 2012. Plastic scintillators with efficient neutron/gamma pulse shape discrimination. Nucl. Instrum. Methods. Phys. Res. Sect. A 668, 88–93.

Chapter 3.1

Synthesis of plastic scintillation microspheres through the organic solvent extraction/evaporation methodology

---

3.1.1. Synthesis of plastic scintillation microspheres: Evaluation of Scintillators.

3.1.2. Synthesis of plastic scintillation microspheres: Alpha/beta discrimination.

3.1.3. Influence of preparation parameters on the synthesis of plastic scintillation microspheres and evaluation of sample preparation.

Influence of preparation parameters on the synthesis of plastic scintillation microspheres and evaluation of sample preparation

Santiago, L.M.; Tarancón, A.*; García, J.F.

Department of Analytical Chemistry of the University of Barcelona. Martí i Franqués, 1-11, E-08028, Barcelona, Spain

Abstract

Plastic scintillation microspheres (PSm) are solid dispersions of fluorescent solutes encapsulated in a polymeric matrix; they are used to measure β and α decay of radionuclides. Since organic solvent evaporation/extraction methods have been successfully employed to produce PSm, this work evaluates the influence of different parameters (i.e., polystyrene (PS) and polyvinyl alcohol (PVA) concentrations, temperature, stirring speed and the organic/aqueous phase ratio) on the final size of the PSm; and the relationship between this final size and the radiometric capacities of the PSm in relation to emitters of both beta (^{3}H, ^{14}C and ^{90}Sr/^{90}Y) and alpha (^{241}Am) radiation.

The results show that when the concentration of PVA is increased, the size of the PSm decreases; meanwhile, an important decrease in particle size is also achieved when the PS concentration is decreased. For almost all the parameters evaluated, the resultant PSm were smoothed and spherical. However, when temperature was increased, the particle size increased and the PSm eventually became amorphous and porous. The observed decrease in particle size correlated with an increase in radiation detection efficiency and a movement in the positioning of the spectra at lower energy values.

We also evaluated the reproducibility of the vial preparation for ^{3}H measurements and confirmed that small variations in the quantity of PSm and preparation of different vials by different experimenters did not influence the radiometric capacities.

Keywords

Plastic scintillation microspheres, mixed waste, organic solvent evaporation/extraction, radioactivity, liquid scintillation.

*Corresponding author: Tel: +34934033702, fax: +34934021233; e-mail address: alex.tarancon@ub.edu

1. Introduction

Plastic scintillation microspheres (PSm) are composed of a polymeric matrix encapsulating a couple of fluorescent solutes [1]. PSm were developed to measure emissions of beta and alpha radiation, based on the same principles as those of liquid scintillation counting (LS), but with the advantage of being solid and inert materials. Therefore, when measuring with PSm, the generation of mixed waste (organic and radioactive waste) is avoided. Moreover, among other applications, PSm can be used as a selective extractive scintillation support [2] in continuous radionuclide monitoring [3], to measure the properties of salty samples while avoiding phase separation [4].

Different methods have been employed to produce polymeric microspheres for different applications (e.g., controlled drug release, inks, cosmetics, pigments and chemical reagents) [5]. Organic solvent extraction/evaporation has been widely used and it is one of the most appropriated techniques, because it is capable of producing microspheres in a safe, economic and simple way; and because it allows control of the size distribution and morphology of the PSm [6]. This method has been successfully employed to obtain PSm with different compositions [1, 7].

When using organic solvent evaporation/extraction, the particle size distribution and morphology of the PSm depend on different variables which influence the evaporation of the organic solvent and the formation of the initial embryonic droplets. Some of these variables are: the polymer concentration, the proportion of surfactant used in the aqueous phase, the organic/aqueous phase ratio and the stirring speed.

When measuring with PSm, the detection efficiency is highly dependent on their size [7]. Therefore, the organic extraction/evaporation formulation (i.e., polymer and emulsifier concentration, and organic/aqueous phase ratio) and process parameters (i.e., temperature and stirring speed) are evaluated in order to establish their influence on the size and morphology of the resulting PSm, and ultimately on their radiometric capacities (i.e., detection efficiency and spectrum position). This allows determining which parameters need to be controlled to obtain microspheres of a desired diameter.

From the point of view of radiometrics, another highly important parameter is the vial preparation reproducibility, since it has an impact on the uncertainty associated with the activity assigned to a measured sample. So, it is worth evaluating the reproducibility

related to sample preparation when performing radiometrics using PSm obtained by organic solvent extraction/evaporation.

This work has two main objectives. On the one hand, to evaluate different formulation and process parameters in the production of PSm, in order to obtain PSm batches with different sizes which can be used for the measurement of radioactivity, depending on the purpose. On the other hand, to evaluate the effects of sample preparation on the reproducibility of the measurements. For the evaluation of the reproducibility, the parameters studied were: the quantity of PSm added to the vial for a fixed volume of aqueous sample; and the influence of the experimenter on this step (vial preparation by different experimenters).

2. Materials and Methods

2.1. Materials

Polystyrene (PS; molecular weight of 250,000 $g.mol^{-1}$) was purchased from Acros Organics (Geel, Belgium). Fully hydrolysed polyvinylalcohol, 2,5-diphenyloxazol (scintillation grade), 2,6-diisopropyl-naphthalene (99% pure) and dichloromethane (99.9% pure) were purchased from Merck (Darmstadt, Germany); while 1,4-bis(5-phenyloxazol-2-yl)benzene (scintillation grade) was supplied by the Montedison Group, Division Chimica (Milan, Italy).

For the radioactivity measurements, Pico Prias polyethylene vials of 6 mL (Perkin Elmer, Massachusetts, USA) were used to prepare the samples, with the following active stock solutions: ^{3}H solution (HTO) with a concentration of 3.94(7) kBq g^{-1} in deionized water prepared by weight from a standard of 69.8(12) $kBq.g^{-1}$; C-14 (labelled glucose) of 114.6(1) Bq g^{-1} prepared from a standard of 2212(27) $Bq.g^{-1}$ from Amersham International (Buckinghamshire, UK) in a carrier solution of 50 μg g^{-1} of glucose and 1 mg g^{-1} of formaldehyde in deionized water; $^{90}Sr/^{90}Y$ active stock solution (Sr^{2+} and Y^{3+}) of 37.2(3) Bq g^{-1} prepared from a standard of 4.07(3) kBq g^{-1} from Amersham International in 0.1 M HCl; and finally, ^{241}Am solution (Am^{3+}) of 185(2) $Bq.g^{-1}$ prepared from a standard of 924(9) kBq g^{-1} supplied by Amersham International in 0.5 M HCl and deionized water.

For the reproducibility of the measurements related to vial preparation, a plastic spoon (Tescoma-Italy) with capacity of 1 tbsp (15 mL) was employed to add the PSm to polyethylene vials of 20 mL (Perkin Elmer).

2.2. Instruments

A "Macrotronic" centrifuge and an "Ultrasons-P" ultrasonic bath (both from JP Selecta, Abrera, Spain) were used to centrifuge and sonicate the measurement vials, respectively.

The radioactive samples were measured using a 1220 QUANTULUS liquid scintillation spectrometer (Perkin Elmer) equipped with logarithmic amplification, a multichannel analyser (4096 channels distributed into four segments of 1024 channels) and background reduction through an active guard detector.

The scanning electron microscopy (SEM) images were obtained using a "JSM-7100F Field Emission Scanning" electron microscope. The samples were attached using double-coated adhesive tape and coated with gold by a sputtering coater.

An "LS 13 320 Coulter" single-wavelength laser diffraction particle size analyser (Beckman-Coulter Inc., Brea, USA) was used to determine the size and size distribution of the plastic scintillation microspheres.

2.3. Preparation of the plastic scintillation microspheres

PSm were synthesized using organic solvent/extraction evaporation described in the work of Santiago et al., 2013b. Briefly, the process involved the preparation of an organic phase in which the PS, the naphthalene or 2,6-diisopropylnaphthalene (DIN) and the fluorescent solutes were dissolved in dichloromethane (DCM). Then, the organic phase was added to an aqueous phase composed of deionized water containing polyvinyl alcohol (PVA). When the phases were in contact, an organic/aqueous emulsion was formed and, with the help of continuous stirring, micro droplets and subsequently embryonic microspheres were formed. The organic solvent was extracted and evaporated causing the microspheres to harden. The PSm were collected by filtration, washed with ethanol and water, and finally dried in the oven to remove residual organic solvent, at 40ºC for 20 hours.

Fifteen different sets of conditions were used in the synthesis (Table 1) resulting in PSm1 to PSm15. In all cases, the synthesis was performed in triplicate. All the syntheses were composed of PS, PPO, POPOP and naphthalene; except PSm12 and PSm15, in which the naphthalene was replaced by DIN, since it is a less toxic compound which also acts as a pulse delayer. PSm1 was adopted as the reference to compare the other PSm to.

The influence of the stirring speed was evaluated by synthesizing at 16.7, 8.3 and 13.3 Hz. To study the influence of the emulsifier concentration, PVA concentrations of 1%, 2% and 5% (w/v) with regard to the aqueous phase, were used. Meanwhile, the influence of polymer concentration was evaluated using proportions of 10%, 5% and 2.5 % (w/v) PS.

The effect of the organic/aqueous phase ratio (O:W) was studied by using 2,000 mL of aqueous phase for each experiment, and adding an increasing amount (100, 200 or 400 mL) of organic phase containing PS, PPO, POPOP and naphthalene for each synthesis. Finally, the influence of temperature was evaluated by keeping the aqueous phase of the synthesis at 20ºC, 35ºC or 50ºC, during the PSm formation process.

After gaining a clear understanding of the influence of these parameters on the final shape and dimensions of the microspheres, PSm13, PSm14 and PSm15 were produced by adjusting more than one of the parameters.

2.4. Radioactivity measurements

2.4.1. Sample preparation

2.4.1.1. Evaluation of radiometric capacities

The measurement samples were prepared by adding 1.5 g of the PSm and 0.75 mL of the counting solution (active or blank solution) to a 6 mL polyethylene vial. The vials were then sonicated with ultrasound for 2 min and centrifuged for 10 min at 83.3 Hz to ensure homogenization.

The active counting solutions were prepared by diluting a known quantity of an active stock solution of the respective radionuclide with a carrier solution of known volume. The activity of the measurement samples was approximately: 475 Bq g^{-1} for ^{3}H in

deionized water; 35.83 Bq g^{-1} for ^{14}C in a carrier solution of 50 μg g^{-1} of glucose and 1 mg g^{-1} of formaldehyde in deionized water; 3.91 Bq g^{-1} for $^{90}Sr/^{90}Y$ in 0.1 M HCl; and 31.41 Bq g^{-1} for ^{241}Am in 0.5 M HCl. Blanks were prepared by adding carrier solution rather than active stock solution. Three replicates were prepared for each radionuclide and all solutions and samples were prepared by weighing.

2.4.1.2. Influence of the quantity of PSm on ^{3}H detection efficiency

Ten blanks and ten counting samples were prepared using different quantities of PSm (PSm15) and a fixed quantity of aqueous solution (blank or ^{3}H) in a 20 mL vial. The activity of ^{3}H samples was around 752 Bq g^{-1}. The quantities of PSm added to each vial were: 2.83, 2.87, 2.91, 2.95, 2.99, 3.03, 3.07, 3.11, 3.15 and 3.19 g; while 1.26 mL of solution was added to each vial. The vials were sonicated for 2 minutes and centrifuged for 10 minutes at 83.3 Hz to ensure homogenization.

2.4.1.3. Reproducibility of the vial preparation

Solutions of three beta emitters (^{3}H, ^{14}C and $^{90}Sr/^{90}Y$, with activities of approximately 747.8, 60.18 and 6.28 Bq g^{-1} respectively) and one alpha emitter (^{241}Am; 53.04 Bq g^{-1}) were placed into 20 mL vials containing 3 g of PSm (PSm15) and 1.25 mL of blank (carrier) or active solution. The vials were prepared by weighing and were sonicated for 2 minutes and centrifuged at 83.3 Hz for 10 min to ensure homogenization, as in the other cases.

2.4.2. Measurement

The measurements for all the vials were performed using the 'low' coincident bias and '^{14}C' multichannel analyser (MCA) configuration. The coincident bias is a default setting of the Quantulus detector which determines the amplitude threshold level (low or high) for summing pulses obtained in each photomultiplier; it is used to prevent the sum of non-symmetric background pulses. When the '^{14}C' configuration is used, no correction for chemiluminescence is applied and more pulses are detected.

The counting times for the blank, ^{3}H, ^{14}C and ^{241}Am samples were 60 min; while the $^{90}Sr/^{90}Y$ samples were measured over 90 min. The duration of the measurement with an external gamma-ray source of ^{152}Eu was adjusted to 10 min.

2.4.3. Data analysis

The spectrum obtained from each measurement was smoothed using a Savitzky-Golay algorithm included in Matlab software (Mathworks, Natwick, USA). The net spectrum of active samples was obtained by subtracting the corresponding blank sample. The detection efficiency was calculated as the ratio between the net number of counts in the entire spectrum and the activity added to the measurement vial. The uncertainty associated with the count rate and the detection efficiency values corresponded to the higher of the values of either the experimental standard deviation between replicates or the combined standard uncertainty considering the canonical values of the main uncertainty sources (i.e., weighing, and the count rate of the active and background sample).

The quenching indicator, SQP(E), was calculated by the detector for each sample and corresponds to the end-point channel that limits 99.75% of the total counts of the spectrum generated by the external gamma-ray source [8].

3. Results and discussion

Different organic solvent extraction/evaporation parameters were studied in order to evaluate their effect on the morphology, size and radiometric capacities of the PSm obtained.

The formulation parameters evaluated were the polymer and emulsifier concentrations, and the organic/aqueous phase ratio. Meanwhile, the process parameters evaluated were the temperature and stirring speed employed during the synthesis of the PSm.

3.1. Influence of the formulation and process parameters on the resulting PSm

3.1.1. Influence of the stirring speed

The synthesis of PSm was performed at three different stirring speeds (16.7, 13.3 and 8.3 Hz; which correspond to PSm1, PSm2 and PSm3, respectively). Figure 1 shows the resulting SEM images. In all cases, the particles were spherical, smooth and apparently compact, with a wide range of diameters. The values in Table 2 and Figure 2 regarding particle size show that PSm3 has the smallest diameter; however, due to the high

diameter dispersion, the three resulting PSm are equivalent, and they are in the same size range.

According to previous research, particle size may be smaller when stirring speed is higher, because the Weber number increases in aqueous emulsion systems [5, 9] producing higher shear forces [10] that provide more energy to disperse the organic phase in the aqueous phase [11]. However, over the range evaluated in this experiment, increasing the stirring speed did not produce any relevant difference between the three resulting PSm. This may be due to the variation in the stirring speed not being highly significantly at this density.

3.1.2. Influence of the surfactant concentration

The presence of a surfactant is needed to decrease the interfacial tension between the embryonic microdroplets and the continuous phase, thereby causing the PSm to harden more and protecting them from coalescence due to collisions during stirring [12, 13]. Moreover, PVA has been reported to be an emulsifier that improves the surface smoothness of the microspheres [14] and helps decrease the mass transfer rate between the disperse and continuous phases [15].

The influence of PVA on the PSm produced was studied by synthesizing microspheres at three different concentrations of PVA in the aqueous solution: 1%, 2% and 5 % (w/v) (PSm1, PSm4 and PSm5, respectively). Table 2 and Figure 2 clearly show the decrease in PSm size as the PVA concentration increases (i.e., 84(26) µm for PSm1, 71(24) µm for PSm4 and 51(21) µm for PSm5). This decrease presents linear behaviour with a negative slope (of the mean size with regard to the emulsifier concentration) following the trend reported by other authors [9, 16]. The decrease in PSm size and size distribution as the PVA concentration increases can be attributed to the decrease in the interfacial tension and the resultant decrease in the initial droplet size.

Another effect that may be taken into consideration when increasing the concentration of surfactant, in accordance with the findings of Yang et al., 2001 [17], is the formation of microspheres with irregular shapes. This is probably because the critical micelle concentration is reached and therefore the emulsion stability is affected [5]. In this situation, interfacial tension does not change after the critical micelle concentration and collisions or irregularly shaped microspheres may occur. Looking at the SEM images in

Figure 3, at higher magnification, some non-spherical shapes can be observed in the PSm obtained at 5% PVA concentration, probably due to this effect. The almost perfectly spherical PSm obtained at 1% PVA concentration demonstrates that the quantity of PVA added shields the entire droplet surface and produces a stable emulsion for microparticle formation.

3.1.3. Influence of polymer concentration

Three experiments (PSm1, PSm6 and PSm7), were performed to evaluate the effect of the polymer concentration, using 10%, 5% and 2.5% (w/v) PS, respectively. Figure 4 shows that the particle size tends to decrease when the PS concentration decreases in the disperse phase. The values in Table 2 and Figure 2 confirm this observation. A decrease in size when a lower polymer concentration was employed could be explained by a lower availability of PS in each liquid drop in the embryonic microparticle, and in the final PSm. Moreover, at lower PS concentrations, there is a decrease in the viscosity of the organic phase and PS droplets break up more easily than at higher dispersed phase viscosities; even at the same stirring speed (lower shear forces are required). Our results are in accordance with those of Viswanathan et al., 1999 [18], who determine that the particle size is directly proportional to the polymeric solution viscosity; and also with those of Heiskanen et al., 2012 [19], who state that when PS concentration is low, the efficiency of the stirring is enhanced and smaller particles are obtained.

3.1.4. Influence of volume ratio of phases

Three different experiments were carried out keeping the quantity of aqueous phase constant (2,000 mL) and increasing the organic phase to 100 mL for PSm1, 200 mL for PSm8 and 400 mL for PSm9.

According to the results shown in Table 2 and Figure 2, the PSm size decreases slightly when the organic/aqueous phase ratio is increased, thus obtaining diameters of 84(26), 68(24) and 57(24) μm for PSm1, PSm8 and PSm9 respectively. This is in agreement with Gabor et al., 1999 [20], who observed that when the ratio of the phases (DCM in water emulsion) is increased, the size of the microsphere decreases. However, according to Jeffery et al., 1993 [21], when the total amount of emulsion is increased, due to the increase in the quantity of the organic phase, it would be expected that the PSm increase

in size, because the efficiency of the stirring speed is lower and therefore the solution becomes more viscous.

In the experiments performed in this work, the quantity of the aqueous phase and the time needed to extract the DCM seems to be adequate, since the continuous phase is large, thereby allowing a rapid distribution of the organic solvent. Moreover, the amount of PVA added (1% w/v) also seems to be high enough to produce stable droplets, even when the proportion of the organic phase is increased four times. Under these conditions, it can be said that the system is stable enough and the increase of the organic phase has a higher impact on the droplet formation than the variations in the speed associated with changes in the viscosity.

3.1.5. Influence of the synthesis temperature

To study the influence of the temperature on PSm size, morphology and radiometric capacities, experiments were performed at three different temperatures: PSm1 at 20ºC, PSm10 at 35ºC and PSm11 at 50ºC. The temperatures chosen were below, close to and higher than the boiling point of DCM.

It is known that solvent evaporation is highly dependent on the temperature and concentration of solvent in the air; whereas solvent extraction depends on its solubility in the aqueous phase and the rate of solvent mass transfer, which are also correlated with temperature. The solubility of DCM in water decreases with increasing temperature (the solubility of DCM in water is around 2.0 wt% (25ºC) [22, 23], but the mass transfer process becomes faster due to an increase in the gradient of the solvent and the diffusion coefficient. When temperatures are high, the driving forces are the evaporation of solvent and mass transfer, resulting in faster saturation of the aqueous phase and faster evaporation of the solvent [24]. This effect is more notable for PSm10 and PSm11, at temperatures close to or exceeding the boiling point of DCM, when diffusion and solvent evaporation are very rapid, making the effect of solubility negligible. Under these conditions, it can be said that solvent escapes from the microspheres during the first minutes, causing faster solidification.

The PSm produced at 20ºC (PSm1), shown in Figure 6, are smaller and have a narrower particle size distribution (84 ± 26 μm) than those produced at 35 ºC (PSm10), with a size of 145 ± 62 μm; or at 50ºC, that can even reach a diameter of 1 mm. At lower

temperatures, the microspheres harden slowly and shear forces due to stirring still have an influence on the particle formation, since there is a time lapse between the initial embryonic microsphere formation and the hardening of the microsphere. In contrast, at 50ºC, the microspheres hardened very fast because the solvent is removed rapidly; and so it is possible to obtain larger mean sizes with a broader particle size distribution and in some cases porous particles.

3.2. Influence of the substitution of naphthalene by 2,6-diisopropylnaphthalene within the PSm composition

Naphthalene is employed as a secondary solvent in PSm formulation. Due to its electronic structure it is considered a suitable compound for delaying scintillation pulses produced by alpha particles and therefore for enhancing the alpha/beta discrimination capacities of organic scintillators. However, naphthalene cannot be considered completely safe and for this reason it has been replaced in PSm composition by 2,6-diisopropylnaphthalene, which accomplishes the same functions as the former [25].

PSm12 was synthesized using the same parameters as PSm1, but replacing the naphthalene by DIN. No differences were observed in particle size or shape and surface of the PSm; as can be observed in Figure 7 and Table 2. It is also possible to observe that size distribution was similar for both experiments (84±26 μm for PSm1 and 83±28 for PSm12).

3.3. Combined procedures

Once the influence of the formulation and process parameters on the resulting PSm was known, three different experiments were performed with specific combined conditions. First, to study the potential synergies between parameters; and second, to develop procedures for obtaining large amounts of PSm with a desired diameter.

Table 1 shows the parameters of these experiments. PSm13 and PSm14 only differ in their organic/aqueous phase ratio, and the polymer concentration was higher for PSm14. A third combined procedure (PSm15) was established to produce PSm composed of PS/PPO/POPOP and DIN, with a higher rate of PSm production but adjusting the size to larger diameters.

As can be observed in the SEM images in Figure 8, most of the particles were spherical. However, some of them showed a deformed appearance (PSm15). Combined changes in the PS and PVA concentrations resulted, as expected, in an important decrease in PSm diameter (shown in Figure 2 and Table 2) and an increase in production yield (100% yield and more PSm than in the initial synthesis).

3.4. Radiometric capacities

Three beta emitters of different energies (^{3}H, E_{max}: 18.6 keV ; ^{14}C, E_{max}: 156.5 keV; ^{90}Sr/^{90}Y, E_{max}= 545.9 keV and E_{max}= 2,279.8 keV respectively) and an alpha emitter (^{241}Am, E_{max}: 5,637.8 keV) were studied using the PSm obtained in each synthesis.

For ^{3}H, the detection efficiencies were spread across a broad range: from 0.34% (PSm11) to 4.51% (PSm14). ^{3}H is a very weak beta emitter and the probability of it being detected when using PSm is highly dependent on the distance that the particle has to travel before reaching the PSm. When the diameter of the PSm is large, the distance that a disintegration particle has to travel is also large and its probability to be detected depends on its interaction with the medium, described as particle quenching [1] which increases with the distance and causes a decrease in the detection efficiency values. It can be seen that the lowest values of detection efficiency (0.34% and 0.81%) were obtained for the PSm with the largest diameters (PSm11 and PSm10, respectively); whereas the highest efficiency values (3.36% and 4.51%) were obtained for the microspheres with the smallest diameters (PSm7 and PSm14, respectively).

Something similar happens in the case of ^{14}C, but to a lesser degree since the energy of ^{14}C beta particles is higher than that for ^{3}H. The lowest value of detection efficiency (19.8%) was obtained in the synthesis performed at 50ºC (PSm11). For the rest of the PSm, the values vary from 45% (PSm10) to 74% (PSm14), with most of them between 55% and 65%.

The correlation between the detection efficiency for ^{3}H and ^{14}C, measured with each PSm, and the mean diameter of every PSm, can be observed in Figure 9.

In the case of ^{90}Sr/^{90}Y, the variation in the detection efficiency is small since the energy of beta particles emitted by ^{90}Sr and especially by ^{90}Y is very high. The values ranged between 185% and 190%; and the two extreme values were 193% for PSm14 and 152%

for PSm11, corresponding again to the smallest and largest mean microspheres, respectively.

In the case of ^{241}Am, although it is an alpha emitter with very high energy, around 5.5 MeV, the detection efficiency is also correlated with the diameter, since the pathway of alpha particles in water is of the same order as the distance between microspheres (tenths of a micrometre). Therefore, for the smallest microspheres, all the alpha events are detected and the detection efficiency is around 100% (PSm14). When the diameter increases, some alpha particles are not detected and the efficiency decreases slightly to 80%, in most of the cases, and to 31% in the worst scenario (PSm11).

SQP(E) values were determined to assess the presence of quenching effects that reduce the number of photons detected in each disintegration. It can be observed that these values ranged from 741 to 805 (Table 2) and the trend was the opposite to that observed for the detection efficiency, as observed in Figure 10a: the smallest PSm (PSm7 and PSm14) presented the lowest SQP(E) values (741 and 743, respectively), while the largest PSm (PSm11 and PSm10) had the highest SQP(E) values (805 and 788, respectively). This behaviour was due to the presence of optical quenching since light transmission is poorer in a medium with small microspheres (due to a high number of optical processes per distance to reach the photomultipliers) than in a medium with larger microspheres, and the consequence is a movement of the spectrum to lower energies and a decrease on the SQP(E).

The inverse correlation between SQP(E) and detection efficiency can be observed in Figure 10b, where the detection efficiency values are plotted versus the SQP(E) parameter. It can be seen that high diameter PSm (PSm10 and PSm11) present the highest values of SQP(E) and the lowest values of ^{3}H detection efficiency; while on the opposite site, the smallest PSm (PSm14 and PSm7) have the lowest SQP(E) and the highest values of detection efficiencies. In contrast, values of SQP(E) and detection efficiencies for the PSm synthesized by including DIN in their composition (PSm12), replacing the naphthalene (PSm1), were correlated to the mean diameter of the PSm1 comparable with the other PSm synthesized, therefore demonstrating that the use of DIN is recommended.

3.5. Evaluation of sample preparation reproducibility

One of the most important aspects when quantifying radionuclide is to know the reproducibility of the measurements and the sources of variation involved. In the case of measurements with PSm, the sample preparation, the specific amount of PSm added and the packing of the PSm, are some of the most important factors that should be addressed in two ways. Firstly, how does the variation in the amount of PSm added to the same volume of sample affect the detection efficiency? and secondly, what is the variability between samples prepared by different experimenters?.

3.5.1. Evaluation of the influence of PSm/sample ratio on ^{3}H radiometric capacities

The variability associated with the PSm vial preparation with regard to the amount of PSm and sample solution added, was evaluated by analysing the variation in ^{3}H detection efficiency when changing the quantity of PSm added to a fixed quantity of active solution.

Initially two different procedures were tested in order to establish which was the more suitable and reproducible method for adding PSm to the vial. In the first, PSm were added from a plastic spoon that was filled to being level, with an amount corresponding to approximately 3 g. In the second, the amount of PSm loaded into the spoon was adjusted using a spatula; removing excess PSm to achieve a completely flat surface. In the first case the average amount of PSm added to the vial (60 measurements were performed) was 3.14(9) g, while in the second, 2.99(8) g was added. The reproducibility of the addition was good (less than 3% deviation was obtained) and similar to that of a liquid scintillator cocktail added with a dispenser. Of the two procedures, that with the spatula was adopted for the experiments, since its value was closer to the expected 3 g.

To evaluate the influence on the radiometric capacities of the amount of PSm added with the plastic spoon (using the second procedure), which entailed a variation of approximately ± 0.2 g of PSm, a series of vials containing a variable amount of PSm and a fixed amount of sample solution (active or background) were prepared. The amount of PSm added was in the range of the mean value ± two standard deviations of the values obtained in the second experiment (from 2.83 to 3.19 g). Therefore, 1.26 mL of ^{3}H solution was added to the vials containing 2.83, 2.87, 2.91, 2.95, 2.99, 3.03, 3.07, 3.11, 3.15 and 3.19 g of PSm.

The average detection efficiency was 0.69(3)% with a relative standard deviation of 5%. This value is considered high, according to the expected value taking into account the fact that ^{3}H is a very weak beta emitter and the detection efficiency when using PSm is highly dependent on the distance between the microspheres and therefore on the packing of the PSm. Our results indicate that the variability of the measurements with PSm, at least for weak beta emitters in the range considered, is associated more with the random packing of the microspheres than with the PSm:solution ratio or other experimental parameters.

3.5.2. Reproducibility of the sample preparation

The reproducibility of the PSm sample vial preparation was studied by measuring four replicates of different radionuclides (^{3}H, ^{14}C, $^{90}Sr/^{90}Y$ and ^{241}Am) prepared by four different experimenters using the same synthesized PSm (PSm15) and following the same experimental conditions and vial preparation protocol. Each person prepared the sample vials following an established procedure (adding 3 g of PSm to a 20 mL polyethylene vial using the abovementioned plastic spoon and spatula, adding 1.25 mL of sample, applying ultrasound for 2 minutes and centrifuging for 10 min at 58.33 Hz).

Our results (Table 3) show that the variability decreases with the energy of the radionuclide. The variability of the ^{3}H measurements (5%) was similar to that obtained when evaluating the sample preparation, which confirms that for this kind of radionuclide, the packing of the microspheres is the main source of variability; it is even more important than other experimental factors (i.e., including the person who prepares the sample). In the case of the particles with medium or high energy, the PSm packing is less important, since the variability decreases and other experimental factors such as weighing, counting and the experimenter are more important.

4. Conclusions

We successfully evaluated the formulation and process parameters in the production of PSm by means of the organic solvent extraction/evaporation method. In almost all cases, the microparticles were spherical and smoothed; and the yield was around 100%, which is promising for scaling up production of PSm from the laboratory to the commercial scale.

Different stirring speeds (16.67, 13.33 and 8.33 Hz) did not produce important changes in the diameter of the PSm obtained; probably due to the surfactant having the predominant effect.

The use of different PVA concentrations in the aqueous phase (1%, 2% and 5% (w/v)) resulted in a clear decrease of particle size as the surfactant concentration increased, due to the resultant decrease in the interfacial tension and droplet size.

The PSm produced with variable PS concentration in the organic phase (10%, 5% and 2.5% (w/v)) presented a decreasing average particle size with the decrease in the PS concentration. This could be attributed to the decrease in viscosity and enhancement of the stirring efficiency.

The volume ratio of organic/aqueous phases was also evaluated. Although we expected the PSm size to increase as the phase ratio increased (because the viscosity increases and the stirring becomes less efficiency), the opposite effect was observed. This could be attributed to the fact that the PVA concentration was controlling the process.

A very clear tendency was observed in the influence of the aqueous phase synthesis temperature: the PSm size and distribution increased as the temperature increased, due to an increase of the solvent evaporation. The PSm synthesized at 20ºC were smaller, more spherical and smoother; while the PSm synthesized at 50ºC were amorphous and porous in some cases.

Naphthalene was successfully replaced by DIN, since both the morphologic and the radiometric properties of the PSm were not changed by the use of the new compound.

The evaluation of the radiometric capacities for ^{3}H, ^{14}C, $^{90}Sr/^{90}Y$ and ^{241}Am showed that smaller PSm have higher detection efficiencies. This is due to lower particle quenching and lower SQP(E) values due higher optical quenching.

Two aspects of vial preparation were evaluated: the ^{3}H detection efficiency with regard to the variation in the quantity of PSm added to the vial; and reproducibility when performed by different experimenters. In the first case, in the range of the quantity of PSm evaluated, no trend in the variation of detection efficiency was observed; the variability was 5%. With regard to the vial preparation reproducibility, it was optimal

for high-energy radionuclides; while for low-energy radionuclides such as ^{3}H, it was about 5%.

5. Acknowledgements

The authors thank the Spanish Ministerio de Economía y Competitividad and the Catalan regional Agència de Gestió d'Ajuts Universitaris i de Recerca *(*AGAUR) for financial support under projects CTM2008-01147/CTM2011-27211 and 2009-SGR-1188 respectively.

6. References

[1] L.M. Santiago, H. Bagán, A. Tarancón, J.F. García, G. Rauret, Systematic study of particle quenching in organic scintillators, Nuclear Instruments and Methods in Physics Research Section A, 698 (2013) 26–36.

[2] H. Bagán, A. Tarancón, L. Stavsetra, J.F. García, G. Rauret, Determination of oil reservoir radiotracer ($S^{14}CN^{-}$) in a single step using a plastic scintillation extractive scintillation resin, Analytica Chimica Acta, 736 (2012) 30-35.

[3] A. Tarancón, A. Padró, J.F. García, G. Rauret, Development of a radiochemistry sensor, part: 2. Application to liquid effluents, Analytica Chimica Acta, 538 (2005) 241.

[4] H. Bagán, A. Tarancón, S. Hartvig, G. Rauret, J.F. García, Plastic vs. Liquid Scintillation for ^{14}C radiotracers determination in high salt matrices, Analytica Chimica Acta, 631 (2009) 229-236.

[5] H. Heiskanen, P. Denifl, P. Pitkänen, M. Hurme, Effect of preparation conditions on the properties of microspheres prepared using an emulsion-solvent extraction process, Chemical Engineering Research and Design, 90 (2012) 1517-1526.

[6] S. Freitas, H. P. Merkle, B. Gander, Microencapsulation by solvent extraction/evaporation: reviewing the state of the art of microsphere preparation process technology, Journal of Controlled Release, 102(2) (2005) 313–332.

[7] L.M. Santiago, H. Bagán, A. Tarancón, J.F. García, Synthesis of plastic scintillation microspheres: Evaluation of scintillators, Nuclear Instruments and Methods in Physics Research Section A, *698*(0) (2013) 106–116.

[8] Instrument Manual: Wallac 1220 Quantulus Ultra Low Level Liquid Scintillation Spectrometer, available at: (2002). http://www.perkinelmer.com/content/manuals/gde_quantulusinstrumentmanual.pdf (accessed on May 05th, 2015)

[9] Y. Mu, A. Lyddiat, A. Pacek, Manufacture by water/oil emulsification of porous agarose beads: effect of processing conditions on mean particle size, size distribution and mechanical properties, Chemical Engineering and Processing: Process Intensification, 44 (2005) 1157-1166.

[10] P. R.Nepal, M.K. Chun, H.K. Choi, Preparation of floating microspheres for fish farming, International Journal of Pharmaceutics, 341 (2007) 85-90.

[11] T. Mateovic, B. Kriznar, M. Bogataj, M. Mrhar, The influence of stirring rate on biopharmaceutical properties of Eudragit RS microspheres, Journal of Microencapsulation, 19 (2002) 29-36.

[12] R. Arshady, Microspheres and microcapsules a survey of manufacturing techniques. Part III. Solvent Evaporation, Polymer Engineering and Science, 30 (1990) 915-924.

[13] R.Dinarvand, S. Mirfattahi, F. Atyabi, Preparation, characterization and in vitro drug release of isosorbide dinitrate microspheres, Journal of Microencapsulation, 19 (2002) 73-81.

[14] W. Yuan, Y. Zhang, F. Wu, H. Li, Y. Cai, T. Zhang, M. Han, T. Jin, Preparation of protein-loaded sustained-release microspheres via 'solid-in-oil-in-hydrophilic oil-in-ethanol (S/O/hO/E)' emulsification, Colloids and Surfaces B: Biointerfaces, 79 (2010) 326-333.

[15] Y.L. Lee, Surfactant effects on mass transfer during the drop formation and drop falling stages, Journal of Materials, Interfaces and Electrochemical Phenomena, 49 (2003) 1859-1869.

[16] H. Rafati, A.G. Coombes, J. Adler, J. Holland, S. Davis, Protein-loaded poly(D,L-lactic-co-glycolic acid) microparticles for oral administration: formulation, structural and release characteristics, Journal of Control Release, 43 (1997) 89-103.

[17] Y. Yang, T.S. Chung, Morphology, drug distribution, and in vitro release profiles of biodegradable polymeric microspheres containing protein fabricated by double-emulsion solvent extraction/evaporation method, Biomaterials, 22 (2001) 231-241.

[18] N.B. Viswanathan, P.A. Thomas, J.K. Pandit, M.G. Kulkarni, R.A. Mashelkar, Preparation of non-porous microspheres with high entrapment efficiency of proteins by a (water-in-oil)-in-oil emulsion technique, Journal of Controle Release, 58 (1999) 9-20.

[19] H. Heiskannen, P. Denifl, P. Pitkänen, M. Hurme, Effect on the concentration and temperature on the properties of the microspheres prepared using an emulsion-solvent extraction process, Advanced Powder Technology, 23 (2012) 779-786.

[20] F. Gabor, B. Ertl, B. Wirth, R. Mallinger, Ketoprofen-poly(D,L-lactic-co-glycolic acid) microspheres: influence of manufacturing parameters and type of polymer on the release characteristics, Journal of Microencapsulation, 1, (1999) 1-12.

[21] H. Jeffery, S.S. Davis, D.T. O'Hogan, The preparation and characterization of poly(lactide-co-glycolide) microparticles. II. The entrapment of a model protein using a (water-in-oil)-in-water emulsion solvent evaporation technique, Pharmaceutical Research, 10 (1993) 362-368.

[22] Air Quality Guidelines. Second Edition (2000). Who Regional Publications, European Series, Nº 91. ISBN 9289013583. Available at http://www.euro.who.int/__data/assets/pdf_file/0013/ 12 3061/ AQG2 ndEd_5_7Dichlo romethane.pdf (accessed on April 1st, 2015).

[23] IUPAC-NIST Solubility Database, version 1.1. (2007). NIST Standard reference Database 106. Available at http://srdata.nist.gov/solubility/ (accessed on april 1st, 2015).

[24] Y.Y. Yang, T.S. Chung, X.L. Bai, W.K Chan, Effect of preparation conditions on morphology and release profiles of biodegradable polymeric microspheres containing protein fabricated by double-emulsion method, Chemical Engineering Science, 55 (2000) 2223-2236.

[25] J.M. Pates, G.T. Cok, A.B. MacKenzie, J. Thomson, The relation between photomultiplier tube output pulse shapes and alpha/beta separation efficiency, in Proc: Liquid Scintillation Spectrometry 1992, Radiocarbon, 25-32. Edited by Noakes, J.E.; Spaulding J.D. Tucson, 1993.

Figures

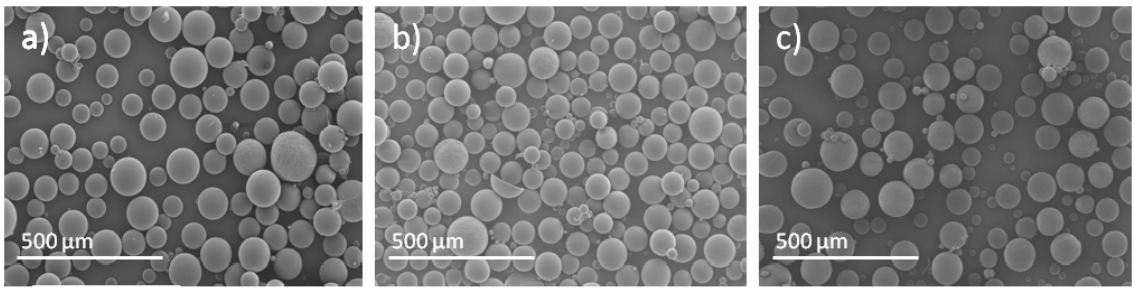

Figure 1. PSm synthesized by varying the stirring speed: (a) PSm1, 16.7 Hz; (b) PSm2, 13.3 Hz and (C) PSm3, 8.3 Hz.

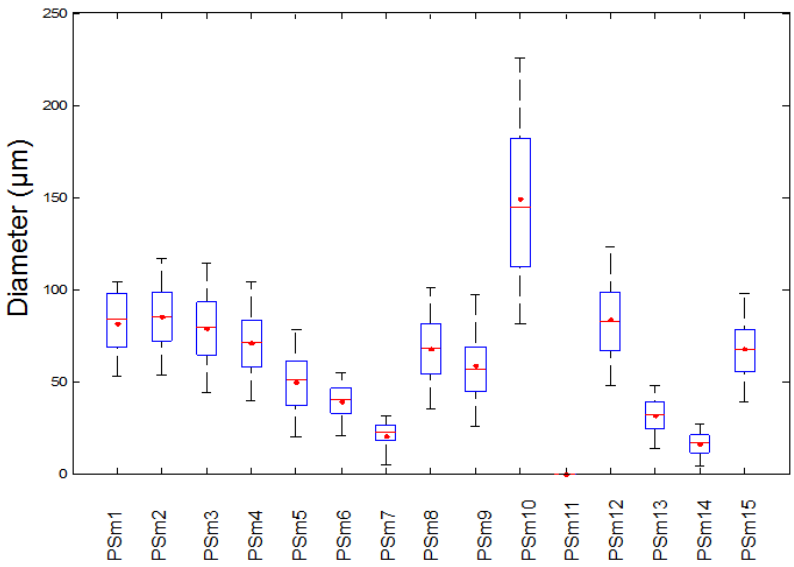

Figure 2. Particle size distribution of the synthesized PSm (PSm11 at 50ºC is not included).

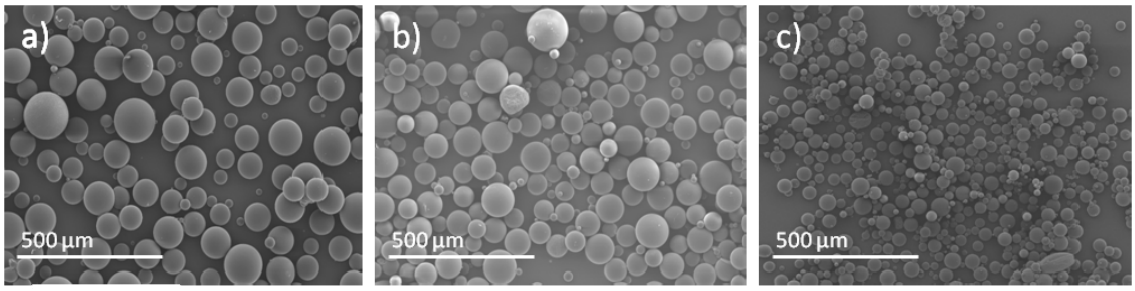

Figure 3. PSm synthesized for evaluating the influence of PVA concentration: (a) PSm1, 1% (w/v); (b) PSm4, 2% (w/v); and (C) PSm5, 5% (w/v).

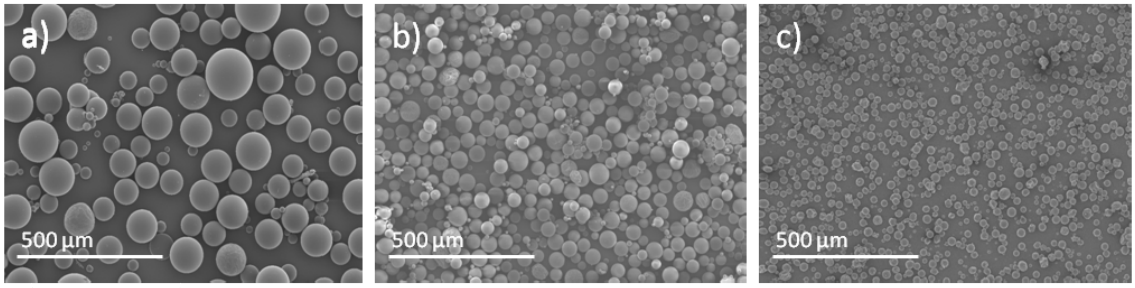

Figure 4. Influence of the PS concentration on the PSm: (a) PSm1, 10% (w/v); (b) PSm6, 5% and (C) PSm7, 2.5% (w/v).

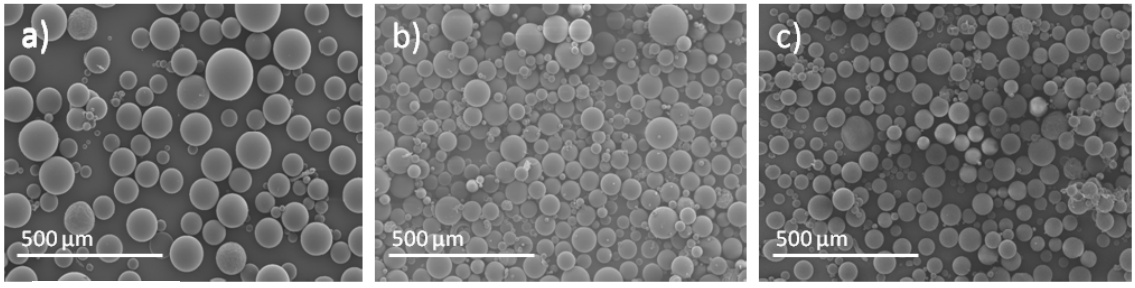

Figure 5. Evaluation of the influence of the organic/aqueous phase ratio. The aqueous phase was kept constant in 2,000 mL, while the organic phase was increased: (a) PSm1, 100 mL; (b) PSm8, 200 mL and (C) PSm9, 400 mL.

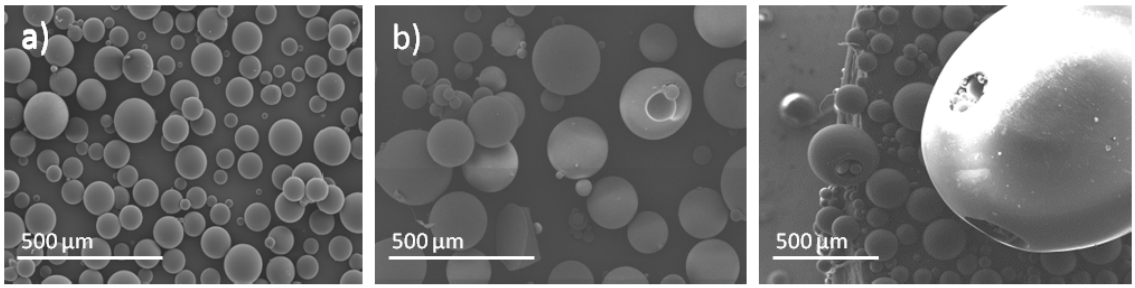

Figure 6. Evaluation of the influence of temperature on synthesized PSm: (a) PSm1, 20ºC; (b) PSm10, 35ºC and (C) PSm11, 50ºC.

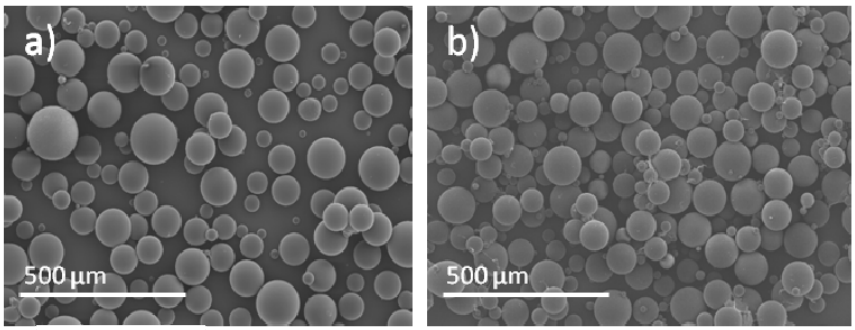

Figure 7. PSm synthesized using naphthalene, PSm1 (a); and using DIN instead of naphthalene, PSm12 (b).

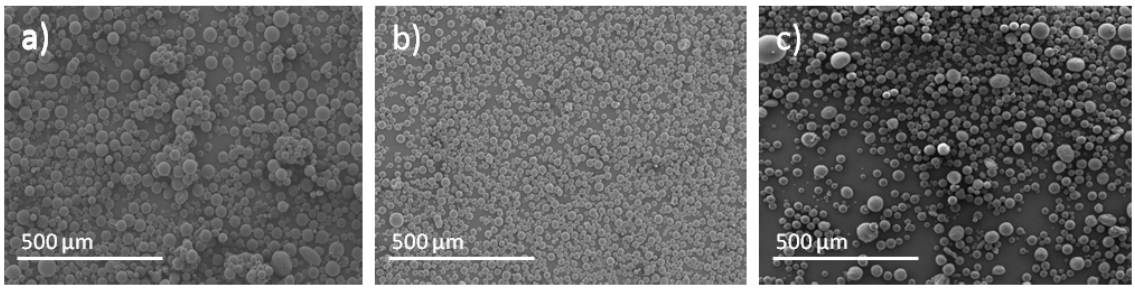

Figure 8. PSm synthesized with different combined procedures: (a) PSm13, PS 10% (w/v), 3:20 (O:W) phase ratio, PVA 6% (w/v); (b) PSm14, 5% (w/v), 6:20 (O:W) phase ratio, PVA 6% (w/v); and (C) PSm15, PS 10% (w/v), 2.5:20 (O:W) phase ratio and PVA 6% (w/v).

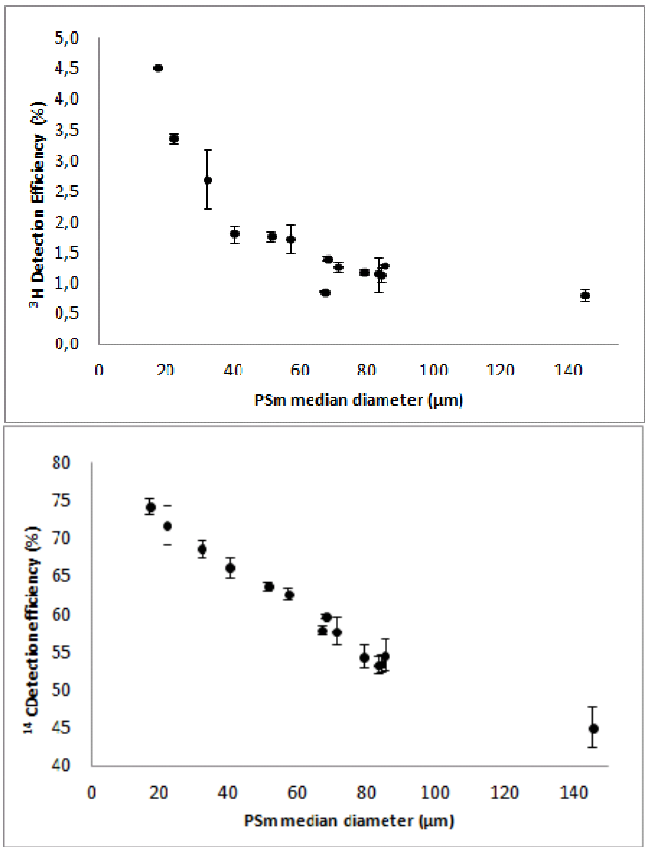

Figure 9. Correlation between detection efficiency and mean diameter measured for each PSm synthesis: a) for ^{3}H and b) for ^{14}C.

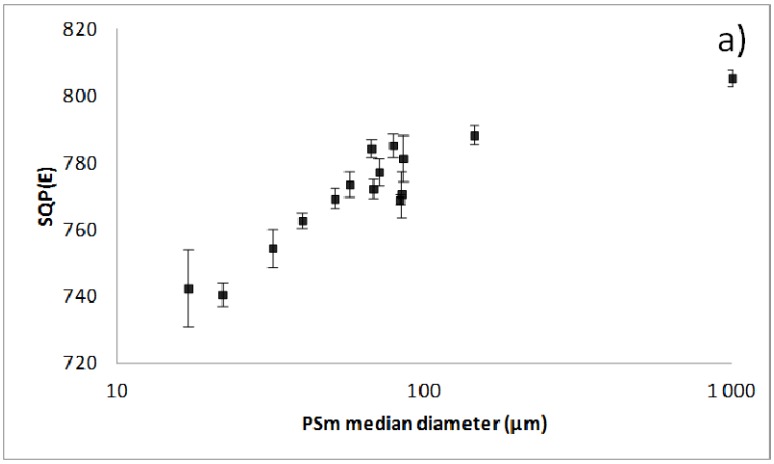

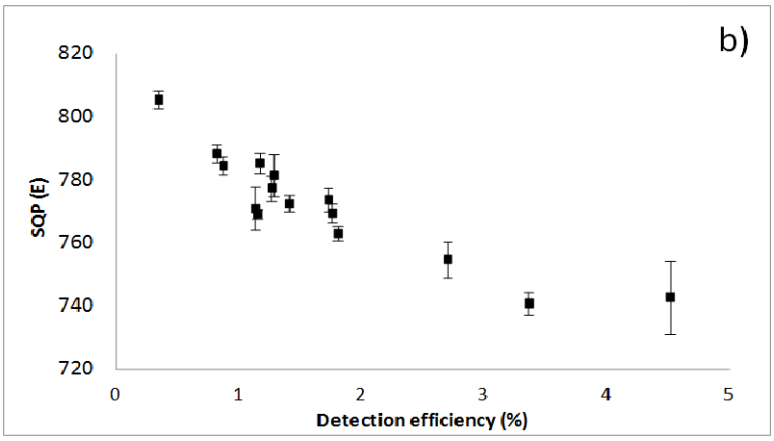

Figure 10. Correlation between the SQP(E) and the mean diameter of the PSm (a) and detection efficiency (b) for each PSm synthesized.

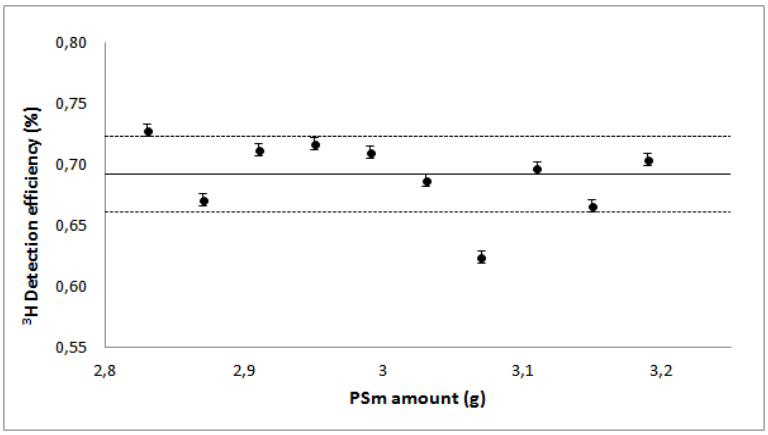

Figure 11. Evaluation of the influence of the amount of PSm added to the vial on the ^{3}H detection efficiency.

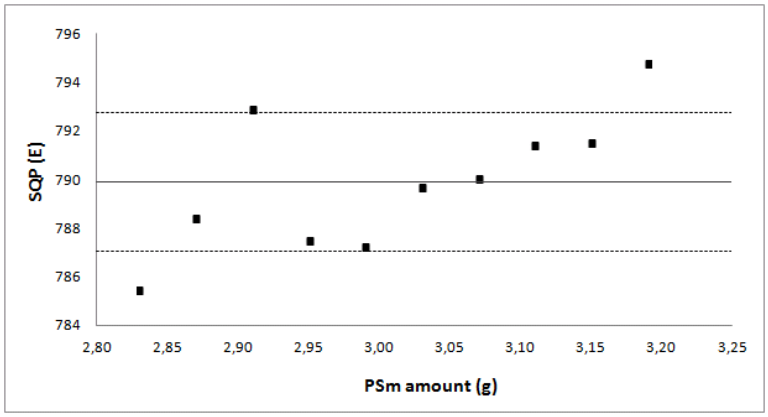

Figure 12. Variation of the SQP(E) parameter with regard to the amount of PSm added to the vial.

Table Captions

Table 1. Different parameters employed for PSm synthesis.

Synthesis	PS (g)	DCM (mL)	Temperature (ºC)	O:W	PVA (%)	Stirring speed (Hz)
PSm1	10	100	20	1:20	1	16.7
PSm2	10	100	20	1:20	1	8.3
PSm3	10	100	20	1:20	1	13.3
PSm4	10	100	20	1:20	2	16.7
PSm5	10	100	20	1:20	5	13.3
PSm6	10	200	20	2:20	1	16.7
PSm7	10	400	20	4:20	1	13.3
PSm8	20	200	20	2:20	1	16.7
PSm9	40	400	20	4:20	1	13.3
PSm10	10	100	35	1:20	1	16.7
PSm11	10	100	50	1:20	1	16.7
PSm12	10	100	20	1:20	1	16.7
PSm13	30	300	20	3:20	6	11.67
PSm14	30	600	20	6:20	6	11.7
PSm15	25	250	20	2.5:20	1	10.0

Table 2. Radiometric capacities and mean diameter of PSm synthesized.

	Particle size (μm)	Background (cpm)	^{3}H (%)	^{14}C (%)	^{90}Sr/^{90}Y (%)	^{241}Am (%)	SQP (E)
PSm1	84(26)	0.94(10)	1.13(12)	53.5(13)	186.3(4)	81.8(16)	771(7)
PSm2	85(25)	0.95(16)	1.28(3)	54.6(22)	188.5(11)	85.1(13)	781(7)
PSm3	79(26)	1.35(45)	1.16(4)	54.5(16)	186.7(15)	85.5(26)	785(3)
PSm4	71(24)	1.07(12)	1.26(8)	57.9(18)	187.9(5)	85.7(8)	777(4)
PSm5	51(24)	1.07(29)	1.75(8)	63.8(5)	190.1(7)	96.3(7)	769(3)
PSm6	40(13)	1.18(9)	1.80(15)	66.2(14)	189.7(18)	99.0(7)	763(2)
PSm7	22(9)	1.19(25)	3.36(8)	71.8(26)	194.4(45)	102.9(7)	741(3)
PSm8	68(24)	1.19(18)	1.40(3)	59.8(2)	188.3(13)	91.9(4)	772(3)
PSm9	57(24)	1.05(9)	1.73(24)	62.7(9)	190.3(11)	95.2(5)	774(4)
PSm10	145(62)	1.02(18)	0.81(9)	45.1(26)	184.8(25)	67.3(49)	788(3)
PSm11	-	0.97(8)	0.34(14)	19.8(92)	152.5(161)	30.7(159)	805(3)
PSm12	83(28)	1.19(6)	1.14(2)	53.4(9)	190.6(25)	83.8(18)	769(2)
PSm13	32(12)	1.29(12)	2.69(28)	68.7(12)	189.8(8)	99.7(14)	755(6)
PSm14	17(8)	1.20(16)	4.51(49)	74.3(10)	192.9(23)	102.9(2)	743(12)
PSm15	67(21)	1.03(16)	0.872(8)	57.9(6)	186.7(4)	83.4(2)	784(3)

Table 3. Detection efficiency and relative standard deviation obtained for the evaluation of vial preparation reproducibility.

Radionuclide	Detection efficiency (%)	Relative standard deviation (%)
^{3}H	0.66(3)	5.1
^{14}C	51.8(17)	3.3
$^{90}Sr/^{90}Y$	184.8(4)	0.3
^{241}Am	83.1(11)	1.3

Chapter 3.2

Production of plastic scintillation microspheres by using methods based on drying.

3.2.1. Polystyrene based sub-micron scintillating particles produced by supercritical anti-solvent precipitation.

3.2.2. Production of polystyrene-based scintillation microspheres for the measurement of radioactivity by spray-drying.

J. of Supercritical Fluids 103 (2015) 18–27

Contents lists available at ScienceDirect

The Journal of Supercritical Fluids

journal homepage: www.elsevier.com/locate/supflu

Polystyrene based sub-micron scintillating particles produced by supercritical anti-solvent precipitation

L.M. Santiago[a,*], Y. Masmoudi[b], A. Tarancón[a], R. Djerafi[b], H. Bagán[a], J.F. García[a], E. Badens[b]

[a] Department of Analytical Chemistry, University of Barcelona, Martí i Franquès 1-11, Barcelona, 08028, Spain
[b] Aix Marseille Université, CNRS, Centrale Marseille, M2P2 UMR 7340, Aix-en-Provence, 13454, France

ARTICLE INFO

Article history:
Received 12 August 2014
Received in revised form 17 April 2015
Accepted 17 April 2015
Available online 25 April 2015

Keywords:
Plastic scintillation microspheres
Plastic scintillation sub-micron particles
Supercritical anti-solvent process
Polystyrene
Radioactivity measurements
Alpha and beta radionuclides determination
Mixed waste
Optical quenching

ABSTRACT

Plastic scintillation microspheres (PSm) are a novel material employed in the measurement of radioactivity (α and β emitters). This work is focused on the formation of plastic scintillation particles through the precipitation and encapsulation of two fluorescent solutes (2,5-diphenyloxazol (PPO) and 1,4-Bis(5-phenyloxazol-2-yl) benzene (POPOP)) and an aromatic solvent 2,6-diisopropyl-naphthalene (DIN), which acts as an enhancer for α and β emitters discrimination, into a polymeric matrix of polystyrene (PS) by Supercritical Anti-Solvent process (SAS) using ethyl acetate (EtAc) for dissolving the PS and supercritical CO_2 as antisolvent. Different process parameters were varied; solute concentration in the organic solution (W, wt%), injection velocity of the organic solution (u, ms^{-1}), molar ratio of the organic solvent regarding to CO_2 (X_{EA}) and injection capillary tube diameter (μm). In the different experimental conditions tested, SAS coprecipitation was successfully achieved resulting in yields higher than 90% and very low quantities of residual solvent (600–1200 ppm). The different polystyrene based particles obtained were nearly spherical sub-micron particles (ranged between 150 and 400 nm) and also agglomerates of a few micrometers were observed in most of the studied conditions. Radiometric capacities of particles were evaluated through measuring different beta and alpha emitting radionuclide. The coprecipitates showed scintillation behavior when fluorescent solutes were added, therefore confirming their encapsulation.

1. Introduction

Plastic scintillators are solid dispersions formed by fluorescent solutes embedded in a polymeric matrix and are commonly used for the detection of neutron, alpha and beta particles and gamma radiation in different fields (i.e. radiation protection, high-energy particle physics, etc). When measuring with plastic scintillators, the energy of the radioactive particle or radiation is transferred to the polymeric matrix whereas the fluorescent solutes (primary and secondary) are responsible to convert this energy deposited into photons that are detected by means of photomultiplier tubes [1,2]. Plastic scintillators produced in form of microspheres with a diameter ranging from ten to hundreds micrometers, named Plastic Scintillation microspheres (PSm) [3], can be applied in the field of the radioactivity measurements and more specifically in the routine determination of beta and alpha emitting radionuclides in different samples. PSm are based on the same principle than liquid scintillation spectrometry (LS), which is the main technique used for these purposes [1,4], but with the advantage of not producing mixed waste (residue containing organic and radioactive compounds) [5]. Additionally, due to the fact of being solid and polymeric, PSm present other advantages that allow innovative and promising applications such as continuous monitoring of radionuclides in fluid streams [6], selective extracting scintillation support (PSm resin) [7] and scintillation reagent for the measurement of samples with a high salt content [8]. The possibility of producing plastic scintillation particles in the sub-micron range would extend the advantages of using them to other applications, such as, nanodosimeters in studies of energy deposition of very low-energy radionuclides (i.e. ^{3}H, ^{55}Fe and others) in bio-substances (DNA, etc).

Due to the lack of regular PSm suppliers, it is necessary to establish new methods for their synthesis, which can provide new compositions with different and controlled sizes [2]. Several methods have been employed for the production of polymeric microspheres: polymerisation of monomer [9] by several techniques (i.e. emulsion, suspension and dispersion); microspheres

* Corresponding author. Tel.: +34 934021281; fax: +34 934021233.
E-mail address: luzmarysantiago@gmail.com (L.M. Santiago).

http://dx.doi.org/10.1016/j.supflu.2015.04.015
0896-8446/

preparation from polymers using organic solvent extraction/evaporation [10]; microfluidic devices [11], electro-spray technique [12] and supercritical fluids [13]. Organic solvent evaporation/extraction methodology has been adapted successfully for the synthesis of polystyrene based PSm using dichloromethane (DCM) as the organic solvent of the polymer and the fluorescent solutes, obtaining spherical microparticles with a diameter around 70 μm and a yield of 100% [2]. However, when particles ranged in the sub-micron size are the target, this methodology presents limitations. Additionally, new procedures that reduce the amount of DCM by a more environmental friendly solvent would be desirable.

Supercritical fluid (SCF) methodology is a powerful tool regarding to the production of microparticles [13] or nanoparticles [14]. It shows potential advantages for the formation of particles with controlled characteristics [15], generally using carbon dioxide (CO_2) as a supercritical fluid, that presents the advantage of its non flammability, non toxicity, low critical temperature and low cost [16]. Since supercritical CO_2 is gaseous under ambient conditions, its separation from the final product is spontaneous upon depressurisation, avoiding thus subsequent separation steps. Compared to conventional processes of particle generation, the volume of organic solvents used can be reduced or even completely avoided resulting in final product containing low levels of solvent or completely free from residual traces. Particle generation can be carried out using the supercritical fluid as a solvent, as an anti-solvent or as a solute depending on the chemical nature and molecular weight of the compound to be precipitated. For polymers like polystyrene, which is not soluble in CO_2, the anti-solvent method can be applied and the resulting methodology that is derived is known as Supercritical Anti-Solvent process (SAS). Different variations of the SAS process have been developed and they differ from each other by the injection mode of the organic solution: Gas Anti-Solvent (GAS), Supercritical Enhanced Dispersion Solution (SEDS), Aerosol Solvent Extraction System (ASES) [17] and SAS using impinging jet (IJ-SAS) [18].

SAS process is based on the low solubility of the component to be precipitated in the supercritical fluid (i.e. CO_2), therefore involving the use of an organic solvent in which the material is first solubilised [19]. This organic solution is introduced in the autoclave through a capillary tube or a nozzle and it enters in contact with the supercritical CO_2. The organic solvent diffuses into the supercritical fluid phase whereas the CO_2 diffuses simultaneously into the liquid solution leading to the supersaturation of the solution and therefore the precipitation of the solute in a semi-continuous process [20].

SAS process has been successfully applied to several kind of compounds including polymers, bio-polymers, pharmaceutical molecules, inorganic and organic materials (i.e. coloring matters, catalysts, precursors of superconductors, etc), explosives and others either through particle micronisation [21] or micro or nanocomposites formation [13,22]. Different phenomena are involved in SAS process such as the phase behavior, the hydrodynamics, the mixing conditions, the kinetics of mass transfer as well as the kinetics of nucleation and growth and play a key role on the precipitate formation and its physical characteristics (i.e. particle size, morphology, polymorphism of crystalline compounds, etc).

Although production of polymeric particles using SCF is widely described, there are only few studies regarding the production of polystyrene micro or nanoparticles using SAS process methodologies, and some of them are based on the use of solvents like DCM or toluene [23,24] which are known by their high capacity to solubilize several polymers but also because of their toxicity. Dixon et al. have synthesized polystyrene microspheres and fibers through Precipitation with a Compressed fluid Anti-solvent (PCA) using toluene as the organic solvent [24]. Jeong et al. have prepared polystyrene submicron particles employing the Aerosol Solvent Extraction System (ASES) using DCM [23] and Reverchon et al. refers to the polystyrene forming solid bridges (coalesced) nanoparticles obtained at 150 bar and 40 °C through SAS using chloroform [14].

The aim of this work was to employ SAS technique in order to produce plastic scintillation sub-micron particles by coprecipitating polystyrene with fluorescent solutes, using ethyl acetate, a generally recognised as safe (GRAS) solvent. The desired composition for the particles will include polystyrene (PS), 2,5-diphenyloxazol (PPO) (primary fluorescent solute), 1,4-Bis (5-phenyloxazol-2-yl) benzene (POPOP) (second fluorescent solute) and 2,6-diisopropyl-naphthalene (DIN) (second organic solvent), all the components being soluble in ethyl acetate.

The production of plastic scintillation sub-micron particles was carried out while varying certain process parameters as: solute concentration in the organic solution (W, wt%), injection velocity of the organic solution (u, ms^{-1}), molar ratio of the organic solvent regarding to CO_2 (X_{EA}, %) as well as the capillary diameter (μm). The particles obtained were characterised by the evaluation of their morphology, size and radiometric capabilities. The quantity of the residual solvent in the formed scintillation was also quantified.

2. Materials and methods

2.1. Materials

Polystyrene (PS) (Mw 250.000) was provided by Acros Organics (Geel, Belgium), 2,6-diisopropylnaphthalene (purity 99%) and 2,5-diphenyloxazol (scintillation grade) were supplied by Merck (Darmstadt, Germany), 1,4-Bis (5-phenyloxazol-2-yl) benzene (scintillation grade) was supplied by the Montedison Group, Division Chimica (Milano, Italy), ethyl acetate (purity 99.8%) was provided by Carlo Erba Reagents (Milano, Italy) and Carbon dioxide (purity 99.7%) was purchased from Air Liquide (Marseilles, France).

For the radioactivity measurements, Pico Prias polyethylene vials of 6 mL (Perkin Elmer, USA) were used to prepare the samples using the following active stock solutions: a low-energy beta emitter, ^{3}H solution (HTO) with a concentration of 4.20(8) KBq g^{-1} in deionised water prepared from a standard of 69.8(12) kBq g^{-1}; a medium-energy beta emitter C-14 in form of labeled glucose of 132(2) Bq g^{-1} prepared from a standard of 2212(27) Bq g^{-1} from Amersham International (Buckinghamshire, UK) in a carrier solution of 50 μg g^{-1} of glucose and 1 mg g^{-1} of formaldehyde in deionised water. A $^{90}Sr/^{90}Y$ active stock solution which are in secular equilibrium and are both high-energy beta emitters of 38.4 (3) Bq g^{-1} prepared from a standard of 4.07(3) kBq g^{-1} from Amersham International in 0.1 M HCl; and finally, a ^{241}Am solution in form of Am^{3+} of 47.4(5) Bq g^{-1} prepared from a standard of 924(9) KBq g^{-1} supplied by Amersham International in 0.5 M HCl and deionised water.

2.2. SAS experimental set-up

The SAS experimental set-up used within this study is illustrated in Fig. 1. It is mainly composed of a 1 L stainless steel high pressure vessel (Top Industrie S.A. France). The CO_2 injection was insured thanks to a high pressure piston pump (LGP50, Separex, France) and the organic solution was injected through a HPLC pump (Gilson 307, France). The pressure was controlled during all the process through the use of a back pressure regulator (BPR) located at the output of the autoclave. The particles were collected on a stainless steel frit filter placed at the bottom of the autoclave.

In a typical SAS experiment, the autoclave is first heated and fed with CO_2 to set the operating pressure and temperature. Then pre-heated and regulated flows of CO_2 and the organic solvent are injected in co-current configuration. Once a steady-state

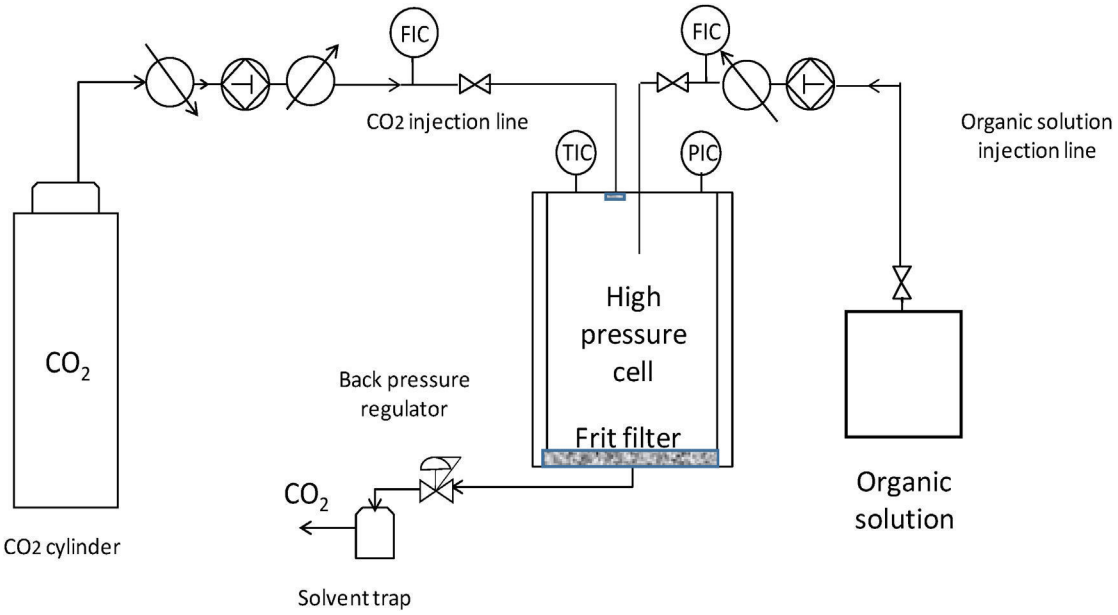

Fig. 1. Schematic diagram set-up for the SAS process.

composition conditions are obtained, the organic solvent is replaced with the organic solution dispersed through a capillary nozzle (127 and 254 μm). Precipitation process is then carried out for a fixed time defined by the final quantity of product to collect. A washing step is then performed to remove the remaining solvent by sweeping the autoclave with pure CO_2 for twice the residence time, considering that the autoclave behaves like a plug flow reactor [25]. Finally, the autoclave is depressurised to atmospheric pressure in order to recover the solid particles.

All the experiments were carried out through the same experimental methodology aforementioned, only the composition of the organic solution injected was varied according to PS micronisation or PS/fluorescent particles coprecipitations.

2.3. Organic solutions

Different organic solution compositions were prepared for the sub-micron scintillating particles micronisations. In all cases, ethyl acetate was employed as the organic solvent.

To perform polystyrene micronisations (P1 and P2 in Table 1), solutions of PS in ethyl acetate were prepared with a concentration of 3 mg mL^{-1} and 12 mg mL^{-1} corresponding respectively to PS mass fraction in the organic solution of 0.3 and 1.2 wt%. For scintillating particles coprecipitation, PS/ethyl acetate organic solutions were prepared with concentrations of 3 mg mL^{-1} (P3–P7) and of 12 mg mL^{-1} (P8–P11) of PS regarding the ethyl acetate. Fluorescent particles (PPO, POPOP) and DIN were added together (P3–P7) or subsequently (P8–P11) to the PS/ethyl acetate organic solution in mass fractions with regard to PS respectively of 2 wt%, 0.05 wt% and 20 wt%.

2.4. Characterisation of the micronized particles

The morphology and the size of micronized particles were observed using a JSM-7100F Field Emission Scanning Electron Microscope. Samples were attached by using double-coated adhesive tape and coated with gold by means a sputtering coater. The mean particle size of individual particles was calculated using Image J analysis software and measuring the size of minimum 100 particles for each synthesis from different SEM images.

2.5. Gas chromatography–mass spectrometry analysis

Two different gas chromatography equipments (Trace GC Thermo Scientific and 6890 N GC Agilent) coupled each one to a Mass Spectrometer (ITQ 900 Thermo Scientific and 5975 Inert Mass respectively) were used for quantifying the residual solvent content in the micronized particles. The measurement was carried out under the following equipment conditions: oven temperature at 40 °C (1 min); temperature ramp profile of 5 °C/min up to 325 °C (10 min); injector temperature 280 °C; injection mode: splitless; splitless time 1 min and transfer line temperature at 300 °C. Helium was used as carrier gas with a flow of 1 mL/min. The column used was composed of 5% diphenyl-95% dimethylpolysiloxane (Agilent GC Column type HP-5 MS 30 m length, 0.25 mm inner diameter). On the other hand, the mass spectrometer was used with a temperature source of 200 °C; solvent delay of 5 min, electronic ionisation mode and scanning from 50 until 550 uma.

2.6. Fourier transform infra-red spectroscopy measurements

A Thermo Scientific Nicolet iZ10 Fourier Transform Infrared equipped with an Attenuated Total Reflectance (ATR) diamond and a Deuterated Triglycerine Sulfate (DTGS) detector (ATR diamond/DTGS detector) was employed to obtain the FT-IR spectra and therefore, information about residual organic solvent in the micronized particles. The measure was performed under the following conditions: number of accumulation scans was 32, spectral resolution 4 cm^{-1} and a spectral range between 4000 and 525 cm^{-1}. For the measurement, the sample was placed directly on the diamond crystal and it was mechanically pressed to create a sample layer that allows the radiation pass through.

2.7. Radioactivity measurements

2.7.1. Sample preparation

Evaluation of the radiometric capabilities was carried out using the micronized plastic scintillation particles. Measuring vials were prepared by adding 0.3 g of plastic scintillation particles and 0.3 mL of solution (active or blank) into a 6 mL polyethylene vial. The active counting solutions were prepared by diluting in ethanol a known quantity of an active solution of the respective radionuclide

Table 1
Experimental conditions of SAS micronisation and coprecipitations.

Synthesis	Composition	Mass of solutes injected (g)	W(wt%)	X_{EtAc} (%)	u (ms^{-1})	Capillary (μm)	Qm CO_2 ($g\,min^{-1}$)	Qv EtAc ($mL\,min^{-1}$)	Particle size (nm)
Polystyrene precipitation									
P1	PS	1	0.3	4.5	4	127	30	3	197(±41)
P2	PS	1	**1.2**	4.5	4	127	30	3	305 (±99)
Polystyrene/PPO/POPOP/DIN coprecipitation									
P3	PS/PPO/POPOP/DIN	1	0.3	4.5	4	127	30	3	189 (±39)
P4	PS/PPO/POPOP/DIN	1	0.3	**9**	4	127	15	3	277 (±79)
P5	PS/PPO/POPOP/DIN	1	0.3	4.5	1	**254**	30	3	301 (±79)
P6	PS/PPO/POPOP/DIN	1	0.3	**9**	1	**254**	15	3	278 (±89)
P7	PS/PPO/POPOP/DIN	1	0.3	4.5	**1**	**127**	7.6	0.76	212 (±40)
Polystyrene/PPO/POPOP/DIN coprecipitation for radioactivity measurements									
P8	PS	**10**	1.2	4.5	4	127	30	3	274 (±85)
P9	PS/**PPO**	**10**	1.2	4.5	4	127	30	3	317 (±70)
P10	PS/PPO/**POPOP**	**10**	1.2	4.5	4	127	30	3	268 (±96)
P11	PS/PPO/POPOP/**DIN**	**10**	1.2	4.5	4	127	30	3	322 (±96)

to obtain the desired activity. Vials contained around 122.4, 6.3, 2.33 and 5.97 $Bq\,g^{-1}$ of ^{3}H, ^{14}C, $^{90}Sr/^{90}Y$ and ^{241}Am respectively. The blank vial was prepared adding 0.3 mL of ethanol into the 0.3 g of PSm.

All samples were prepared by triplicate and by weighing. To ensure a complete homogenisation, the vials were sonicated during 2 min using an Ultrasons-P ultrasonic bath (both from JP Selecta, Abrera, Spain) and they were centrifuged at 58.33 Hz during 10 min using a Macrotronic centrifuge (JP Selecta, Abrera, Spain).

2.7.2. Measurements

The radioactive samples were measured using two instruments. A 1220 Quantulus Liquid Scintillator Spectrometer (Perkin Elmer, USA) equipped with logarithmic amplification, a multichannel analyser (4096 channels distributed into four segments of 1024 channels) and background reduction through an active guard detector and a Triathler Liquid Scintillation Spectrometer (Hidex, Turku, Finland), which is a single sample detector equipped with one photomultiplier, a multichannel analyzer with 2048 channels and has alpha/beta discrimination capacities.

The measurements done in the Quantulus detector were performed using the configuration settings at low coincidence bias, and a ^{14}C multichannel analyzer. The counting time in the Quantulus for the blank, ^{3}H, ^{14}C and ^{241}Am samples was 60 min and 90 min for the $^{90}Sr/^{90}Y$ samples. The measurement of the external standard quenching parameter SQP(E) was fixed at 10 min. Background, $^{90}Sr/^{90}Y$ and ^{241}Am samples were also measured in the Triathler detector during 120 min in the "open" mode [26].

2.7.3. Data analysis

The detection efficiency (in percentage) was calculated as the ratio between the net count rate (in counts per minute) in the entire spectrum and the added activity to the measurement vial (in disintegrations per minute).

The SQP(E) parameter is calculated by the detector and it can be used to evaluate the degree of quenching in the sample. It corresponds to the channel of the spectrum generated by the external gamma source in which the cumulative area is 99.75% of the total area [27]. Specific details about data treatment are given in the supplementary material section.

3. Results and discussions

As far as it is known, no bibliographical study reports PS micronisation through SAS process using ethyl acetate solvent. In this study, different experiments were carried out varying the operating conditions to produce sub-micron scintillating particles. Values selected for carrying out the experiments are shown in Table 1. For all the experiments the temperature and the pressure were kept constant at 307 K and 10 MPa. The temperature was set at this value to work at mild conditions and avoid as far as possible the plasticisation of the polystyrene which can result in agglomerated and coalesced particles or even the formation of films (reported by some authors at 313 K [24]).

According to previous works on PS micronisation, Dixon et al. [24] showed that the variation of the pressure between 8 and 19 MPa at 308 K does not result in significant variation in particle characteristics (size and morphology). Jeong et al. [23] observed fine particles of PS at 308 K and at 10 and 15 MPa, whereas further increase in the pressure (20 and 25 MPa) leads to larger particles.

Therefore, for this work, pressure was kept constant at a relative low value (10 MPa). According to previous works on the ethyl acetate/CO_2 phase equilibria [28–30], this pressure ensures a monophasic state of the mixture. The ternary phase diagram formed by solute/solvent/anti-solvent can behave like the binary system solvent/anti-solvent [22] when the solute concentration is very low and can be considered as negligible. It is estimated that at solute concentration lower than 1 wt%, the solution is close to the dilute region [24].

3.1. Production of polystyrene particles

SAS process was first applied to micronize polystyrene (experiments P1 and P2 in Table 1). For these experiments the molar ratio solvent/CO_2, (X_{EA}), was set to 4.5%, the injection velocity to 4 ms^{-1} and the capillary diameter to 127 μm. According to previous works [23] [24], increasing the polystyrene concentration in the organic solution leads to a severe increase in particle size and even the formation of fibers since increasing the viscosity of the solution favors stabilizing viscous forces and therefore delaying the jet disintegration during the organic solution dispesion. In order to limit particles agglomeration and fiber formation, the concentration of polystyrene in the organic solution was tested at 0.3 wt% and 1.2 wt%.

In both tested conditions, precipitation yield was higher than 90%. It was not possible to recover the entire product due to high static electricity. Nearly spherical sub-micron particles (150 to 400 nm) were obtained as illustrated in Fig. 2 with a slight increase in particle size when increasing the concentration of polystyrene in the organic solution. Nevertheless, as it is shown in Fig. 3, a second population of more aggregated (fused and coalesced) particles was also observed by SEM.

The presence of these two populations of particles can be explained by the mixing conditions leading to different local supersaturations in the autoclave, either in the dispersed phase or in the continuous one.

Moreover, the plasticizing effect of CO_2 could favor the agglomeration of these particles. Indeed, contact between softened

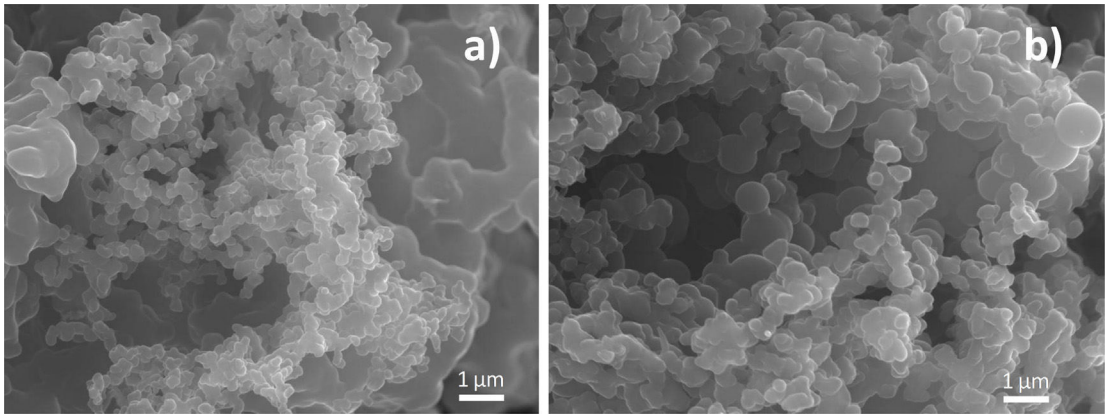

Fig. 2. Polystyrene particles obtained by SAS process (at 10 MPa, 307 K, X_{EA} = 4.5 wt%, u = 4 ms^{-1}, capillary = 127 μm) at a polystyrene concentration in the organic solution of (a) 0.3 wt% (P1) and (b) 1.2 wt% (P2).

particles enhances their coalescence. Increasing the polymer concentration in the organic solution from 0.3 wt% to 1.2 wt% does not seem to induce large modifications on the morphology of the resulting particles, which can also affect the radiometric capacities.

3.2. Production of scintillating particles

Scintillating particles were produced by the sequential coprecipitation of polystyrene with PPO, POPOP and DIN. In order to study the influence of the operating conditions on coprecipitation, experimental conditions were varied according to Table 1 (experiments P3–P7).

The presence of the fluorescent particles does not seem to induce significant modifications on the morphology of the resulting particles. Indeed, coprecipitations in the same experimental conditions than PS micronisation (experiments P3 and P11 comparing to experiments P1 and P2) lead to similar morphologies of resulting particles and comparable particles sizes. As illustrated in Fig. 4, submicron particles were also obtained when the fluorescent particles are added as well as a population of coalescent particles.

The influence of some operating conditions on coprecipitation was then evaluated while keeping a PS concentration in the organic solution of 0.3 wt%.

The influence of the hydrodynamic conditions was first evaluated by decreasing the velocity of the organic solution from 4 ms^{-1} to 1 ms^{-1} with the same capillary diameter of 127 μm which reduces the Reynolds number by a factor of 4 (P3 and P7 respectively in Table 1). As it was mentioned, micronized coprecipitates for P3 (at 4 ms^{-1}) were basically composed by nearly spherical particles ranged around 200 nm and more coalescent particles. However, coprecipitates formed at a jet velocity of 1 ms^{-1} (P7), showed a more homogeneous morphology since only the population of sub-micron particles were observed through SEM characterisations (Fig. 5b).

This unexpected result could be explained by the different mixing efficiencies. Indeed, for lower Reynolds number, the mixing conditions are less favorable which can lead to high local supersaturations in the dispersion zone resulting in small particles.

By increasing the capillary diameter from 127 μm to 254 μm (P5) at a velocity of the organic solution of 1 ms^{-1} the hydrodynamic conditions were intermediary between those of P3 and P7 (Fig. 6c). In these conditions, the resulting powders show two populations of particles comparable to those of P3 (Fig. 6a). The influence of the solvent/CO_2 molar ratio was evaluated for the two capillary diameters by increasing X_{EA} from 4.5% to 9% (P3/P4 and P5/P6 in Table 1).

For a capillary diameter of 127 μm, the morphology of the obtained powder was similar for the two molar solvent/CO_2 ratios (P3 and P4). By increasing the solvent/CO_2 molar ratio at a capillary diameter of 254 μm, the obtained particles still show two populations of particles; however the population of coalesced particles was more present for the highest solvent molar ratio (P6). The increase in particle agglomeration can be explained by slower mass transfer phenomena. Indeed, by increasing the capillary diameter, the surface to volume ratio of the plain jet (above the break-up zone) is reduced limiting the mass transfer phenomena. Moreover,

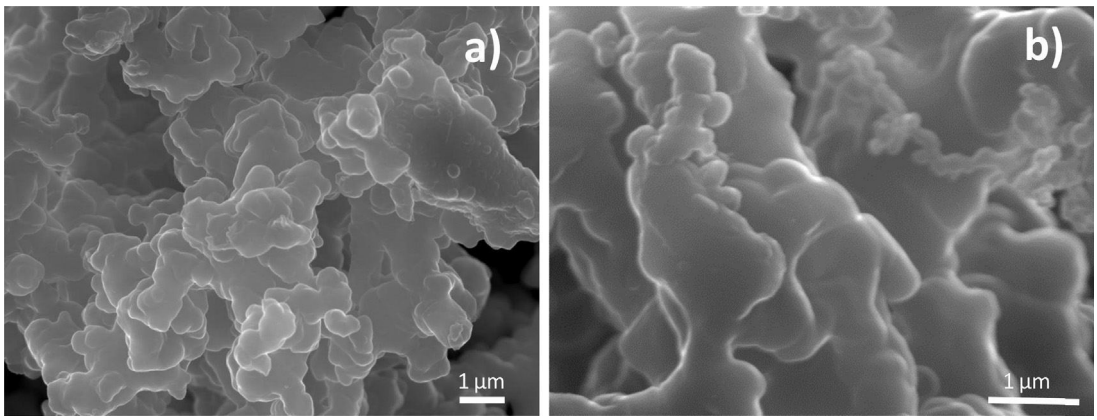

Fig. 3. Fused and coalesced polystyrene particles obtained by SAS process (at 10 MPa, 307 K, X_{EA} = 4.5 wt%, u = 4 ms^{-1}, capillary = 127 μm) at a polystyrene concentration in the organic solution of (a) 0.3 wt% (P1) and (b) 1.2 wt% (P2).

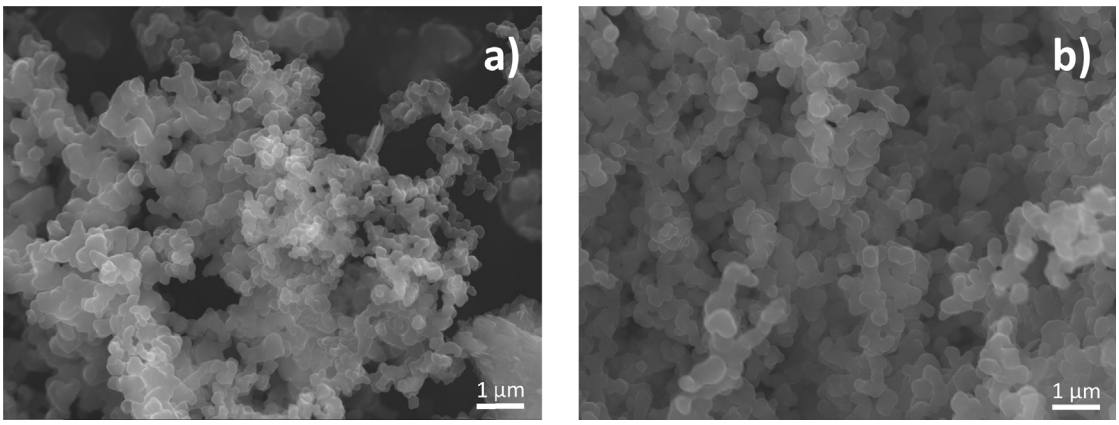

Fig. 4. Influence of polystyrene concentration in the organic solution on the resulting PS/PPO/POPO/DIN coprecipitates (at 10 MPa, 307 K, X_{EA} = 4.5 wt%, u = 4 ms^{-1}, capillary = 127 μm) (a) 0.3 wt% (P3); (b) 1.2 wt% (P11).

by increasing the solvent/CO_2 molar ratio, the concentration gradient between the continuous phase and the dispersed one is lowered leading also to slower mass transfer kinetics.

As a result, lower supersaturations are reached leading to lower nucleation frequencies favoring thus particle growth. Coalescence is then enhanced on those biggest softened particles.

The reproducibility of the production of sub-micron polystyrene and scintillating particles can be evaluated taking into account the reproducibility of PS micronisation of P8 compared to P2. Moreover, a series of coprecipitations was carried out by adding sequentially to the polystyrene solution (P2) the primary fluorescent solute PPO (P9), then the secondary fluorescent solute POPOP (P10), and finally the alpha/beta discrimination enhancer DIN (P11). Those experiments were carried out in order to evaluate the radiometric capabilities of the produced coprecipitates and to confirm the encapsulation of the fluorescent solutes and DIN within the polystyrene matrix. According to the obtained results and SEM images, the morphology, particle diameters and populations for all the obtained particles were similar, therefore ensuring a reproducible behavior.

3.3. Radioactivity measurements

The optimal encapsulation of the fluorescent solutes within the polymeric matrix can be determined by evaluating the radiometric capabilities. Detection efficiency, SQP(E) and spectrum position are determined by using the sub-micron particles and measuring beta emitters of different energies and an alpha emitter.

3.3.1. Beta and alpha emitting radionuclides

The results obtained when beta emitters (^{3}H, E_{max}: 18.6 KeV; ^{14}C, E_{max}: 156.5 KeV; ^{90}Sr/^{90}Y, E_{max} = 545.9 keV and E_{max} = 2279.8 keV respectively) and alpha emitter (^{241}Am, E_{max}: 5637.8 KeV) are measured with the sub-micron particles and they are summarised in Table 2.

As it can be seen in the Table 2, when beta emitters of low and medium energy (^{3}H and ^{14}C, respectively) were measured using the P8, the resulting detection efficiency was very low, since the particles were composed only by PS, which has a fluorescent wavelength emission around 270 nm and corresponds to a region of the spectra in which the photomultipliers (PMT) quantum efficiency is low, taking into account that the quantum efficiency of the PMT is wavelength-dependent and it has a maximum around 400 nm. On the other hand, in the case of ^{90}Sr/^{90}Y and ^{241}Am, the values of detection efficiency are higher because they are more energetic and as a consequence, more photons are produced for each disintegration and the probability to be detected increases. However these values of detection efficiency are far from those expected (180% and 100% respectively from previous experiments) [2].

An increase of the detection efficiency was observed for all the measured emitters when P9 were employed, since the PPO was correctly encapsulated. PPO is a primary fluorescent solute which has the capability to shift the photon wavelength to a higher value, since it absorbs the energy deposited in PS and reemits it at 354 nm. The same behavior was observed when the second fluorescent solute (POPOP) was encapsulated in P10. The detection efficiency increased significantly for all the radionuclides, since the POPOP is a wavelength shifter with a maximum emission wavelength at

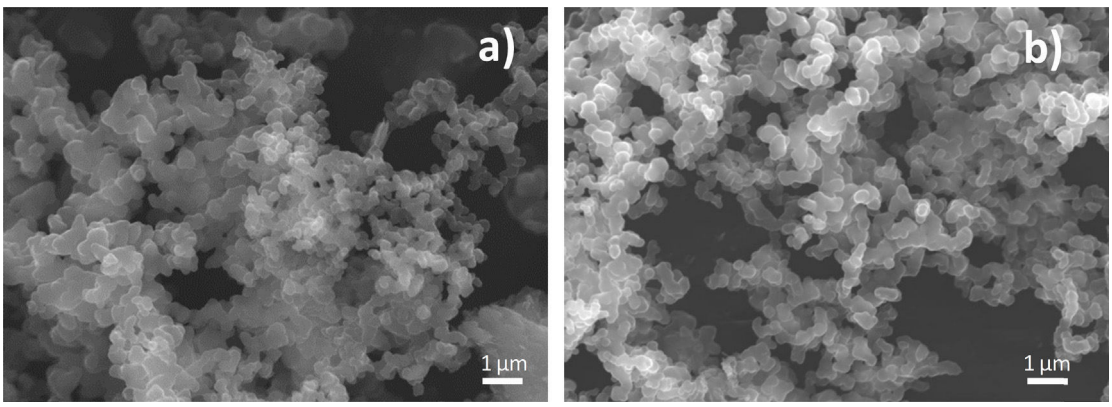

Fig. 5. Influence of the jet velocity (u) on the resulting PS/PPO/POPO/DIN coprecipitates (at 10 MPa, 307 K, 0.3 wt%, X_{EA} of 4,5% and both using 127 μm capillary diameter) (a) u = 4 ms^{-1} (P3); (b) u = 1 ms^{-1}(P7).

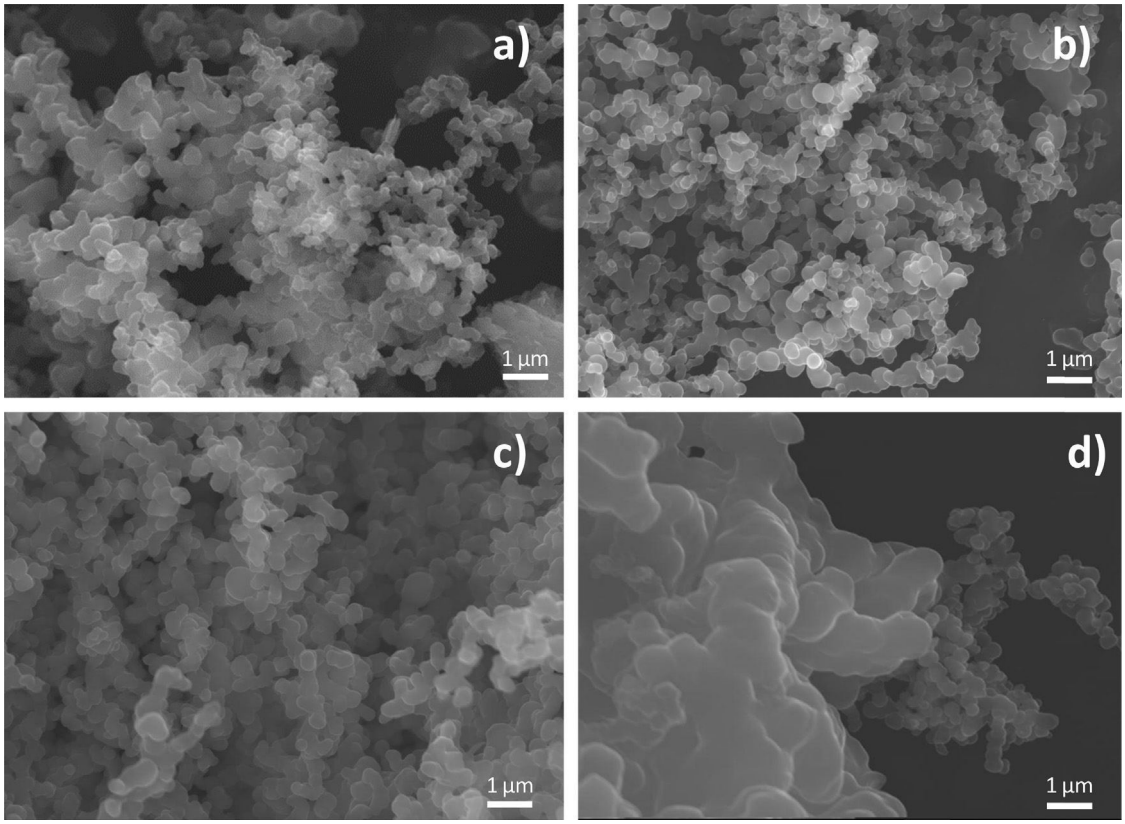

Fig. 6. Influence of the solvent/CO_2 molar ratio (X_{EA}) and the capillary diameter (d_c) on the resulting PS/PPO/POPO/DIN coprecipitates (at 10 MPa, 307 K, 0.3 wt%) (a) d_c = 127 µm, u = 4 ms^{-1} X_{EA} = 4,5 (P3); (b) d_c = 127 µm, u = 4 ms^{-1}, X_{EA} = 9 (P4); (c) d_c = 254 µm, u = 1 ms^{-1}, X_{EA} = 4,5 (P5); (d) d_c = 254 µm, u = 1 ms^{-1}, X_{EA} = 9 (P6).

407 nm and matches much better with the wavelength of maximum quantum efficiency of the PMT. However, detection efficiency values were still lower than those obtained in a previous work developed by Santiago et al., especially for ^{3}H and ^{14}C, where PSm of the same composition were synthesized by the organic solvent extraction-evaporation methodology [2].

In scintillation measurements, the decrease on the detection efficiency is associated to losses on the transfer of energy from the initial energy of the radioactive particle until the pulse generated when the photons are detected by the PMTs (i.e. quenching). When measuring with PSm, particle and optical quenching effects are the more relevant. Decrease of the detection efficiency for submicron particles is due to a balance between both phenomena and its relationship with the scintillating particle diameter.

Particle quenching is related to the lost of energy of the particle before it reaches the scintillating particle surface, since it is stopped by interactions with the medium in which it is travelling (i.e. aqueous solution). It may be expected that scintillating polymeric particles obtained in the sub-micrometric range suffer less particle quenching than microspheres of higher diameter, because the distance they have to travel is lower and as consequence detection efficiency may be higher. However, this effect is compensated negatively by the inefficient light transmission caused by the optical quenching. When produced light photons travel along of a non homogeneous track composed by polymeric particles and aqueous solutions with different refraction index (1.5 and 1.33, respectively), the photons suffer multiple reflection and transmission processes which may lead the loss of all or part of its energy. The probability that at least one photon reaches the photomultiplier is correlated with the energy of the radionuclide and with the size of the scintillating particles, since smaller particles implies a more tortuous track for the photons.

3.3.2. Spectrum and SQP(E)

SQP(E) provides information about how efficient is the transformation of the particles energy into scintillation photons and therefore, about the quenching processes that are taking place in the measurement. As it can be observed on the Table 2, values of SQP(E) were around 410 for all the synthesis. These values were very low regarding to those obtained by Santiago et al. [2] when PSm of 130 µm of diameter and containing PS/PPO/POPOP were used in the measurement of beta and alpha radionuclides (around 780).

On the other hand, the spectrum position in Fig. 7 shows clearly that fluorescent solutes have been encapsulated. The spectrum corresponding to P8 is shifted to very low energies, while, when the

Table 2
Values obtained for the background (in counts per minute); detection efficiencies (in %) and SQP(E) in the measurement of ^{3}H, ^{14}C, ^{90}Sr/^{90}Y and ^{241}Am solutions using the particles obtained in synthesis P8, P9, P10 and P11.

	^{3}H (%)	^{14}C (%)	^{90}Sr/^{90}Y (%)	^{241}Am (%)	SQP(E)
P8 (PS)	0.008(2)	0.9(1)	58.4(6)	35.6(38)	412(9)
P9 (PS/PPO)	0.032(7)	2.8(4)	68.2(22)	55.0(40)	406(10)
P10 (PS/PPO/POPOP)	0.237(22)	13.8(6)	101.2(12)	88.9(28)	416(3)
P11 (PS/PPO/OPOPOP/DIN)	0.092(2)	7.7(4)	95.8(5)	79.9(29)	410(5)

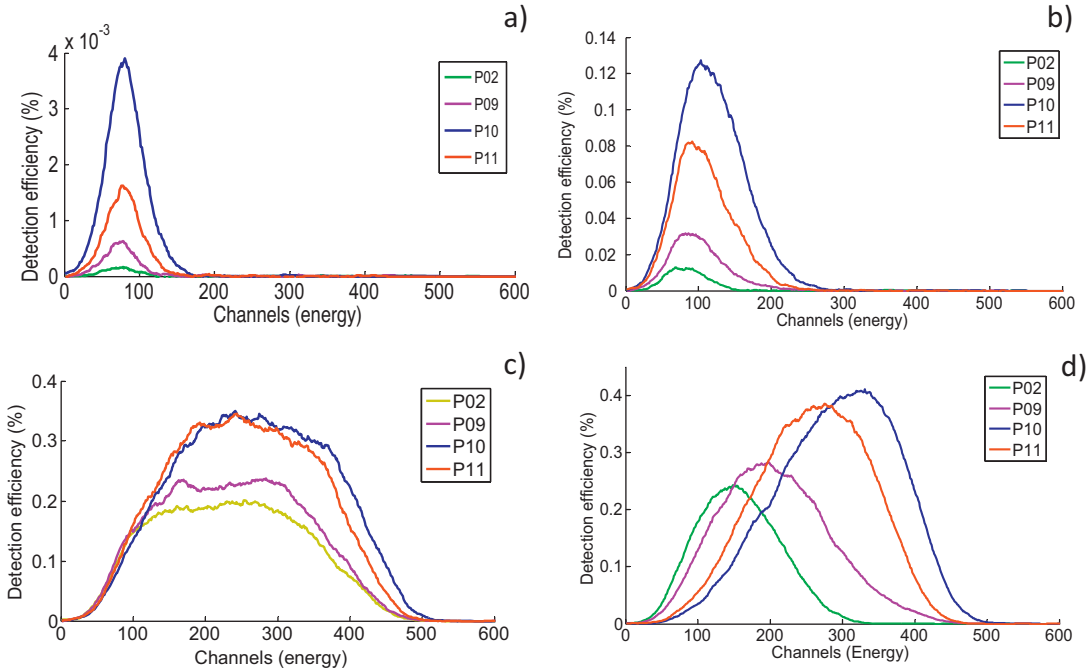

Fig. 7. Spectra obtained in the measurement of: (a) ^{3}H; (b) ^{14}C; (c) ^{90}Sr/^{90}Y and (d) ^{241}Am with the sub-micron particles synthesized in P8, P9, P10 and P11.

PPO and POPOP were encapsulated (P9 and P10, respectively) the spectra were located at higher energies in comparison with P8. However the maximum of the spectra (i.e. channel 500 for ^{90}Sr/^{90}Y in sub-micron particles containing PS/PPO/POPOP) is located at lower channels if when comparing with PSm of higher diameter (i.e. channel 900 for ^{90}Sr/^{90}Y in PSm containing PS/PPO/POPOP).

Values of SQP(E) and spectra of the alpha and beta emitters in the Fig. 7 confirm that even when the fluorescent solutes are encapsulated, enhancing the detection efficiency, a quenching phenomenon is affecting the measurement leading to obtain a spectrum located at very low energies. Since particle quenching may be reduced when sub-micron particles are used, the main reason of this lost of energy may be due to the optical quenching.

3.3.3. Alpha/beta measurements

Plastic scintillation sub-micron particles containing DIN (P11), were used to evaluate their alpha/beta discrimination capabilities. Since this compound causes a delay on energy transmission between the different components of the scintillator leading to a delay of the alpha pulses regarding to the beta ones. This delay is the basis of the alpha/beta discrimination methods and can be detected by electronics devices [31,32].

In the Fig. 8, the two spectra obtained from the measurement of ^{90}Sr/^{90}Y and ^{241}Am with the Triathler spectrometer are shown. As it can be observed, the ^{241}Am spectrum shows a small difference regarding to the ^{90}Sr/^{90}Y one in the time axis. Although there is small evidence of discrimination, it is necessary to remark that an optimal discrimination is not possible and the main responsible of this fact is the optical quenching, which has shifted the spectra to lower energies in the range of the luminescence signal.

3.4. Residual solvent quantification

Plastic scintillation sub-micron particles were characterised by Fourier Transform Infrared Spectroscopy (IR-FT) and Headspace Gas Chromatography coupled with Mass Spectrometry (GC/MS) in order to evaluate the organic solvent retained during the microencapsulation process.

The IR-FT spectrum (attached in the supplementary material) suggests that the solvent was not included within the sub-micron

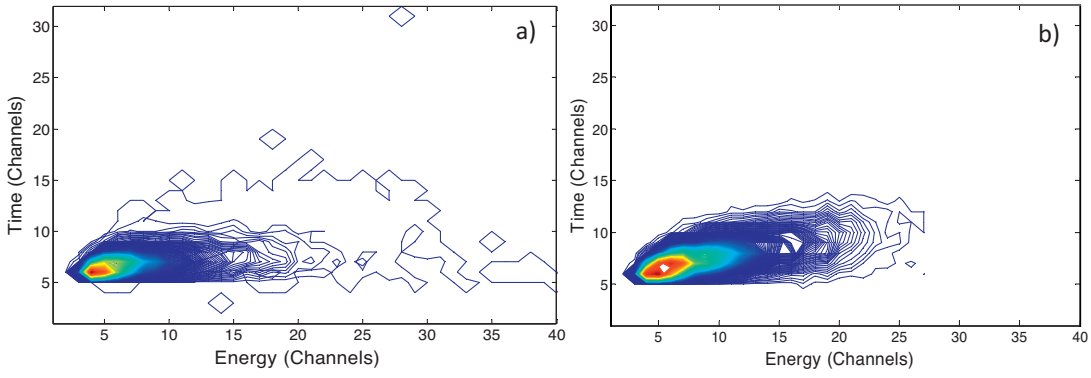

Fig. 8. 2D spectra obtained with the Triathler spectrometer: (a) ^{90}Sr/^{90}Y, (b) ^{241}Am.

scintillating particles synthesized by SAS, since the main peak of ethyl acetate located at 1725 cm^{-1} and corresponding to the C=O stretch was not observed in the spectrum of P8. To confirm this result, a more sensitive analytical technique, Headspace Gas Chromatography coupled with Mass Spectrometry (GC/MS), was employed to analyse the particles and by means of the characteristic signal of EtAc at 6.72 min the values of remaining solvent were determined. They were ranged between 550 and 1250 ppm for the synthesis (P8, P9, P10 and P11). These values were low taking into account that according to the European Medicines Agency, ethyl acetate is considered to be a Class 3 solvent and 5000 ppm is accepted as a limit for pharmaceutical purposes [33] and additionally, because of these remaining quantities of solvent does not produce any significant interference on the scintillation process.

4. Conclusions

Plastic scintillation sub-micron particles composed by polystyrene, fluorescent solutes and DIN were synthesized successfully by SAS process achieving yields around 90%. Different synthesis parameters were evaluated. In almost all the synthesis conditions, two populations of nearly spherical sub-microns particles sizing between 150 and 400 nm and more coalescent particles were obtained. Parameters used in the P7 synthesis (PS/PPO/POPOP/DIN, 307 K, 10 MPa, 4.5% X_{EA}, 0.3% W, 1 ms^{-1} and capillary diameter of 127 μm) seem to be the most appropriated for obtaining one population of more homogeneous sub-micron coprecipitates with narrower particle sizes.

According to the information obtained by multiple headspace GC-MS, quantities of residual solvent (between 550 and 1250 ppm) were observed in the synthesized particles, considered as a low value according to the European Medicine Agency, which establishes the limit in 5000 ppm for pharmaceutical products.

Radiometric capabilities were evaluated resulting in low values of detection efficiency for ^{3}H and ^{14}C and acceptable values for $^{90}Sr/^{90}Y$ and ^{241}Am. The encapsulation of the fluorescent solutes was achieved and demonstrated because the detection efficiency values observed for the synthesis including PPO (P9), were higher than those obtained for the synthesis containing only the PS (P8), and the one including the PPO and POPOP (P10) was even higher than the P9.

The low SPQ(E) values obtained and the location of the sample spectra at low energies indicated the existence of an important degree of optical quenching.

The availability of scintillating particles in the sub-micron range opens new possibilities to the measurement of radioactivity employing plastic scintillators at the nanoscale range.

Acknowledgments

The authors thank the Ministerio de Ciencia e Innovación (Spain) (MICINN) and Agència de Gestió d'Ajuts Universitaris i de Recerca (AGAUR) (Spain) for financial support under CTM2008-01147/CTM2011-27211 and 2009-SGR-1188 respectively.

Appendix A. Supplementary data

Supplementary data associated with this article can be found, in the online version, at http://dx.doi.org/10.1016/j.supflu.2015.04.015

References

[1] M.F. L'Annunziata, Handbook of Radioactivity Analysis, 2nd ed., Academic Press, San Diego, 2012, pp. 439–576.
[2] L.M. Santiago, H. Bagán, A. Tarancón, J.F. García, Synthesis of plastic scintillation microspheres: evaluation of scintillators, Nuclear Instruments and Methods in Physics Research A 698 (2013) 106–116.
[3] L.M. Santiago, H. Bagán, A. Tarancón, J.F. García, G. Rauret, Systematic study of particle quenching in organic scintillators, Nuclear Instruments and Methods in Physics Research A 698 (2013) 26–36.
[4] S.S. Moebius, T.L. Moebius, Handbook of Liquid Scintillation Spectrometry, 1st ed., Karlsruhe Institute of Technology, Karlsruhe, 2012, pp. 6–9, ISBN:392370478X, 9783923704781.
[5] A. Tarancón, J.F. García, G. Rauret, Reusability of plastic scintillators used in beta emitter activity determination, Applied Radiation and Isotopes 59 (2003) 373–376.
[6] A. Tarancón, A. Padro, J.F. García, G. Rauret, Development of a radiochemistry sensor, part: 2. Application to liquid effluents, Analytica Chimica Acta 538 (2005) 241–249.
[7] H. Bagán, A. Tarancón, L. Stavsetra, G. Rauret, J.F. García, Determination of oil reservoir radiotracer ($S^{14}CN^{-}$) in a single step using a plastic scintillation extractive scintillation resin, Analytica Chimica Acta 736 (2012) 30–35.
[8] H. Bagán, A. Tarancón, S. Hartvig, G. Rauret, J.F. García, Plastic vs. liquid scintillation for ^{14}C radiotracers determination in high salt matrices, Analytica Chimica Acta 631 (2009) 229–236.
[9] S. Freiberg, X.X. Zhu, Polymer microspheres for controlled drug release, International J. Pharmaceutics 282 (2004) 1–18.
[10] J.K. Vasir, K. Tambwekar, S. Garg, Bioadhesive microspheres as a controlled drug delivery system, International J. Pharmaceutics 255 (2003) 13–32.
[11] B. Amsdem, The production of uniformly sized polymer microspheres, Pharmaceutical Research 16 (1999) 1140–1143.
[12] H. Moghadam, M. Samimi, A. Samimi, M. Khorram, Electro-spray of high viscous liquids for producing mono-sized spherical alginate beads, Particuology 6 (2008) 271–275.
[13] J. Jung, M. Perrut, Particle design using supercritical fluids: literature and patent survey, J. Supercritical Fluids 20 (2001) 179–219.
[14] E. Reverchon, I. De Marco, E. Torino, Nanoparticles production by supercritical antisolvent precipitation: a general interpretation, J. Supercritical Fluids 43 (2007) 126–138.
[15] E. Reverchón, M. Cleofe, G. Caputo, Supercritical fluid processing of polymers: composite particles and porous materials elaboration, Current Opinion in Solid State and Materials Science 7 (2003) 391–397.
[16] E. Beckman, Supercritical and near-critical CO_2 in green chemical synthesis and processing, J. Supercritical Fluids 28 (2004) 121–191.
[17] S. Yeo, E. Kiran, Formation of polymer particles with supercritical fluids: a review, J. Supercritical Fluids 34 (2005) 287–308.
[18] S. Careno, O. Boutin, E. Badens, Drug recrystallization using supercritical antisolvent (SAS) process with impinging jets: effect of process parameters, J. Crystal Growth 342 (2012) 34–41.
[19] O. Boutin, E. Badens, E. Carretier, G. Charbit, Co-precipitation of a herbicide and biodegradable materials by the supercritical anti-solvent technique, J. Supercritical Fluids 31 (2004) 89–99.
[20] L. Lesoin, C. Crampon, O. Boutin, E. Badens, Preparation of liposomes using the supercritical anti-solvent (SAS) process and comparison with a conventional method, J. Supercritical Fluids 57 (2011) 162–174.
[21] J. Fages, H. Lochard, J. Letourneau, M. Sauceau, E. Rodier, Particle generation for pharmaceutical applications using supercritical fluid technology, Powder Technology 141 (2004) 219–226.
[22] E. Reverchón, R. Adami, G. Caputo, I. De Marco, Spherical microparticles production by supercritical antisolvent precipitation: Interpretation of results, J. Supercritical Fluids 47 (2008) 70–84.
[23] H. Jeong, K. Yoo, J. Lim, Preparation of polystyrene submicron particles using ASES process in supercritical carbon dioxide, J. Industrial and Engineering Chemistry 14 (2008) 77–83.
[24] D. Dixon, P. Johnston, Polymeric materials formed by precipitation with a compressed fluid antisolvent, Materials Interfaces and Electrochemical Phenomena 39 (1993) 127–139.
[25] E. Carretier, E. Badens, P. Guichardon, O. Boutin, G. Charbit, Hydrodynamics of supercritical anti-solvent precipitation: characterisation and influence on particle morphology, Industrial & Engineering Chemistry Research 42 (2003) 331–338.
[26] Triathler Manual Procedure. Hidex Oy, Turku, Finland, (2010), pp. 5–30.
[27] Quantulus™ Instrument Manual, 1220-931-06, 2002. Perkin Elmer Life Sciences. Ultralow level liquid scintillation spectrometer ⟨http://www.perkinelmer.com/content/manuals/gde_quantulusinstrumentmanual.pdf⟩, 2014. (accessed 22.01.14).
[28] H.S. Byun, M.Y. Choi, J.S. Lim, High pressure phase behavior and modeling of binary mixtures for alkyl acetate in supercritical carbon dioxide, J. Supercritical Fluids 37 (2006) 323–332.
[29] G.R. Borges, A. Junges, E. Franceschi, F.C. Corazza, M.L. Corazza, J.V. Oliveira, C. Dariva, High-pressure vapor–liquid equilibrium data for systems involving carbon dioxide + organic solvent + carotene, J. Chemical Engineering 52 (2007) 1437–1441.
[30] R. Djerafi, Y. Masmoudi, C. Crampon, A. Meniai, E. Badens, Supercritical antisolvent precipitation of ethyl cellulose, J. Supercritical Fluids (2015), http://dx.doi.org/10.1016/j.supflu.2015.02.033
[31] J. Thomson, Di-isopropylnaphthalene—a new solvent for liquid scintillation counting, In Liquid Scintillation Counting and Organic Scintillators (H. Ross, J. E. Noakes, and J. D. Spaulding, Eds). pp. 19–34. Lewis Publishers, Chelsea, MI.

[32] J.M. Pates, G. T. Cook, A. B. MacKenzie, Alpha/beta separation liquid scintillation spectrometry: current trends, In: G. T. Cook, D.D., Harkness, A.B., MacKenzie, B. F. Miller, E. M. Scott (Eds), Proceedings of Advances in Liquid Scintillation Spectrometry, 1994., Radiocarbon Publishers, University of Arizona, 1996,pp. 267–281.

[33] European Medicine Agency, CPM/ICH/283/95. ICH Topic Q3C(R4). Impurities: guideline for residual solvents. ⟨http://www.ema.europa.eu/docs/en_GB/document_library/Scientific_guideline/2009/09/WC500002674.pdf⟩, 2009.

Chapter 3.2

Production of plastic scintillation microspheres by using methods based on drying.

3.2.1. Polystyrene based sub-micron scintillating particles produced by supercritical anti-solvent precipitation.

3.2.2. Production of polystyrene-based scintillation microspheres for the measurement of radioactivity by spray-drying.

Production of polystyrene-based scintillation microspheres for the measurement of radioactivity by spray-drying

Luz M. Santiago[1], Alex Tarancón[1]*, Héctor Bagán[1, 2], José F. García[1]

[1]*Department of Analytical Chemistry, University of Barcelona, Martí i Franqués, 1-11, E-08028, Barcelona, Spain*

[2] *Department of Pure and Applied Biochemistry, Lund University, Getingevägen 60, hus II, SE-22100, Lund, Sweden*

Abstract

The use of plastic scintillation microspheres (PSm) is an innovative technique for measuring the radioactivity of beta-emitting radionuclides. PSm can be produced via different methods; none of which has been assayed at the industrial scale. In the present paper, we evaluate the production of PSm by spray-drying on an industrial scale. Our results indicate that fluorescent solutes were indeed encapsulated within polystyrene producing spherical particles of 10 micrometers in diameter. Detection efficiencies for the measurement of ^{3}H and ^{14}C were 3%-5% and 60%-75%, respectively, depending on the diameter of the PSm. These efficiencies are comparable to those of PSm produced via other methods.

Keywords

Spray-drying, Microspheres, Plastic scintillation, Quenching.

1. Introduction

Plastic scintillation microspheres (PSm) are a novel scintillating material which, due to its solid state and polymeric nature, is of interest in the design and development of new methodologies for analyzing radionuclides that emit alpha or beta particles. PSm are formed of a solid mixture of fluorescent solutes in a polymeric solvent, in a spherical shape, and with a diameter in the range of tens to hundreds of micrometers. When a solution of radionuclides is mixed with PSm, it fills the interstices between the PSm. Beta particles that are emitted then travel through the solution until they arrive at the

PSm, in where they deposit some or all of their energy into the polymeric solvent [1]. Part of the energy deposited is converted into photons, due to the fluorescent molecules, which can be detected by means of photomultipliers using a commercial scintillation counter [2]. Thus, a good organic scintillator for this purpose will be composed of a solvent with the capacity to absorb the energy deposited by the radionuclide efficiently and linearly (e.g., polystyrene or polyvinyltoluene) and will contain appropriate amounts of fluorescent solutes to ensure energy transfer from the solvent to the secondary solute while avoiding auto absorption of the photons produced (approximately 2% of the primary and 0.1% of the secondary solute).

The capacity of PSm to detect low-, medium- and high-energy beta emitters, as well as alpha emitters, has been demonstrated previously [2-3]. PSm can be used in certain novel applications: to take certain measurements in salty samples [5]; to develop new radioactivity sensors [6,7]; and as PSresins (PSm covered with a selective extractant), in which the same support is used to extract and detect radionuclides [8-10]. Despite these potential applications, no large-scale production of PSm has been reported, and the usual suppliers of plastic scintillators (e.g., Bicron and Detec-Rad) only produce them on demand and at considerable cost.

Several methods can be utilized to produce solid solutions in polymers [11,12]. Of those methods, polymerization [13,14], evaporation-extraction [15,16], the use of supercritical fluids [17-19] and spray-drying [20,21] are among the most frequently used. The different methods rely on different principles for the production of microspheres and therefore their shape and size varies depending on the method used. Moreover, other aspects, such as the cost of production, the mass-scale extension, and the degree of residual solvent in the polymer, should be considered to determine which method is most appropriate for a specific purpose.

Previous experience in the production of PSm has shown that the evaporation/extraction method is a simple and valid technique at the laboratory scale for obtaining microspheres in the micrometric range with success in the encapsulation of the fluorescent solutes [22, 23]. However, the amount of residual solvent may be high, and scaling up the process would not be simple since very large reactors are needed, where the dynamics of the solution would be different from that at the laboratory scale.

Furthermore, management of the auxiliary operations, such as filtration or cleaning, would also be difficult at the industrial scale. Scintillation particles obtained by polymerization perform well as radioactivity detectors and can even be used with aggressive and organic media, due to the presence of cross-linking agents [24]. The particles obtained present an amorphous shape and are a few micrometers in diameter. Main drawback of this method is that scaled-up would need reactors adapted to a process that is too specific. Finally, production of scintillation particles with supercritical fluids is possible, although little material is obtained and the particles are slightly larger than the nanometric range [25]. For this size of particles, optical quenching is very high and the scintillation signal obtained decreases dramatically compared to that from microspheres with a size of tens of a micrometer.

Meanwhile, spray-drying has been used for many years to dry solid materials in various fields (e.g., food and cosmetics) and on an industrial scale (tons of products). Moreover, in recent years, the need to encapsulate pharmacological compounds within degradable polymeric matrices has led to the enhancement of this methodology using polymeric materials and at different production scales (grams or kilograms). Furthermore, the use of small spray-dryers and closed-cycle systems has extended the technique to laboratory testing, the development of nanomaterials and use with organic solvents for solving the polymer and solutes. In spray-drying, the solution of the polymer, known as the feed, is sprayed through a nozzle via the action of an inert gas, nitrogen, to form droplets. Once in the chamber, the droplets enter into contact with the drying gas, also nitrogen, which is at a high temperature, to cause the feed solvent to evaporate and consequently lead to the formation of solid particles before they arrive at the walls of the chamber. The size and shape of the particles formed depend on the parameters involved in the formation of the droplet, the process of evaporation of the solvent and the process of solidification of the polymer.

Several spray-drying methods are described in the literature that use various polymers (e.g., poly(lactic-co-glycolic acid), polycaprolactone, polylactic acid, and polyvinylpyrrolidone) [26-27] in which different compounds could be encapsulated using different solvents [29] (e.g., water, dichloromethane, methanol, ethanol, or ethylacetate) or combinations of solvents [30, 31] to obtain reasonable yields and nanometric or micrometric particles [32, 33]. However, whereas reports of the method

at the laboratory scale are quite common in the literature, very few examples can be found related to the large-scale production of particles and most of these are related to patent applications [34, 35]. The situation is even worse when considering the use of polystyrene as the polymer and organic solvents that demand the use of closed-cycle systems [36]. It should therefore be emphasized that the extension from the laboratory scale to an industrial production scale is by no means because the size of the spray-drying chamber, the working variables and the variables associated with the components involved (i.e., the drying gas and feed material) play a very important role in the shape and dimension of the final product. Thus, the aim of this paper is to evaluate the production of PSm based on polystyrene in a closed-cycle Gea Niro MOBIL MINOR™ spray-dryer using two organic solvents, toluene and dichloromethane, under various conditions of polymer concentration, flow of feed material and nozzle mass flow rate, to determine the optimum conditions for obtaining microspheres of different sizes (from tens of a micrometer to one or two hundred micrometers) in the greatest quantity possible with an acceptable production yield. Moreover, the determination of detection efficiencies when the PSm obtained in this way are used for the measurement of emissions from low-energy beta emitters, such as ^{3}H, and medium-energy beta emitters, such as ^{14}C, would permit us to evaluate their suitability for measuring radioactivity and obtain more information about the detection process with PSm.

2. Experimental

2.1. Reagents

All the reagents used were of analytical or scintillation grade. Polystyrene (PS) (MW 250,000 g mol^{-1}) was provided by Acros Organics (Geel, Belgium). 2,5-diphenyloxazole (PPO) was supplied by Merck (Darmstadt, Germany). 1,4-Bis (5-phenyloxazol-2-yl) benzene (POPOP) was supplied by the Montedison Group, Division Chimica (Milan, Italy).

The solvents used, dichloromethane and toluene, were of reagent grade.

2.2. Equipment

An AJ2-HS centrifuge (Beckman-Coulter Inc., Brea, USA) was used to centrifuge the measurement vials and an Ultrasons-P ultrasonic bath (JP Selecta, Abrera, Spain) was used to sonicate the vials (at 40 kHz).

The radioactivity of the samples was measured using a 1220 Quantulus detector. The 1220 Quantulus liquid scintillation spectrometer (Perkin Elmer, USA) is equipped with logarithmic amplification, a multichannel analyzer with 4096 channels distributed into four segments of 1024 channels (four spectra). The background signal is reduced by a combination of passive shielding and active shielding based on a guard detector.

An LS 13 320 single-wavelength laser diffraction particle size analyzer (Beckman-Coulter Inc., Brea, USA) was used to determine the size distribution of the scintillating particles.

Secondary-electron images of the PSm were obtained with a Stereoscan S-360 scanning electron microscope.

The spray-dryer equipment used was a closed-cycle QSD-0.8 MOBILE MINOR™ with a co-current two-fluid nozzle (GEA Niro, Søborg, Denmark).

The feed was introduced into the MOBILE MINOR™ Spray-dryer with a peristaltic pump (Watson Marlow, Wilmington, USA).

The feed solutions were prepared in a 20 liter jacketed glass vessel with a mechanical stirrer.

2.3. Synthesis procedure

Feed solutions were prepared by dilution of a concentrated solution of polystyrene and the fluorescent solvents in the corresponding solvent. Concentrated feed solutions were prepared in all cases by using a 20 L reactor with blade agitation. The concentrated feed solution prepared in dichloromethane had a proportion of polystyrene of 15% (m/m); whereas the concentrated feed solution prepared in toluene had a proportion of polystyrene of 5% (m/m). The proportions of PPO and POPOP were 2% and 0.05%,

respectively, with respect to the amount of polystyrene added. The concentrated feed solution was diluted gravimetrically.

Production of PSm was completed using feed solutions of polystyrene and the fluorescent solutes in dichloromethane or toluene at concentrations ranging from 1% to 9% (m/m). Different production runs were executed with these solutions at different feed flow rates (from 1 to 6 kg h^{-1}) and nozzle flow (measured in kg h^{-1}). The flow of nitrogen in the nozzle was selected using two parameters: the pressure of nitrogen, (in bars), and the degree of split (in %). Taking into consideration the boiling points of the solvent used, the inlet temperature was adjusted to give an outlet temperature of between 30ºC and 35ºC in the case of dichloromethane, and between 80ºC and 85ºC in the case of toluene. The temperature of the nitrogen in the nozzle was adjusted to 20ºC in the case of production with dichloromethane and to 50ºC in the case of toluene.

After each change involving a variation of the feed flow rate, the system was preconditioned for 30 minutes by injecting only the solvent. In all cases, the polymer production from the first 5 minutes was discarded to avoid cross contamination with previous production. If the formation of threads was observed, the injection of the feed was stopped and the system was fed only with solvent until the threads on the walls of the chamber disappeared. The amount of feed injected was determined gravimetrically in all cases. Table 1 summarizes the conditions of each production run.

The sprayed product was recovered in a bottle and weighed to calculate the yield of the process.

2.4. Radioactivity measurements

2.4.1. Sample preparation

The measurement vials were prepared by adding 0.3 g of the synthesized PSm and 0.3 mL of the counting solution (active or blank solution) into a 6 mL Pico Prias polyethylene scintillation vial (Perkin Elmer, USA). After this preparation, the vials were sonicated for 2 minutes and then they were centrifuged for 10 minutes at 16.7 Hz, to ensure homogenization and to improve the detection efficiency and reproducibility of the measurement.

The counting solutions were prepared by diluting a known amount of active stock solution (^{3}H or ^{14}C) in a known volume of ethanol to obtain the desired activity in the measurement sample. The activities in the measurement samples were approximately: 450 Bq for ^{3}H and 35 Bq for ^{14}C. A blank counting solution was prepared for each active measurement sample by the addition of carrier solution instead of active stock solution. All the solutions were prepared by weight.

The active stock solutions used were: ^{3}H solution (HTO) with a concentration of 3.94(14) kBq g^{-1} in deionized water prepared from a standard of 69.8(24) kBq g^{-1} provided by Eckert-Ziegler (Berlin, Germany); a ^{14}C solution (labeled glucose) of 114.6(29) Bq g^{-1} prepared from a standard of 44.7(11) kBq g^{-1} from Amersham International (Buckinghamshire, UK) in a carrier solution of 50 μg g^{-1} of glucose and 1 mg g^{-1} of formaldehyde in deionized water.

2.4.2. Measurements

The measurements with the Quantulus detector were performed with a “low” coincident bias and a multichannel analyzer (MCA) in the "C14" configuration. The counting times were 60 minutes for all the samples: blank, ^{3}H and ^{14}C. The spectrum produced by an external standard gamma radiation source (^{152}Eu) was obtained by measuring for 10 minutes. In all cases, the measurement vials were stored in the dark for 2 h before counting.

2.4.3. Data treatment

The detection efficiency was calculated as the ratio between the net count rate over the whole spectrum and the activity added to the measurement vial; and expressed as a percentage. The net count rate was obtained after subtracting the count rate of the blank sample from the count rate of the active sample. The SQP(E) parameter is the quenching parameter of the Quantulus detector. It was calculated by the detector for each sample and corresponds to the end-point channel that limits 99.75% of the total counts of the spectrum of the Compton electrons generated when the external ^{152}Eu gamma radiation source irradiated the sample.

3. Results and discussion

Since the objective of this work is to obtain microspheres with a diameter of tens of a micrometer and in the highest production yield, different production conditions were evaluated. The variables studied included the solvent of the polymer, the flow of the feed, the feed concentration the nozzle mass flow rate. The use of different solvents permitted us to assay different drying speeds, depending on the boiling point of the solvent, which is what finally determines whether microspheres or other kinds of shapes are formed (flakes, threads, etc.). Meanwhile, varying the feed speed and feed concentration determined the amount of material to be dried; too much material will not lead to the formation of droplets before drying, and will therefore lead to the formation of threads. Finally, the nozzle mass flow rate defines the size of the droplets, since high nozzle mass flow rates produce a large number of small droplets; whereas low nozzle mass flow rates lead to few droplets of larger size. The final product is the result of the equilibrium between the different variables; with optimum conditions being those that permit the formation of spherical droplets that are dried progressively before the particle reaches the wall of the chamber.

To evaluate each condition set of production conditions, three aspects were assessed: the yield of the process, the shape and size of the polymeric material obtained, and their radiometric capacities. Table 2 summarizes the results of each production run in terms of yield, appearance, size, ^{3}H and ^{14}C detection efficiencies, and the SQP(E) parameter.

3.1. Production using dichloromethane

Dichloromethane has been demonstrated to be a good solvent for polystyrene in previous work [22,23] and has the capacity to dissolve up to of 15% (m/m) polystyrene. The first experiment (SD_DC_1) was performed at a concentration of polystyrene of 3% (m/m), a flow rate of 6 kg h^{-1} and a nozzle mass flow rate of 3 bar (60%); conditions which are within the average range of those reported in the literature for spraying using the MOBILE MINOR™. The result was the formation of aggregates and a solid with a very low density that blew into the chamber as if it were snow (Figure 1). By decreasing the feed flow rate to 3 kg h^{-1} and the nozzle mass flow rate to 1 bar (40%), we reduced the formation of aggregates (SD_DC_2). In the next experiment (SD_DC_3), the concentration of polystyrene was increased to 9% (m/m); resulting in the formation of

very large aggregates and large threads, probably due to fast evaporation of the solvent and no capacity to form single droplets from the feed.

These first tests indicated that the conditions for the formation of microspheres using dichloromethane should be gentle, and so the subsequent experiments were performed at lower concentrations, with lower feed flows and lower nozzle mass flow rates.

In experiment SD_DC_4, the feed flow and nozzle mass flow rates were decreased, and the feed concentration was kept in the same range as in the first two experiments. As happened before, long aggregates were formed due to inefficient formation of droplets before the solvent dried. Reduction of the feed concentration to 1% (m/m) (SD_DC_5) made it possible to obtain good spraying with the formation of microparticles and a yield close to 50%. Under these conditions, droplets were formed correctly before the solvent dried and therefore particles were formed. However, analysis by SEM (Figure 2) revealed that the particles had the shape of deflated microspheres. This may have been caused by the surface of the microparticle hardening too fast. Since dichloromethane has a very low boiling point and the inlet temperature was higher than the boiling point, the surface of the droplet would have become hard very quickly while the inside was still liquid. The solvent inside the droplet then escapes quickly and the surface collapses, creating deflated microspheres by the time they arrive at the walls of the chamber.

The next two experiments were performed by increasing the feed concentration to 2% (m/m) (SD_DC_6) or the feed flow to 2 kg h^{-1} (SD_DC_7), with similar results; although from both parameters the increase in concentration had a greater impact on the formation of threads.

A dramatic decrease of the nozzle mass flow rate to 1 bar (15%), SD_DC_8, produced inefficient spraying and large drops of feed fell straight into the chamber, resembling a shower.

In the next experiments, an increase in the feed concentration and feed flow rate to 2% and 3 kg h^{-1}, were followed by an increase in the nozzle mass flow rate, since the increase in material to be dried can only be balanced by the fast formation of droplets from the nozzle before the solvent dries.

In SD_DC_9, the nozzle mass flow rate was increased to 1 bar (60%), and microparticles in the form of deflated microspheres were obtained again. It is also worth mentioning an important decrease in the yield to 25%. This can be attributed to the size of the microspheres obtained and some difficulty in retaining particles of the size produced. The size distribution analysis (Figure 3) revealed that the product obtained in this test presented two different populations with a mean diameter smaller than that obtained in the previous experiments.

Under the same conditions but increasing the feed concentration to 3% (m/m) (SD_DC_10), the formation of threads was observed again (Figure 4). To avoid the formation of threads, the nozzle mass flow rate was increased to 2 bar (60%) (SD_DC_11); but no improvement was observed. The next experiments, performed using a feed concentration of 2% (m/m) and a feed flow rate of 2 kg h^{-1} (SD_DC_12) or 3 kg h^{-1} (SD_DC_13 and SD_DC_14), again led to the formation of threads. This shows that if threads are formed, increasing the injected mass does not lead to any improvement.

The experiments performed show that it is possible to obtain polystyrene particles with diameters of approximately ten micrometers by spray-drying using dichloromethane as the solvent and with a 50% yield. However, the products obtained always formed deflated microspheres, and gentle production conditions are required to avoid the formation of threads, thereby reducing the production rate. These results are mainly due to the low boiling point of dichloromethane and its fast evaporation at these working temperatures, which make the formation of feed droplets and their homogeneous drying difficult.

3.2. Production using Toluene

Toluene has a higher boiling point and is also capable of dissolving polystyrene; although the solubility of polystyrene in toluene is lower than in dichloromethane and the highest concentration reached was 5% (m/m).

The first experiment, SD_TO_15, was performed under conditions similar to those that resulted in the best performance in dichloromethane: a high nozzle mass flow rate (3 bar (60%)), low feed flow rate (1 kg h^{-1}) and low feed concentration (2% (m/m)). Under

these conditions, very fine particles were obtained and, as happened with dichloromethane, the yield was poor, just 18%, due to the difficulties in recovering the particles, which had a small mean diameter (Figure 5). Another relevant aspect that should be noted is that the particles obtained presented spherical forms, which indicates that the droplets were drying correctly.

To determine the limits of the system in terms of the feed concentration and therefore of mass production per unit of time, we performed a test (SD_TO_16) with the feed concentration increased to 5% (m/m). Again, threads were formed, which indicates that production of polystyrene microspheres is limited in terms of the feed concentration to values between 2% and 5%.

Returning to the conditions of test SD_TO_15, a small increase on the feed flow to 2 kg h^{-1} (SD_TO_17) had no impact on the formation of particles; although some threads were observed. The yield obtained was 50%, in accordance with the increase in the mean size of the particles. In the next experiment, SD_TO_18, an increase in the feed concentration to 3 % (m/m) again resulted in the formation of threads; showing once again the sensitivity of production to this variable.

At this point, a series of experiments was performed at different nozzle mass flow rates and feed flows with a constant feed concentration of 2% (m/m) to find the conditions in which most particles per unit time are obtained without the formation of threads. Table 3 indicates the experiments and results in terms of means size, yield and the appearance of the end product.

Comparing these experiments, the extremely delicate equilibrium at which microspheres are formed can be observed. At a feed flow rate of 2 kg h^{-1}, an increase in nozzle mass flow rate leads to a decrease in the size of the particles (Figure 6). At high nozzle mass flow rates, the particles are too small and recovery decreases due to difficulties in collecting the deposited microspheres. Moreover, at high nozzle mass flow rates, threads start to form; although not a very high proportion of them.

When keeping the nozzle mass flow rate constant at 3 bar (20%) and increasing the feed flow rate from 2 to 5 kg h^{-1}, small changes in the shape and size of the particles were observed; whereas the yield reached a maximum of 80% at 4 kg h^{-1}. However, when

looking at the SEM images, we can see that particles obtained at 5 kg h^{-1} presented an imperfect spherical shape (Figure 7). This finding correlates with the fact that some drops appeared on the walls of the chamber during production, as if at such a high feed flow rate, there was not enough time and gas for all the droplets formed to dry completely and consequently the microspheres are too soft and become deformed when they impact on the walls of the chamber.

It seems clear that when the production parameters, such as the feed flow rate, are too large, the system becomes less robust and the production of microspheres diminishes. As an example and as observed previously, when working at 5 kg s^{-1} and at a nozzle mass flow rate of 3 bar (20%), the droplets formed are not completely dry when they arrive at the walls of the chamber. However, if we increased the nozzle mass flow rate to 3 bar (40%), particles were formed but the yield and amount of product recovered was very low. Finally, in experiment SD_TO_25, using a nozzle mass flow rate of 3 bar (25%), spherical microspheres were obtained with good recovery rate and a diameter of approximately 10 micrometers (Figure 8).

The aim of the last two series of experiments was to increase the microsphere production rate. In the first experiment, feed flow rates of 6 kg h^{-1} and 7 kg h^{-1}, and a 2% (m/m) feed concentration were used (SD_TO_28 and SD_TO_29). In both cases, microspheres were obtained but with low recovery rates. Finally, changing the feed concentration to 3% (m/m) (SD_TO_30 and SD_TO_31) at the highest feed flow rates possible (5 kg h^{-1} and 6 kg h^{-1}) generated products that were too small to be collected in an acceptable yield. These conditions seem to be the upper limit beyond which it is not possible to obtain microspheres.

In summary, conditions for obtaining microspheres are more flexible with toluene than with dichloromethane, due to its higher boiling point, and yields higher than 50% were obtained. In addition, the particles obtained presented a spherical shape due to the droplets drying better.

3.3. Radiometric capacities

The particles obtained in the experiments we performed were successfully used to measure two radionuclides, ^{3}H (maximum energy 18.6 keV) and ^{14}C (maximum energy

156.8 keV), to evaluate their radiometric performance. Apart from detection efficiencies for both radionuclides, the SQP(E) parameter was also used as an indicator of possible quenching phenomena in the scintillation process.

The scintillation samples were prepared by mixing the particles and the radioactive solution in an ethanol medium. The radioactive solution was prepared in an ethanol medium to facilitate the introduction of the radionuclide into the interstices between microparticles, as mixing the polymer with the solution in an aqueous medium proved not to be efficient due to the high electrostatic electricity of the microspheres, which repel water molecules. This situation is different from that of microspheres obtained in previous evaporation/extraction experiments or polymerization methods [23, 24], which can be mixed easily with aqueous solutions; but it is similar to that of the nano/microparticles obtained by using the supercritical anti-solvent fluids. The use of ethanol and homogenization by ultrasound and centrifugation is useful in overcoming this problem, and in producing adequate mixing of the microspheres and the solution.

The detection efficiencies obtained for ^{3}H were between 2% and 5%. These values were similar for the particles produced using either dichloromethane or toluene (Figure 10). A clear correlation between diameter and detection efficiency was observed: the increase in detection efficiency upon decreasing the diameter is due to a decrease in particle quenching. This is because for small microspheres, the distance a beta particle has to travel to reach a microsphere is shorter and therefore the probability of hitting a microsphere before interacting with the medium and losing its energy is higher [25]. The fact that diameter depends on the conditions of drop formation during the spraying process offers us the possibility to predefine the final mean diameter of the PSm by changing the production conditions. However, the diameter range will be limited to those described here, and for higher or lower diameters different conditions should be tested or another drying chamber should be used.

The values obtained for ^{3}H are in agreement with those reported in the literature for PSm [22-25]. Microspheres obtained by the evaporation/extraction method present a diameter of between a few tens and hundreds of micrometers, and their detection efficiencies are between 4% (for 20-micrometer microspheres) and 0.4% (for 200-micrometer microspheres) mainly due to the decrease in particle quenching with the

decrease in size. However, particles obtained by extraction with supercritical fluids, although having a very small diameter (less than 1 micrometer), present very low detection efficiencies (0.09%) due to the poor optical transmission of the photons in such a medium, which has a greater effect than the decrease in particle quenching due to their smaller size. Our spray-drying results permit us to note that, for this range of size (approximately 10 micrometers), the improvement in the detection efficiency due to the reduction of particle quenching is still more important than losses of photons due to optical quenching; and this explains why the detection efficiency is high but of the same order as microspheres of larger diameters.

These high values of detection efficiency for the microspheres produced by spray-drying also imply that encapsulation of the fluorescence solutes within the polymer was successful. If this were not the case, the efficiency for ^{3}H would have been similar to that obtained when the PSm contain only polystyrene (less than 0.1%) [23].

The detection efficiencies obtained for ^{14}C were also high (between 60% and 70%) and the relation between diameter and detection efficiency still held, but to a lesser extent because beta particles emitted by ^{14}C are more energetic. The values when using dichloromethane as the solvent seem to be lower than those for toluene; probably because the microspheres produced using dichloromethane were larger.

Finally, in the case of the parameter related to the efficiency of the energy transfer from the solvent to the photomultipliers, the SQP(E) parameter (Figure 9), the values obtained when using the particles produced using dichloromethane (approximately 625) are significantly lower than those obtained when using the microspheres produced using toluene as the solvent (approximately 670). This difference may be attributed to a chemical quenching effect caused by the amount of residual solvent present in the particles or to the different shape of the particles: deflated in the case of dichloromethane (Figure 2) and spherical in the case of toluene (Figure 8). The values obtained using both solvents are lower than those obtained with larger microspheres produced by the evaporation/extraction method (around 750), but higher than those obtained with supercritical fluids (below 500). This behavior is related to the diameter of the microspheres and the associated optical quenching because, for the smaller

microspheres, light transmission is poorer due to the high density of discontinuities in the medium, and as consequence the SQP(E) parameter decreases.

As happens with the ^{3}H and ^{14}C measurements, the values of SQP(E) are high enough to confirm the encapsulation of the fluorescent solutes (PPO and POPOP), as the absence of these solutes would have resulted in SQP(E) values lower than 500, due to the low sensitivity of the photomultipliers to the photons emitted at the wavelength of emission of polystyrene [23].

With regard to the stability of the PSm, we should mention that they are not the result of a polymerization of styrene with a cross-linker and therefore this PSm can be used with polar solvents (e.g. water, ethanol, etc.) but not with less-polar organic solvents (e.g. toluene, ketone, etc.) in which pure polystyrene is soluble. PSm can be reused after filtration, which causes no degradation of their properties and PSm are not damaged when used with activity levels of the order used in this work.

Our results show that the particles obtained by spray-drying can be used for the detection and measurement of beta-emitting radionuclides and that the encapsulation of fluorescent solutes by polystyrene is effective. Thus, the decision concerning the use of this technique for the production of PSm will depend mainly on the economic balance.

4. Conclusions

A method for producing polystyrene microparticles with encapsulated fluorescent solutes by spray-drying at an industrial scale using industrial equipment has been evaluated successfully here. The results indicate that production is possible and that the solutes are successfully encapsulated within the polystyrene.

When dichloromethane is used as the solvent for the polymer feed solution, deflated microspheres with diameters of between 5 to 25 micrometers are obtained, provided that gentle conditions of feed concentration and feed flow rate are used. In the case of high feed flow rates and high feed concentrations, threads are obtained. Both results, the acquisition of deflated microspheres and the formation of threads, are probably caused by the fast evaporation of dichloromethane due to the high inlet temperature of industrial equipment of such dimensions and the low boiling point of dichloromethane.

When toluene is used as the solvent, the particles obtained have a spherical form. In this case, the evaporation of the solvent seems to be more progressive, spherical droplets are formed via injection and the microparticles become consolidated before arriving at the walls of the drying chamber. These microspheres present a diameter of approximately 10 micrometers. The conditions of production are more flexible than in the case of dichloromethane, and feed flow rates of up to 5 kg h^{-1} can be used. Under more extreme conditions, threads, or very small microparticles, are obtained.

Comparing the two solvents, toluene provides better results, since the production yield is higher and the particles present a spherical form. Under the optimum conditions, using toluene as the solvent, a feed concentration of 2%, a feed flow rate of 5 kg h^{-1} and a nozzle mass flow rate of 3 bar (25%), microspheres of 10-micrometer diameter can be obtained with a 50% yield and a production rate of 300 g per day.

The particles obtained can be used to measure beta-emitting radionuclides. The detection efficiency for ^{3}H is approximately 3%-4%; and for ^{14}C, approximately 65%. The microparticles present high electrostatic charge and therefore the samples must be prepared in a water/ethanol medium. The radiometric results, efficiency and SQP(E) parameter are all in agreement with those obtained using PSm of 22 micrometers in diameter (produced by the evaporation/extraction method), which have a detection efficiency of 3.4% and 72% for ^{3}H and ^{14}C respectively [22].

As a whole, spray-drying is a technique that is capable of producing PSm in the range of ten micrometers in diameter for use in the detection of radioactivity in aqueous samples. The implementation of this method at a production scale using a MOBILE MINOR™ system depends only on the economic balance.

5. Acknowledgments

The authors thank the Spanish *Ministerio de Economia y Competitividad* (MINECO) and Catalan regional *Agència de Gestió d'Ajuts Universitaris i de Recerca* (AGAUR) for financial support under grants CTM2008-01147/CTM2011-27211 and 2009-SGR-1188, respectively. The authors are indebted with to Marti Bartra, Pere Talavera and Stephen Winter for their support and advice on the use of the spray-drying technique at Esteve Química.

6. References

[1] L'Annunziata, MF. (2013) Handbook of Radioactivity Analysis (third edition). San Diego. Academic Press. ISBN: 978-0-12-384873-4.

[2] Bertrand, GHV., Hamel, M., Sguerra, F. (2014) Current status on plastic scintillators modifications. Chemistry, 20(48), 15660–15685

[3] Brooks, FD. (1979) Development of organic scintillators. Nuclear Instruments and Methods, 162(1-3), 477–505.

[4] Santiago, LM., Bagán, H., Tarancón, A., Rauret, G., García JF (2013) Systematic study of particle quenching in organic scintillators. Nuclear Instruments and Methods in Physics Research, Section A: Accelerators, Spectrometers, Detectors and Associated Equipment, 698, 26–36.

[5] Bagán, H., Hartvig, S., Tarancón, A., Rauret, G., García, JF, (2009) Plastic vs. Liquid Scintillation for ^{14}C radiotracers determination in high salt matrices. Analytica Chimica Acta, 631(2), 229–236.

[6] Tarancón, A., Padró, A., García, JF., Rauret, G. (2005) Development of a radiochemical sensor, Part 2: application to liquid effluents. Analytica Chimica Acta, 538(1-2), 241–249.

[7] Fjeld, RA., DeVol, TA., Leyba, JD., Paulenova, A.. (2005) Measurement of radionuclides using ion chromatography and on-line radiation detection. Journal of Radioanalytical and Nuclear Chemistry, 263(3), 635–640.

[8] Bagán, H., Tarancón, A., Rauret, G., García, JF. (2011) Radiostrontium separation and measurement in a single step using plastic scintillators plus selective extractants. Application to aqueous sample analysis. Analytica Chimica Acta, 686(1-2), 50–56.

[9] Bagán, H., Tarancón, A, Stavsetra, L., Rauret, G., García, JF. (2012) Determination of oil reservoir radiotracer ($S14CN^-$) in a single step using a plastic scintillator extractive resin. Analytica Chimica Acta, 736(0), 30–35.

[10] Egorov, OB., O'Hara, JW., Grate, JW. (2006) Equilibration-Based Preconcentrating Minicolumn Sensors for Trace Level Monitoring of Radionuclides and Metal Ions in Water without Consumable Reagents. Analytical Chemistry, 78(15), 5480–5890.

[11] Rao, JP., Geckeler, KE .(2011) Polymer nanoparticles: Preparation techniques and size-control parameters. Progress in Polymer Science, 36(7), 887–913.

[12] Bettencourt, A., Almeida, AJ. (2012) Poly(methyl methacrylate) particulate carriers in drug delivery. Journal of Microencapsulation, 29(4), 353–67.

[13] Tsagkatakis, I., Peper, S., Retter, R., Bell, M., Bakker, E. (2001) Monodisperse Plasticized Poly(vinyl chloride) Fluorescent Microspheres for Selective Ionophore-Based Sensing and Extraction. Analytical Chemistry, 73(24), 6083–6087.

[14] Sánchez-Silva, L., Rodríguez, JF., Romero, A., Borreguero, AM., Carmona, M., Sánchez, P. (2010) Microencapsulation of PCMs with a styrene-methyl methacrylate copolymer shell by suspension-like polymerisation. Chemical Engineering Journal, 157(1), 216–222.

[15] Freitas, S., Merkle, HP., Gander, B. (2005) Microencapsulation by solvent extraction/evaporation: reviewing the state of the art of microsphere preparation process technology. Journal of Controlled Release, 102(2), 313–332.

[16] Li, M., Rouaud, O., Poncelet, D. (2008) Microencapsulation by solvent evaporation: state of the art for process engineering approaches. International Journal of Pharmaceutics, 363(1-2), 26–39.

[17] Reverchon, E., De Marco, I., Torino, E. (2007) Nanoparticles production by supercritical antisolvent precipitation: A general interpretation. The Journal of Supercritical Fluids, 43(1), 126–138.

[18] Yeo, SD., Kiran, E. (2005) Formation of polymer particles with supercritical fluids: A review. The Journal of Supercritical Fluids, 34(3), 287–308.

[19] Badens, E., Boutin, O., Charbit, G. (2005) Laminar jet dispersion and jet atomization in pressurized carbon dioxide. J. Supercrit. Fluids 36, 81–90.

[20] Vehring, R. (2008) Pharmaceutical particle engineering via spray drying. Pharmaceutical Research, 25(5), 999–1022.

[21] Paudel, A., Worku, ZA., Meeus, J., Guns, S., Mooter, G. (2013) Manufacturing of solid dispersions of poorly water soluble drugs by spray drying : Formulation and process considerations. International Journal of Pharmaceutics, 453(1), 253–284.

[22] Santiago, LM, Bagán H, Tarancón A, García JF (2015) Influence of preparation parameters on the synthesis of plastic scintillation microspheres and evaluation of sample preparation. Sent to Advanced Powder Technology.

[23] Santiago L M, Bagán H, Tarancón A, García JF (2013) Synthesis of plastic scintillation microspheres: Evaluation of scintillators. Nuclear Instruments and Methods in Physics Research Section A: Accelerators, Spectrometers, Detectors and Associated Equipment, 698(0), 106–116.

[24] Bagán H, Tarancón A, Ye L, García JF (2014) Crosslinked plastic scintillators: A new detection system for radioactivity measurement in organic and aggressive media. Analytica Chimica Acta, 852, 13–19.

[25] Santiago L, Masmoudi Y, Tarancón A, Djerafi R, Bagán H, García JF, Badens E (2015) Polystyrene based sub-micron scintillating particles synthesized by supercritical anti-solvent precipitation. Journal of Supercritical Fluids, 103, 18-27.

[26] Fu Y, Shyu S, Su F, Yu P (2002) Development of biodegradable co-poly (D , L - lactic / glycolic acid) microspheres for the controlled release of 5-FU by the spray drying method, Colloids and Surfaces B: Biointerfaces, 25 (4), 269-279.

[27] Moretti D L, Gavini E, Juliano C, Pirisino G (2001) Spray-dried microspheres containing ketoprofen formulated. Journal of Microencapsulation 18(1), 111-21.

[28] Lee DH, Yang M, Kim SH, Shin M J, Shin, J S (2011) Microencapsulation of Imidazole Curing Agents by Spray-Drying Method. Journal of Applied Polymer Science, 122, 782-788.

[29] Rivera, PA., Martínez-Oharriz, C., Rubio, M., Irache, JM., Espuelas, S. (2004) Fluconazole encapsulation in PLGA microspheres by spray-drying, Journal of Microencapsulation, 21(2), 203–211.

[30] Shin, MJ., Kim, JG., Shin, JS. (2012) Microencapsulation of imidazole curing agents by spray-drying method using W/O emulsion. Journal of Applied Polymer Science, 126, 108–115.

[31] Shim, JB., Kim, MJ., Kim, SJ., Kang, SJ., Lee, JH., Kim, HS., Khang, G. (2012) Dissolution properties of control released solid dispersion of carvedilol with HPMC and Eudragit RS. Journal of Pharmaceutical Investigation, 42(5), 285–291.

[32] Hugo, M., Kunath, K., Dressman, J. (2013) Selection of excipient, solvent and packaging to optimize the performance of spray-dried formulations: case example fenofibrate. Drug Development and Industrial Pharmacy, 39(2), 402–12.

[33] Gupta, NV., Natasha, S., Getyala, A., Bhat, RS. (2013) Bioadhesive vaginal tablets containing spray dried microspheres loaded with clotrimazole for treatment of vaginal candidiasis. Acta Pharmaceutica, 63(3), 359-72.

[34] Burke, P., French, D., Herberger, J., Klumb, L., Murphy, K., (Amgen Inc), WO200103032 0A1, 1999.

[35] Verhoeven, E., Voorspoels, J., Gonnissen, Y., Ruysschaert, Y. (AiCuris GmbH & Co., Germany), EP20090170133, 2009.

[36] Carné-Sánchez, A., Stylianou, KC., Carbonell, C., Naderi, M., Imaz, I., Maspoch, D. (2015) Protecting metal–organic framework crystals from hydrolytic degradation by Spray-Dry encapsulating them into polystyrene microspheres. Advanced Materials, 27, 869–873.

Figures

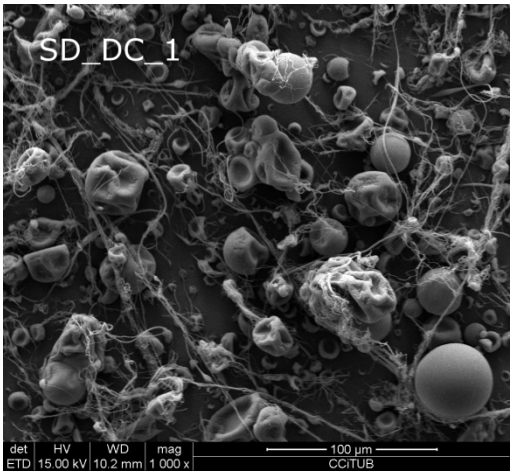

Figure 1. SEM images of the product obtained in test SD_DC_1

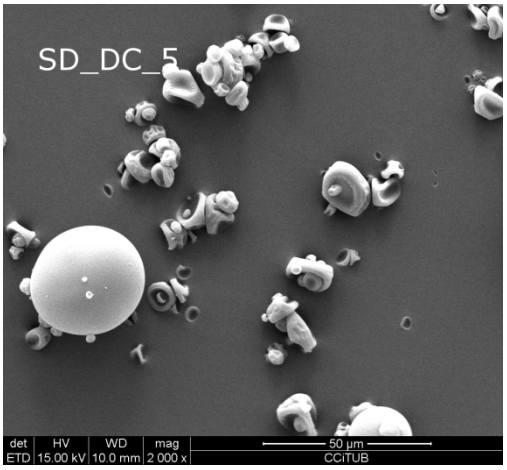

Figure 2. SEM images of the product obtained in test SD_DC_5

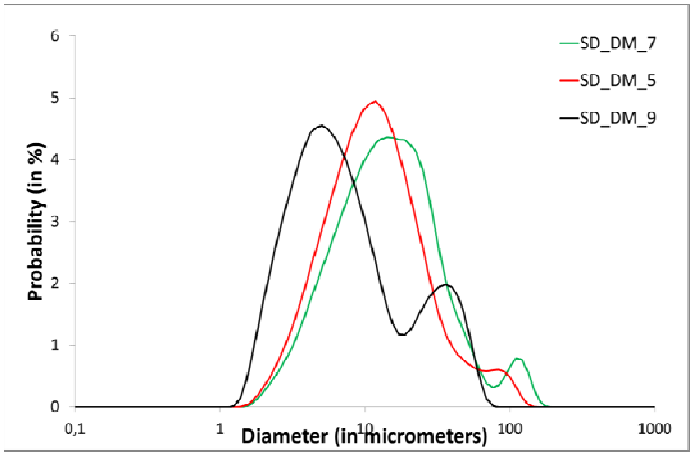

Figure 3. Size distribution of the particles obtained in tests SD_DC_5, SD_DC_7 and SD_DC_9

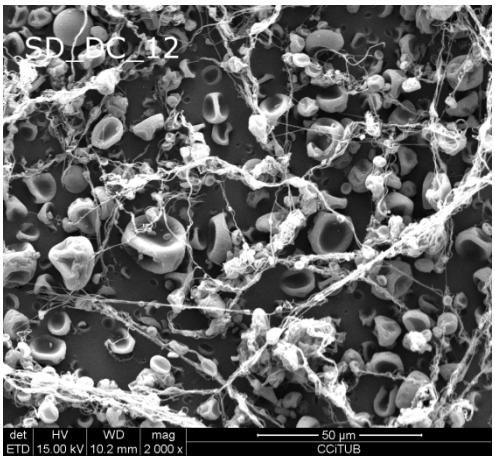

Figure 4. SEM image of the microparticles obtained in test SD_DC_12

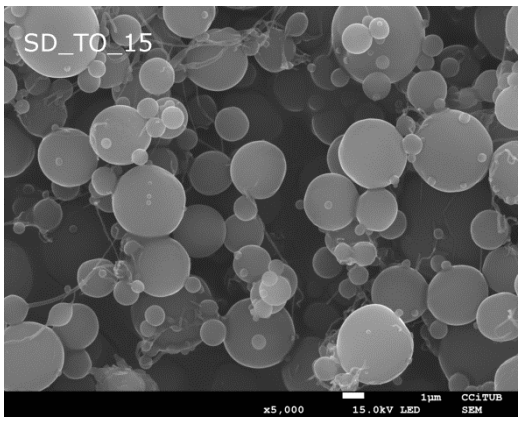

Figure 5. SEM image of the microparticles obtained in test SD_TO_15

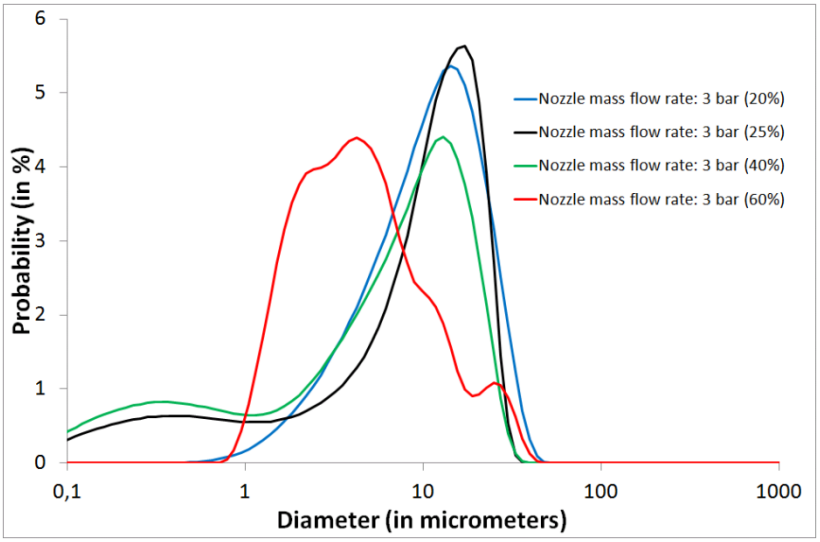

Figure 6. Size distribution of the microparticles obtained with toluene at 2 kg h^{-1} and 2% (m/m)

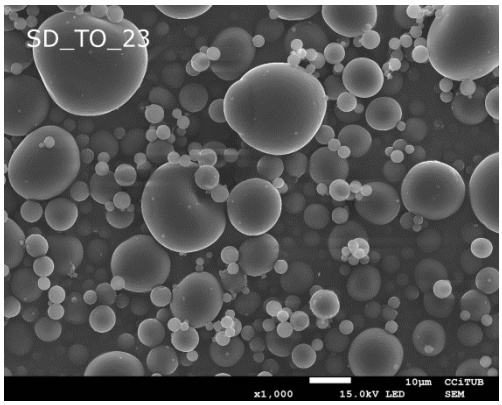

Figure 7**.** SEM image of the particles obtained in test SD_TO_23

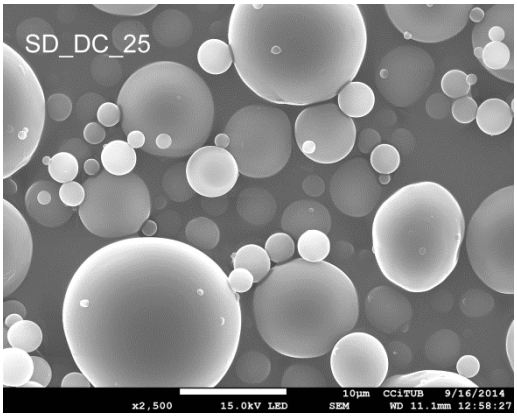

Figure 8. SEM image of the particles obtained in test SD_TO_25

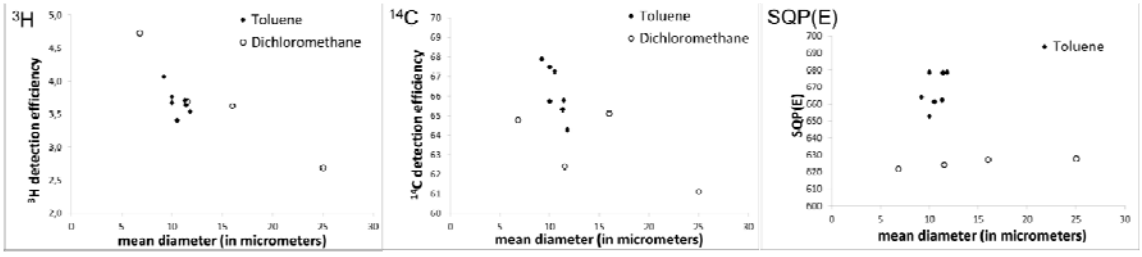

Figure 9. Values of ^{3}H and ^{14}C detection efficiency and the SQP(E) parameter obtained using the particles produced using toluene and dichloromethane

Tables

Table 1. Conditions of the production runs

Test	Solvent	Feed Concentration (%)	Feed Flow Rate (kg h^{-1})	Nozzle Mass Flow Rate (bar and %)
SD_DC_1	Dichloromethane	3	6	3 (60%)
SD_DC_2	Dichloromethane	3	3	1 (40%)
SD_DC_3	Dichloromethane	9	3	1 (40%)
SD_DC_4	Dichloromethane	3	1	1 (20%)
SD_DC_5	Dichloromethane	1	1	1 (20%)
SD_DC_6	Dichloromethane	2	1	1 (20%)
SD_DC_7	Dichloromethane	1	2	1 (20%)
SD_DC_8	Dichloromethane	1	2	1 (15%)
SD_DC_9	Dichloromethane	1	2	1 (60%)
SD_DC_10	Dichloromethane	3	2	1 (60%)
SD_DC_11	Dichloromethane	3	2	2 (60%)
SD_DC_12	Dichloromethane	2	2	2 (60%)
SD_DC_13	Dichloromethane	2	3	2 (60%)
SD_DC_14	Dichloromethane	2	3	2 (40%)
SD_TO_15	Toluene	2	1	3 (60%)
SD_TO_16	Toluene	5	1	3 (60%)
SD_TO_17	Toluene	2	2	3 (60%)
SD_TO_18	Toluene	3	2	3 (60%)
SD_TO_19	Toluene	2	2	3 (20%)
SD_TO_20	Toluene	2	3	3 (60%)
SD_TO_21	Toluene	2	3	3 (20%)
SD_TO_22	Toluene	2	4	3 (20%)

SD_TO_23	Toluene	2	5	3 (20%)
SD_TO_24	Toluene	2	5	3 (40%)
SD_TO_25	Toluene	2	5	3 (25%)
SD_TO_26	Toluene	2	2	3 (25%)
SD_TO_27	Toluene	2	2	3 (40%)
SD_TO_28	Toluene	2	6	3 (25%)
SD_TO_29	Toluene	2	7	3 (40%)
SD_TO_30	Toluene	3	5	3 (25%)
SD_TO_31	Toluene	3	6	3 (25%)

Table 2. Results obtained in each production run

Test	Shape*	Yield (%)	Mean Particle Size (µm)	^{3}H Det. Eff. (%)	^{14}C Det. Eff. (%)	SQP
SD_DC_2	Particles	--	25	2.7	61.1	628
SD_DC_5	Particles	54	11.5	3.7	62.4	624
SD_DC_6	Particles/Threads	72	17.3	3.2	61.1	628
SD_DC_7	Particles	44	16	3.6	65.1	627
SD_DC_9	Particles	28	6.8	4.7	64.8	622
SD_TO_15	Particles	18	4.2	3.7	52.3	603
SD_TO_17	Particles/Threads	50	4.8	5.2	65.4	635
SD_TO_19	Particles	55	10.5	3.4	67.3	661
SD_TO_20	Particles	6	3.7	--	--	--
SD_TO_21	Particles/Threads	74	8.7	4.5	66.2	673
SD_TO_22	Particles	80	11.4	3.6	65.8	678
SD_TO_23	Particles	56	11.8	3.5	64.3	679
SD_TO_24	Particles	26	9.2	4.1	67.9	664
SD_TO_25	Particles	65	10	3.7	65.8	679
SD_TO_26	Particles	54	10	3.8	67.5	653
SD_TO_27	Particles/Threads	43	9	5.1	71.2	656
SD_TO_28	Particles	28	11.3	3.7	65.3	662
* Experiments resulted in the formation of threads and were not included in the table						

Table 3. Results obtained in tests performed using toluene as the solvent at 2% (m/m) feed concentration and variable feed flow rate and nozzle mass flow rate

Feed flow rate (kg h^{-1})	**Nozzle mass flow rate**			
	3 bar (20%)	**3 bar (25%)**	**3 bar (40%)**	**3 bar (60%)**
2	n: SD_TO_19 55%, 10.5 µm, microspheres	n: SD_TO_26 54%, 10 µm, microspheres	n: SD_TO_27 43%, 9 µm, microspheres and threads	n: SD_TO_17 50%, 4.8 µm, microspheres and threads
3	n: SD_TO_21 74%, 8.7 µm, microspheres	--	--	n: SD_TO_20 6%, 3.7 µm, microspheres
4	n: SD_TO_22 80%, 11.4 µm, microspheres	--	--	--
5	n: SD_TO_23 56%, 11.8 µm, microspheres	n: SD_TO_25 65%, 10.0 µm, microspheres	n: SD_TO_24 26%, 9.2 µm, microspheres	--
6	--	n: SD_TO_28 28, 11.3, microspheres	n: SD_TO_29 very small microspheres	--

Chapter 3.3

Study of the energy transfer mechanism in organic scintillators

---

3.3.1. Systematic study of particle quenching in organic scintillators

Nuclear Instruments and Methods in Physics Research A 698 (2013) 26–36

Contents lists available at SciVerse ScienceDirect

Nuclear Instruments and Methods in Physics Research A

journal homepage: www.elsevier.com/locate/nima

Systematic study of particle quenching in organic scintillators

L.M. Santiago, H. Bagán, A. Tarancón *, G. Rauret, J.F. Garcia

Department of Analytical Chemistry of the University of Barcelona, Diagonal 645, E-08028 Barcelona, Spain

ARTICLE INFO

Article history:
Received 2 March 2012
Received in revised form
12 September 2012
Accepted 19 September 2012
Available online 27 September 2012

Keywords:
Plastic scintillation
Particle quenching
Optical quenching
Liquid scintillation

ABSTRACT

Among the different factors that affect measurements by organic scintillators, the majority of attention has been focused on those related to the scintillator (i.e., ionization, chemical, color and optical quenching), and less attention has been paid to the loss of energy before the particle (i.e., alpha or beta) arrives at the scintillator (i.e., particle quenching). This study evaluates the effect of particle quenching in different scintillation methods (i.e., using two plastic scintillation microspheres (PSm1 and PSm2), liquid scintillator and gel scintillator) by measuring solutions that contain increasing concentrations of NaCl, $BaCl_2$ and glycerin. The results show the importance of particle quenching in PSm measurements because detection efficiency decreases with increasing concentrations of the quenching component, although the spectrum position and external standard parameter remain constant. The results have shown evidence of particle quenching, although at a lower magnitude, in the liquid scintillation or gel scintillation measurements. Moreover, the use of two PSm with different diameters and salty compound that alters the equilibrium of the liquid and gel emulsions also exemplified the importance of the transmission of optical photons through different scintillation media (i.e., optical quenching). Improvement and deterioration of the optical conditions on the scintillation media is manifested as a movement of the spectrum to higher and lower energies, respectively. The results obtained with PSm were confirmed by Monte Carlo simulation.

1. Introduction

The development of organic scintillators began at the end of the 40 decade with the aim to use these compounds to transform the kinetic energy of electrons that are emitted by radionuclides into optical photons that could be detected by photomultipliers [1–3]. During the following years the developments were focused in: the development of organic scintillators in different physical states (e.g., crystal, liquid, gel, or plastic), the formulation of new scintillators, the establishment of the main properties of scintillators [4] and the mechanism(s) involved in these properties [5], and the development of analytical applications that can be used to determine radioactivity [6]. Liquid scintillation, LS, was early established as the best technique for determining and quantifying beta and alpha emitters. During the last twenty years, main developments have been guided by the necessity to find selective, efficient and reproducible analytical procedures, and a few studies have focused on a better understanding of some of the mechanisms that are involved in the scintillation process [7–9].

The detection efficiency of organic scintillators depends on the efficiency in which the kinetic energy of the particle (i.e., alpha or beta) is transformed into optical photons and is detected by photomultipliers. This transformation can be divided into three consecutive stages:

A. The path of the particle from the point in the solution where the disintegration is produced, through the medium, and until the particle interacts with the scintillator. In this stage, energy can be lost due to excitations or ionizations of the molecules of the medium (e.g., water or sample compounds).
B. Transformation of the energy that is deposited in the organic solvent molecule into photons that are emitted by the secondary scintillation solute. In this stage, energy can be lost by the excessive density of the solvent molecules excited (i.e., ionization quenching [10]), the excitation of non-scintillating molecules (i.e., chemical quenching [11]) or other inefficient processes (e.g., autoabsorption).
C. Travel of optical photons from the scintillator, through the medium and the detection chamber, until they reach the PMT surface. In this stage, energy and photons can be lost due to absorption by colored samples (i.e., color quenching [12]) or by inefficient photon transmission processes [13].

Although a large number of studies have focused on understanding and calibrating the effects of the two last stages, little information exists on the effects on the measurement by the

* Corresponding author. Tel.: +34 934021281; fax: +34 934021233.
E-mail address: alex.tarancon@ub.edu (A. Tarancón).

0168-9002/$ - see front matter © 2012 Elsevier B.V. All rights reserved.
http://dx.doi.org/10.1016/j.nima.2012.09.041

processes that cause energy losses before the particle arrives at the scintillator. In this sense, the use of Plastic Scintillation microspheres, PSm, provides a new opportunity to understand the phenomena that cause the transformation, partially or not, of the kinetic energy of a particle into detectable scintillation photons. PSm are a solid mixture of organic fluorescent molecules in a completely polymerized solvent (e.g., polystyrene or polivinyltoluene) and have a size that is in the tens or hundreds of microns. The aqueous sample can be mixed with the PSm to obtain a heterogeneous scintillation medium, which presents some advantages over LS (e.g., Scintillation proximity assay [14], continuous measurements [15,16], non-production of mixed waste [17–19] and others [20,21]).

It can be assumed that the scintillation mechanism of PSm must be similar to that of LS, but previous experiments [22] have demonstrated that the loss of energy during the path of a particle through the sample until it arrives to the scintillator is of high importance because it causes an important decrease in the detection efficiency for weak beta emitters (e.g., ^{3}H). However, for high-energy beta emitters, detection efficiency values are similar to those of LS. Moreover, it has also been observed that efficiency decreases with an increase in the diameter of microspheres [23].

These experimental findings, which were observed when measuring with PSm, can be compared with Monte Carlo simulation of the transport of electrons through the aqueous phase before they reach the scintillator. During the last decades and in parallel to the increase in computing power, different codes have been successfully developed to simulate the track of the alpha and beta particles and gamma rays in different media. One example is the Penelope [24,25] software, which was developed to simulate electrons and gamma radiation in a wide range of energies (from a few eV to MeV) and in geometries of different sizes (from micrometers to meters). This software has been successfully applied in the measuring of radionuclides with PSm in a Triple to Double Coincidence Ratio detector (TDCR) [26].

The aim of this work is to evaluate and quantify the effect of different solutions (e.g., salty and dense solutions) on measurements with PSm and, by comparing the results with those of other organic scintillators, i.e., liquid scintillators and gel scintillators, to determine a general mechanism for particle quenching in organic scintillators. To fulfill this objective, we have determined the experimental detection efficiencies when measuring ^{3}H and ^{36}Cl with PSm of different diameter, liquid scintillator and gel scintillator. Values obtained with both PSm were compared to those obtained by the Monte Carlo simulation using a modification of the Penelope software. In a second stage, we have evaluated the effect of variation in the detection efficiency with the variation of the concentrations of different compounds (e.g., NaCl, $BaCl_2$ and glycerin) on measuring ^{3}H and ^{36}Cl when using different PSm (PSm1 and PSm2), liquid scintillator and gel scintillator.

2. Experimental

2.1. Reagents and solutions

All reagents that were used were analytical or scintillation grade and deionized water was used to prepare the solutions.

Detec (Ottawa, Canada) supplied the plastic scintillation microspheres (Polystyrene UPS-89). The PSm were separated by sieving, and two different PSm, which were named PSm1 (which was segregated with a sieve with pores between 120 μm and 180 μm) and PSm2 (which was segregated with a sieve with pores between 400 μm and 500 μm), were used in the experiments. OptiPhase Supermix (liquid scintillator) and Insta-Gel Plus (gel scintillator) Scintillation Cocktails were supplied by PerkinElmer (Waltham, MA. USA). Measurement solutions were prepared in 6-ml Pico Prias polyethylene vials (PerkinElmer).

A ^{3}H, active stock solution of 350.8 ± 5.8 Bq/g was prepared from a standard that contained 3589 ± 58 Bq/g of ^{3}H (Eckert–Ziegler, Berlin, Germany) in water; and a ^{36}Cl, active stock solution of 2.22 ± 0.03 Bq/g, which was prepared from a standard that contained 22.24 ± 0.26 Bq/g of ^{36}Cl in a water solution that contained 65 μg/l of NaCl (from CERCA/LEA, Pierrelatte, France), were used to prepare the measurement solutions.

NaCl (from Merck, Darmstadt, Germany), $BaCl_2$ and Glycerin (from Panreac, Castellar del Vallés, Spain) were also used to prepare the measurement solutions.

2.2. Apparatus

An AJ2-HS centrifuge (Beckman-Coulter Inc., Brea, USA) was used to centrifuge the measurement vials, and an Ultrasons-P ultrasonic bath (from JP Selecta, Abrera, Spain) was used to apply ultrasonic waves to the solutions.

A 1220 Quantulus liquid scintillation spectrometer (PerkinElmer) was used to measure the count rate and the energy spectrum of the PSm, LS and GS samples. The detector has two photomultipliers to detect the scintillation pulses of the samples and two photomultipliers to detect the scintillation pulses caused by the cosmic rays in the active guard. The signals coming from the sample detector that are not in coincidence with a signal in the active guard detector (true sample signals) are stored in a 1024 channel multichannel analyzer in function of the height of the pulse (energy spectrum). Correlation between channel numbers and pulse height of the pulses (energy of the pulse)) is logarithmic and unknown for the end user. As a result for each sample measurement we obtain the number of pulses detected (coincident counts that are recordered), the real time of measurement and the energy distribution of the pulses detected.

A LS 13 320 single-wavelength laser diffraction particle size analyzer (Beckman-Coulter Inc., Brea, USA) was used to determine the probability size distribution of the plastic scintillation microspheres that were used (i.e., PSm1 and PSm2).

2.3. Sample preparation

Measurement samples were prepared by adding 2 g of the organic scintillator (i.e., PSm1 or PSm2 plastic scintillation microspheres, liquid scintillator or gel scintillator) and 1 ml of the counting solution (i.e., active or blank) to a 6-ml polyethylene vial. After preparation, the vials were shaken using ultrasonic waves for 2 min and then centrifuged for 10 min at 83.3 Hz to ensure homogenization and to improve the efficiency and reproducibility of the experiments.

The counting solutions were prepared by diluting a known quantity of the active stock solution (^{3}H or ^{36}Cl) and the corresponding quenching agent (NaCl, $BaCl_2$ or Glycerin) into a known volume of the carrier solution to obtain the desired activity and concentration of the quenching agent in the measurement sample.

The activity of the measurement samples was around 350 Bq for the ^{3}H solutions and 2.17 Bq for the ^{36}Cl solutions.

The measurement samples contained an increasing concentration of the various quenching agents (NaCl, $BaCl_2$ or Glycerin). The concentrations of the measurement samples that contained NaCl were as follows: 0 M, 0.3 M, 0.7 M, 1.4 M, 2.1 M and 2.6 M. The concentrations of the $BaCl_2$ measurement solutions were as follows: 0 M, 0.05 M, 0.10 M, 0.15 M, 0.2 M, 0.25 M, 0.3 M, 0.7 M and 1.4 M. Finally, the glycerin solutions had the following percentage of weight values: 0%, 14.42%, 28.85%, 43.33%, 57.75%, and 72.17%.

A blank was prepared for each active measurement sample by adding the carrier solution instead of the active stock solution.

All solutions were prepared by weighing.

2.4. Measurements

Measurements were done in the following default setting configuration of the Quantulus detector: "low coincident" bias (right and left pulses with high differences in their amplitude are accepted) and "^{14}C" multichannel analyzer configuration (no correction for chemiluminescence). The counting times were 60 min for each vial and 10 min for the external gamma source (^{152}Eu).

2.5. Data treatment

The spectrum that was obtained for each measurement was smoothed using a Savitzky–Golay algorithm. Net spectrum was obtained by subtracting from an active spectrum, the spectrum of the corresponding blank solutions. The detection efficiency was calculated to be the ratio of the net counts in the entire spectrum and the activity that was added to the measurement vial. The uncertainty associated with the detection efficiency of the samples without quenching agent (Tables 1 and 2) corresponds to the experimental standard deviation of three replicates. The uncertainty associated to the detection efficiency of the rest of the samples corresponds to the combined standard uncertainty considering the canonical values of uncertainty of the main sources of uncertainty (weighting, count rate of the active sample and count rate background sample).

Normalized spectra (NC_i) were calculated by dividing the number of counts in each channel of the spectrum (C_i) with regard to the total area of the same spectrum (ΣC_i) (thus, the area of the normalized spectrum is one). The residual spectrum plot of a quenched sample ($NNE_{q,i}$) was obtained from the detection efficiency spectrum ($E_{q,i}$), normalized with regard to its value of detection efficiency($\Sigma E_{q,i}$) (the value of each channel is divided with regard to the value of detection efficiency), and normalized again with regard to the normalized spectrum of the sample without quenching agent ($E_{0,i}/\Sigma E_{0,i}$)

$$NC_i = \frac{C_i}{\sum_{j=1}^{1024} C_j} \quad (1)$$

Table 1
SQP(E) values and ^{3}H and ^{36}Cl experimental detection efficiencies obtained for the different organic scintillators.

	SQP	^{3}H (%)	^{36}Cl (%)
Liquid scintillation	750 ± 4	24.2 ± 0.2	94.6 ± 1.4
Gel scintillation	760 ± 5	22.1 ± 1.1	96.7 ± 0.7
Plastic scintillation (PSm1)	680 ± 9	0.51 ± 0.03	88.2 ± 1.0
Plastic scintillation (PSm2)	737 ± 4	0.40 ± 0.02	83.3 ± 0.5

$$NNE_{q,i} = \frac{NE_{q,i}}{NE_{0,i}} = \frac{E_{q,i}/\sum_{j=1}^{1024} E_{q,j}}{E_{0,i}/\sum_{j=1}^{1024} E_{0,j}} \quad (2)$$

Once a sample is measured in the Quantulus detector, it can be irradiated (in the same detector) with a external gamma source (^{152}Eu). The interaction of the gamma rays with the atoms of the sample solution generates by Compton effect a high number of electrons that finally are converted into photons that could be measured by the detector. Typically the Compton spectrum of the external gamma source is used to know the degree of quenching (color and chemical) that the sample suffers, since the spectrum will be shifted to low energies when samples have quenching. In the case of the Quantulus detector the result of the measurement of the sample when irradiated by the gamma external source is the spectrum and a parameter, named SQP(E). The SQP(E) is calculated by the detector and corresponds to the channel of the spectrum generated by the external gamma source in which the cumulative area is 99.75% of the total area. The decrease of the

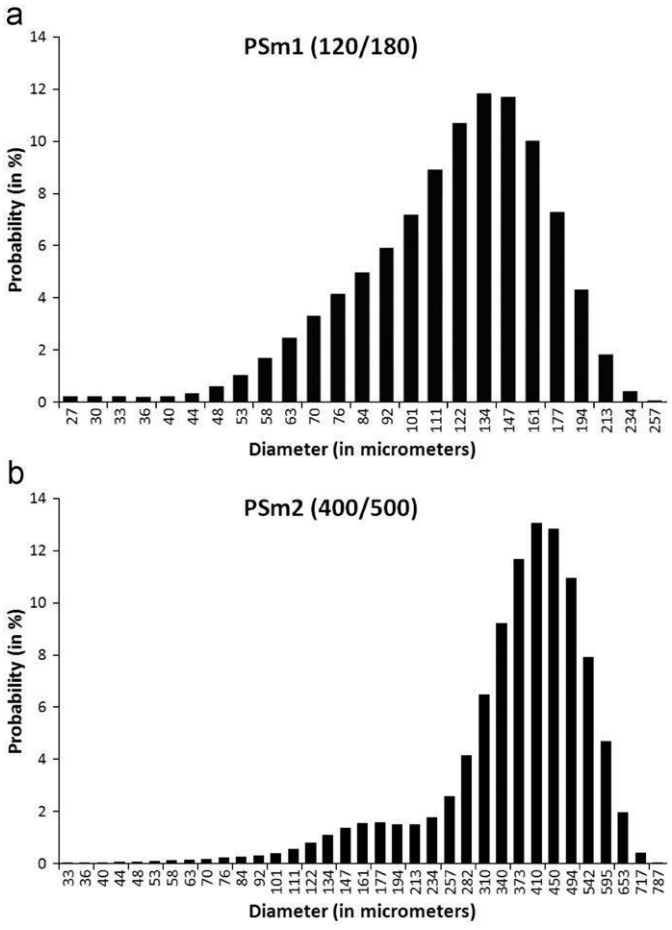

Fig. 1. Probability size distribution of the PSm (PSm1 in Fig. 1a and PSm2 in Fig. 1b).

Table 2
Experimental and Simulated detection efficiencies for PSm1 and PSm2.

	^{3}H efficiency (%)		^{36}Cl efficiency (%)	
	Experimental	Simulated	Experimental	Simulated
Plastic scintillation (PSm1)	0.51 ± 0.03	1.64 ± 0.03	88.2 ± 1.0	91.6 ± 0.1
Plastic scintillation (PSm2)	0.40 ± 0.02	0.51 ± 0.01	83.3 ± 0.5	83.3 ± 0.3

SQP(E) value indicates the presence of quenching agents in the sample [8].

2.6. Monte Carlo simulation

The simulation of electron transport was performed using a Monte Carlo simulation and the 2004 version of the PENELOPE code package, which was supplied by the Nuclear Energy Agency. The program was modified to allow for the simulation of the track of the electrons in a 1-mm^3 cube that was filled with polystyrene spheres and water [26].

The geometries that were used in the simulation were created by following a procedure that was previously established by the authors and was based on the location of the spheres in the lowest possible position until the 1-mm^3 cube were completely filled with microspheres [26]. The diameter of the microspheres was selected using random numbers and the real diameter distribution of the microspheres, which was measured previously by particle size analysis. Fig. 1 show the probability distribution of the diameters for the PSm1 and PSm2. Five geometries were created for each type of microsphere and the degree of space filling was $63.3 \pm 0.6\%$ for PSm1 and $62.6 \pm 0.5\%$ for PSm2.

The compositions of the materials used in the simulation were polystyrene for the microspheres and water for the space between the microspheres.

In the simulation, the beta particle emitted in the radioactive disintegration is located at a random position in the aqueous phase, and the transport of this particle through this media is simulated until the energy is lower than the absorption energy (i.e., 50 eV) or it enters into a microsphere. In this last case it is considered that the disintegration is detected, the energy of the beta particle when arriving to the microsphere is recorded and the simulation of the event is ended. Once all events are simulated, the results obtained comprised the number of beta particles that arrived to the microspheres (efficiency) and their energy distributions.

The emission spectrum of the ^{36}Cl and ^{3}H used in the simulation were obtained from the MICELLE2 code [27]. 5.7×10^5 events were simulated for each geometry (five geometries for both PSm1 and PSm2). Final values of efficiency for each PSm correspond with the mean value of the five geometries; whereas the uncertainty associated correspond with the standard deviation between the five geometries.

2.7. Safety considerations

All of the experimental procedures were carried out in accordance with the regulations of the Spanish Nuclear Authorities (Consejo de Seguridad Nuclear) and the University of Barcelona.

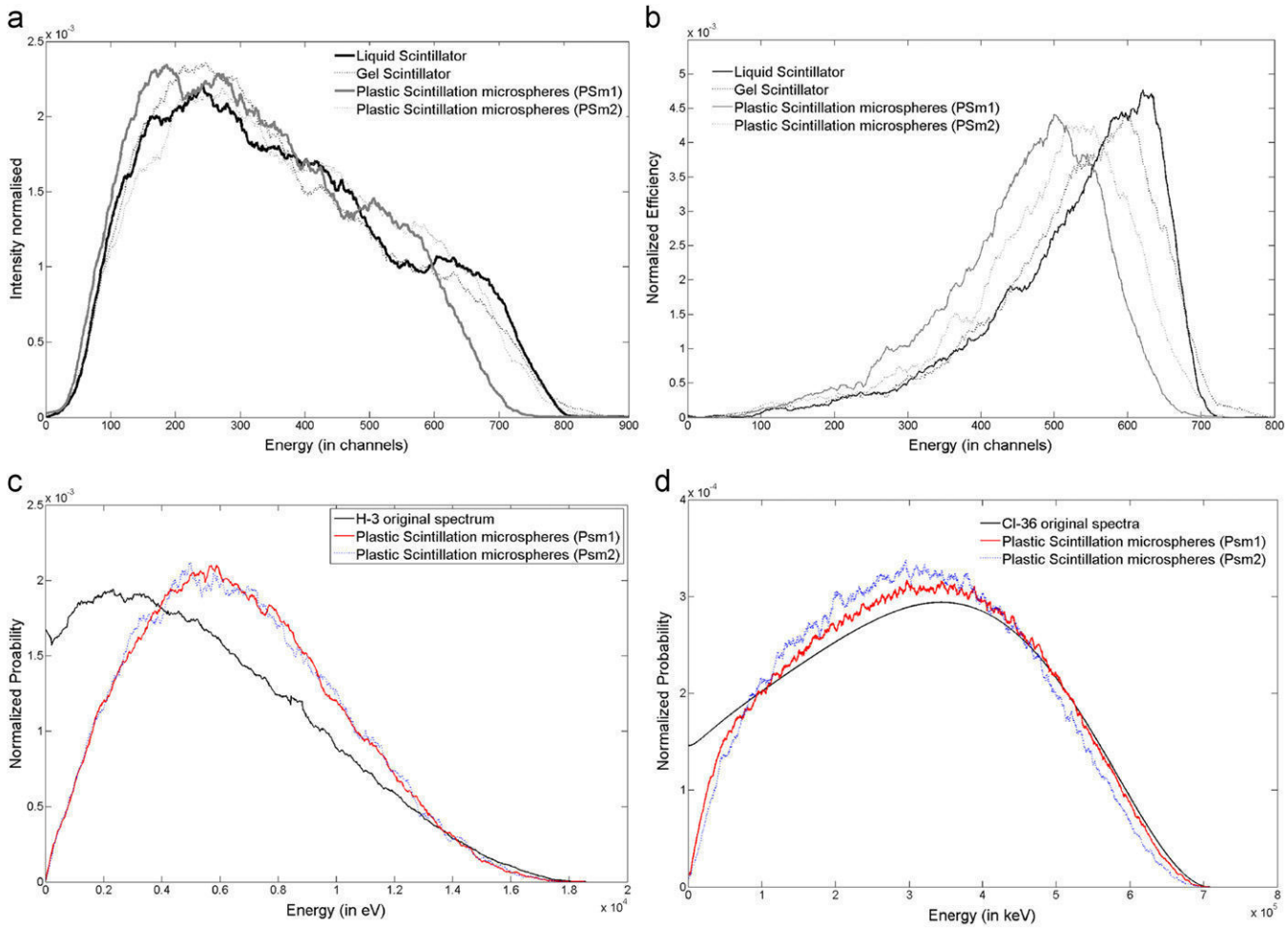

Fig. 2. (a) Spectra of a background sample irradiated by an external gamma source in LS, GS, PSm1 and PSm2; (b) ^{36}Cl-normalized, experimental detection efficiency spectra obtained by using LS, GS, PSm1 and Psm2; (c) the original ^{3}H and ^{3}H spectra obtained for PSm1 and PSm2 by using the Monte Carlo simulation; and (d) the original ^{36}Cl and ^{36}Cl spectra obtained for PSm1 and PSm2 by using the Monte Carlo simulation.

3. Results and discussion

3.1. Detection efficiency in organic scintillators

Experimental values of detection efficiency obtained with the different organic scintillators are shown in Table 1. The values obtained by using LS and GS were similar, and the differences that occurred could be attributed to the different scintillating properties of the scintillation cocktails (Optiphase Supermix and Insta Gel). In both cases, the mixture of sample and scintillator provides a quasi-homogenous medium (i.e., nanomicelles of water into the organic scintillator) in which the distance between the emitted particle (i.e., beta or alpha) and the organic solvent is on the order of nanometers, and, as consequence, a great proportion of the beta particles emitted in the ^{3}H decay are capable of arriving to the scintillator to produce photons and almost all of the beta particles emitted in the ^{36}Cl decay are detected.

In measurements with PSm, the distance between microspheres is on the order of tens or hundreds of microns; therefore, the distance that a particle (i.e., beta or alpha) must travel in the aqueous media to reach the scintillator can be higher than its range. When ^{3}H is measured with PSm, only a small proportion of the beta particles emitted are capable of reaching the surface of the microsphere, and, therefore, the detection efficiency obtained is low.

In case of ^{36}Cl, since the beta particles emitted in the decay are more energetic, more betas are capable of reaching the scintillator to produce photons. However, the low-energy ones lose all of their energy in interactions with the aqueous media without being detected, as it can be deduced from the detection efficiency values obtained using PSm, which are slightly lower than those of LS and GS (Table 1).

When comparing both PSm, the experimental detection efficiencies of PSm1 are slightly higher than those of PSm2 (Table 1). This behavior could be related to the distance between the microspheres. In PSm1, since the diameter of the microspheres is lower, the distance between microspheres is lower and as consequence the probability of an electron reaching the microspheres without losing its energy is slightly higher. However, this behavior enters into contradiction with the values of the SPQ(E), since the values for PSm1 are smaller than those for PSm2, and values for PSm2 are slightly smaller than those obtained for LS and GS. When analyzing the spectrum of a background sample that is irradiated by the external standard source (Fig. 2a) and the detection efficiency ^{36}Cl (Fig. 2b) obtained by the four scintillators, it can be seen that the spectra of PSm2, LS and GS appear in the same position, whereas the spectrum of PSm1 is shifted to lower energies, as if it had suffered some quenching process.

To obtain a better understanding of the differences between PSm1 and PSm2, a Monte Carlo simulation for the loss of energy of the electrons that are emitted in the PSm media was performed. As a result of the simulation, it is obtained the proportion of beta particles that arrive at the surface of a plastic scintillation microsphere (and could have their energies converted into photons), and the energy distribution probability of those particles (Fig. 2c and d, together with the original ^{3}H and ^{36}Cl spectra used in the simulation).

The probability of beta particles emitted in the ^{3}H decay of reaching the microspheres is low (Table 2). Furthermore, the effect of the diameter of the microspheres in the detection efficiency was evidenced (1.64% for PSm1 versus 0.51% for PSm2). For ^{36}Cl, most of the beta particles achieve the microspheres (91.6% for PSm1 versus 83.3% for PSm2) but the existence of a proportion of particles which are fully halted, explains why the experimental efficiency values for PSm are lower than the obtained with LS and GS (Table 1).

The analysis of ^{3}H spectra (Fig. 2c, original spectrum of ^{3}H and spectra of the beta particles that arrive to the microspheres) show that all the low-energy beta particles are fully halted and are not

Table 3
Density of the NaCl, $BaCl_2$ and glycerin solution measured.

NaCl concentration (mol/l)	NaCl solution density (g/ml)	$BaCl_2$ concentration (mol/l)	$BaCl_2$ solution density (g/ml)	Glycerin proportion (w/w%)	Glycerin solution density (g/ml)
0.3	1.006	0.3	1.052	14.42	1.038
0.7	1.020	0.7	1.122	28.85	1.086
1.4	1.045	1.4	1.245	43.33	1.135
2.1	1.069			57.75	1.185
2.8	1.093			72.71	1.236

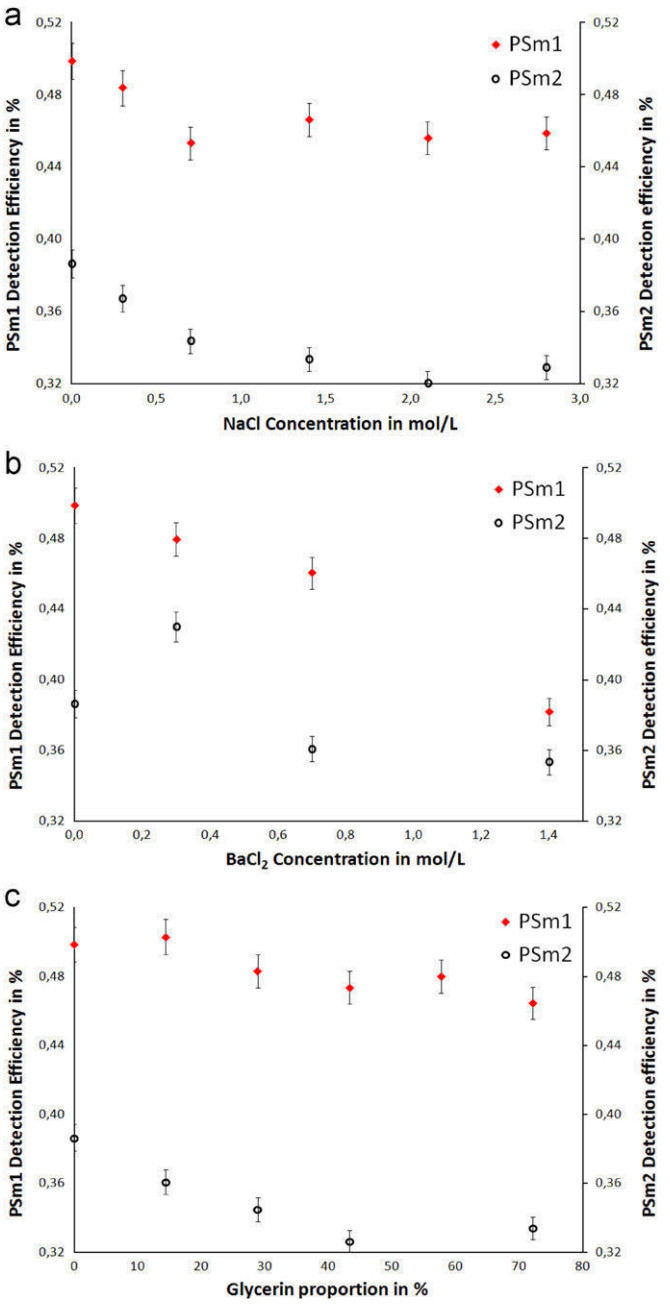

Fig. 3. ^{3}H experimental detection efficiency for PSm1 and PSm2 samples with different concentrations of NaCl (a), $BaCl_2$ (b) and Glycerin (c).

detected, whereas a small proportion of those beta particles of high energy are capable to reach the scintillator. The resulting simulated spectra are apparently shifted to high energies (since they are the normalize spectra) with regard to the original spectrum.

However, the simulated spectra obtained for PSm1 and PSm2 are similar, probably because the PSm diameter (134 μm and 410 μm) is too high, the range of ^{3}H particles too low (as can be seen from the efficiency values) and as consequence, the particles detected are only those that are emitted very close of the surface of the microsphere and do not lose energy (or only a small proportion). As a result no important differences are observed in the simulated spectra of PSm1 and PSm2.

The analysis of ^{36}Cl spectra (Fig. 2d) show relevant differences between the original spectrum of ^{36}Cl and the simulated spectra at low energies (as in the case of ^{3}H) but only small differences at high energies. In this case, as the energy of most of the particles emitted in the ^{36}Cl decay is high, their range is higher than the diameter of the microspheres. As consequence, the effect on changing the PSm diameter is slightly evidenced by a shift to low energies of the simulated spectrum of PSm2 with regard to PSm1 (i.e., the beta particles emitted in the farthest position in Psm2 (410 mm of diameter) may travel more distance than those that are farthest in Psm1 (134 mm of diameter) and as consequence may lost part of its energy).

These effects on the detection efficiency and the spectrum distribution in PSm measurements are caused by *particle quenching*, which can be defined as the process of a particle (i.e., beta or alpha) losing energy by interacting with the molecules in the medium before the particle reaches the scintillator. The consequences of particle quenching are a reduction in the detection efficiency and changes on the spectrum distribution. These effects are more important for low-energy beta particles and minimal for high-energy particles. Particle quenching can be considered the most important cause of the loss of energy in measurements with plastic scintillation microspheres, especially for low-energy emitters.

It is also interesting to note that although the energy distributions of the beta particles that arrive to the scintillator are similar for PSm1 and PSm2 and are also similar to the original spectrum of the radionuclide (Fig. 2c), the experimental spectrum of PSm1

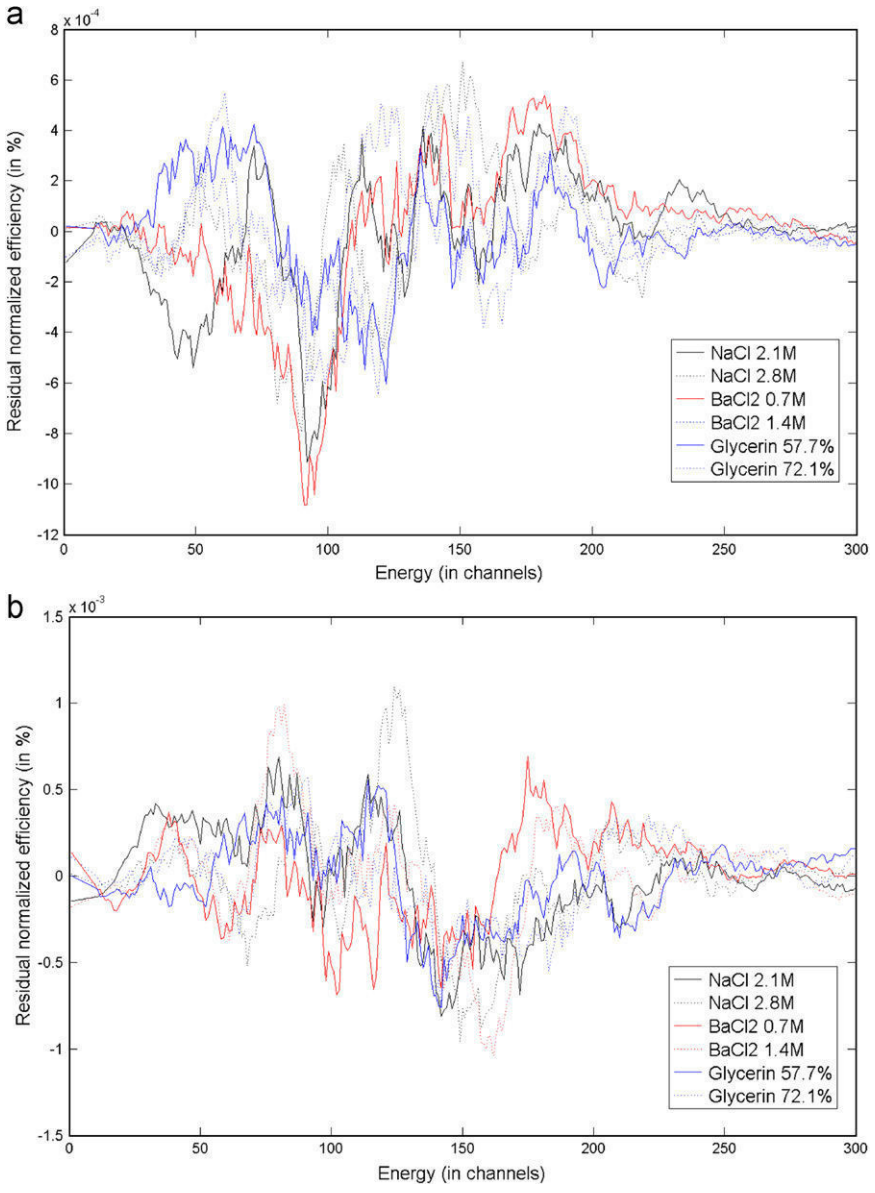

Fig. 4. ^{3}H normalized detection efficiency residual spectra (referred to "without salt" sample) for PSm1 (a) and PSm2 (b) samples with different concentrations of NaCl, $BaCl_2$ and Glycerin.

is shifted to lower energies, when compared to that of PSm2 (Fig. 2b). Moreover, the difference between the ^{3}H theoretical detection efficiency and the experimental value (Table 2) is higher for PSm1 (from 1.65% to 0.51%) than for PSm2 (from 0.51% to 0.40%). Because the spectrum of beta particles that arrive at the scintillator is similar for both scintillators, it can be deduced that these differences originate after the beta particles reach the scintillator. Discarding chemical and color quenching, because the sample composition is the same, the differential loss of energy between PSm1 and PSm2 can only be attributed to inefficient transmission of scintillation photons. For PSm1, the path traveled by a photon generated at one point of the vial contains more changes in materials and, as consequence, in the refractive index than a photon that is produced in the PSm2 medium. From the optical point of view the situation in PSm2 is simpler and this explains why the SQP(E) values (Table 1), the Compton spectrum (Fig. 2a) and the spectrum of ^{36}Cl (Fig. 2b) are more similar to those of LS and GS. For PSm1, the multiple changes in refractive index causes that a proportion of beta particles emitted in the ^{3}H and ^{36}Cl decay that are capable arrive at the scintillator to produce photons that are not capable of reaching the photomultipliers. Consequently, the spectrum of both radionuclides is shifted to lower energies, and the values of the SQP(E) decrease.

This behavior, termed *optical quenching*, is defined as the quenching process that can be attributed to inefficient transmission of the optical photons that are generated by the scintillator. Consequences of this quenching process include a decrease in the efficiency of low-energy beta emitters and a small decrease in the efficiency and movement of the spectrum to lower energies for high-energy beta emitters.

Table 4
The appearance of liquid scintillation and gel scintillation vials before measurement.

	Liquid	Gel
NaCl (0.3 M and 0.7 M)	Clear	Clear
NaCl (1.4 M, 2.1 M and 2.8 M)	Phase separation	Precipitation
$BaCl_2$ (0.05 M to 0.25 M)	Precipitation	Milky
$BaCl_2$ (0.3 M to 1.4 M)	Precipitation, milky and phase separation	Milky
Glycerin (14.4% to 43.3%)	Clear	Precipitation
Glycerin (57.7%)	Clear	Phase separation
Glycerin (72.1%)	Phase separation	Phase separation

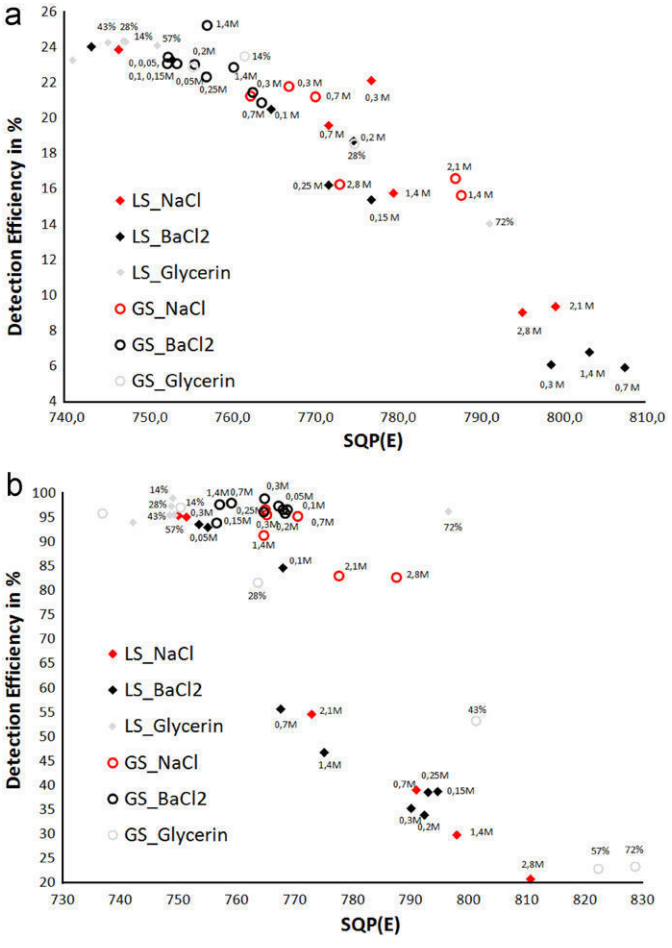

Fig. 5. Variation of the ^{3}H (a) and ^{36}Cl (b) detection efficiencies for LS and GS with the SQP(E) values for samples with different NaCl, BaCl2 or Glycerin concentrations.

3.2. Particle quenching in organic scintillators

Particle quenching was evaluated by measuring the detection efficiencies of samples with increasing amounts of NaCl or $BaCl_2$. In both cases, an increase in salt concentration produces an increase in the density of the solution and introduces elements of different atomic radius that can interact with the beta particle emitted. Glycerin ($C_3H_8O_3$) was also considered in the evaluation by measuring solutions with an increasing glycerin proportion (from 14% to

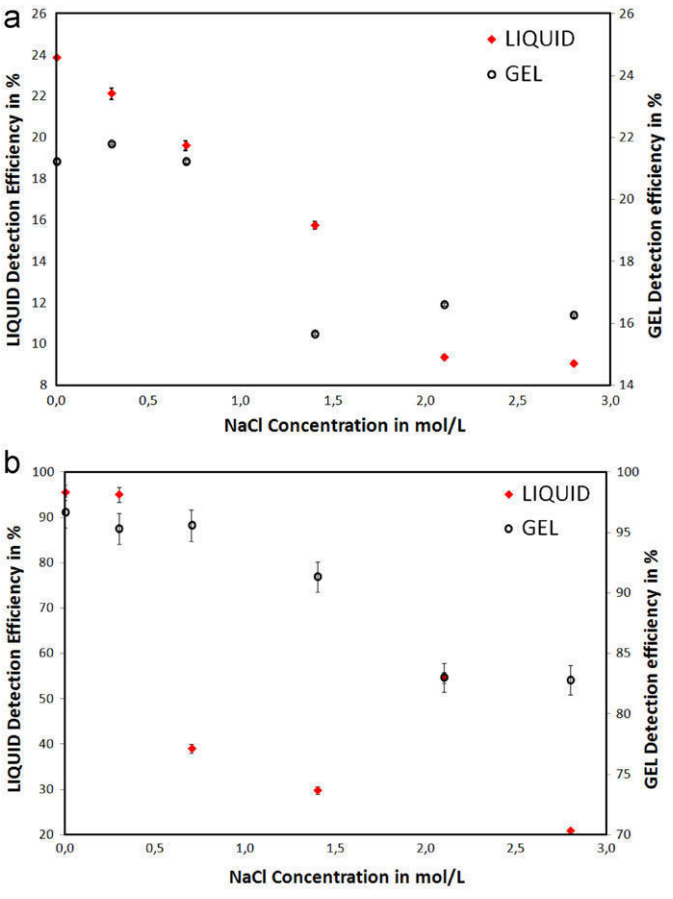

Fig. 6. Variation of the detection efficiency for ^{3}H (a) and ^{36}Cl (b), as measured by LS and GS, with the NaCl concentration.

72%), which leads to an increase on the solution density. Densities of the solutions evaluated are given in Table 3 [28].

3.2.1. Plastic scintillation

When measuring ^{3}H with PSm1 and PSm2, a decrease in the detection efficiency with the increase in the concentration of NaCl, $BaCl_2$ and glycerin can be observed (Fig. 3). This decrease is caused by a decrease in the number of beta particles that are capable of arriving to the scintillator, since the increase of the density of the solution causes an increase on the interactions of the beta particle with the molecules and atoms of the medium (i.e., particle quenching).

The variation of the ^{3}H detection efficiency is not correlated with a variation of the SQP(E) value, which remains constant in all cases (PSm1: NaCl—678 ± 5; $BaCl_2$—672 ± 9 and Glycerin—676 ± 2; PSm2: NaCl—737 ± 2; $BaCl_2$—736 ± 5; and Glycerin—736 ± 4). Moreover, the ^{3}H spectrum is always in the same position and is not shifted to lower energies as it can be seen in the residual plots (Fig. 4a and b). Both results can be explained by the increase in the density of the solution, which leads to a decrease on the range of the beta particles emitted in ^{3}H decay, causing an increase of beta particles halted before they arrive to the microspheres. As a whole, the beta particles that are still capable of arriving to the microspheres do so with the same energy distribution as the beta particles measured when only water was added (i.e., the reduction on the number of beta particles is proportional in the ^{3}H energy range). This behavior is similar to what was previously observed with the simulated spectra of PSm1 and PSm2 (Fig. 2c).

It is important to highlight the differences between the effect of particle quenching when comparing the ^{3}H original spectrum with the ^{3}H spectra measured with PSm1 and PSm2, and the effect when comparing the spectra of ^{3}H sample without salt or with salt. In the former case, the spectrum gravity center moves to high energies because only the high-energy particles emitted in the ^{3}H decay that are close to a microsphere, have probabilities to reach the microspheres. In the second case, the increase on the density causes a small decrease in the range of the betas and as consequence the reduction on the probability to be detected, due to collisions with atoms or molecules in the medium, is proportional for all energies and the spectra measured are always in the same position.

When comparing the different compounds that were used in this study (i.e., NaCl, $BaCl_2$ and glycerin), the behavior observed for PSm1 and PSm2 seems not homogenous. This can be probably related to different factors that affect the measurement, among which density is the most important.

In the case of ^{36}Cl, since the energy of the beta particles emitted in the decay is high, the effect of the increase in density is negligible; therefore, the detection efficiency and the SQP(E) are constant, and the spectrum remains in the same position.

3.2.2. Liquid and gel scintillation

For LS and GS, the organic scintillator and the aqueous solution form a heterogeneous emulsion of aqueous nanomicelles that are surrounded by the organic scintillation cocktail. As happens for PSm, an increase in the density of the solution can lead to an increase in the number of particles that are halted before they

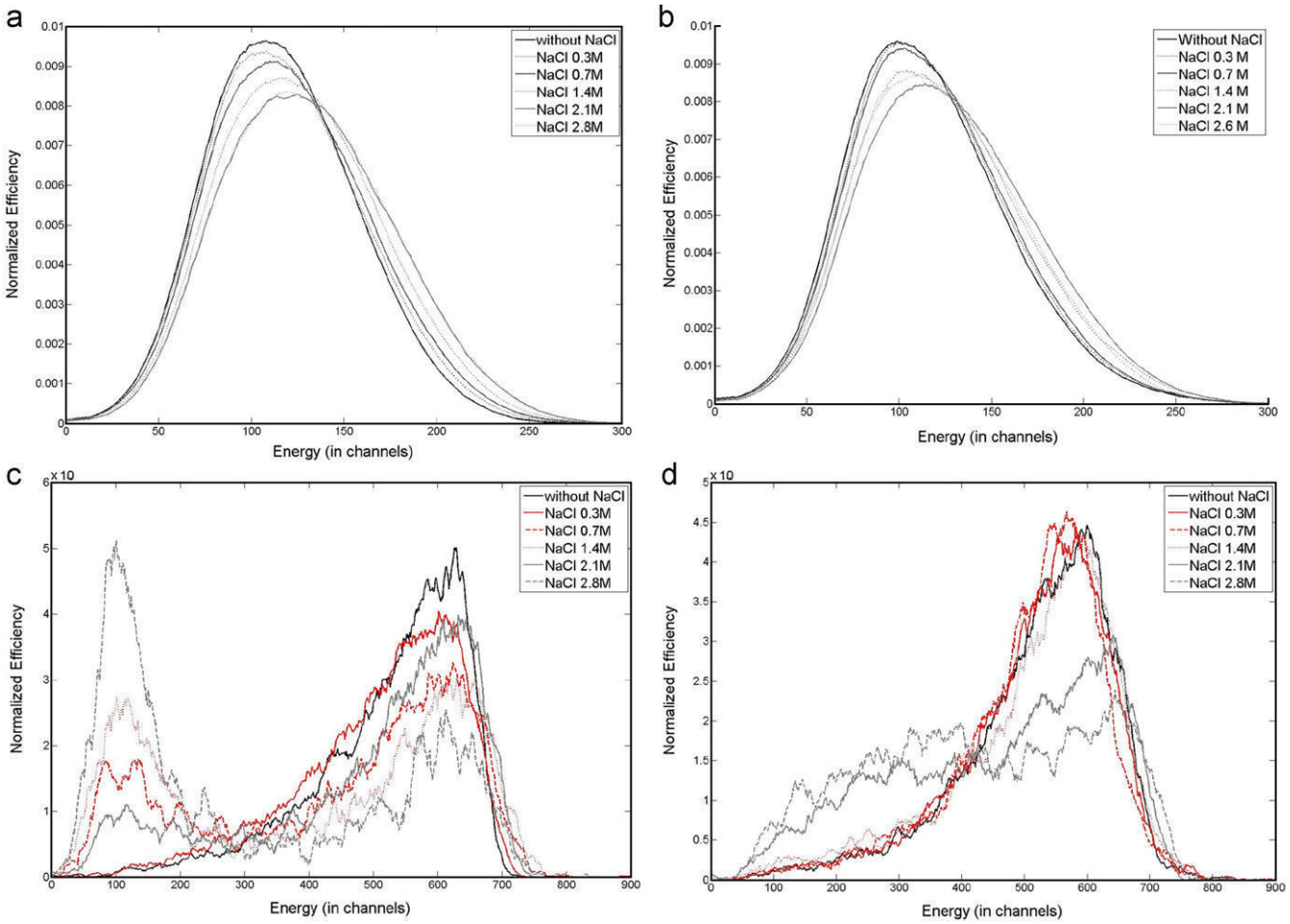

Fig. 7. Normalized efficiency spectra obtained for samples with differing NaCl concentrations. ^{3}H with LS (a); ^{3}H with GS (b); ^{36}Cl with LS (c); and ^{36}Cl with GS (d).

reach the scintillator (i.e., particle quenching), and as consequence, a reduction in the detection efficiency occurs. However, the presence of salts can have other effects such as changing the equilibrium between the scintillator and the aqueous solution, thus causing the appearance of turbidity, which is commonly known as milky solutions, and phase separation, which can change the scintillation properties of the mixture. Table 4 summarizes the appearance of the LS and GS vials after adding NaCl, $BaCl_2$ or glycerin immediately before these solutions were measured.

3.2.2.1. NaCl. The detection efficiency of ^{3}H in LS (Fig. 6a) decreases when the NaCl concentration increases; and when phase separation occurs, this value decreases abruptly to a constant value. However, the SQP(E) value (Fig. 5a) increases and the ^{3}H spectrum shifts to higher energies (Fig. 7a) with the increase in the NaCl concentration. Similarly, ^{36}Cl (Fig. 5b) efficiency is inversely correlated with the SQP(E) value (i.e., the efficiency decreases with an increase in the SQP(E) value) and the spectrum is shifted to higher energies (Fig. 7c). In this case, we also observe a peak at low energies that increases with the increase in the NaCl content.

Using a GS, the detection efficiency is constant for ^{3}H and ^{36}Cl at low NaCl concentrations. When the concentration is higher than 1.4 M and the NaCl precipitates, the efficiency decreases to a constant value for both radionuclides, the SQP(E) parameter increases (Fig. 5a and b), and the spectra move to higher energies (Fig. 7b and d). As it happens for LS, a broad band at low energies also appears in the ^{36}Cl spectra for the two samples that exhibit phase separation.

Although there are not experimental direct evidences (not in the bibliography either) and by comparison with the results obtained in PSm measurements, It can be thought that the presence of NaCl at low concentrations causes an increase in the size of the aqueous nanomicelles into the organic scintillator and a small decrease of the probability of the low-energy beta particles (e.g., ^{3}H) arriving at the scintillator. However, in a way similar to that of PSm samples, an increase in the size of nanomicelles could cause a reduction in the number of micelles and an improvement in the optical transmission of photons through this media. Consequently, the spectra would shift to higher energies, and the SQP(E) values would increase due to a reduction in optical quenching.

When micelles become saturated and cannot expand, the phase separation occurs and an aqueous phase with NaCl dissolved appears. ^{3}H (in form of $^{3}H_2O$) or ^{36}Cl (in form of $^{36}Cl^-$) are then distributed between the organic and the aqueous phase depending on the quantity of water in each phase. In one hand, the organic phase contains the scintillator and is saturated with water micelles (containing H_2O and NaCl), that included part of the radionuclide (^{3}H or ^{36}Cl). On the other hand, the aqueous phase ($^{3}H_2O$) contains most of the NaCl (^{36}Cl) and can contain also some scintillator solved (the solvent and fluorescent solute).

In the case of ^{36}Cl, the presence of the radionuclide in the aqueous phase can be the reason that explains the presence of the peak at low energies. Two hypotheses can be considered to explain this fact; First, that the signal corresponds to Cherenkov radiation by emitted by the ^{36}Cl in the aqueous (with an efficiency around 22% and a signal peak located up to channel 200) and second, that the aqueous phase contains enough scintillator dissolved to produce scintillating signals, that are detected at the low energy region due to the limited optical properties of the aqueous phase (optical quenching).The intensity of this signal increases with the increase in NaCl concentration, since the volume of the aqueous phase increases (increasing also the quantity of radionuclide included in it). The final detection efficiency is the sum of the contribution of both phases and it is affected by several factors (stability, height of the vial, lensing effect due to the meniscus,…), which makes its determination inaccurate.

3.2.2.2. $BaCl_2$. The addition of $BaCl_2$ to the liquid scintillator causes the appearance of a white, gelatinous precipitate, even at the lowest-tested concentration. When the concentration is higher than 0.3 M, two phases are observed. However, with GS, the scintillation solution is always milky, and neither precipitate nor separated phases are detected.

The behavior that is observed when measuring using LS reproduces the pattern that is observed for NaCl (Fig. 8a and b). The efficiency decreases due to the presence of a precipitate, which may occlude ^{3}H and partly precipitated ^{36}Cl, but the SQP(E) increases, and the normalized spectrum shifts to high energies because of improved optical conditions of the organic phase. For ^{36}Cl, a peak at low energies is observed as a consequence of the scintillation signal of the aqueous phase and/or due to Cherenkov radiation from ^{36}Cl.

In GS measurements, the detection efficiency (Fig. 8a and b), SQP(E) values (Fig. 5a) and spectra position (Fig. 9a and b) remain constant for both radionuclides, which implies that optical quenching is constant (i.e., the organic phase is always constant) and that particle quenching does not occur (i.e., the presence of more $BaCl_2$ does not change the probability of the beta particle to be halted). A hypothesis to explain that behavior is that $BaCl_2$ form crystals that are suspended in the gel solution (as happens with $BaSO_4$ [29]) and are not deposited on the bottom. Since all

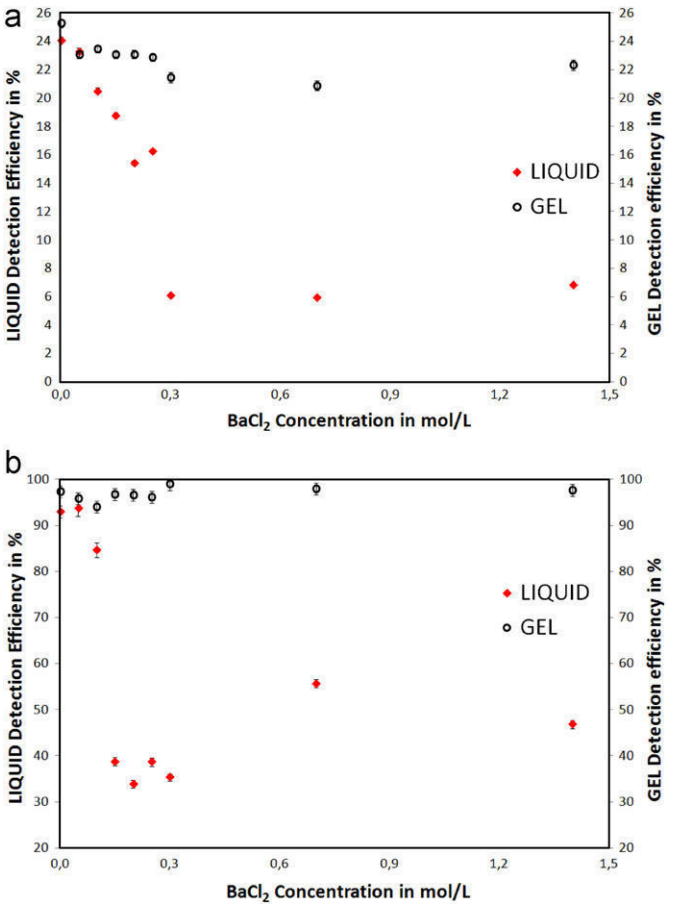

Fig. 8. Variation of the detection efficiency for ^{3}H (a) and ^{36}Cl (b), measured by LS and GS, with the $BaCl_2$ concentration.

the $BaCl_2$ is suspended, no optical effects are expected. Furthermore, crystal must be on the nano or micro scale, to avoid autoabsorption and the distance between crystals must be high, and therefore, the probability of a beta particle interacting with other crystals is negligible.

3.2.2.3. Glycerin. When glycerin solutions were added to the liquid scintillator samples, the measurements solutions remained clear and homogenous, except for the solution with a higher proportion of glycerin where two phases were clearly identified. On the contrary, in GS, even the solution with a lower concentration of glycerin produced the appearance of a gelatinous precipitate, and the formation of two phases.

In LS, detection efficiency and SQP(E) values (Figs. 10 and 5a) are constant, and the spectra are in the same position for all homogeneous samples. In the sample with 72% glycerin and phase separation, the ^{3}H efficiency decreases, the SQP(E) increases, the main part of the spectrum (^{3}H and ^{36}Cl) shifts to lower energies, and a small proportion of the spectrum appears at higher energies (Fig. 11a and b).

When only one phase exists the detection efficiency and the SQP(E) are constant with regard to the glycerin proportion and the spectra are always in the same position. This constant behavior suggests that the mixture scintillator/glycerin/water is constant for this range of glycerin proportions. The glycerin is dissolved into the organic phase of the mixture, and the aqueous nanomicelles always have the same composition and dimensions, thus, the efficiency is constant. When phase separation happens two phases are formed: A glycerin phase, with water and part of the organic scintillator dissolved in it, and an organic phase, with glycerin and water dissolved in it. The radionuclide, which is in an inorganic chemical form, is mostly dissolved into the glycerin phase, which has poor optical properties. This explains why the main part of the spectrum moves to lower energies. However, a small proportion of the radionuclide remains in the organic phase (with less water and improved optical properties), and this explains why a small tail at high energies and an increase in the SQP(E) value are observed.

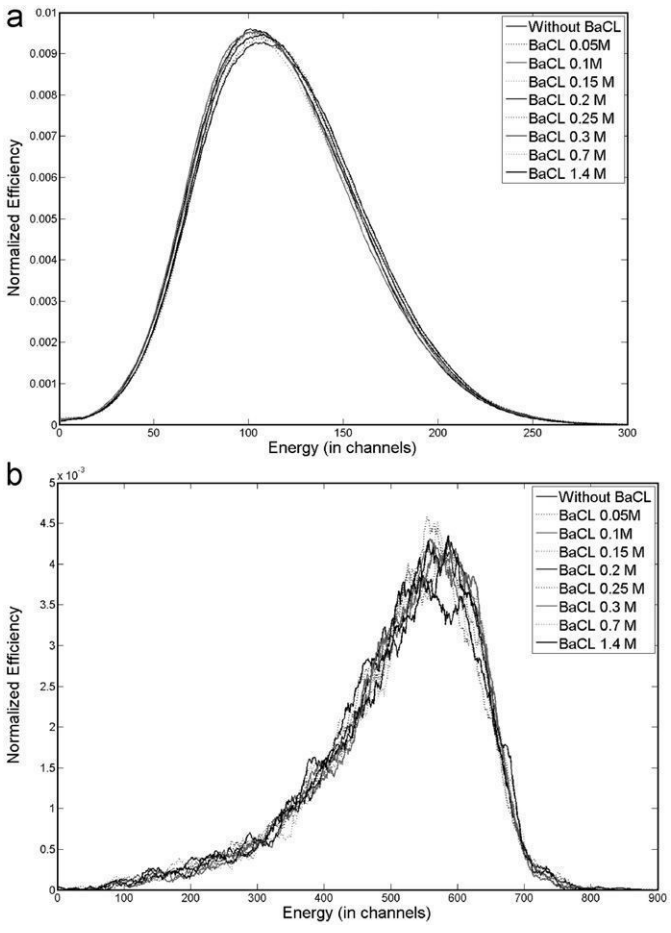

Fig. 9. Normalized efficiency spectra obtained when measuring ^{3}H (a) and ^{36}Cl (b) samples with different $BaCl_2$ concentrations with the Gel Scintillator.

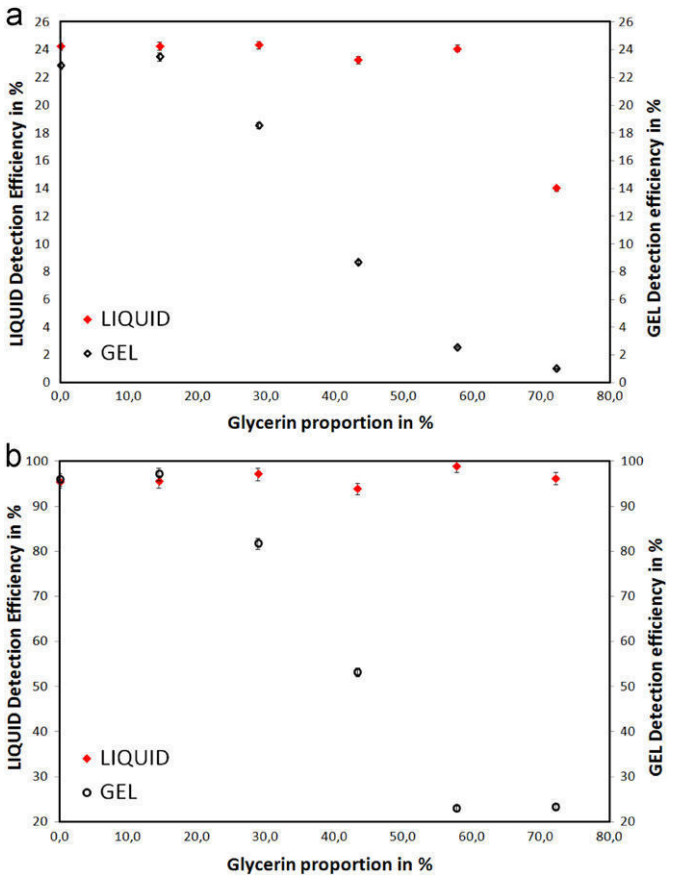

Fig. 10. Variation of the detection efficiencies for ^{3}H (a) and ^{36}Cl (b), when measured by LS and GS, with the proportion of glycerin.

Measuring by using GS is very similar to what was observed in LS NaCl and $BaCl_2$ solutions. Efficiency decreases (Fig. 10a and b), the spectra shift to higher energies, and the SQP(E) increase (Fig. 5a and b) due to the increase on the dimensions of the micelles. When phases are separated, the efficiency and SQP(E) values became constant, and a peak at low energies appears for ^{36}Cl, which is due to the signal from the aqueous phase and/or from ^{36}Cl Cherenkov emission.

4. Conclusions

Evidences on the effects of particle quenching and optical quenching on measurements by organic scintillators have been found.

Particle quenching, which is defined as the process of a particle (i.e., beta or alpha) losing its energy before it interacts with the scintillators, is the main quenching effect when measuring PSm and is responsible for the decrease in the detection efficiency when the diameter of the PSm is increased or when solutions of increasing density are measured. In liquid scintillation, this effect is lower and, in some cases, negligible, but it can also be observed

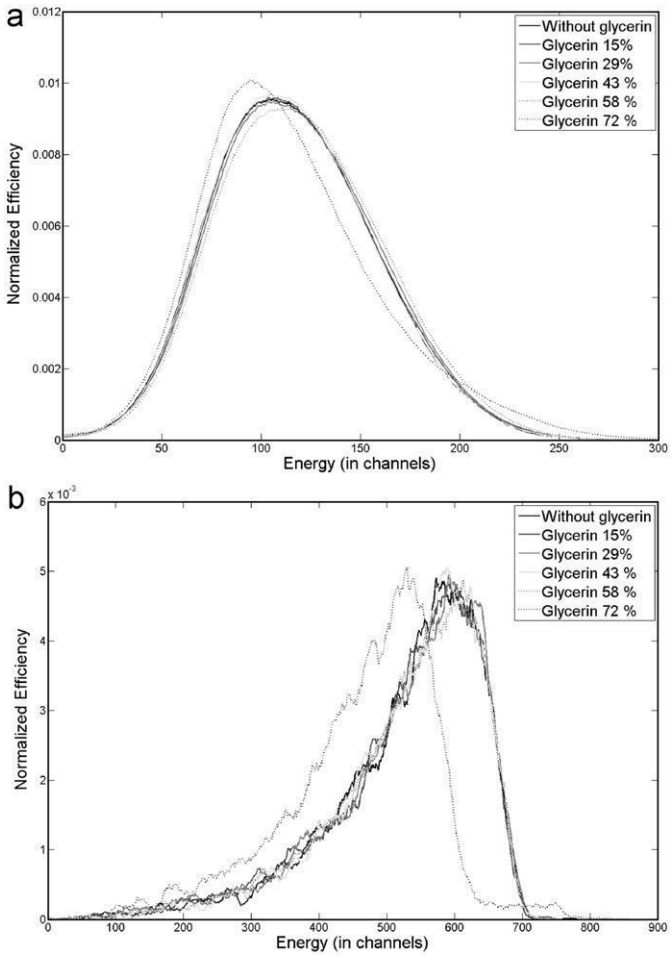

Fig. 11. Normalized efficiency spectra obtained when measuring ^{3}H (a) and ^{36}Cl (b) samples that had different Glycerin proportions with a liquid scintillator.

when the size of the nanomicelles of water in the scintillator is increased (which may be the case of environmental samples with high salinity content). From the experimental point of view, this effect implies a decrease in the detection efficiency, but the distribution of the measured spectrum is not affected, since this reduction is proportional for the entire range of energies. In this sense, the Monte Carlo simulation was in agreement with the experimental evidences that are obtained on particle quenching in PSm measurements.

Optical quenching in organic scintillators, which is defined as the process of reduction of the number of scintillation photons capable to reach the photomultipliers due to poor optical transmission, is associated with the size of the aqueous phase and the organic phase in the mixture and with the number of optical discontinuities that the optical photons must cross in that media. In this sense, an increase in the size of the nanomicelles, in LS, or the increase in the diameter of the microspheres, in PSm, improve the optical properties of the solution due to a simplification in the optical path of the photons. Consequently, more photons are detected, and the spectrum shifts to higher energies. However, a decrease in the size of the nanomicelle or microsphere causes a loss of optical photons in the optical transmission, which leads to a decrease of the detection efficiency, and a movement of the spectra to lower energies.

Acknowledgements

The authors would like to thank the Ministerio de Ciencia e Innovación (Spain) (MICINN) for financial support under CTM2008-01147 and CTM2011-27211 and a research grant (CTM2008-01147).

References

[1] D. Steinberg, Nature 183 (1959) 1253.
[2] D. Steinberg, Nature 182 (1958) 740.
[3] H. Kallmann, Physical Review 78 (1950) 621.
[4] J.B. Birks, The Theory and Practice of Scintillation Counting, Pergamon Press, Oxford, 1964.
[5] F.D. Brooks, Nuclear Instruments and Methods 162 (1979) 477.
[6] J.A.B. Gibson, A.E. Lally, The Analyst 96 (1971) 681.
[7] D.L. Horrocks, Applications of Liquid Scintillation Counting, Academic Press, New York San Francisco London, 1974.
[8] M.F. L'Annunziata, Handbook of Radioactivity Análisis, second ed., Academic Press, San Diego, 2003.
[9] F. Schoenhofer, Science of the Total Environment 173/174 (1995) 29.
[10] G. Grau Carles, E.G. García, A. Grau Malonda, Applied Radiation and Isotopes 60 (2004) 447.
[11] A. Grau Carles, Applied Radiation and Isotopes 64 (2006) 1505.
[12] M. Villa, G. Manjón, M. García-León, Nuclear Instruments and Methods in Physics Research Section A: Accelerators, Spectrometers, Detectors and Associated Equipment 496 (2003) 413.
[13] R. Broda, P. Cassette, K. Kossert, Metrologia 44 (2007) S36.
[14] N. Bosworth, P. Towers, Nature 341 (1989) 167.
[15] O.B. Egorov, S.K. Fiskum, M.K. O'Hara, J.W. Grate, Analytical Chemistry 71 (1999) 5420.
[16] A. Tarancon, A. Padro, J.F. Garcia, G. Rauret, Analytica Chimica Acta 538 (2005) 241.
[17] D.A. Kalbhen, V.J. Tarkkanen, in: E. University of Alberta (Ed.), Review of the Evolution of Safety, Ecological and Economical Aspects of LSC Materials and Techniques. 1984, pp. 66–70.
[18] A. Tahnassian, J. Eveloff, H. Tisdale, in: Lewis Publishers Inc. Chelsea. (Ed.), Liquid Scintillation Waste. 1991, pp. 573–575.
[19] A. Tarancon, J.F. García, G. Rauret, Analytica Chimica Acta 463 (2002) 125.
[20] H. Bagán, A. Tarancón, G. Rauret, J.F. García, Analytica Chimica Acta 686 (2011) 50.
[21] H. Bagán, S. Hartvig, A. Tarancón, G. Rauret, J.F. García, Analytica Chimica Acta 631 (2009) 229.
[22] A. Tarancon, E. Alonso, J.F. Garcia, G. Rauret, Analytica Chimica Acta 471 (2002) 135.
[23] A. Tarancon, J.F. Garcia, G. Rauret, Analytica Chimica Acta 590 (2007) 232.
[24] J. Baró, J. Sempau, J.M. Fernández-Varea, F. Salvat, Nuclear Instruments and Methods in Physics Research Section B 100 (1995) 31.
[25] F. Salvat, J.M. Fernandez-Varea, J. Sempau, PENELOPE, A Code System for Monte Carlo Simulation of Electron and Photon Transport, NEA, 2008.
[26] A.T. Sanz, K. Kossert, Nuclear Instruments and Methods in Physics Research Section A 648 (2011) 124.
[27] A. Grau Carles, Computer Physics Communications 176 (2007) 305.
[28] David R. Lide. Handbook of Chemistry and Physics. Chemical Rubber, Cleveland (Ohio) (1977) pp. 8–60.
[29] C.P. Willis, D.G. Olson, C.W. Sill, Analytical Chemistry 42 (1) (1970) 124.

Chapter 4

Global Discussions

This thesis has been focused on the evaluation of the feasibility of three different methodologies for producing plastic scintillation microspheres (PSm), the study of the influence of their operational parameters and the formulation in the yield of production, morphology, diameter and shape, and the radiometric capacities of the PSm produced to measure alpha and beta emitters.

The first methodology evaluated was the organic solvent extraction/evaporation (E/E) for producing PSm in a simple way from laboratory to commercial scale; the second one was the supercritical antisolvent (SAS) methodology to micronise particles in the order of the submicron range; and the third one, the spray drying (SD) technique to evaluate the production of PSm at industrial scale.

In addition to the production of PSm, factors like the possibility of varying their composition, the optimization of their formulation to enhance the ability for discriminating alpha/beta particles, the production of PSm of different diameters and, the systematic modification of the sample composition, allowed to develop a better understanding of the energy transfer mechanism when PSm were employed in the measurement of some beta and alpha emitters such as ^{3}H, ^{14}C, $^{90}Sr/^{90}Y$ and ^{241}Am, respectively.

Finally, the PSm production at laboratory scale through the organic solvent extraction/evaporation methodology was optimized and first steps towards the industrial production of PSm were performed.

4.1. PRODUCTION OF PSm THROUGH METHODS BASED ON THE ORGANIC SOLVENT EXTRACTION/EVAPORATION

4.1.1. Feasibililty of the organic solvent extraction/evaporation methodology and synthesis of PSm of variable composition.

The first technique used to produce PSm was the organic solvent (E/E). The procedure followed to produce PSm of seven different compositions (Table 1) is shown in Figure 1 and described as follows:

1. Preparation of the organic phase by dissolving 10 g of polystyrene and the corresponding amount of solutes in 100 mL of dichloromethane.
2. Preparation of the aqueous phase by dissolving polyvinylalcohol (PVA) in water (1 % w/v).
3. Pouring of the organic phase into the aqueous phase and mixing at 16.7 Hz during 5 hours to achieve the extraction/evaporation of the dichloromethane and the hardening of the microspheres.
4. Harvesting of the particles by filtration.
5. Washing with a solution of ethanol in water (1:10) and drying in an oven at 40ºC during 24 h.

Table 1. Composition of the organic phase of the different PSm synthesised batches.

PSm	Composition in 100 mL of dichloromethane
PSm1	10 g of polystyrene
PSm2	10 g of polystyrene and 0.1 g of PPO
PSm3	10 g of polystyrene and 0.1 g of pT
PSm4	10 g of polystyrene, 0.1 g of PPO and 0.01 g of POPOP
PSm5	10 g of polystyrene, 0.1 g of pT and 0.01 g of Bis-MSB
PSm6	10 g of polystyrene, 1.2 g of naphthalene, 0.1 g of PPO, 0.01 g of POPOP
PSm7	10 g of polystyrene, 1.2 g of naphthalene, 0.1 g of pT, 0.01 g of Bis-MSB

Figure 1. Synthesis of PSm performed at the laboratory through the organic solvent extraction/evaporation methodology.

When both phases were mixed, microdroplets of the disperse phase (organic phase) were formed in the continuous phase (aqueous phase) and were stabilized by the presence of the polyvinlalcohol (PVA).

The dichloromethane contained within the microdroplet was extracted by the water of the continuous phase and evaporated. Once all the solvent was removed from the microdroplet, the solid microsphere was formed and precipitated (Figure 2).

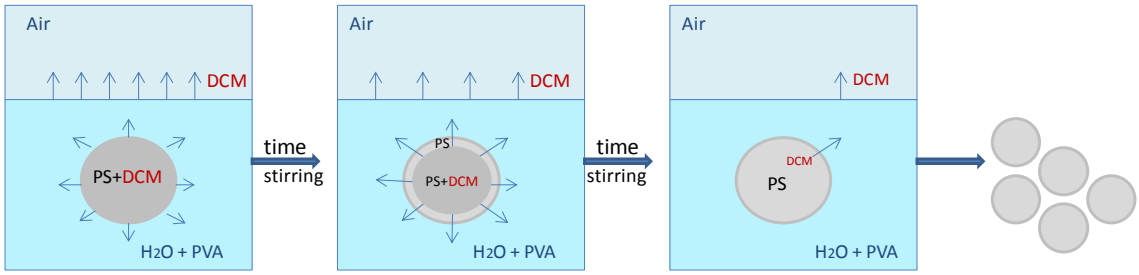

Figure 2. Graphical representation of the extraction and evaporation of the dichloromethane and the hardening of the PSm.

The addition of components within the microspheres was addressed to create PSm with the ability of transforming the energy of the decaying particles into detectable photons. Therefore, primary (2,5-diphenyloxazole (PPO) or p-terphenyl (pT)) and secondary (1,4-bis(5-phenyloxazol-2-yl) benzene (POPOP) or p-bis-(o-methylstyryl)-Benzene (bis-MSB)) fluorescent solutes were added within the solution containing the

polystyrene. Moreover, a second organic solvent (naphthalene) was added to produce a pulse delay for alpha emitters for enhancing the ability of PSm to discriminate between alpha and beta particles.

Microspheres composed only by PS (PSm1) were produced under the aforementioned conditions with a yield of about 100%. The performance of the methodology proved easy and did not present technical difficulties. A series of syntheses was carried out by varying their composition, from PSm2 to PSm7 (Table 1), while keeping the operational parameters constant in order to evaluate the influence of the PSm components on the final physical features, their radiometric capacities and to get a better understanding of the energy transfer mechanism.

The obtained PSm were spherical and showed a smooth morphology in almost all the cases, as it is shown in Figure 3, probably due to three facts:

- An optimal stirring speed applied during the formation of the emulsion and the drying of the PSm.
- A gradual extraction and evaporation of the organic solvent.
- An optimal and total hardening of the microspheres.

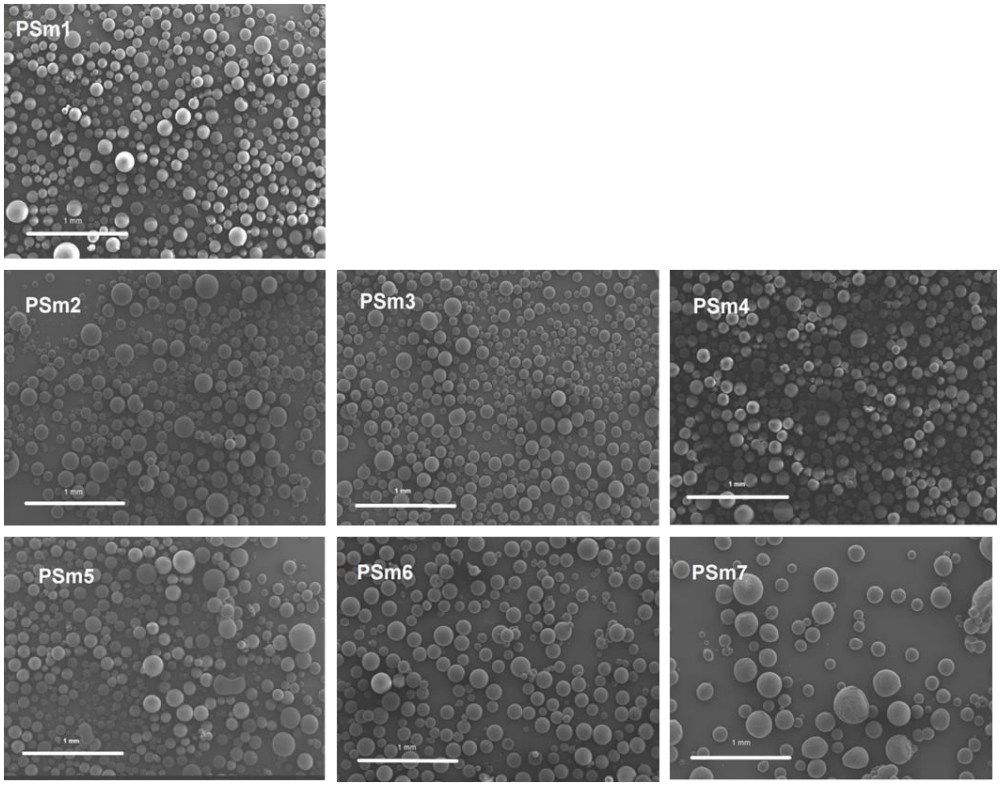

Figure 3. Scanning electron microscopy images of the synthesized PSm.

It can be said that, for the applied conditions, stable organic droplets were formed in the aqueous phase when both phases were mixed and an optimal evolution of these droplets during the continuous process of the organic solvent extraction and evaporation was achieved.

According to the boxplot in Figure 4, in general, PSm containing PPO (PSm2, PSm4 and PSm6) resulted in a smaller size, around 125 µm of median diameter and a narrower size distribution than those containing pT (PSm3, PSm5 and PSm7), which presented a slightly higher median diameter value, around 135 µm, and a wider size distribution. The encapsulation of the fluorescent solutes and the naphthalene was proved by the enhancement of the radiometric capacities in comparison with those for PSm1 (results shown in higher detail in section 4.3.1).

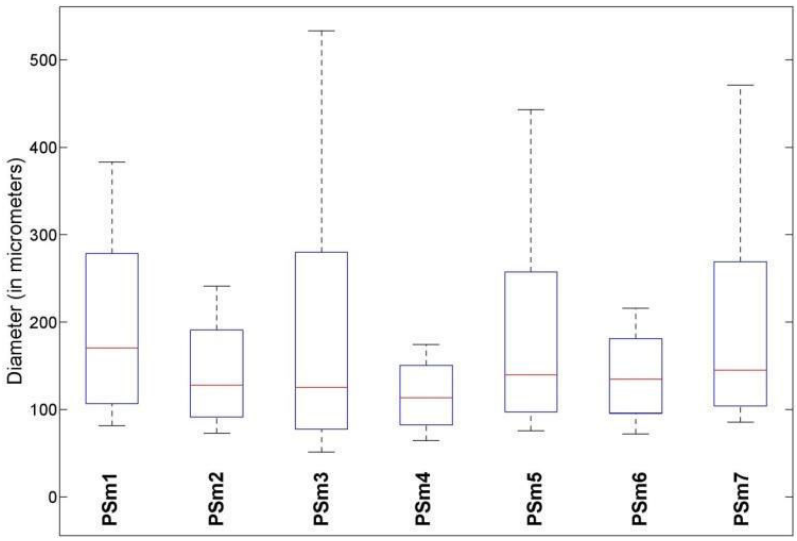

Figure 4. Boxplot of diameter size and size distribution for the synthesized PSm.

The reproducibility of the synthesis was evaluated by using the PSm obtained in three replicate syntheses of PSm6 and PSm7, before and after being homogenized. The parameters used to assess the reproducibility were: the median particle diameter, the particle size distribution and the detection efficiency when PSm were used to measure a low-energy beta emitter (i.e. ^{3}H).

The results shown in Table 2 and Figure 5 demonstrate that uncertainty associated to the ^{3}H detection efficiency decreased when homogenized PSm were employed. This is probably caused by the difference between the diameters obtained in different PSm

synthesis. This difference is reduced when the PSm from the homogeneous bulk are employed.

Table 2. Detection efficiency values and relative standard deviation of the measurement of ^{3}H with the PSm before and after their homogenization.

PSm		^{3}H Detection efficiency (%)	RSD (%)
Before homogenization	PSm6	1.03(3)	3.2
	PSm7	0.75(7)	9.7
After homogenization	PSm6	1.02(2)	1.5
	PSm7	0.82(1)	1.1

(A) (B)

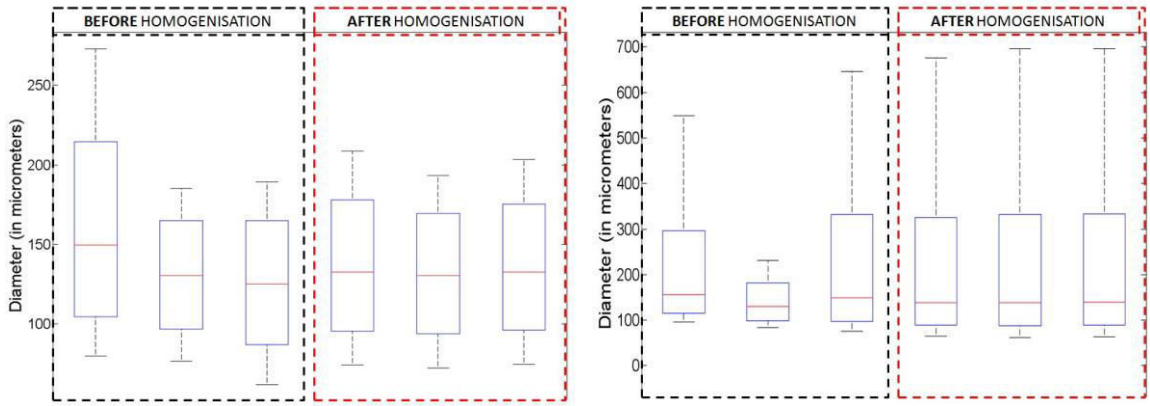

Figure 5. Boxplot of the particle size distribution of PSm6 and PSm7 before and after their homogenization: (A) PSm6 and (B) PSm7.

The obtained results suggest that there is certain variability in the synthesis process and that PSm should be homogenized before their use.

4.1.2. Synthesis of PSm adding naphthalene in their composition through the organic solvent extraction/evaporation methodology.

With the aim of evaluating the alpha/beta discrimination capacities of the PSm, two series of PSm composed of polystyrene/PPO/POPOP and polystyrene/pT/bis-MSB were synthesized, following the aforementioned procedure, and adding increasing concentrations of naphthalene to the organic phase (Table 3), since naphthalene has been widely described as a pulse length delayer [Rodríguez-Barquero y Grau-Carles, 1998].

Table 3. Amount of naphthalene added in each synthesis.

	Naphthalene (g)							
Synthesis	PSm1_n	PSm2_n	PSm3_n	PSm4_n	PSm5_n	PSm6_n	PSm7_n	PSm8_n
PPO/POPOP	0	0.6	0.8	1.2	2.0	2.5	3.0	-
pT/bis-MSB	0	0.01	0.05	0.1	0.3	0.5	0.8	1.2

The PSm size and morphology were similar in almost all cases, except when the amount of naphthalene in the PSm containing PPO/POPOP was higher than 2 g, in which flattened microspheres were obtained, probably due to a slow extraction of the organic solvent and to the collisions with other microspheres during the stirring/hardening process. The PSm which contained PPO/POPOP showed a slight increase in size when the concentration of naphthalene was increased and their mean diameter ranged between 100 and 160 µm (Figure 6a). On the other hand, the PSm containing pT/bis-MSB did not show a correlation with the naphthalene concentration and presented a median diameter around 150 µm with a lower dispersion (Figure 6b).

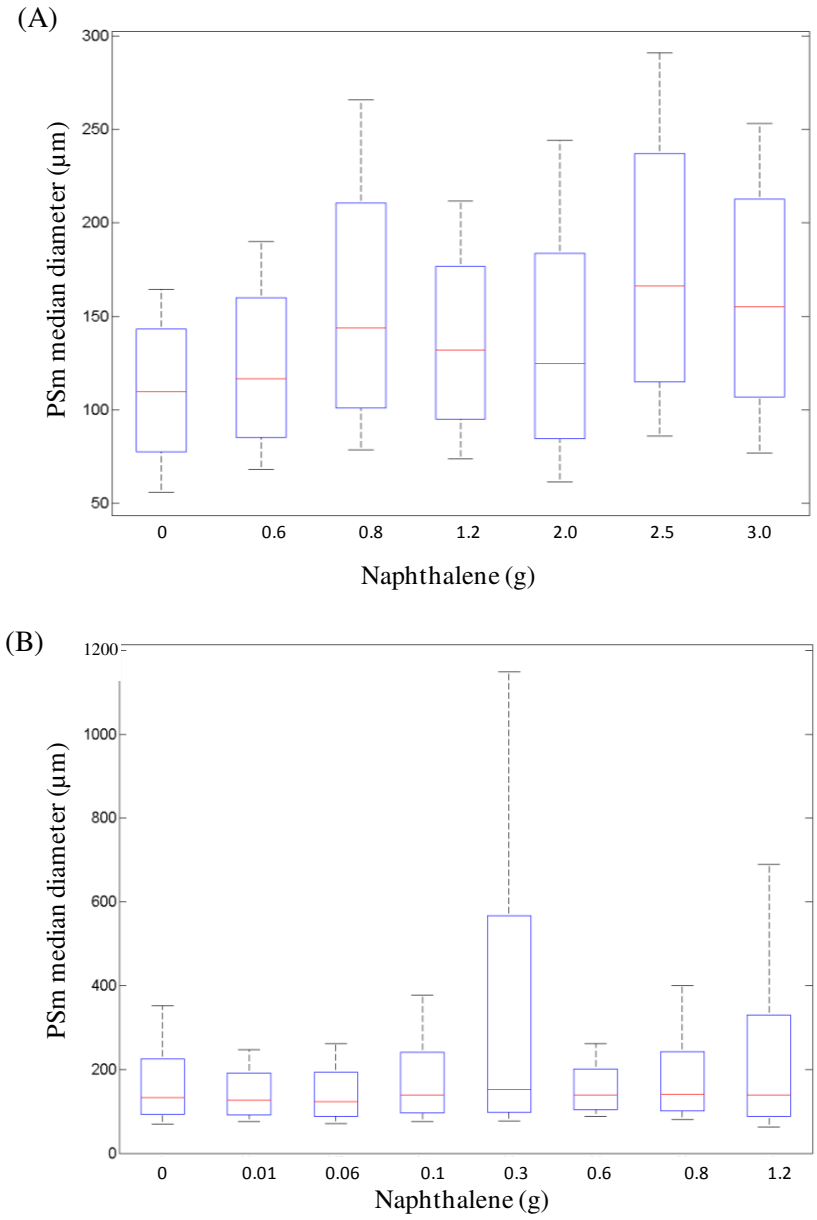

Figure 6. Boxplot of the PSm diameter: (A) PSm containing polystyrene/PPO/POPOP and naphthalene; (B) PSm containing polystyrene/pT/bis-MSB and naphthalene.

4.1.3. Evaluation of parameters in the production of PSm by the organic solvent extraction/evaporation methodology.

Once the methodology has been implemented and proved valid to produce PSm with a high yield, some operational (i.e. temperature and stirring speed) and formulation parameters (i.e. polymer concentration, organic/aqueous phase ratio and surfactant

concentration) were varied in order to determine their effect on the physical features of the resulting PSm (i.e. morphology, size, size distribution, shape and yield) (Table 4).

Table 4. Different conditions employed for the production of PSm.

Synthesis	PS (g)	DCM (mL)	Temperature (ºC)	O/W	PVA(%)	Stirring speed(Hz)
PSm01_p	10	100	20	1:20	1	16.7
PSm02_p	10	100	20	1:20	1	8.3
PSm03_p	10	100	20	1:20	1	13.3
PSm04_p	10	100	20	1:20	2	16.7
PSm05_p	10	100	20	1:20	5	13.3
PSm06_p	10	200	20	2:20	1	16.6
PSm07_p	10	400	20	4:20	1	13.3
PSm08_p	20	200	20	2:20	1	16.6
PSm09_p	40	400	20	4:20	1	13.3
PSm10_p	10	100	35	1:20	1	16.7
PSm11_p	10	100	50	1:20	1	16.7
PSm12_p*	10	100	20	1:20	1	16.7
PSm13_p	30	300	20	3:20	6	11.7
PSm14_p	30	600	20	6:20	6	11.7
PSm15_p	25	250	20	2.5:20	1	10

* DIN was used instead of naphthalene.

In all cases, syntheses were performed by triplicate and PSm1 was taken as a reference synthesis to which other syntheses were compared with. Table 5 shows also the median diameter and standard deviation of the different synthesis classifying them by parameters. Size distribution is represented in Figure 7.

Table 5. Median diameter of PSm produced under different operational and formulation parameters

Parameter	Condition	Synthesis name	Median dia. (STD) (µm)
Stirring speed (Hz)	16.67	PSm01_p*	84(26)
	8.33	PSm02_p	85(26)
	13.33	PSm03_p	79(26)
PVA (%)	2	PSm04_p	71(24)
	5	PSm05_p	51(21)
DCM (mL)	200	PSm06_p	40(13)
	400	PSm07_p	22(9)
Organic/aqueous ratio	2:20	PSm08_p	68(24)
	4:20	PSm09_p	57(24)
Temperature	35	PSm10_p	145(62)
	50	PSm11_p	-
Composition	DIN	PSm12_p	83(28)
Combined procedures	-	PSm13_p	32(12)
		PSm14_p	17(8)
		PSm15_p	67(21)

* Synthesis conditions are taken as a reference for the rest.

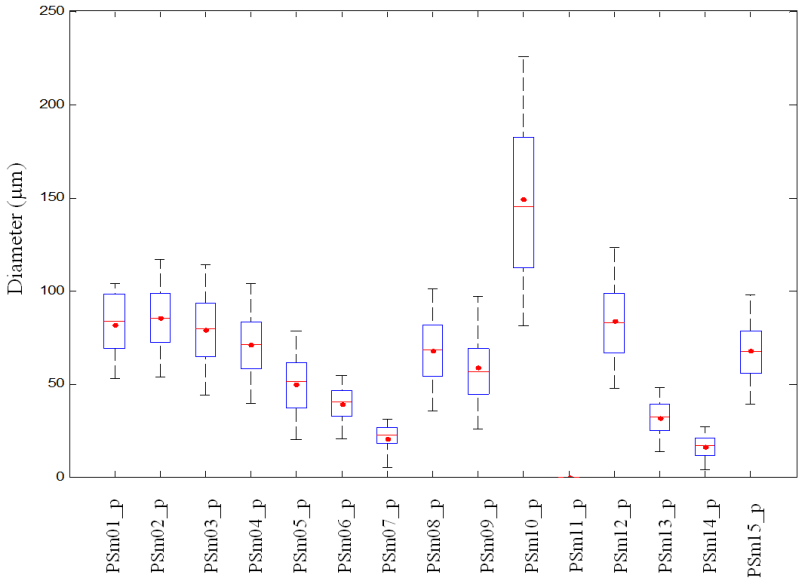

Figure 7. Size distribution of the PSm produced under different operational and formulation conditions

The main remarks about the influence of each parameter in the physical features of the obtained PSm are detailed as follows:

- **Effect of the polymer concentration (PSm01_p, PSm06_p and PSm07_p)**

PSm size diminished when the polystyrene concentration decreased due to the lower availability of polymer within the microdroplets and also, because a decrease in the organic phase viscosity causes an easier droplet break up, therefore enhancing the stirring efficiency (Figure 8).

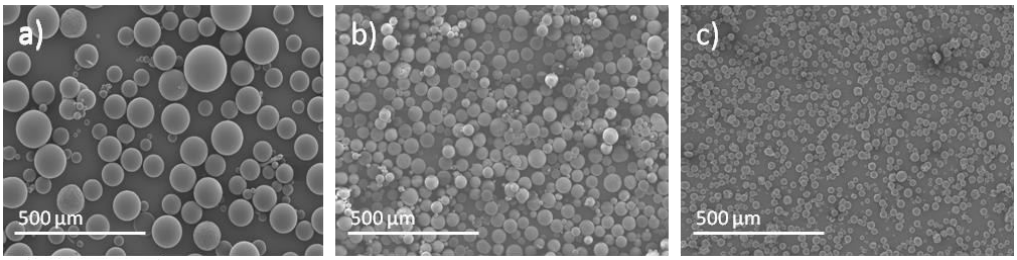

Figure 8. PSm synthesized at different PS concentrations: (A) PSm01_p, 10% (w/v); (B) PSm06_p, 5% (w/v) and (C) PSm07_p, 2.5% (w/v).

- **Effect of the PVA concentration (PSm01_p, PSm04_p, PSm05_p).**

PSm size decreased when the surfactant concentration was increased (Figure 7 and 9). According to Heiskanen et al., 2012 and Lee, 2003 the surfactant decreases the interfacial tension resulting in a decrease of the coalescence between droplets, since there is an increased film drainage time between the approaching droplets. Another reason of the decreasing of the microspheres size could be attributed to the decrease of the mass transfer rate produced between the dispersed and continuous phases by the action of the surfactant. It is worth to remark that 1% (w/v) PVA was enough to shield the microdroplets surface and to maintain the stability of the emulsion.

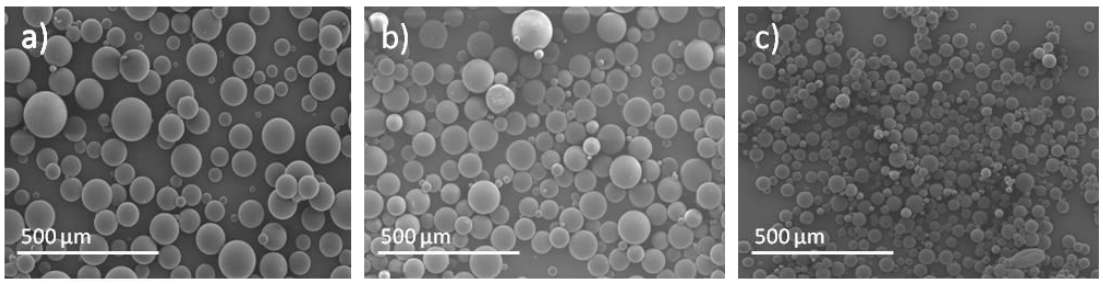

Figure 9. PSm synthesized at different PVA concentrations: (A) PSm01_p, 1% (w/v); (B) PSm04_p, 2% (w/v); and (C) PSm05_p, 5% (w/v).

- **Effect of the temperature (PSm01_p, PSm10_p, PSm11_p).**

PSm size and size distribution increased (Figure 7 and 10) when higher temperatures were employed. At higher temperatures the saturation of the aqueous phase and the evaporation of the solvent which escapes from the microdroplets at the very first minutes are faster, thus causing a faster precipitation and resulting in porous particles with larger mean sizes.

At lower temperatures, PSm hardened slowly and were influenced by the shear forces produced by stirring, since there is a time gap between the initial microsphere and the hardened microsphere (with a reduction of size estimated around 30% of the total initial droplet size).

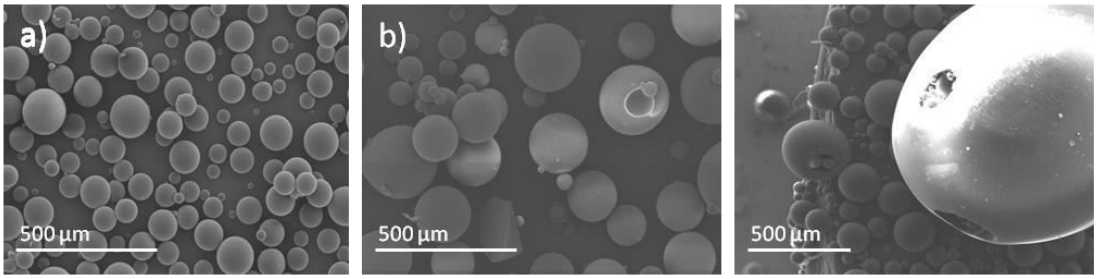

Figure 10. PSm synthesized at different temperatures: (A) PSm01_P, 20ºC; (B) PSm10_p, 35ºC and (C) PSm11_p, 50ºC.

- **Effect of the organic/aqueous phase ratio (PSm01_p, PSm08_p, PSm09_p).**

PSm diameters slightly decreased when the organic/aqueous phase ratio increased (Figure 7 and 11). It was expected that PSm increased the diameter size when the ratio increased, since the efficiency of stirring becomes lower when the solution is more viscous. However, the PVA concentration of 1% (w/v) was high enough to produce stable microdroplets even when the ratio was increased four times; demonstrating that excess of surfactant exerts a higher influence on the PSm formation. Also comparing these results with the microspheres obtained in PSm06 and PSm07, the increase in the amount of polymer result in an increase of the PSm diameter.

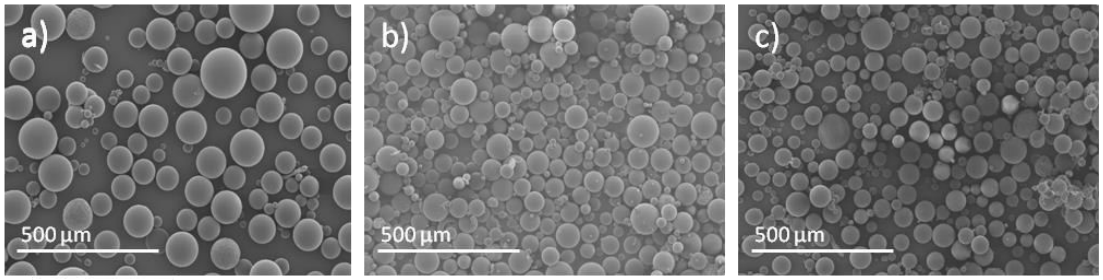

Figure 11. PSm synthesized at different organic/aqueous phase ratios: (A) PSm01_p, 100 mL/2000 mL; (B) PSm08_p, 200 mL/2000 mL and (C) PSm09_p, 400 mL/2000mL.

- **Effect of the stirring speed (PSm01_p, PSm02_p, PSm03_p)**

The PSm diameter did not show significant changes when the stirring speed was increased, since the median diameter of the three syntheses was very similar (Figure 7 and 12). This was mainly attributed to the fact that at this density, the variation of the conditions due to the stirring speed was not significant.

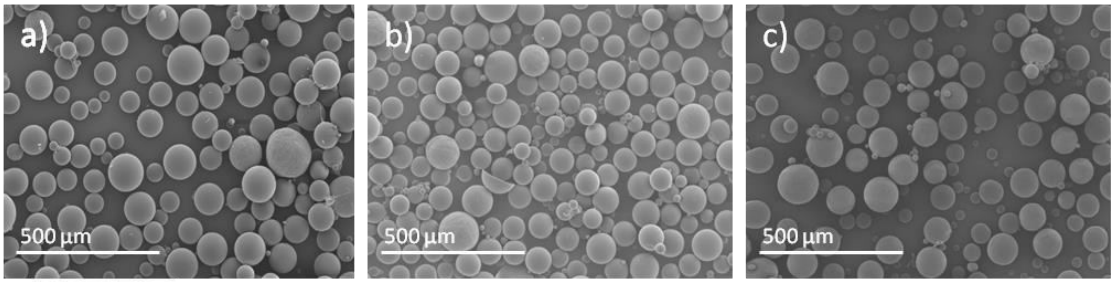

Figure 12. PSm synthesized with different stirring speeds: (A) PSm01_p, 16.7 Hz; (B) PSm02_p, 13.3 Hz and (C) PSm03_p, 8.3 Hz.

As a conclusion, it can be said that the temperature, the polymer and the surfactant concentration were the parameters which presented the biggest influence in the PSm median diameter and particle size distribution. On the other hand, the organic/aqueous phase ratio and stirring speed parameters did not have a significant impact.

- **Combined procedures (PSm13_p, PSm14_p, PSm15_p).**

Taking into account the results obtained in the syntheses performed and the skills developed for handling the methodology, three combined procedure syntheses were performed in order to study the potential synergies between parameters and to obtain a higher amount of PSm of the desired diameter per batch. In Figure 13, the SEM images of the three syntheses are shown.

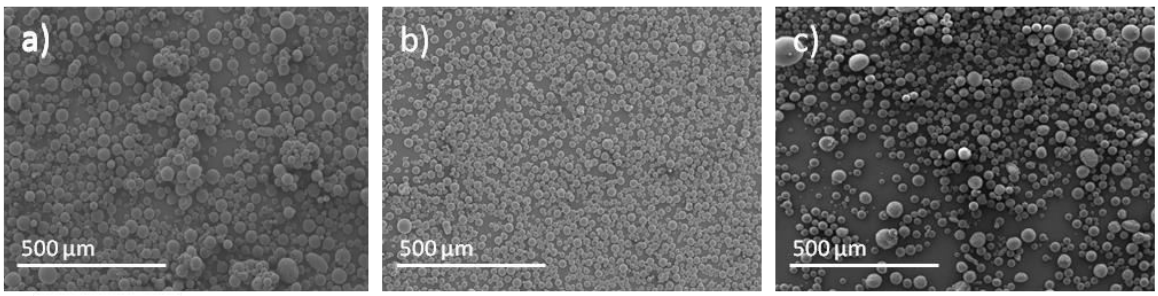

Figure 13. PSm synthesized with different combined procedures: (A) PSm13_p, (B) PSm14_p and (C) PSm15_p.

Optimized conditions were able to produce 40 g of PSm per synthesis with a yield of 100%. In all cases, a decrease of the median diameter of the PSm was also observed. This fact opened the possibility to explore the production of PSm at commercial scale using the organic solvent extraction/evaporation methodology with potential acceptable cost by the market.

- **Replacement of naphthalene by DIN (PSm12_p)**

Finally, in the optimization process of the synthesis procedure, the naphthalene was replaced by 2,6-diisopropylnapththalene (DIN) in order to enhance the PSm formulation by diminishing the toxicity of the microspheres without losing the alpha/beta discrimination capacities. The PSm morphology and size diameters were very similar to the corresponding PSm containing naphthalene (PSm01), as can be observed in the SEM images of Figure 14.

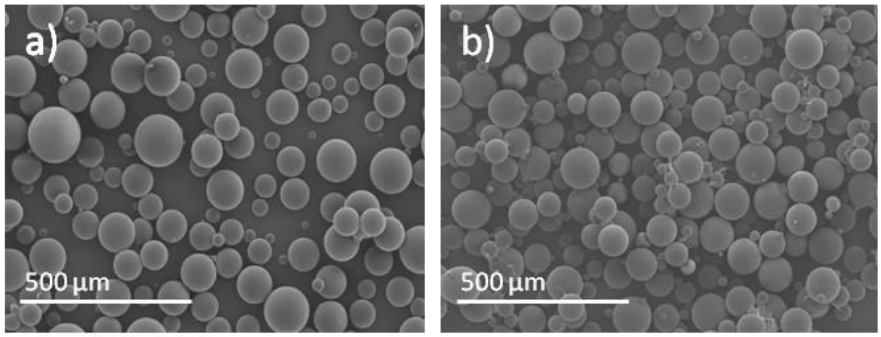

Figure 14. PSm synthesized using: (A) PSm01_p, naphthalene; (B) PSm12_p, DIN.

4.2. PRODUCTION OF PSm TRHOUGH METHODS BASED ON AUTOMATIC DRYING TECHNIQUES.

Although the organic solvent extraction/evaporation methodology has been successfully employed for obtaining polymeric microspheres at the laboratory scale, other aspects like mass scale extension, automation of the process, degree of residual solvent within the polymeric particle and production cost should be kept in mind when the production is aimed to be increased from grams to kilograms.

For this reason, two techniques based on the drying of the organic solution containing the polystyrene and the fluorescent solutes were employed to produce plastic scintillation particles. Both are potentially scalable to industrial production and based on automated equipment which are commercially available or can be rented. In both cases the organic solvent contained in the nebulized droplet was extracted by a solvent contained in the vessel (in gaseous or supercritical state), allowing the coprecipitation of the scintillating particles.

The techniques were the supercritical anti-solvent methodology (SAS) and the Spray Drying methodology (SD). SAS was performed at the laboratory M2P2 of the Aix-Marseille Universitè (Aix-Marseille – France) and SD was carried out at the facilities of the research and development department of the pharmaceutical company Esteve Q using a Mobile Minor closed cycle (Figure 15).

Figure 15. Equipment employed for the micronisation of PSm: (A) Supercritical Fluids; (B) Closed cycle Mobile Minor ™.

Apart from the objective of evaluating the mass scale production of PSm, the performed research also represented a challenging and innovative work since the micronisation of polystyrene using the drying methodologies has not been widely studied nor evaluated until the present.

4.2.1. Evaluation of the Supercritical Anti-Solvent methodology for producing polystyrene based sub-micron particles.

The Supercritical Anti-Solvent technique employed CO_2 as anti-solvent and ethyl acetate as organic solvent to dissolve the polystyrene and the fluorescent solutes. This represented an advantage with regard to the methodology of organic solvent extraction/evaporation since CO_2 and ethyl acetate are less toxic compounds than dichloromethane.

The coprecipitation of the polystyrene initially consisted in feeding the vessel with the anti-solvent CO_2 to set the optimal pressure and temperature conditions. It was followed by the injection of the organic solvent and anti-solvent in a co-current

configuration to reach the steady state. At this point, the organic solvent was replaced by the organic solution and the coprecipitation process took place. Finally, the vessel was washed with CO_2 to remove any remaining organic solvent from the product and the micronized product was recovered from the filter frit (Figure 16).

Figure 16. Polystyrene based submicron particles obtained by the SAS.

The coprecitipation of the polystyrene and the fluorescent solutes was carried out while varying different process parameters, among them the solute concentration (polystyrene), the injection velocity of the organic solution, the molar ratio of the organic solvent regarding to CO_2 and the capillary diameter (Table 6). Furthermore, regarding the formulation of the particles, the evaluation was divided into three main stages:

- Micronisation of polystyrene at two different solute concentrations.
- Micronisation of polystyrene together with PPO/POPOP and DIN at different operational parameters.
- Micronisation of particles with different compositions: polystyrene, polystyrene/PPO, polystyrene/PPO/POPOP and polystyrene/PPO/POPOP/DIN, while keeping the operational parameters constant and modifying the formulation to confirm the encapsulation of the components and their influence in the final particle characteristics.

Table 6. Experimental conditions of PSm micronisation through SAS.

Particles	Composition	Mass of solutes injected (g)	W (wt %)	X_{EtAc} (%)	u (m s^{-1})	Capillary (µm)	Qm CO_2 (g min^{-1})	Qv EtAc (mL min^{-1})
Polystyrene precipitation								
SAS-P1	PS	1	0.3	4.5	4	127	30	3
SAS-P2	PS	1	**1.2**	4.5	4	127	30	3
Polystyrene/PPO/POPOP/DIN coprecipitation								
SAS-P3	PS/PPO/POPOP/DIN	1	0.3	4.5	4	127	30	3
SAS-P4	PS/PPO/POPOP/DIN	1	0.3	**9**	4	127	15	3
SAS-P5	PS/PPO/POPOP/DIN	1	0.3	4.5	1	**254**	30	3
SAS-P6	PS/PPO/POPOP/DIN	1	0.3	**9**	1	**254**	15	3
SAS-P7	PS/PPO/POPOP/DIN	1	0.3	4.5	**1**	**127**	7.6	0.8
Polystyrene/PPO/POPOP/DIN coprecipitation for radioactivity measurements								
SAS-P8	PS	**10**	1.2	4.5	4	127	30	3
SAS-P9	PS**/PPO**	**10**	1.2	4.5	4	127	30	3
SAS-P10	PS/PPO**/POPOP**	**10**	1.2	4.5	4	127	30	3
SAS-P11	PS/PPO/POPOP**/DIN**	**10**	1.2	4.5	4	127	30	3

W solute (solute mass fraction, %); X (molar ratio solvent/CO_2, %); u (organic solution velocity, m s^{-1}; Qm CO_2 (mass flow are of CO_2, mL min^{-1}); Qv solvent (volumic flow rate of the organic solution, mL min^{-1})

In all cases, the micronisation of polystyrene particles was achieved with a yield of about 90%. The particles were highly electrostatic and a total recovery was difficult. The diameter of single particles was below 1 µm and for that reason they were classified as submicron particles.

In general, morphology, particle size and populations were similar for all the PSm micronised with different compositions, thus ensuring a reproducible production. SAS methodology allowed the production of sub-micron scintillation particles by successfully replacing the dichloromethane with the ethyl acetate.

Residual organic solvent amounts within the particles were determined using Headspace Gas Chromatography coupled with Mass Spectrometry. Values were ranged between 550 and 1250 µg g^{-1} and were considered below the accepted limit for pharmaceutical purposes (5000 µg g^{-1}) according to the European Medicine Agency [European Medicine Agency, 2009].

Polystyrene particles were produced at two concentrations (0.3 and 1.2 % (w/v), SAS-P1 and SAS-P2, respectively). In both cases, two particle populations were obtained. The first one was composed of particles ranging between 150-400 nm and the second one was formed by fused or coalesced particles (Figure 17). This was probably due to the presence of different local supersaturations in the autoclave during the mixing of the organic solution containing the polymer and the supercritical phase as well as the plasticization of polystyrene caused by CO_2, producing changes in the mechanical and thermal properties of the polymer such as a decrease in the temperatures at which deformations can be produced.

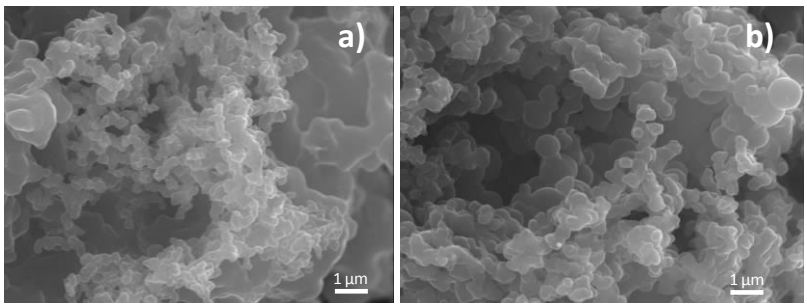

Figure 17. Polystyrene particles obtained by the SAS process while varying the polystyrene concentration in the organic solution of (A) 0.3 % (w/v) (SAS-P1) and (B) 1.2 % (w/v) (SAS-P2).

Hydrodynamic conditions were evaluated by decreasing the organic solution injection velocity from 4 to 1 m s^{-1} (SAS-P3 and SAS-P7, respectively), while the rest of parameters remained constant. Higher injection velocity resulted in nearly spherical particles sized around 200 nm and distributed in two populations, whereas scintillating particles produced at the lowest injection velocity showed only one population and homogeneous morphology. This fact was probably attributed to the flow regime of the organic phase. It was behaving as a laminar flow, which caused less favorable mixing conditions and produced high local supersaturations in the dispersion phase and therefore producing smaller particles.

With regard to the increase of the capillary diameter (SAS-P5 and SAS-P6) and the solution/CO_2 molar ratio (SAS-P3 and SAS-P4), it can be observed (Figure 18) that in both cases, two populations were still obtained but the number of agglomerates increased when the capillary diameter increased. This could be due to the low mass transfer caused by the increase of the volume of the jet and the decrease of available solvent.

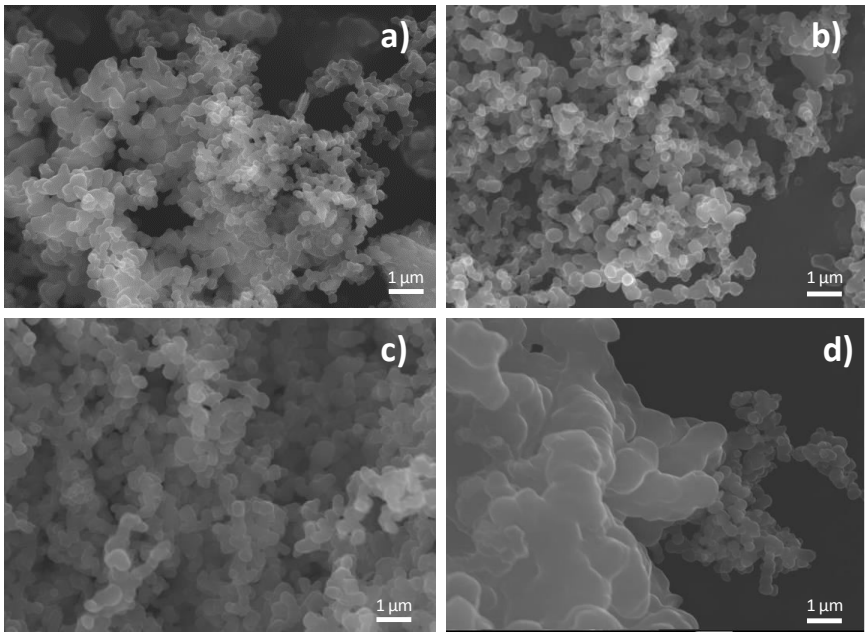

Figure 18. Influence of the solvent/CO_2 molar ratio X_{EtAa} (%) and the capillary diameter (d_c): (A) d_c =127 µm, u=4 m s^{-1} X_{EtAc} = 4,5% (SAS-P3); (B) d_c =127 µm, u=4 m s^{-1}, X_{EtAc} = 9% (SAS-P4); (C) d_c=254 µm, u=1 m s^{-1}, X_{EtAc} = 4,5% (SAS-P5); (D) d_c=254 µm, u=1 m s^{-1}, X_{EtAc} =9 % (SAS-P6).

Micronised particles were able to encapsulate the components, as it will be described in detail in chapter 4.3.3 dealing with the radioactivity measurements. However, the production cost of the SAS technique for micronising polystyrene is high and limits its application to routine production of PSm.

4.2.2. From laboratory to commercial scale PSm production: Spray Drying methodology.

The Spray Drying methodology, employing a closed cycle Gea Niro Mobile Minor™ was used for the coprecipitation of polystyrene together with the fluorescent solutes (PPO and POPOP) dissolved in an organic solvent. Due to its size equipment, allows the micronisation in the range of kg per hour for several materials.

In a typical procedure, the system is preconditioned by injecting the solvent. During the injection process the solvent (or the feed) is mixed with the gas (nitrogen) and nebulized by the nozzle at a determined flow rate and nozzle mass flow rate. The feed is sprayed through the nozzle to form droplets, which entered in contact with the nitrogen gas contained in the chamber, which is at a determined temperature and flowing in the opposite direction than the feed, therefore causing the evaporation of the organic solvent (which contains the polymer) and hence the coprecipitacion of the particles.

The feasibility to micronise the polymer was evaluated and the operational and formulation parameters were varied to explore the optimal conditions for obtaining PSm with the largest yield and the optimum size and shape. The feed flow rate, nozzle mass flow rate, concentration of the polymer in the organic solution (feed concentration) and the organic solvent employed to dissolve the polymer and fluorescent solutes were studied. The nozzle mass flow rate was selected according to the pressure of N_2 (drying gas) and the degree of splitting (%) in the nozzle.

Two different organic solvents were employed: dichloromethane and toluene. The inlet and outlet temperature was varied according to the organic solvent, and were adjusted to obtain an outlet temperature higher than the boiling point of the organic solvent ensuring its drying.

- **Micronisation of plastic scintillation particles using dichloromethane**

The operational parameters employed for the polystyrene micronisation using dichloromethane as organic solvent are given in Table 7. The value of the feed concentration was ranged between 1 and 9% (w/w) of polystyrene, the feed flow rate varied between 1 and 6 kg h^{-1} and the nozzle mass flow rate from 1 to 3 with a degree of splitting between 15% and 60%. The inlet temperature was adjusted to obtain an outlet temperature between 30 and 35ºC and the temperature of N_2 in the nozzle was fixed at 20ºC. Results in term of yield, shape and median diameter in the cases when particles were obtained are shown in Table 8.

Table 7. Established conditions for the micronisations performed with dichloromethane.

Test	Feed Concentration (%)	Feed Flow Rate (kg h^{-1})	Nozzle Mass Flow Rate (bar and %)
SD_DCM_1	3	6	3 (60 %)
SD_DCM_2	3	3	1 (40 %)
SD_DCM_3	9	3	1 (40 %)
SD_DCM_4	3	1	1 (20 %)
SD_DCM_5	1	1	1 (20 %)
SD_DCM_6	2	1	1 (20 %)
SD_DCM_7	1	2	1 (20 %)
SD_DCM_8	1	2	1 (15 %)
SD_DCM_9	1	2	1 (60 %)
SD_DCM_10	3	2	1 (60 %)
SD_DCM_11	3	2	2 (60 %)
SD_DCM_12	2	2	2 (60 %)
SD_DCM_13	2	3	2 (60 %)
SD_DCM_14	2	3	2 (40 %)

Table 8. Results obtained in the micronisation of polystyrene using dichloromethane

Test*	Shape	Yield (%)	Median Particle Size (µm)
SD_DCM_2	Particles	--	25
SD_DCM_5	Particles	54	12
SD_DCM_6	Particles/Threads	72	17
SD_DCM_7	Particles	44	16
SD_DCM_9	Particles	28	7

*Experiments with very low yield are not shown

For the first micronisations (SD_DCM_1, SD_DCM_2 and SD_DCM_3), mild operational conditions in comparison with those described in the literature, were employed. Microspheres, deflated microspheres, threads and flakes were obtained with some degree of agglomeration (Figure 19). The formation of threads could be attributed to the fast evaporation of the organic solvent and the inability to create single droplets from the feed.

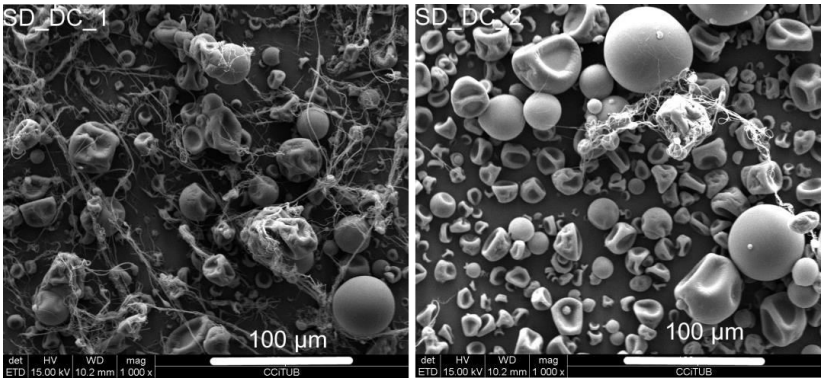

Figure 19. Micronisations performed using a feed concentration of 3% (w/w): (A) feed flow rate 6 Kg h^{-1} and nozzle mass flow rate 3 bar (60%) for SD_DCM_1; (B) feed flow rate 3 Kg h^{-1} and nozzle mass flow rate 1 bar (40%) for SD_DCM_2.

Despite choosing operational conditions that were considered mild, they were still not soft enough, and as a consequence the morphology was not optimum. Thus, other experiments were performed by adjusting the parameters to even more moderated values. Therefore, lower feed concentrations, flow feed and nozzle mass flow rates were employed (SC_DCM_4). Still, long aggregates were produced, probably due to the inefficient formation of droplets before the solvent was extracted.

When decreasing the polystyrene concentration to 1% (w/w) and the nozzle mass flow rate to 1 bar (20%), SD_DCM_5, deflated particles were obtained, probably due to the fast hardening of the microsphere before the organic solvent was completely removed producing a collapse of the microsphere surface. Changes in the conditions (SD_DCM_6, SD_DCM_7, SD_DCM_8 and SD_DCM_9) did not lead to the improvement of the shape, but resulted in threads, deflated microspheres, etc. It can be seen that in the cases in which polymeric particles are obtained (SD_DCM_5, SD_DCM_9) the increase of the mass flow rate and feed flow rate led to a decrease of the particle size (Figure 20).

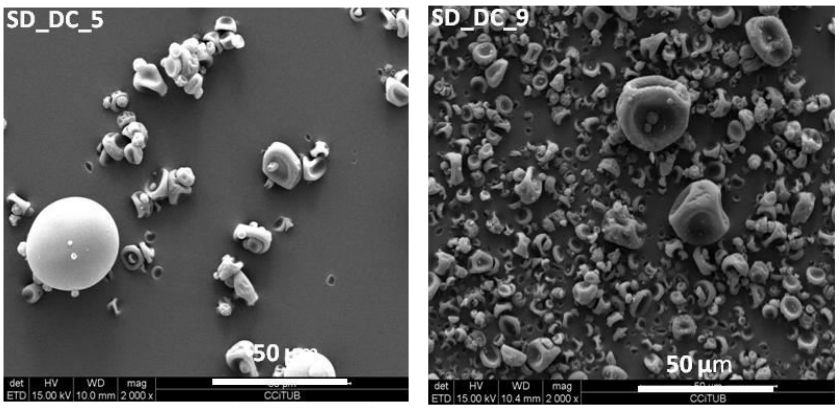

Figure 20. SEM images of the products obtained in the experiments SD_DC_5 and SD_DC_9

A series of micronisations (from SD_DCM_10 to SD_DCM_14) was performed by increasing the values of the feed concentrations, feed flow rate and nozzle mass flow rate parameters, but especially the last one, since the increase of the amount of material to be dried can be balanced by a fast formation of droplets from the feed before the

solvent is removed. However, for all these conditions, the precipitated particles were threads, microparticles and deflated microspheres, as it is shown in Figure 21.

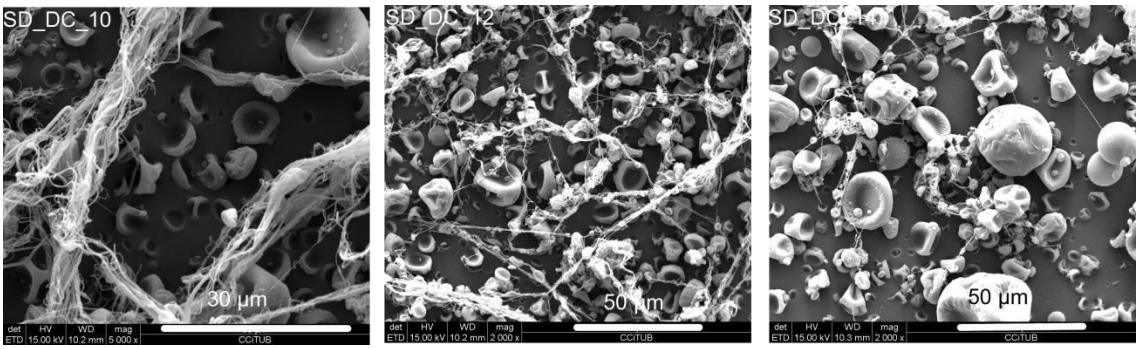

Figure 21. SEM image of the microparticles obtained in tests SD_DC_10, SD_DC_12 and SD_DC_14.

The use of dichloromethane allowed obtaining polymeric particles from few to about 30 µm with a yield of about 50% and a production rate of 20 g per hour. The particles were mainly threads and deflated microspheres. The production of large amounts of PSm was not possible due to the low boiling point of the dichloromethane.

- **Micronisation of plastic scintillation particles using toluene**

Toluene was employed instead of dichloromethane since its boiling point is higher (110.6 ºC) and because of its ability to dissolve polystyrene. The parameters were fixed employing feed concentrations from 2 to 5% (w/w), feed flow rates from 1 to 7 kg h^{-1} and a nozzle mass flow rate of 3 bar by varying the degree of splitting from 20 to 60%. The inlet temperature was adjusted to ensure an outlet temperature of about 80-85ºC and the temperature of N_2 in the nozzle was 50ºC (Table 9). The results in term of shape, yield and median diameter are shown in Table 10.

Table 9. Conditions employed for the micronisation of PSm using toluene

Test	Feed Concentration (%)	Feed Flow Rate (kg h^{-1})	Nozzle Mass Flow Rate (bar and %)
SD_TO_15	2	1	3 (60 %)
SD_TO_16	5	1	3 (60 %)
SD_TO_17	2	2	3 (60 %)
SD_TO_18	3	2	3 (60 %)
SD_TO_19	2	2	3 (20 %)
SD_TO_20	2	3	3 (60 %)
SD_TO_21	2	3	3 (20 %)
SD_TO_22	2	4	3 (20 %)
SD_TO_23	2	5	3 (20 %)
SD_TO_24	2	5	3 (40 %)
SD_TO_25	2	5	3 (25 %)
SD_TO_26	2	2	3 (25 %)
SD_TO_27	2	2	3 (40 %)
SD_TO_28	2	6	3 (25 %)
SD_TO_29	2	7	3 (40 %)
SD_TO_30	3	5	3 (25 %)
SD_TO_31	3	6	3 (25 %)

Table 10. Results of the micronisations performed using toluene.

Test	Shape*	Yield (%)	Median Particle Size (µm)
SD_TO_15	Particles	18	4
SD_TO_17	Particles/Threads	50	5
SD_TO_19	Particles	55	11
SD_TO_20	Particles	6	4
SD_TO_21	Particles/Threads	74	9
SD_TO_22	Particles	80	11
SD_TO_23	Particles	56	12
SD_TO_24	Particles	26	9
SD_TO_25	Particles	65	10
SD_TO_26	Particles	54	10
SD_TO_27	Particles/Threads	43	9
SD_TO_28	Particles	28	11

Toluene showed an enhancement of the results of the micronisation from the very first experiments (SD_TO_15), since spherical particles were obtained, thus demonstrating that droplet formation and drying by solvent evaporation is possible (Figure 22). Although the shape of the particles was improved in comparison with the micronisations employing dichloromethane, the median diameter was considered too small and the yield of production not high enough (it was about 10 g of PSm per hour).

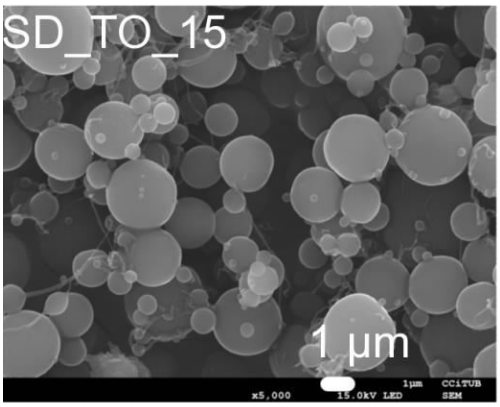

Figure 22. SEM image of the microparticles obtained in the test SD_TO_15.

At the same conditions as SD_TO_15, but increasing the feed concentration to 5% (w/w) in SD_TO_16, threads were obtained, demonstrating in that way that feed concentrations between 2-5% (w/w) are the optimal range for obtaining particles. At feed concentrations of 2% (w/w), a feed flow rate of 2 kg h^{-1} and a nozzle mass flow rate of 3 bar (60%) (SD_TO_17), microspheres of about 5 µm and some threads were obtained with a yield of about 50% (Figure 23)

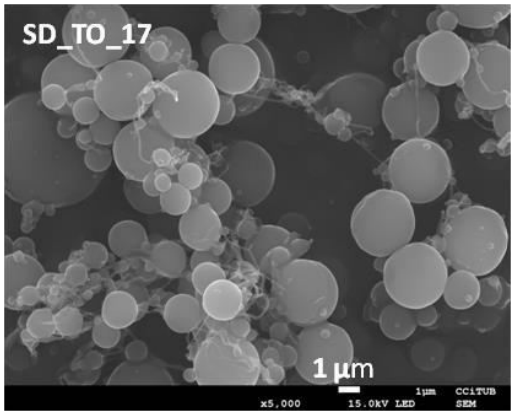

Figure 23. SEM image of the microparticles obtained in the test SD_TO_17.

Other experiments were performed by varying the parameters until finding the optimal conditions for obtaining microspheres. In SD_TO_18 a small increase of the feed concentration until 3% resulted in the formation of flakes and with a very low yield. Therefore, feed concentration of 2% was established to obtain microspheres and the feed flow rate and the nozzle mass flow rate were evaluated in a range from 2 to 7 kg h^{-1} and 3 bar (20%) to 3 bar (60%), respectively, for experiments from SD_TO_19 to

SD_TO_31. In those experiments it could be observed the delicate equilibrium between variables and its effect on the formation of particles. Thus, it was observed that an increase of the feed flow rate could be only compensated with an increase on the nozzle mass flow rate. In general, when the feed flow rate was increased, droplets were dried slowly and even in some cases (SD_TO_23) droplets were not completely dried when arriving to the wall of the chamber. On the other hand, the increase of the nozzle mass flow rate lead to the formation of small droplets and therefore to small microspheres, which in some cases were not recovered (SD_TO_24). Finally in the case of feed flow rates of 6 or 7 kg h^{-1} flakes are produced instead of microspheres (SD_TO_28).

As a conclusion, it can be said that it was possible to obtain spherical particles using toluene due to a better drying process of the droplet and because toluene seems to allow working with more flexible operational conditions than dichloromethane. The steps of droplet formation, organic solvent extraction and drying of the coprecipitated particles are more uniform for toluene, allowing to obtain particles instead of threads at certain conditions. Optimal conditions for obtaining spherical PSm of about 10-12 µm and a good recovery yield (about 50%) were those in which the feed concentration rate was 2 kg h^{-1}, the feed speed was 5 kg h^{-1} and the nozzle mass rate was 3 bar (25%) (SD_TO_25) (Figure 24). These conditions allowed a yield production rate of 300 g per day. It was also observed that varying these conditions threads could be obtained instead of microspheres

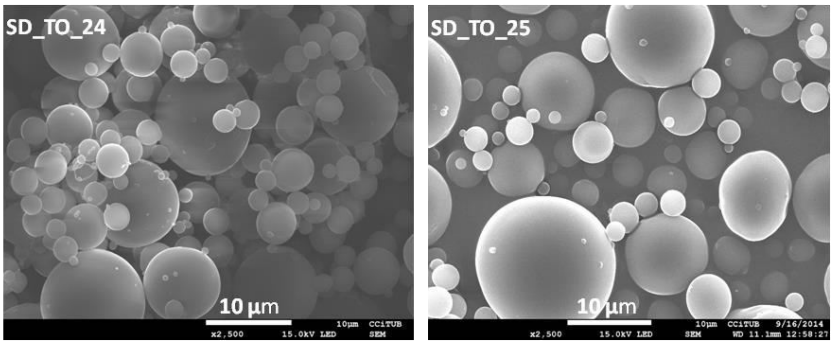

Figure 24. SEM images of the microparticles obtained with toluene at 5 kg h^{-1} and 2% (w/w): (A) SD_TO_24; (B) SD_TO_25.

Although the production of scintillating particles by Spray-Drying was possible and it was proven that the particles were able to measure alpha and beta emitters, as will

be seen later in the chapter 4.3.3, the production yield does not compensate the associated operational cost, especially due to the amount of solvent involved in the process and the cost of the equipment.

4.3. STUDY OF THE ENERGY TRANSFER MECHANISM IN THE PSm.

The energy transfer mechanism of the liquid scintillation (LS) methodology has been studied and not totally elucidated [L'Annunziata, 2013]. However, three quenching phenomena have been established when measuring with liquid scintillation cocktail (LSc): chemical quenching, ionization quenching and color quenching. On the other hand, the mechanism when PSm are employed is supposed to be similar to the liquid scintillation one, although it presents some differences. One of the clearest aspects is that PSm are solid particles and this fact causes that the decaying particle must travel some distance from the place where the disintegration occurs to the scintillator, which could be of hundreds of micrometers while in LS it could be of only a few nanometers.

Previous measurements with PSm have shown evidence that the detection efficiency and spectral position may change according to the diameter of the microsphere. This behavior could be related to two additional types of quenching: the particle quenching and the optical quenching, which should be taken into account to fully understand the mechanism of detection when using PSm for the measurement of radionuclides.

Particle quenching is defined as the process in which a decaying particle loses its energy by interacting with the molecules of the sample solution before it reaches the solid mixture of solvent and scintillators, resulting in a reduction of the detection efficiency and very small changes in the spectra distribution. On the other hand, optical quenching can be attributed to the inefficient transmission of the photons generated by the scintillator due to the change of media that photons may pass through in their way to the PMT. This can be evidenced by a decrease on the detection efficiency and a shift on the spectrum position toward lower energies.

The measurement of beta and alpha particle emitters employing the PSm obtained through the different methodologies implemented in this thesis has been useful for a

better understanding of the energy transfer mechanism in the PSm. The study has been focused on evaluating systematically:

- The effect on the radiometric capacities when fluorescent solutes and naphthalene are added within the PSm composition.
- The influence of adding naphthalene within the PSm to enhance the discrimination of alpha and beta particles.
- The effect on the radiometric capabilities when PSm of various diameters are employed for measuring different radionuclides.
- The influence of the solution composition in the radiometric capacities. The evaluated compounds were: NaCl, $BaCl_2$, glycerine, methyl orange and nitromethane.

In all cases, the detection efficiency, quenching parameter and spectra position were the parameters used to identify the presence of quenching effects.

4.3.1. Addition of fluorescent solutes and naphthalene within the PSm composition.

Values of detection efficiency and SPQ(E) obtained when measuring different radionuclides (^{3}H, ^{14}C, ^{90}Sr/^{90}Y and ^{241}Am) with the PSm obtained in 4.1.1. through the organic solvent extraction/evaporation methodology are shown in Table 11.

Table 11. Values of background, ^{3}H, ^{14}C, ^{90}Sr/^{90}Y and ^{241}Am detection efficiency and SQP(E) for the different PSm compositions

	Composition	^{3}H (%)	^{14}C (%)	^{90}Sr/^{90}Y (%)	^{241}Am (%)	SQP(E)
PSm1	PS	0.014(1)	8.6(15)	134.9(35)	52.9(11)	428(5)
PSm2	PS/PPO	0.829(26)	48.6(9)	182.4(27)	74.4(21)	732(6)
PSm3	PS/pT	0.650(12)	45.7(7)	180.3(27)	72.3(17)	694(6)
PSm4	PS/PPO/POPOP	1.185(18)	51.2(8)	180.6(27)	76.7(11)	782(5)
PSm5	PS/PPO/bis-MSB	1.135(29)	49.8(7)	178.7(27)	73.2(14)	783(4)
PSm6	PS/PPO/POPOP/ naphthalene	1.025(15)	48.7(16)	180.9(27)	74.9(29)	791(4)
PSm7	PS/PPO/POPOP/ naphthalene	0.819(12)	45.9(17)	178.1(27)	70.9(39)	790(5)

According to the obtained results, it can be seen that detection efficiency and SQP(E) values increase and the spectrum (Figure 25) shifts toward higher energy values when adding the primary (PPO or pT) fluorescent solutes, if comparing with the PSm1 which was composed only by polystyrene, thus indicating an enhancement in detection of scintillating photons. This behavior was emphasized when the secondary (POPOP or bis-MSB) fluorescent solutes were also added within the composition.

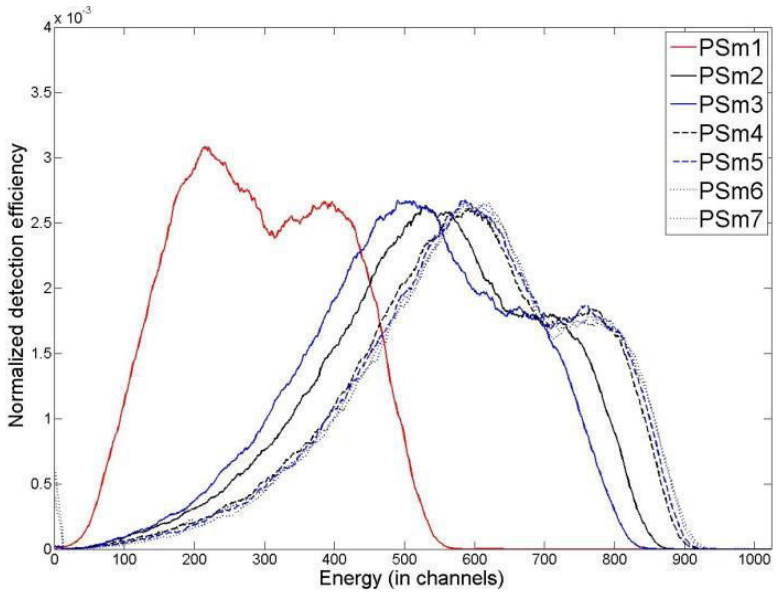

Figure 25. Normalised detection efficiency spectra obtained for $^{90}Sr/^{90}Y$ measurements with the differently synthesised PSm.

Polystyrene is able to scintillate by itself (poorly), in addition the photons are emitted at a wavelength of around 270 nm, while the more sensitive detection wavelength of the photomultiplier is around 400 nm. Therefore, the collection of photons produced by polystyrene is inefficient. A graphical representation of the emission wavelengths of the components employed in this work is represented in Figure 26. The addition of the primary fluorescent solute within the PSm composition (either PPO or pT) improved the detection of the energy deposited into the polystyrene by enhancing the emission at a higher wavelength value (maximum at 354 nm for PPO and 337 nm for pT) and producing an increase of the detected photons by the PMT, thus enhancing the radiometric capacities.

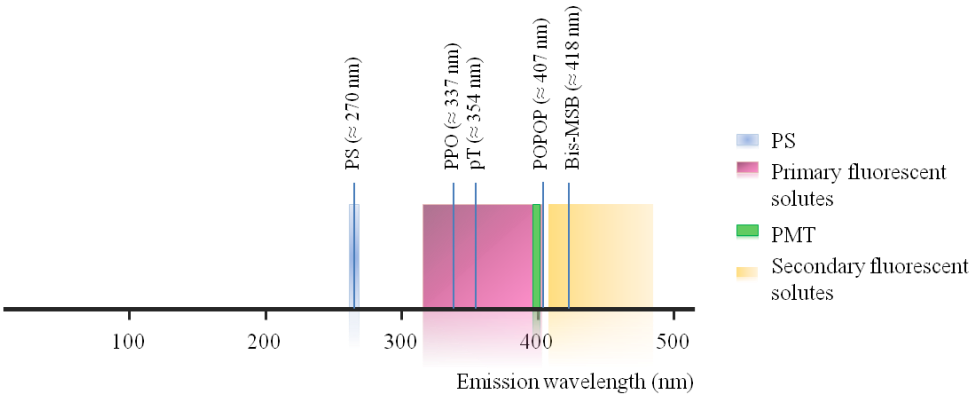

Figure 26. Emission wavelengths of the components of the PSm and the PMT.

However, in order to reach the maximum quantum efficiency of the PMT, the secondary scintillators were added since the maximum emission of POPOP and bis-MSB are at 407 nm and 418 nm, respectively. The influence of the secondary solutes was also observed by the SQP(E), resulting in higher values, and a spectrum shifted toward higher energy values. In all cases, the PPO/POPOP couple showed better results than the pT/bis-MSB one.

Finally, the addition of naphthalene within the PSm composition caused a small decrease of the detection efficiency values, SQP(E) and position of the spectra, since it introduces the addition of a new step in the energy transfer process that caused the loss of energy transferred within the scintillator.

For all the radionuclides measured, the detection efficiency kept a correlation with the energy of the measured radionuclide. Hence, low and medium energy beta emitters, ^{3}H and ^{14}C, respectively, showed lower detection efficiency values due to the difficulty of the beta emitted particle to reach the scintillating surface, by its interaction with molecules in the medium (particle quenching).

Radiometric capacities measured using the produced PSm were similar to those obtained when commercial PSm are employed [Tarancón et al., 2007] (detection efficiency values of around 0.5% for ^{3}H; 42% for ^{14}C; 186% for $^{90}Sr/^{90}Y$ and 63% for ^{241}Am). These results demonstrated that the use of organic solvent E/E methodology is valid for the production of PSm which are able to measure radioactivity.

4.3.2. Addition of naphthalene within the PSm for enhancing their alpha/beta discrimination capacities.

Liquid scintillation counting has been widely employed for the determination of mixtures of alpha and beta emitting radionuclides through alpha/beta discrimination. Since the PSm composition is similar to that of liquid scintillation cocktails, the energy transfer mechanism can be considered similar too. However, two main differences should be taken into account when comparing both scintillators in term of alpha/beta discrimination. As previous mentioned, the first, is the distance that a disintegrated particle must travel to reach the scintillating particle, while the second one, is regarding the rigid structure of the solid scintillator which may affect the relaxation process of the triplet states of the solvent, this last one is more related to the alpha/beta discrimination capacities

Radiometric capacities of the produced PSm when adding increasing amounts of naphthalene to the organic solution, which contained the polystyrene together with a couple of fluorescent solutes (PPO/POPOP or pT/bis-MSB), were determined by measuring ^{3}H, ^{14}C, $^{90}Sr/^{90}Y$ and ^{241}Am (Table 12 and 13).

According to the results, the addition of naphthalene only influenced the radiometric capacities of ^{3}H and ^{14}C. In the case of the PPO/POPOP scintillators, the detection efficiency showed a decrease with the increase of naphthalene concentration, specifically when 2.5 and 3.0 g were employed. The effect of naphthalene was more prominent for the PSm containing pT and bis-MSB when measuring ^{3}H, since naphthalene, as a secondary solvent, seems to modify the energy transfer process between the polystyrene and the pT molecules. Detection efficiency values obtained for $^{90}Sr/^{90}Y$ and ^{241}Am for both fluorescent solute couples were not influenced by the addition of naphthalene.

Table 12. Values for the background, ^{3}H, ^{14}C, $^{90}Sr/^{90}Y$, and ^{241}Am detection efficiencies and the SQP(E) for the PSm containing PPO and POPOP and increasing naphthalene concentrations.

Naphthalene (g)	BKG (cpm)	^{3}H (%)	^{14}C (%)	$^{90}Sr/^{90}Y$ (%)	^{241}Am (%)	SQP(E)
0	1.10 (5)	1.19(7)	51.2(4)	180.6(9)	76.7(6)	782(5)
0.6	1.36(8)	1.10(2)	49.6(6)	185.6(25)	76.2(9)	781(2)
0.8	0.97(15)	0.96(1)	47.3(6)	174.9(23)	72.4(9)	791(5)
1.2	1.10(13)	1.03(2)	48.7(6)	180.9(27)	74.9(29)	791(4)
2.0	1.09(16)	1.12(2)	51.1(6)	180.7(24)	77.3(9)	796(4)
2.5	1.50(18)	0.64(1)	39.9(5)	191.2(25)	74.3(9)	767(7)
3.0	1.46(18)	0.72(2)	44.0(6)	194.1(26)	64.3(9)	776(0)

Table 13. Values for the background, ^{3}H, ^{14}C, $^{90}Sr/^{90}Y$, and ^{241}Am detection efficiencies and the SQP(E) for the PSm containing pT and Bis-MSB and increasing naphthalene concentrations.

Naphthalene (g)	BKG (cpm)	^{3}H (%)	^{14}C (%)	$^{90}Sr/^{90}Y$ (%)	^{241}Am (%)	SQP(E)
0	1.16(14)	1.14(3)	49.8(3)	178.7(26)	73.2(14)	783(4)
0.01	1.18(16)	0.90(2)	48.9(6)	-	75.5(9)	781(2)
0.05	1.19(16)	0.78(1)	48.7(6)	-	76.4(9)	771(5)
0.1	1.21(16)	0.74(1)	46.4(6)	187.8(25)	72.6(9)	747(9)
0.3	1.09(16)	0.77(11)	45.9(6)	178.7(24)	72.8(9)	761(2)
0.6	0.89(14)	0.79(12)	44.4(6)	181.6(24)	70.9(9)	791(9)
0.8	0.81(13)	0.75(1)	45.3(6)	182.8(24)	69.0(8)	782(4)
1.2	1.28(21)	0.82(1)	45.9(17)	178.1(30)	70.9(39)	790(5)

Regarding the SQP(E) values and spectra positions, small variations were observed and may be attributed to the quenching effects, which were probably caused by the energy transfer in presence of naphthalene or to the optical quenching due to variations in the packaging of the PSm during the sample preparation.

Samples containing $^{90}Sr/^{90}Y$ (two beta emitters in secular equilibrium with $E_{máx}$= 545.9 and 2279.8 keV, respectively) and ^{241}Am (an alpha emitter with $E_{máx}$= 5637.82 keV) were measured in the Quantulus 1220 and in the Triathler liquid scintillation detectors to evaluate the discrimination ability of the synthesized PSm. In both equipment, the discrimination was based on an analysis of the time pulse distribution of the photons produced by the particles in the scintillator. In general, a beta pulse has a shorter length than an alpha pulse.

- **Quantulus detector**

In a Quantulus detector, pulses are classified as beta or alpha by analysis of their length with regard to a threshold level, which is selected through the PSA parameter (0 to 250) that is related to the pulse duration. The proportion of correctly classified beta and alpha signals was determined by measuring the vials at different PSA values.

PSm containing PPO, POPOP and naphthalene

In general, as it can be observed in Figure 27a and 27b, when naphthalene concentration increased within the PSm composition for a fixed PSA value, more beta particles were misclassified, while more alpha particles were correctly classified. As expected, naphthalene produces a delay in the photon emission of both radionuclides, and consequently, there is an improvement in the correct discrimination of alpha pulses.

When PSm composed only by polystyrene and PPO/ POPOP were employed, beta particles were correctly classified at PSA values higher than 100 (Figure 27a). However, even when PSm containing the highest naphthalene amount (3.0 g) were employed, approximately 10% of alpha particles remained misclassified. This could be due to the conjunction of two factors: the detection of Compton electrons generated by the gamma rays emitted by ^{241}Am, which could be detected as beta particles, and the non detection of alpha particles due to particle quenching, since efficiency is lower than 100%.

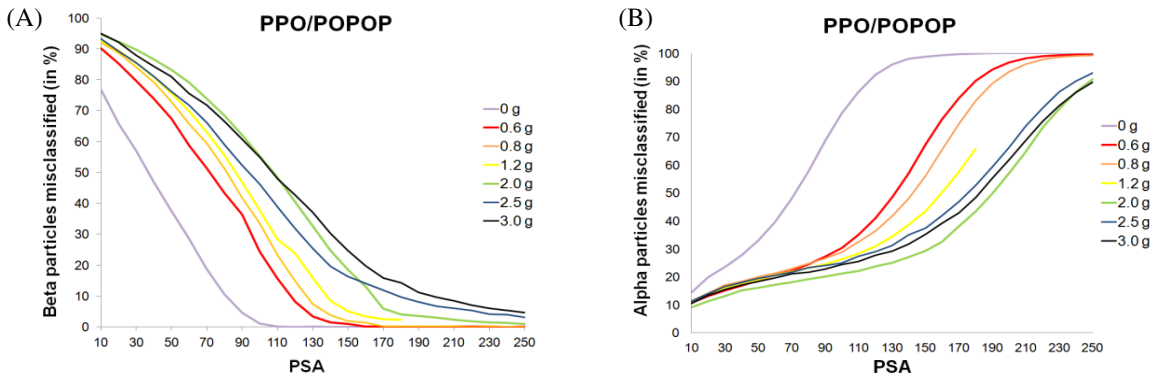

Figure 27. Misclassification of beta and alpha particles measured with the PSm containing PPO/POPOP and increasing amounts of naphthalene.

Figure 28 shows the spectrum of ^{241}Am. It can be observed that it is composed of a band at low energies (probably caused by Comptom electrons) and a peak at high energies (originated by the alpha particles). The fact that the detection efficiency of ^{241}Am is lower than 100% makes it possible to detect gamma rays as beta particles, when the alpha particle is not detected.

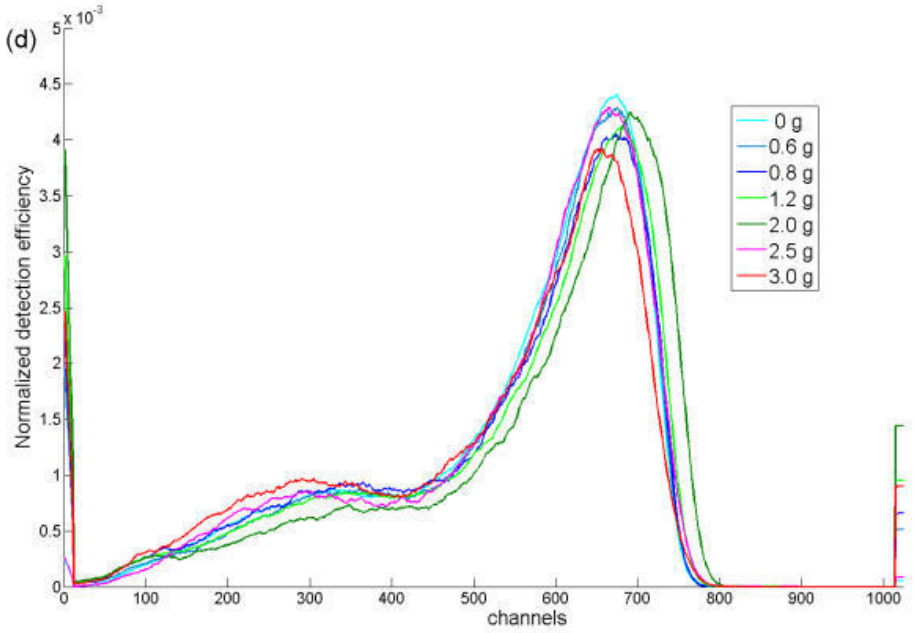

Figure 28. Normalized spectra of ^{241}Am, samples measured with PSm containing PPO/POPOP and increasing amounts of naphthalene in the Quantulus detector.

PSm containing pT, bis-MSB and naphthalene

A similar behavior in the particle discrimination was observed regarding the PSm containing the pT/bis-MSB and naphthalene. When increasing amounts of naphthalene were employed, more beta particles were misclassified while more alpha particles were correctly classified (Figure 29).

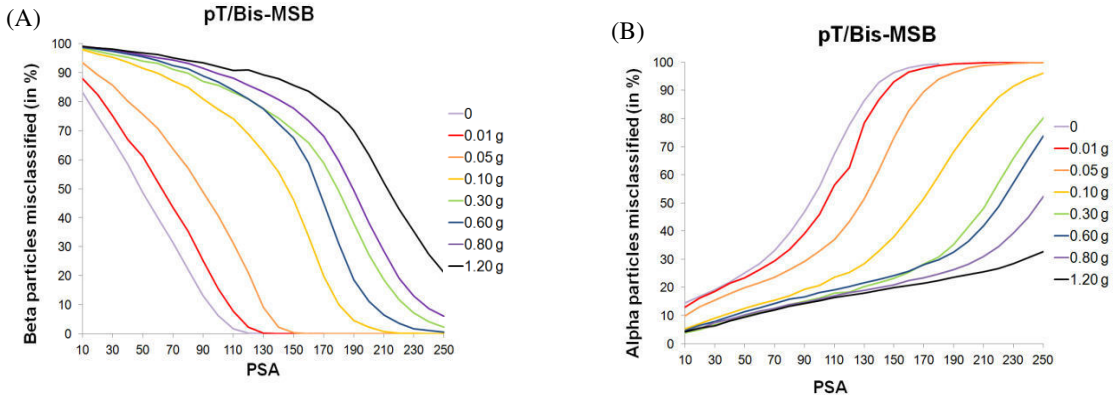

Figure 29. Misclassification of beta and alpha particles measured with the PSm containing pT/bis-MSB and increasing amounts of naphthalene.

The influence of naphthalene in the pulse delay of the emitters was more remarkable for the PSm composed by pT and bis-MSB than for those containing PPO and POPOP, probably because the energy transfer between naphthalene and pT seems to be more difficult than the energy transfer between naphthalene and PPO. Increasing amounts of naphthalene introduces an additional delay of the pulses, influencing in the classification of the particles.

In order to determine the most appropriate conditions for alpha/beta discrimination (i.e. solutes, amount of naphthalene and PSA value) employing the synthesized PSm, the mean misclassification for each PSA value was calculated (Figure 30). The lowest proportion of wrongly classified signals was about 23% for both emitters. The conditions in which these values were obtained were: 2.0 g of naphthalene at PSA 170 for PSm containing PPO/POPOP and 0.6 g of naphthalene at PSA 210 for the PSm containing pT/bis-MSB.

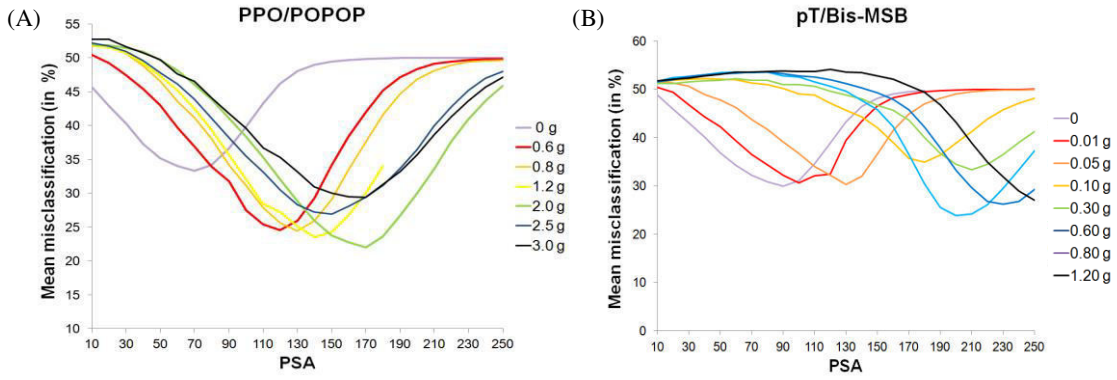

Figure 30. Misclassification with the Quantulus detector when increasing amounts of naphthalene are added: (A) PSm containing PPO/POPOP and (B) PSm containing pT/bis-MSB.

These optimum values of misclassification are high if we compare to the obtained when using liquid scintillation cocktails. This can be mainly attributed to:

- The detection of alpha particles as beta signal through the non-coincident detection of the Compton electron produced by gamma radiation.
- The intrinsic characteristics of the plastic scintillators due to the fast decay time of the scintillation based on polymers.
- The discrimination capabilities of the detector employed, since it classifies the signals into only two classes (alpha and beta) and uses a time threshold value independent of the energy of the signal.

➢ Triathler detector

The Triathler detector has only one PMT, therefore detection efficiency and background performances with regard to the Quantulus detector are poorer. However, in this detector, the pulses are classified by the duration and the energy of each event in a three dimensional plot.

PSm containing PPO, POPOP and naphthalene

A shift of the spectra toward longer time durations in accordance with the amount of naphthalene was observed (Figure 31). The pulse delay was more significant for alpha particles, therefore it could be deduced that naphthalene affected more the energy transfer from the solvent to the primary fluorescent solute which involves triplet states, while the transfer from the singlet state (produced by beta particles) to the primary fluorescent solute was less interfered.

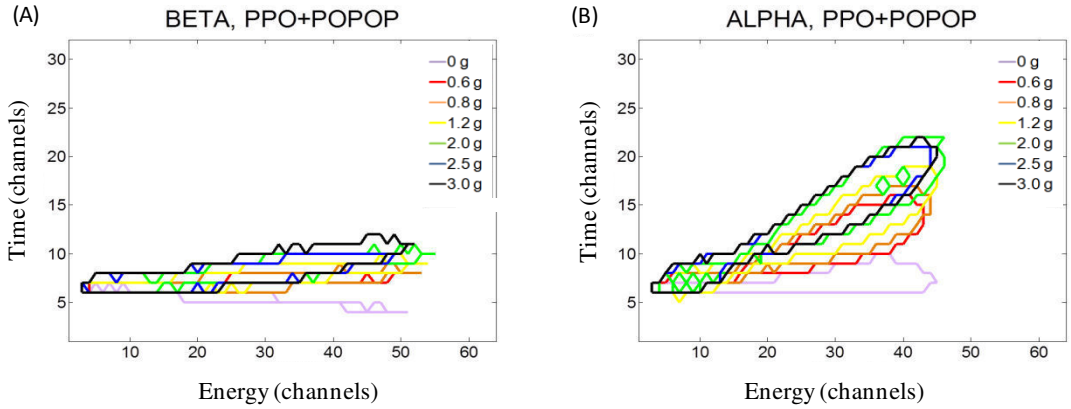

Figure 31. Contours of the spectra obtained with the Triathler detector in the time vs. energy (in channels) space, when measuring PSm containing increasing amounts of naphthalene and PPO/POPOP: (A) beta particles; (B) alpha particles.

PSm containing pT, bis-MSB and naphthalene

Addition of naphthalene within the PSm composition, even at small concentrations, caused an important and similar increase in the delayed component of the pulse for both alpha and beta emitters, producing an overlapping of both pulses in time and energy distribution (Figure 32). This may be caused by a delay in the energy transfer from the solvent, to the primary fluorescent solute, which affects the excitation of both alpha and beta signals.

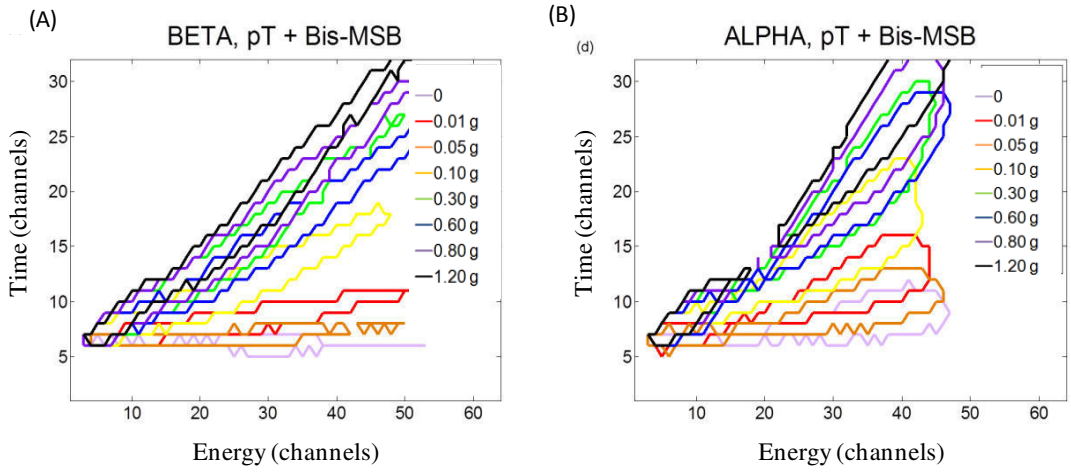

Figure 32. Contours of the spectra obtained with the Triathler detector and measured with PSm containing increasing amounts of naphthalene and pT/Bis-MSB: (A) beta particles, (B) alpha particles.

With the help of a computational method, the integrated regions with the lowest percentages of misclassification for alpha and beta emitters (less than 5%) were determined (Figure 33). Using a 3D analysis, it was possible to define regions of energy and time with a misclassification value lower than 5% (used as a threshold) in both PSm compositions. Following this optimization procedure, detection efficiencies in these regions for PPO/POPOP were higher (around 100% for $^{90}Sr/^{90}Y$ and 20% for the ^{241}Am) than those of the pT/bis-MSB scintillator (lower than 60% for $^{90}Sr/^{90}Y$ and lower than 20% for the ^{241}Am). As a consequence, better performance was obtained using PSm composed of PPO/POPOP and containing 2 grams of naphthalene.

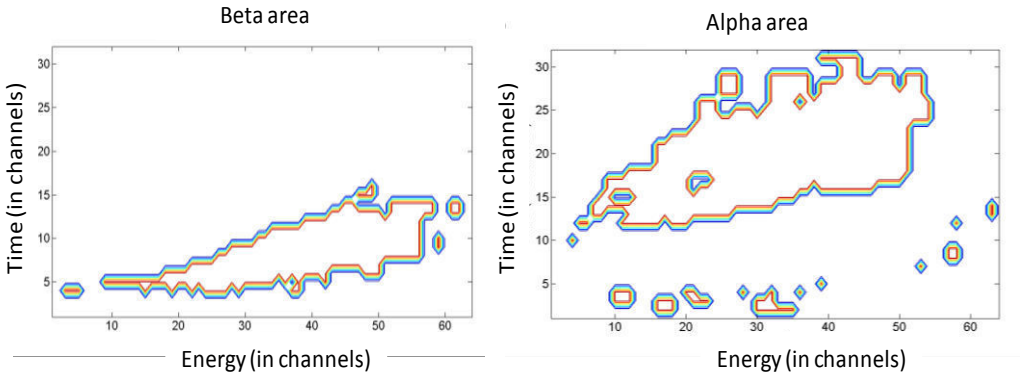

Figure 33. Perimeter of the alpha and beta regions defined for PSm containing PPO and POPOP and 2.0 g of naphthalene.

PSm composed of PPO/POPOP and less than 2.0 g of naphthalene showed the highest ability for discriminating particles. Values of less than 2% misclassification for beta particles in the alpha window and less than 0.5% for alpha particles in the beta window were obtained. Detection efficiencies for alpha particles were about 25% and for beta particles about 90%. Limits of detection obtained were 20 Bq L^{-1} for alpha and 80 Bq L^{-1} for beta particles. They were considered low taking into account the features of the spectrometer (since the equipment possesses one photomultiplier and no passive nor active shielding) and the measurement conditions (120 min counting time and 0.75 mL of sample). These values were achieved since the delimitating areas allowed a significant reduction of the background in the selected integration areas (especially for the alpha emitter).

Results obtained demonstrate that an optimal discrimination can be achieved if the detection is performed with an appropriate electronic system.

4.3.3. Evaluation of the influence of the PSm diameter on the radiometric capacities

In this part of the work the relationship between the diameter of the PSm and their radiometric capacities are discussed. The evaluation is performed measuring with the PSm obtained by different methodologies, which cover different ranges of diameters.

- The PSm produced by the organic solvent extraction/evaporation methodology (particle diameter between 17 μm and 1 mm).
- The polystyrene based sub-micron particles obtained through the supercritical anti-solvent technique (particle diameters below than 1 μm).
- The PSm and scintillating particles obtained through the Spray-Drying methodology (particle diameter between 4 and 12 μm).

- **PSm obtained by the organic solvent extraction/evaporation methodology (particle diameter between 17 µm and 1 mm).**

Fifteen different PSm batches produced by triplicate were obtained by organic solvent extraction/evaporation according to the conditions established in Table 4 in the section 4.1.3. Different radionuclides (^{3}H, ^{14}C, ^{90}Sr/^{90}Y and ^{241}Am) were measured with each PSm batch to determine their radiometric capacities. Values of detection efficiency, SQP(E) parameter and median diameter of the PSm are shown in Table 14.

Table 14. Radiometric capacities and median diameter of PSm synthesized.

	^{3}H (%)	^{14}C (%)	^{90}Sr/^{90}Y (%)	^{241}Am (%)	SQP (E)	Median diameter (µm)
PSm1_p	1.13(12)	53.5(13)	186.3(4)	81.8(16)	771(7)	84(26)
PSm2_ p	1.28(3)	54.6(22)	188.5(11)	85.1(13)	781(7)	85(25)
PSm3_p	1.16(4)	54.5(16)	186.7(15)	85.5(26)	785(3)	79(26)
PSm4_ p	1.26(8)	57.9(18)	187.9(5)	85.7(8)	777(4)	71(24)
PSm5_p	1.75(8)	63.8(5)	190.1(7)	96.3(7)	769(3)	51(24)
PSm6_p	1.80(15)	66.2(14)	189.7(18)	99.0(7)	763(2)	40(13)
PSm7_p	3.36(8)	71.8(26)	194.4(45)	102.9(7)	741(3)	22(9)
PSm8_p	1.40(3)	59.8(2)	188.3(13)	91.9(4)	772(3)	68(24)
PSm9_p	1.73(24)	62.7(9)	190.3(11)	95.2(5)	774(4)	57(24)
PSm10_p	0.81(9)	45.1(26)	184.8(25)	67.3(49)	788(3)	145(62)
PSm11_p	0.34(14)	19.8(92)	152.5(161)	30.7(159)	805(3)	-
PSm12_p	1.14(2)	53.4(9)	190.6(25)	83.8(18)	769(2)	83(28)
PSm13_p	2.69(28)	68.7(12)	189.8(8)	99.7(14)	755(6)	32(12)
PSm14_p	4.51(49)	74.3(10)	192.9(23)	102.9(2)	743(12)	17(8)
PSm15_p	0.872(8)	57.9(6)	186.7(4)	83.4(2)	784(3)	67(21)

The obtained results show a clear correlation between the detection efficiency and the PSm diameter, especially for those radionuclides of weak and medium energy, ^{3}H and ^{14}C, respectively. Detection efficiency values tended to decrease when PSm of higher diameters were employed, as it can be seen in Figure 34.

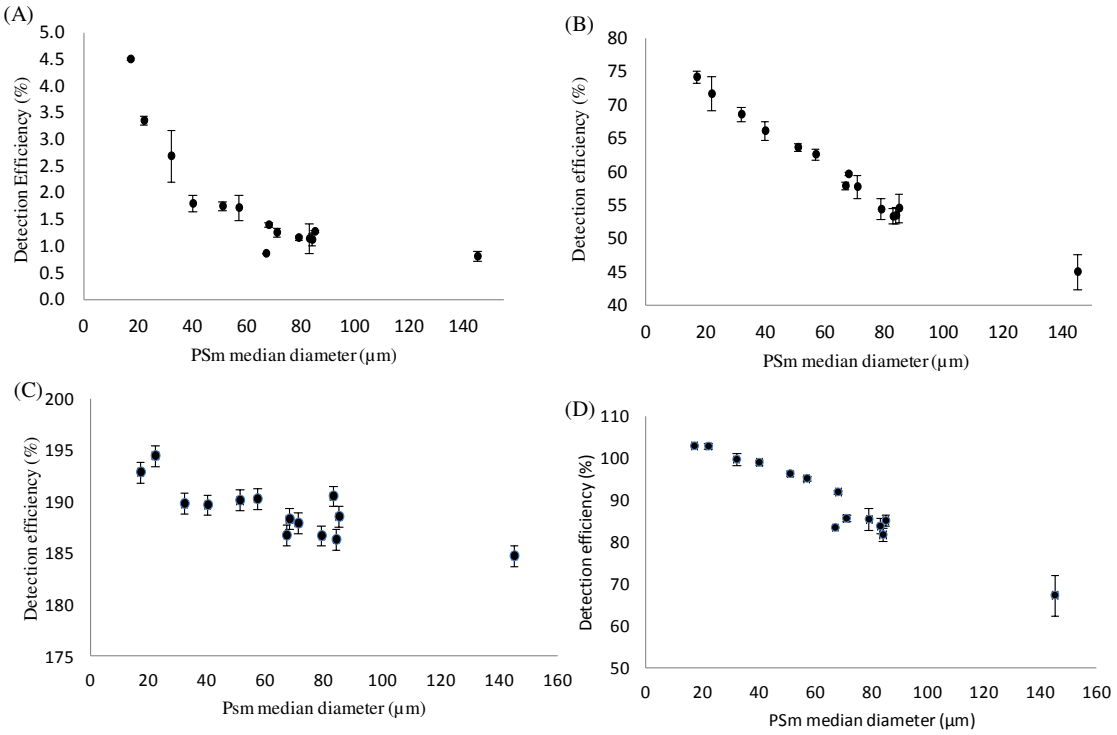

Figure 34. Correlation between detection efficiency and PSm median diameter measured for each synthesis: (A) ^{3}H; (B) ^{14}C; (C) $^{90}Sr/^{90}Y$ and (D) ^{241}Am.

Detection efficiency for ^{3}H increased from 0.34% for PSm of about 1 mm diameter to 4.51% for those with a median diameter of about 17(8) µm, which were the smallest ones. It has been confirmed that smaller PSm diameter implies higher detection efficiencies, since the distance that the disintegrated particles travel to reach the scintillator is shorter, and therefore, the probability for detecting the particle is higher. The same tendency was observed for the rest of the radionuclides, especially for ^{14}C and ^{241}Am.

Regarding $^{90}Sr/^{90}Y$, the influence of the PSm diameter was less significant than for ^{3}H or ^{14}C, but not negligible, since for the highest and lowest diameters, the detection efficiency varied from 193% to 153%. In the case of the alpha particles of ^{241}Am, since they have a very short path in water (around 50 µm) when the PSm diameter is higher than 50 µm not all alpha particles are detected. However, when the PSm median diameter is smaller the distance is lower and the efficiency can achieve values of 100%. These variations on the detection efficiency are related to the particle quenching as a consequence of the diameter size of the PSm.

With regard to the SQP(E) values, they increased when the median diameters of PSm increased and the detection efficiency decreased, as observed in Figure 35.

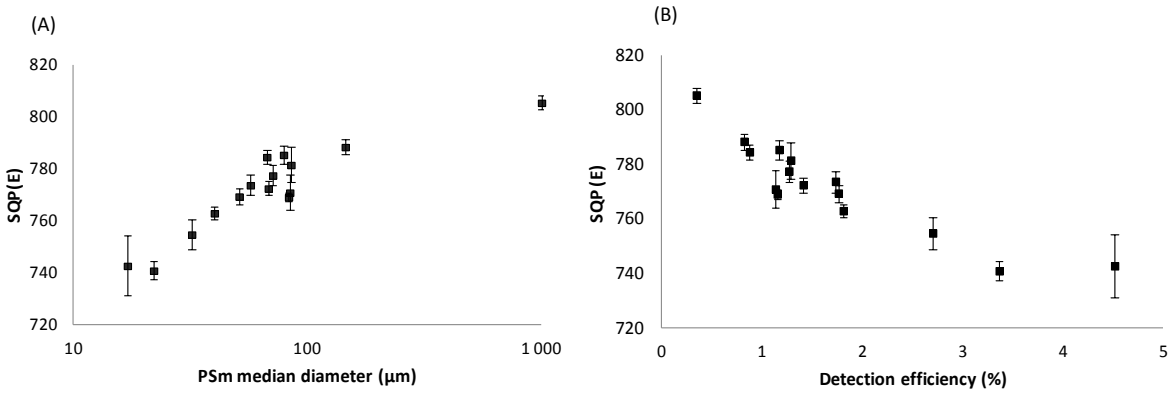

Figure 35. Correlation between the SQP(E) and: (A) median diameter of the PSm; (B) ^{3}H detection efficiency.

This behavior is opposite to what is usually observed for the organic scintillators, in which the detection efficiency decreases with the increase of the quenching parameter. To explain this behavior, it is necessary to take into account the optical quenching when measuring with microspheres, as well as the fact that optical quenching is more significant when measuring with small microspheres than when microspheres of big diameters are employed.

When a photon is produced, it can be transmitted through a microsphere or reflected (more probably) on its surface. In a medium with small microspheres the number of optical processes (transmissions and reflections) is very high and this leads to an increase on the probability that the photons cannot be detected. On the contrary, when big microspheres are used, the path is less tortuous and less photons are lost.

This behavior is confirmed by the position of the spectra (Figure 36 shows the spectra of ^{241}Am as an example). It can be seen that the maximum and the end of the spectra shift toward higher energy values with the increase of the PSm diameter, thus indicating the presence of a quenching phenomena (optical quenching). However, detection efficiency decreases, due to the particle quenching.

In the case of the alpha emitter, it is also worth to highlight how the band at lower energies almost disappears when the diameter decreases indicating that all the alpha particles are detected and only few gammas are detected in non-coincidence with the

alphas. In this situation, the alpha/beta discrimination would improve. The obtained results confirmed the importance of the diameter of the PSm on the measurement and the relevance of particle and optical quenching for the analytical parameters.

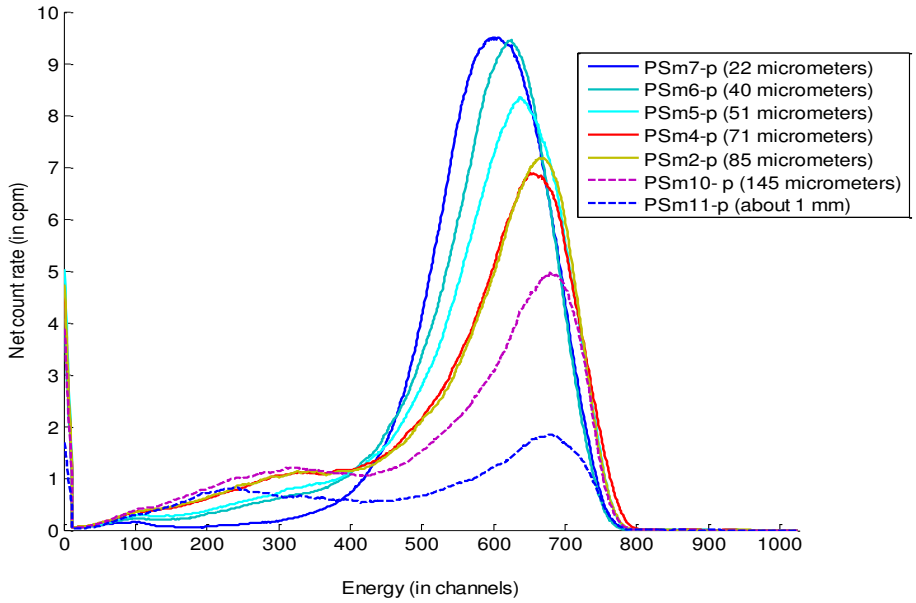

Figure 36. Spectra position for the ^{241}Am measured by using PSm of different median diameters

- **Sub-micron particles obtained through supercritical anti-solvent methodology (particle diameters below than 1 μm).**

Evaluation of the capacity of the SAS technique was carried out by a series of micronisations performed by adding the fluorescent solutes (PPO and POPOP) and DIN one by one to the organic solution (containing polystyrene) and coprecipitating the particles under the operational parameters reported in Table 6 in the section 4.2.1. Different radionuclides (^{3}H, ^{14}C, ^{90}Sr/^{90}Y and ^{241}Am) were measured employing each micronised PSm composition to confirm the encapsulation of the components within the matrix and to determine their radiometric capacities. The samples were prepared in ethanol medium for making the polarity between the scintillating polymeric particles and the solution more similar, since they were highly electrostatic and mixing with water solution was not possible.

Detection efficiency values (Table 15) and spectra position of ^{241}Am (shown as an example) (Figure 37) confirmed the encapsulation of the PPO/POPOP and DIN. The addition of PPO and POPOP caused an increase of the detection efficiencies values and a shift of the spectra toward higher energy values with regard to the obtained detection efficiency for PSm composed only by polystyrene.

Table 15. Radiometric capacities of the submicron particles obtained for the measuring of ^{3}H, ^{14}C, ^{90}Sr/^{90}Y and ^{241}Am.

	^{3}H (%)	^{14}C (%)	^{90}Sr/^{90}Y (%)	^{241}Am (%)	SQP(E)
SAS_P8 (PS)	0.008(2)	0.9(1)	58.4(6)	35.6(38)	412(9)
SAS_P9 (PS/PPO)	0.032(7)	2.8(4)	68.2(22)	55.0(40)	406(10)
SAS_P10 (PS/PPO/POPOP)	0.237(22)	13.8(6)	101.2(12)	88.9(28)	416(3)
SAS_P11 (PS/PPO/OPOPOP/DIN)	0.092(2)	7.7(4)	95.8(5)	79.9(29)	410(5)

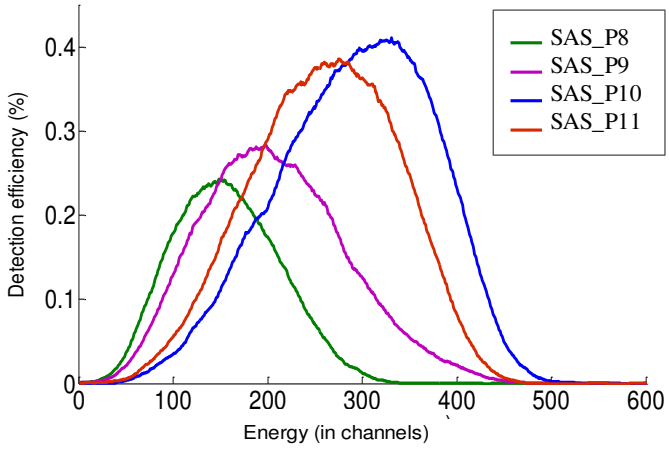

Figure 37. Detection efficiency of the ^{241}Am determined employing submicron scintillating particles with different compositions.

However, the radiometric performances of the sub-micron particles were very low in comparison with those determined for the PSm obtained by the organic solvent extraction/evaporation methodology, especially for the obtained SQP(E) values.

This behavior can be attributed to a balance between the optical quenching and the particle quenching phenomena and their relationship to the scintillating particle diameter, which was, in this case, in the submicron range.

Submicron particles have smaller diameter than the PSm obtained through the organic solvent extraction/evaporation method, thus the path that the disintegrated particle should travel to reach the scintillator is shorter and the probability to reach the surface should be higher. However, this positive effect was compensated by the loss of photons as a consequence of the non-homogeneous, long and tortuous path that they follow. In this path there are multiple reflection and transmission processes resulting in a decrease of the possibility to detect the photons produced in the scintillation event. For this reason values of SQP(E) of about 410 were obtained, which are considered very low values compared to those obtained when PSm were employed (about 720).

It can be concluded that in the sub-micron range the balance between optical and particle quenching is dominated by the increase of the optical quenching and as a consequence no benefit is obtained when the scintillating particles sizes are reduced to the submicrometric scale.

On the other hand, DIN was added to enhance the alpha/beta discrimination capabilities of the sub-micron particles. Results obtained in the measurement of a beta (^{90}Sr/^{90}Y) and an alpha emitter (^{241}Am) in the Triathler detector (Figure 38) showed that discrimination was not possible since quenching phenomena (optical) shifted the spectra toward very low energy values and caused an overlap of the time/energy spectra.

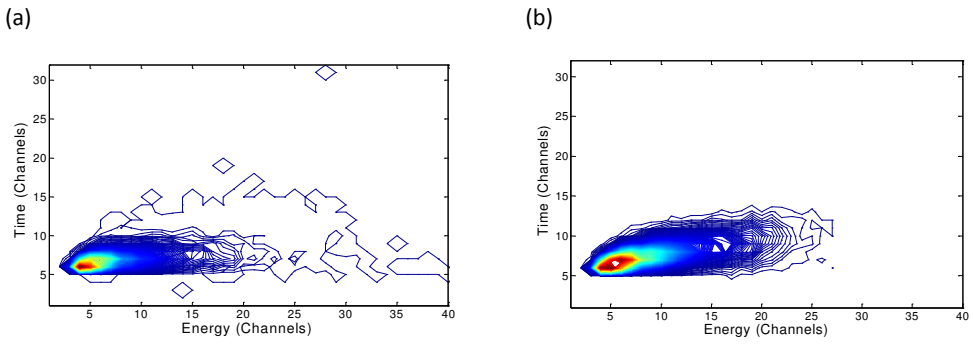

Figure 38. 2D spectra obtained with the Triathler detector employing the submicron particles for measuring: (A) ^{90}Sr/^{90}Y, (B) ^{241}Am.

- **PSm particles obtained through spray-drying methodology (particle diameter between 4 and 12 µm).**

Two beta radionuclides, ^{3}H and ^{14}C, were employed to determine the radiometric capacities of the micronised scintillating particles obtained by Spray Drying under different operational conditions described in the Tables 7 and 9 in section 4.2.2. Once again the samples were prepared by adding ethanol to the counting solution.

Detection efficiency values for the measurement of ^{3}H and ^{14}C with the micronised particles, ranged between 2-5% and 52-70%, respectively (Figure 39). In the case of ^{3}H, a clear correlation can be observed between the detection efficiency and the diameter of the microspheres. These values are comparable to those obtained when measuring with the PSm produced by the organic solvent extraction/evaporation methodology, described in sections 4.3.1 and 4.3.3, which possesses a higher diameter. Moreover, Figure 40 shows the spectral position for ^{3}H and ^{14}C measured employing the microspheres micronised with toluene, in which spectra were located at high energy position, indicating that the PPO, POPOP and DIN were encapsulated within the polystyrene matrix through the Spray-Drying methodology.

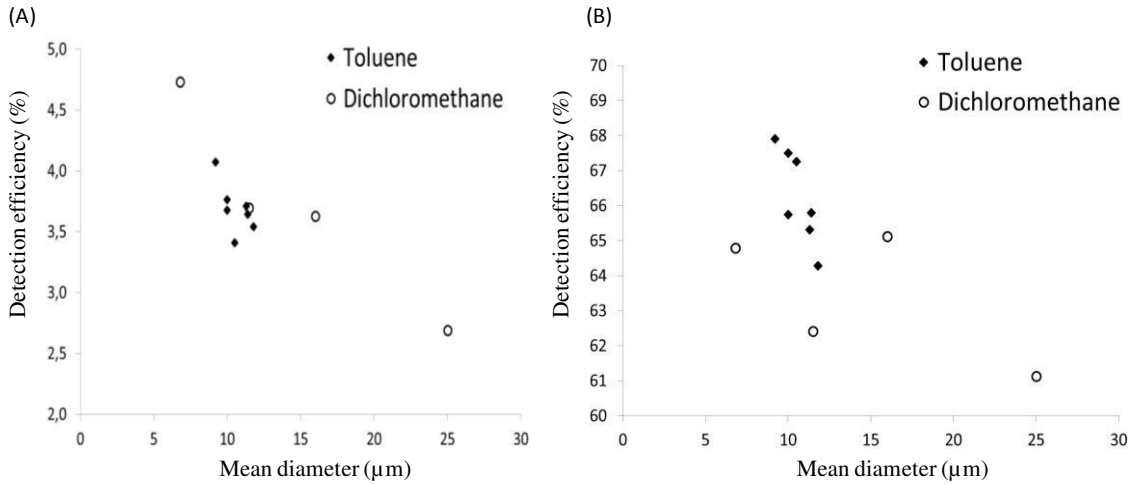

Figure 39. Detection efficiency values obtained by using the PSm obtained by SAS unsing toluene and dichloromethane: (A) ^{3}H; (B) ^{14}C.

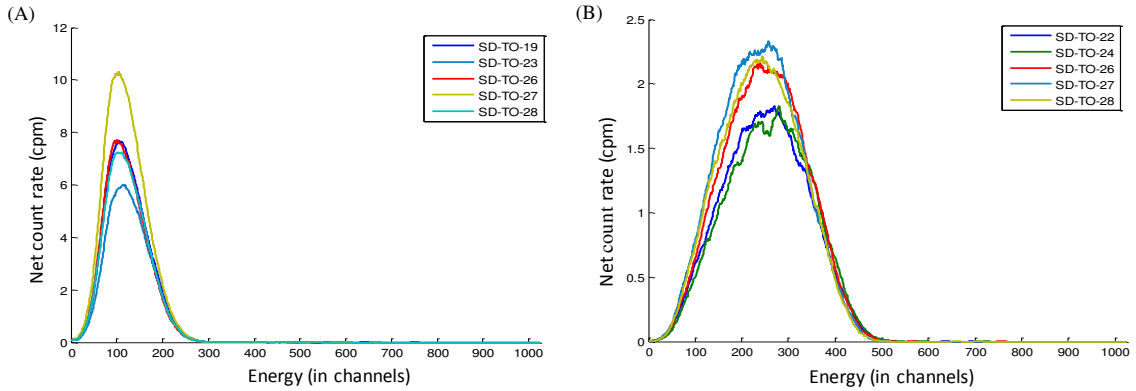

Figure 39. Spectral position obtained for the measurement of PSm micronised by Spray Drying using toluene: (A) ^{3}H; (B) ^{14}C.

The SQP(E) values obtained for the scintillating particles produced by using dichloromethane were about 625, while the values obtained when toluene was employed were about 670. This difference between the values can be attributed to a less efficient light transmission produced by the deflated microspheres obtained when dichloromethane was employed or due to a chemical quenching produced for the residual solvent within the microparticle. Values of SPQ(E) were lower than those obtained when measuring with the PSm obtained through the organic solvent evaporation/extraction methodology and higher than the obtained by employing the submicron particles produced through SAS.

It can be said that higher detection efficiencies are obtained with PSm of 10 µm (especially for ^{3}H) due to the reduction on the particle quenching. However, the optical quenching starts to be relevant at this diameter, as it can be observed in the spectral position and in the SPQ(E) values. Probably for medium and high energy beta emitters the use of PSm with higher diameters is recommended. The use of very small or very big PSm diameters in nanometric or milimetric scale, is not suitable, due to the particle and the optical quenching, respectively.

4.3.4. Evaluation of the solution composition: quenching mechanism.

To complete the evaluation of the quenching mechanism in plastic scintillators, samples containing different quenching agents were evaluated employing different organic scintillators (i.e. liquid scintillation cocktail, gel scintillation cocktail,

commercial PSm of 137 µm (PSm1_c) and PSm of 450 µm (PSm2_c)) for the measurement of two beta emitters of low and high energy, ^{3}H ($E_{\beta max}$=18.5 keV) and ^{36}Cl ($E_{\beta max}$= 710 keV), respectively.

The quenching agents evaluated were:

- NaCl, $BaCl_2$ and glycerine in concentrations of 0.3, 0.7, 1.4, 2.1 and 2.6 M; 0.05, 0.10, 0.15, 0.20, 0.25, 0.30, 0.70 and 1.4 M; and 14.4, 28.9, 43.3, 57.8 and 72.2 % (w/v), respectively. These quenching agents were supposed to increase the density of the solution and introduce elements of higher atomic radius, which could interact with the emitted particle to produce particle quenching.
- Nitromethane in concentrations of 1.52, 3.03, 4.55, 6.06 and 7.58 µL mL^{-1} was also evaluated. This compound is known to interfere in the energy transfer between the molecules of the liquid scintillators causing chemical quenching.
- Methyl orange in concentrations of 9.2, 18.4, 27.6, 33.2, 41.4 µL mL^{-1} which caused colored samples producing color quenching.

The main remarks of the results are summarised as follows.

- **NaCl, $BaCl_2$ and glycerin**

Adding increasing concentrations of each compound into the vials containing PSm1_c and PSm2_c for measuring the ^{3}H resulted in a decrease of the detection efficiency in all cases, as it is shown in Figure 40. This behavior was attributed to the particle quenching, since increasing the density of the solution also increases the probabilities of interaction between the weak beta emitter and the molecules of the solution, and therefore, increases the possibilities to be stopped before reaching the PSm surface to deposit its energy. SQP(E) values and spectra position remained constant, thus indicating that those beta particles which reached the PSm surface did it with the same energy distribution.

With regard to ^{36}Cl, the radiometric capacities remained constant and the effect of increasing the density of the solution was negligible. This was probably due to the high energy of the particle emitted which was not influenced by the interferences.

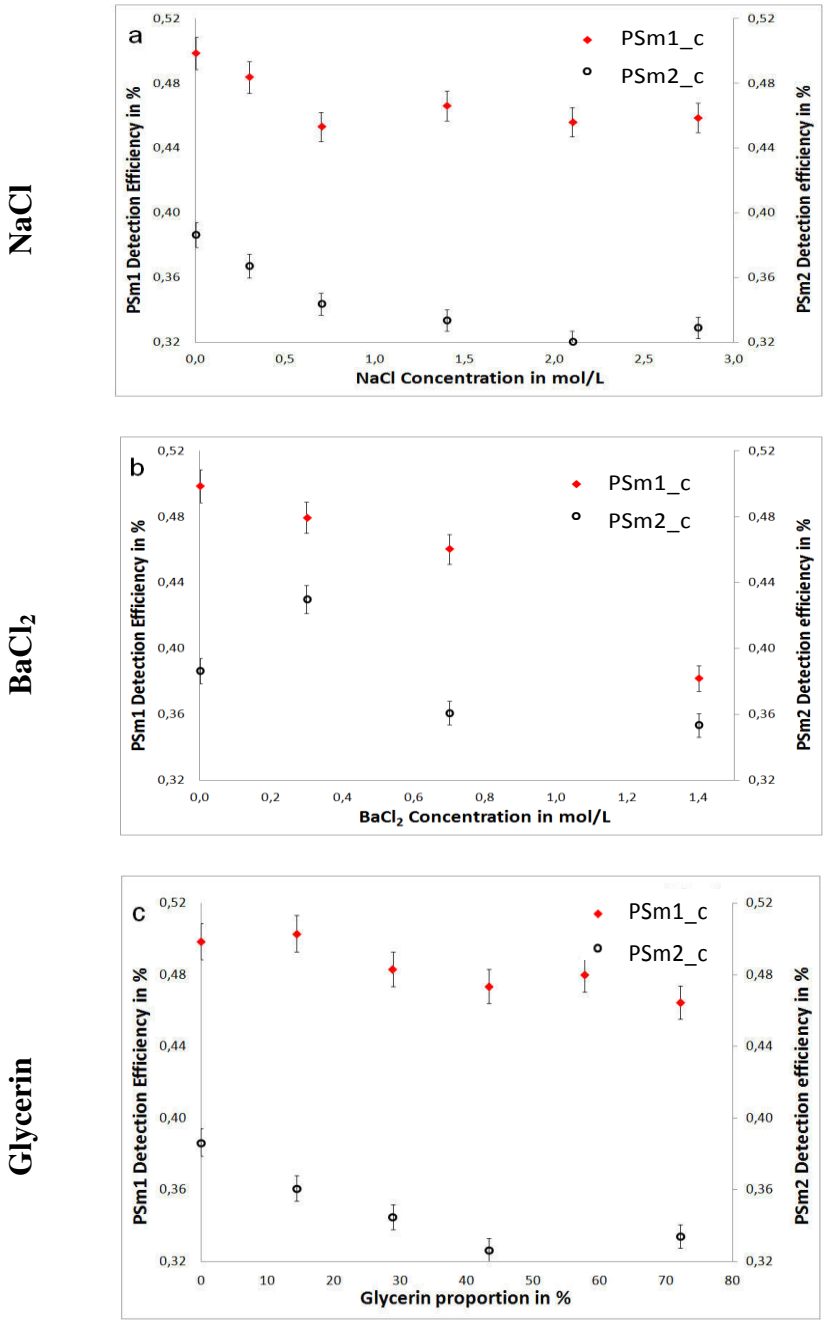

Figure 40. Detection efficiency of ^{3}H employing PSm1_c and PSm_c and different concentrations of (A) NaCl; (B) $BaCl_2$ and (C) Glycerin.

When liquid and gel scintillation cocktails were employed for measuring ^{3}H, and ^{36}Cl in presence of increasing amounts of NaCl, $BaCl_2$ and glycerine, factors related to the physical aspect of the entire sample gained importance besides the importance of the emitter energy.

Increasing concentrations of NaCl or $BaCl_2$ added into a vial containing the liquid or gel scintillation cocktail for measuring ^{3}H, decreased the detection efficiency until

phase separation was observed; at that point, the lowest detection efficiency value was reached and the detection efficiency became constant. SQP(E) increased and the spectra shifted toward higher energies. This behavior can be attributed to an increase in the size of the aqueous nanomicelles into the organic scintillator produced by the addition the salt.

Increasing the size of the nanomicelles is supposed to decrease the total number of micelles in the sample, leading to an improvement in the optical transmission of photons through the medium and causing an improvement of the SQP(E) and spectra position. However, when the micelles became saturated and could not expand anymore, phase separation did occur. The radionuclides were present in both, aqueous and organic phases, proportionally to the amount of water included in each phase.

Similar results to the above mentioned were observed for ^{36}Cl when increasing concentrations of NaCl were added to the vials containing LSc, but in this case a second peak at lower energies was observed. This peak increased proportionally to the increase of NaCl concentration. It was attributed to the presence of the radionuclide in the aqueous phase and it could correspond to the Cherenkov radiation emitted by the ^{36}Cl in the aqueous phase or to the optical quenching phenomenon, since the aqueous phase could contain enough dissolved scintillators to produce a scintillating signal, which was detected at the low region of the spectrum (Figure 41).

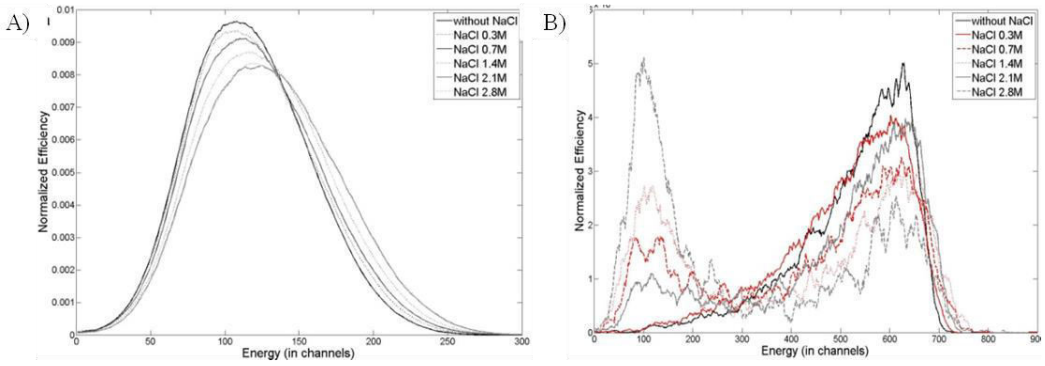

Figure 41. Normalized efficiency spectra obtained for samples with different NaCl concentrations when using liquid scintillation cocktail: (A) ^{3}H; (B) ^{36}Cl.

However, when gel scintillation cocktail (GSc) was employed to measure ^{3}H and ^{36}Cl, the detection efficiency was constant at low NaCl concentrations for both radionuclides, until the salt precipitated, resulting in a decrease of the detection

efficiency until a constant value was reached. As what happens with the liquid scintillation cocktail, the SQP(E) value increased and the spectra were shifted toward higher energy values. Once again, high concentrations of NaCl led to the formation of a peak at lower energies in the case of ^{36}Cl.

The effect of $BaCl_2$ in the radiometric performances for ^{3}H and ^{36}Cl when gel scintillation cocktail was employed was different to that obtained with liquid scintillation. For all the added salt concentrations, the mixture became milky and the detection efficiency (Figure 42), the SQP(E) and the spectra position remained constant. It could be due to a quenching constant, since the organic phase remained constant and the particle quenching did not occur. Nanometric crystals of $BaCl_2$ of about the same size were formed and suspended in the gel solution, and it is supposed that the emitted beta particles did not interact with them.

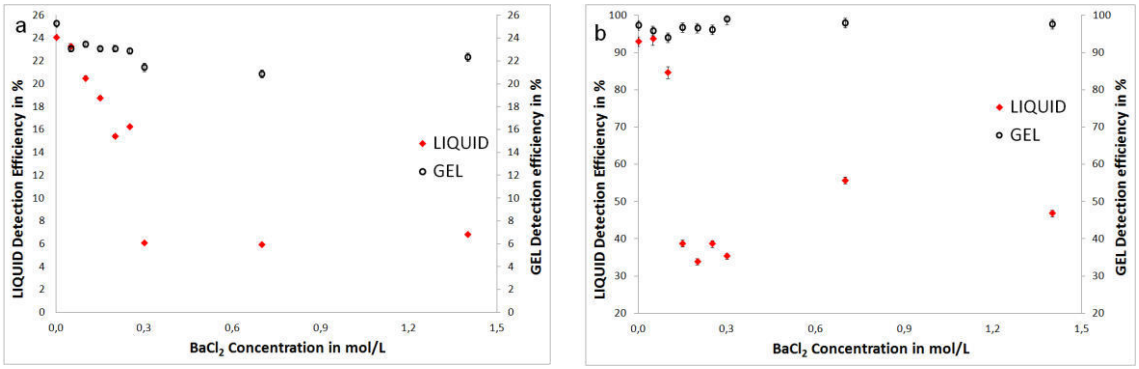

Figure 42. Variation of the detection efficiency measured by liquid and gel scintillation cocktails when increasing amounts of $BaCl_2$ were added: (A) ^{3}H; (B) ^{36}Cl.

On the other hand, the addition of glycerin to the liquid scintillation cocktail produced clear and homogeneous samples in which the detection efficiency, the SQP(E) values and the spectra position remained constant. This was probably due to the amount of glycerin which was dissolved into the organic phase of the mixture and because the aqueous nanomicelles always had the same composition and dimensions. However, when the highest concentration of glycerin was added for both radionuclides, phase separation was observed, resulting in a decrease of the detection efficiency, higher values of SQP(E) and shift of the spectrum to higher energies, due to an improvement of the optical properties of the sample.

When GSc was employed, a gelatinous precipitate and phase separation was observed for all concentrations and the obtained results were similar to those obtained for the vials containing LSc with salts (NaCl, $BaCl_2$), showing a decrease of the detection efficiency (Figure 43), increasing the values of SQP(E) and a part of the spectra shifted towards higher energies due to the increase of the micelle size and therefore, the enhancement of the optical properties of the sample.

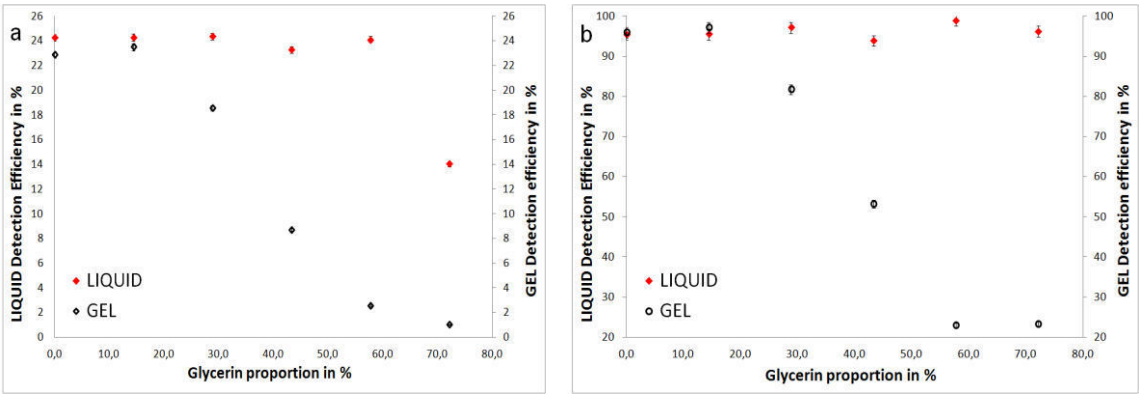

Figure 43. Variation of the detection efficiencies when measuring LSc and GSc with increasing amounts of glycerin: (A) ^{3}H; (B) ^{36}Cl.

- **Nitromethane and methyl orange**

When increasing amounts of nitromethane or methyl orange were added to the vials containing PSm1_c, PSm2_c, liquid and gel scintillation cocktails for measuring ^{3}H and ^{36}Cl solutions, the resulting radiometric capacities corresponded to a typical quenching behavior, in which the detection efficiency decreases according to the amount of added quenching agent with the SQP(E) values and the spectral position shifted towards lower energy values. As a result, the detection efficiency can be correlated with the SQP(E) parameter. The same behavior was observed when ^{36}Cl was measured with PSm1_c and PSm2_c, and in a smaller degree with LSc and GSc, especially for methyl orange. Figure 44 shows the detection efficiency and SQP(E) behavior when PSm1_c and PSm2_c were employed.

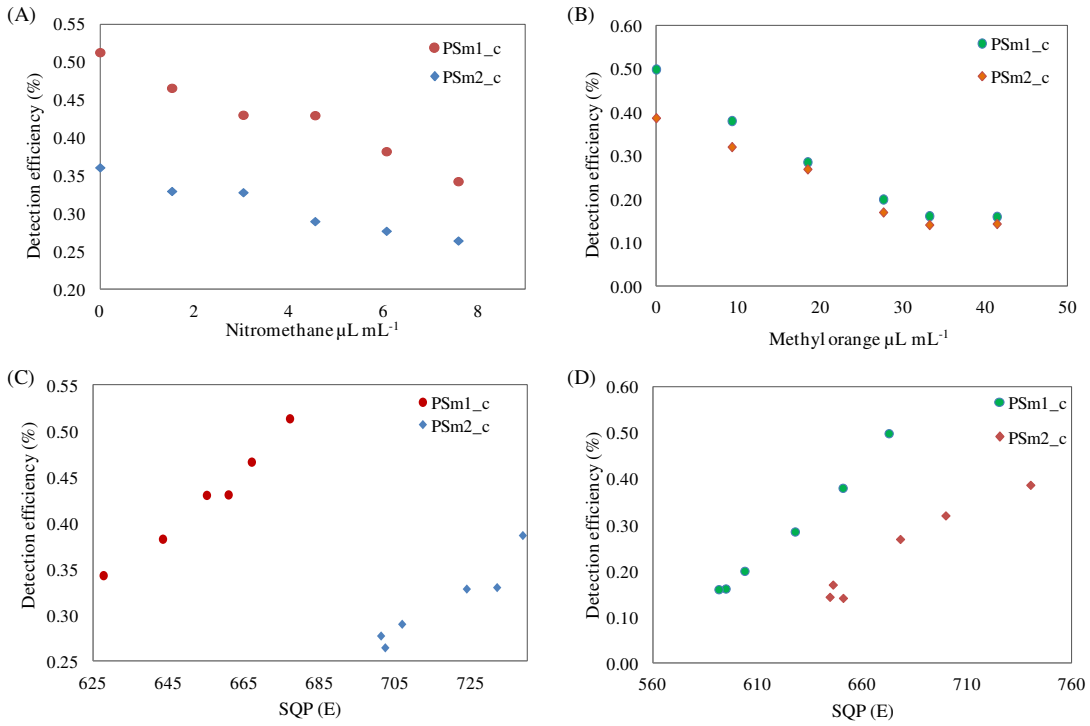

Figure 44. Detection efficiency and SQP(E) obtained when adding increasing amounts of nitromethane (A,C) and methyl orange (B,D) for the measurements with PSm1_c and PSm2_c.

The color quenching produced by the methyl orange was expected in all the organic scintillators evaluated, since colored samples tend to absorb the photons thus decreasing the amount of photons detected by the PMT. However, chemical quenching produced in the PSm by the presence of the nitromethane was an unexpected result, since the solution containing nitromethane is supposed to be only in contact with the PSm on the surface and a minimal interference in the energy transfer process should be expected. However, two hypotheses were considered to explain this behavior. The first one is that nitromethane was absorbed within the PSm and, the second one, that the energy transfer is very fast and at some moment, it took place in the microsphere surface.

Figure 45 shows the detection efficiency (%) and the spectra obtained for ^{3}H and ^{36}Cl when increasing concentrations of nitromethane and methyl orange were added within the sample and measured with PSm1_c and PSm2_c. As it is mentioned before, detection efficiency tends to decrease, mainly for the low and medium beta emitters,

while spectra is shifted toward lower energy values when quenching agent concentration increases.

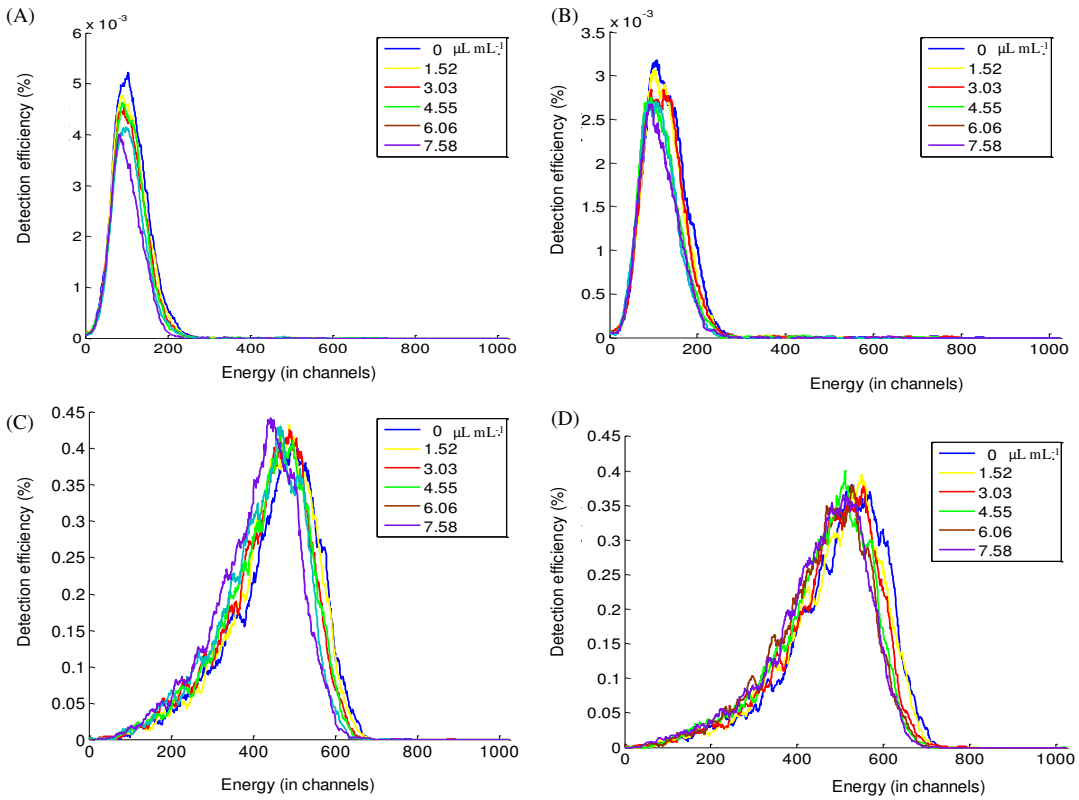

Figure 45. Influence of the increasing concentration of nitromethane when measuring with PSm1: (A) ^{3}H; (B) ^{36}Cl; and with PSm2: (C) ^{3}H; (D) ^{36}Cl

The most important highlights when measuring ^{3}H with LSc are summarised in Figure 46. Nitromethane and methyl orange produced a classical quenching behaviour, while adding glycerine produced phase separation, which resulted in the modification of the optical properties of the sample, and $BaCl_2$ acted as an interference for the disintegrating particle to reach the scintillator, to a lesser extent than when PSm are employed.

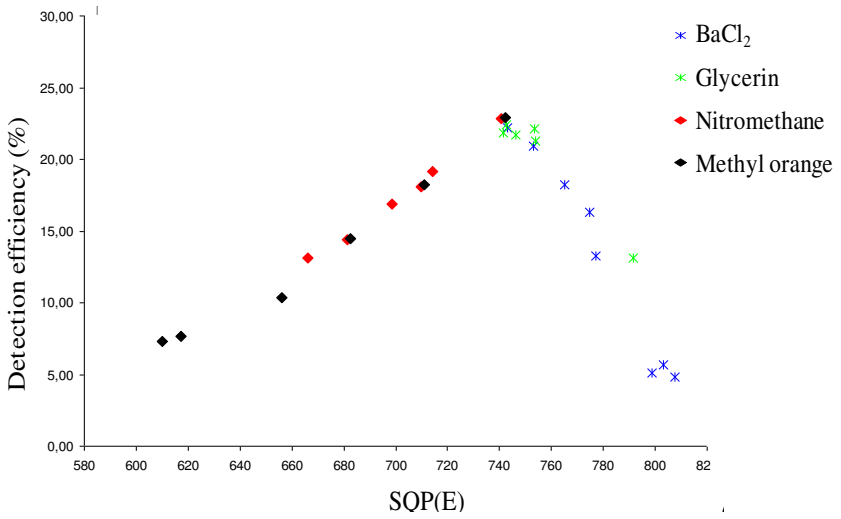

Figure 46. Quenching behavior when ^{3}H is measured employing liquid scintillation cocktail and adding increasing amounts quenching agents.

4.4. Practical aspects of sample preparation

4.4.1. Evaluation of the reproducibility of vial preparation

In order to understand better the variability associated to operational aspects related to the preparation of sample with PSm, the following parameters were evaluated: PSm/solution amount ratio and operator influence in the radiometric capacities when measuring a low energy beta emitter (^{3}H).

A series of vials containing increasing amounts of PSm (from 2.83 to 3.19 g) and a constant volume of ^{3}H counting solution (1.26 mL) were prepared to evaluate the dependence of the detection efficiency on the PSm amount. The obtained results (Figure 47) showed that there is no a clear correlation between the detection efficiency and the amount of PSm added into the vial. This can be due to the fact that for weak emitters, the variation on the efficiency is more dependent on the packaging of the PSm and the distance between microspheres, than on the PSm/solution ratio in the evaluated range. Mean values of detection efficiency and SQP(E) were 0.69(3)% and 789(3), respectively.

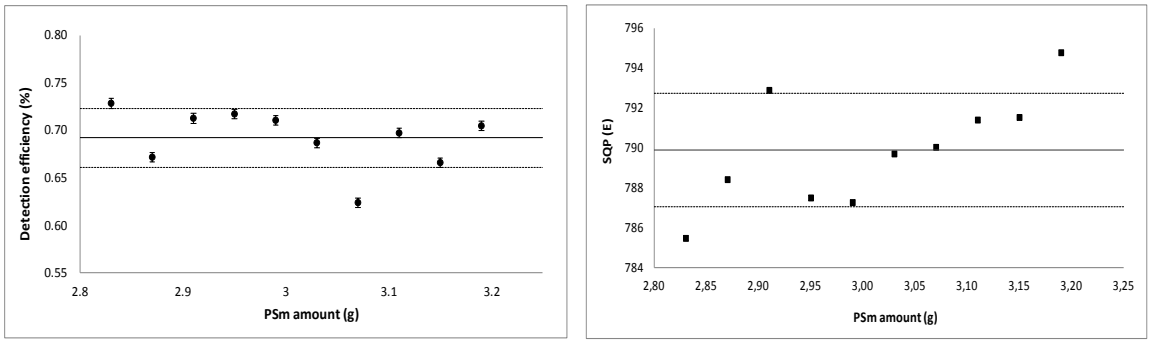

Figure 47. Radiometric capacities in function of the amount of PSm added into the vial for measuring ^{3}H: (A) detection efficiency; (B) Variation of the SQP(E) parameter.

On the other hand, three replicate samples of four different radionuclides (^{3}H, ^{14}C, $^{90}Sr/^{90}Y$ or ^{241}Am) were prepared by four different operators following a defined protocol to evaluate the reproducibility of the measurement.

The results showed that the variability decreases with regard to the energy of the measured radionuclide, as it is shown in Table 16. The variability between operators when preparing ^{3}H samples (0.66(3)%) is similar to that obtained when varying the amount of PSm added into the vial (0.69(3)%). These results indicate that for low energy beta emitters (^{3}H), the packaging of the PSm is the main source of variability and even more important than experimental factors, such as weighing, the way of adding the PSm into the vial and counting statistics. On the contrary, when high energy beta emitters are measured (Figure 48), the variability decreases, this indicates that variability due to changes in the packaging is reduced, and other factors, like the operator, weighing, etc, are more significant.

Table 16. Average values of the detection efficiency obtained for different radionuclides prepared and measured by different operators and its corresponding RSD value.

Radionuclide	Det. Eff. (%)	RSD (%)
^{3}H	0.66(3)	5.09
^{14}C	51.8(2)	3.3
$^{90}Sr/^{90}Y$	183.8(5)	0.3
^{241}Am	83.1(11)	1.3

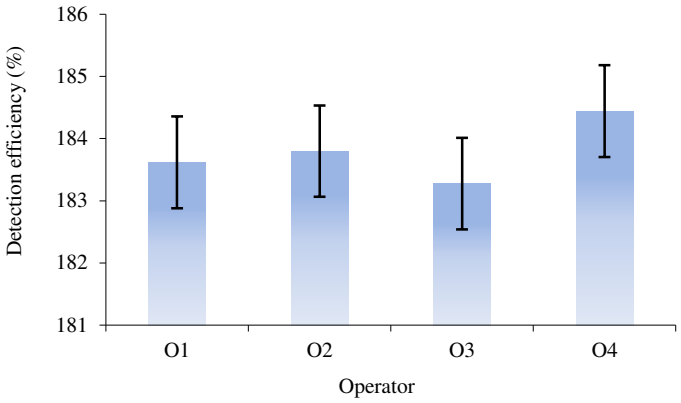

Figure 48. Detection efficiency of the $^{90}Sr/^{90}Y$ for the vials prepared by different operators.

4.5. Production of PSm: from laboratory to industrial scale.

4.5.1. PSm production at laboratory scale for different applications

The organic solvent extraction/evaporation methodology has been successfully implemented at the laboratory as it has been described in this thesis. For this reason, different batches of PSm were produced through this methodology using different operational parameters and formulations (Table 17) in order to obtain PSm of desired diameters and compositions to be employed in the following applications:

- **PSm_WS:** Experimental practices of the "International Workshop of Plastic Scintillation in Practice" and additionally, to supply 50 g of PSm to each participant. Total amount produced: 1000 g.

- **PSm_WS2:** For the own research of the group and also supplied to the University of Sofia (Bulgary) and to the National Institute of Ionizing Radiation Metrology (ENEA) (Italy) in the framework of research collaborations. Total amount produced: 1000 g.

- **PSm_ER**: Studies of immobilization of selective extractants for the development of PSresins (Plastic scintillation resins) (^{99}Tc and ^{210}Pb) done by the research group in collaboration with the company Triskem International. Total amount produced: 1000 g.

- **PSm_Bu:** Supplied to the University of Sofia (Bulgary) for a collaboration project a on the detection of ^{222}Rn. Total amount produced: 600 g.

Table 17. Different batches of PSm produced at the laboratory through the organic solvent extraction/evaporation methodology

	PSm_WS	**PSm_WS2**	**PSm_Bu**	**PSm_ER**
Dichloromethane (mL)	250	250	200	167
Polystyrene (g)	25	25	25	25
PVA (w/v) (%)	1	1	1	0.6
Temperature (ºC)	20	20	25	35
Stirring speed (Hz)	10	10	10	6.7
Composition	PS/PPO/POPOP/DIN			PS/PPO/POPOP

In all cases, the continuous phase was composed of 2000 mL of deionized water and the concentrations of PPO, POPOP and DIN were 2 % (w/w), 0.5% (w/w) and 20% (w/w), respectively, regarding the amount of polystyrene.

In each production three syntheses of 25g of PSm were performed per day. PSm were washed twice, for 4 hours in a end-over-end shaker, with a solution composed of ethanol:water (1:10), dried in an oven at 40ºC, stored and in labeled plastic bottles after their homogenization. PSm were characterised by measuring their radiometric capacities (Table 18) and observing their morphology through SEM (Figure 49) and determining their diameter and size diameter distribution (Figure 50).

Table 18. Radiometric capacities measured for the different batches of PSm.

	PSm_WS	**PSm_WS2**	**PSm_ER**	**PSm_Bu**
^{3}H Efficiency (%)	0.7(3)	0.78(0.1)	0.51(0.01)	0.73(0.07)
^{14}C Efficiency (%)	51.5(1.7)	45.5(0.9)	34.7(0.4)	46.4(0.9)
^{90}Sr/^{90}Y Efficiency (%)	185(1)	178.9(0.1)	177.8(2.4)	181.1(0.3)
^{241}Am Efficiency (%)	83(1)	79.7(1.0)	52(1.7)	78.7(0.2)
SQP(E)	791(1)	800(4)	792(3)	805(2)
Median diameter (µm)	68(24)	63(14)	180(51)	87(22)

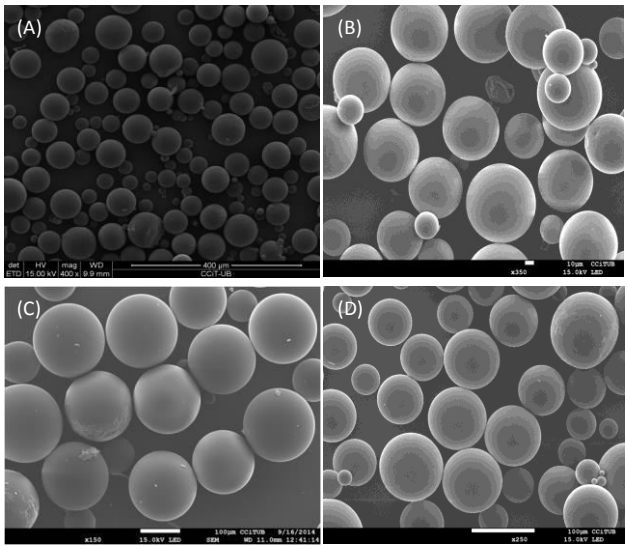

Figure 49. SEM images of the PSm synthesised through organic solvent E/E methodology: (A) PSm_WS, (B) PSm_WS2, (C) PSm_ER and (D) PSm_Bu.

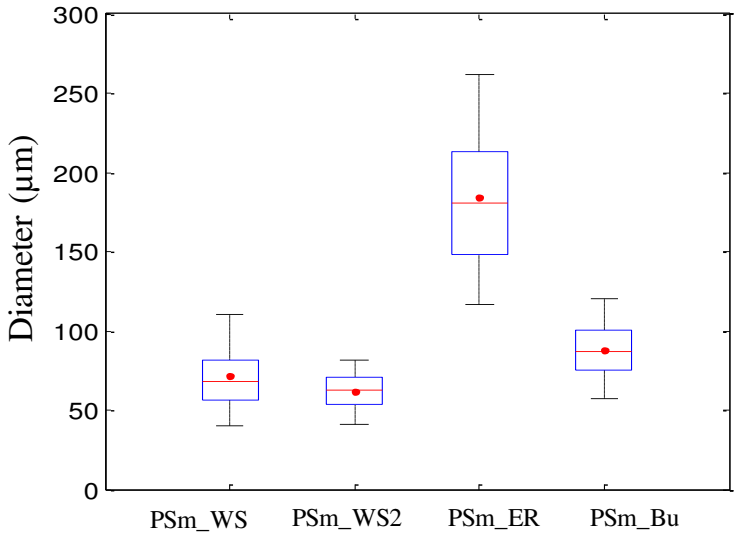

Figure 50. Boxplot of the size and size distribution of the PSm synthesised

4.5.2. Proof of concept for commercial scale production of PSm.

First attempts for producing PSm at the commercial scale were performed using the organic solvent extraction/evaporation methodology at the facilities of the company Trastamo. The aim of this work was focused on producing a batch of about two kilograms of PSm per synthesis, reproducing the process employed at the laboratory at the University of Barcelona at a larger scale. The conditions employed at Trastamo were extrapolated from those ones employed at laboratory scale for obtaining PSm with physical features and radiometric capacities similar to PSm_WS or PSm_WS2 described in 4.4.2. (Table 19). The polymer and the fluorescent solutes were solved in dichloromethane to create the disperse phase, while the continuous one was formed by dissolving PVA in water.

Table 19. Compounds used for the performance of the proof of concept for the production of PSm at Trastamo.

Reagent/Compound	Quantity
Polystyrene (g)	1875
PPO (g)	37.5
POPOP (g)	0.94
DIN (g)	375
DCM (L)	18.75
DCM (L)	3
Deionized water (L)	150
PVA (g)	1500

Production of PSm at Trastamo was performed in avessel of high capacity by stirring at about 5 Hz to simulate the vortex created at laboratory conditions (room temperature in a 5 L glass vessel). The microemulsion formed when the dispersed and the continuous phases were mixed, was stirred during 20 hours to ensure the extraction/evaporation of the organic solvent and the hardening of the PSm.

The obtained material corresponded to about 700 g of microspheres of around 40 µm diameter with a wide size distribution and a smooth and uniform surface as can be seen in the Figure 51. Production yield was about 30%.

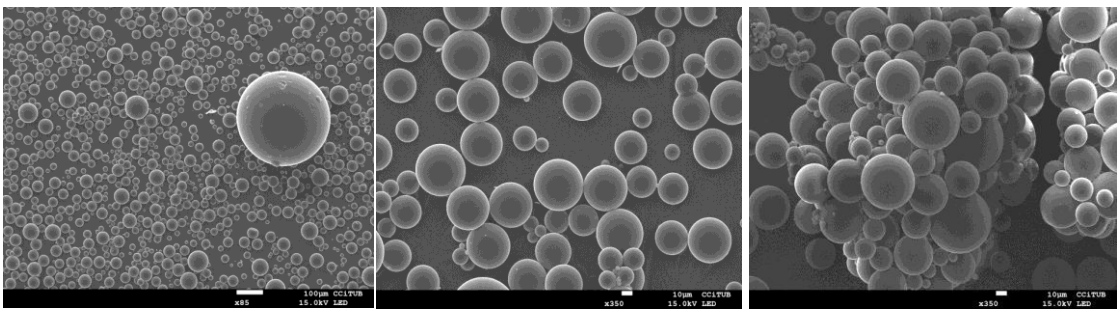

Figure 51. SEM images of the PSm obtained in the first batch produced at Trastamo.

The rest of the material (~1100 g) was obtained in form of agglomerated microspheres, microspheres of irregular shape and with some holes, polymeric flakes, sheets (Figure 52) and threads. The incorrect drying of the droplets could be due to the inefficient extraction of the organic solvent, the inefficient stirring or the rapid evaporation of solvent at the surface of the aqueous phase where there is a direct contact with the air, etc.

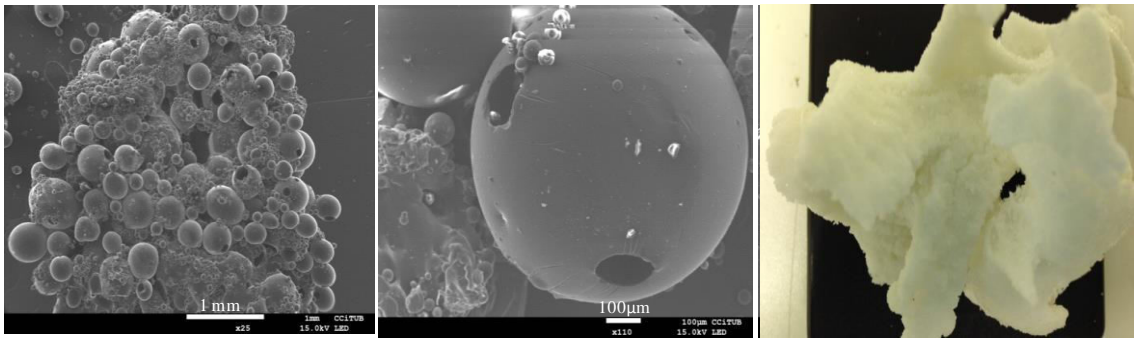

Figure 52. SEM images of the obtained polymeric particles and PSm after drying.

Regarding the radiometric capacities, PSm were employed to measure ^{3}H and ^{14}C (Table 20). The fluorescent solutes were indeed encapsulated, since radiometric capacities were similar to those determined by using the commercial PSm and the ones obtained at the laboratory by the organic solvent extraction/evaporation methodology.

Table 20. Radiometric capacities determined for the PSm obtained in the production of Trastamo

PSm	Background (cpm)	^{3}H (%)	^{14}C (%)	SQP (E)	Particle size (µm)
Trastamo	1.06(17)	1.14(12)	53.7(9)	738(4)	47(39)

Radioactivity can be measured by employing the PSm produced in the PSm proof of concept at Trastamo. These results makes feasible the production of PSm in a kg scale with acceptable cost feasible. However, the process should be optimized to increase the yield, reproducibility and quality of the PSm batches, and to permit the selection of the optimal parameters which result in the production of PSm of the desired diameters.

4.6. References

European Medicine Agency. February 2009. CPM/ICH/283/95. ICH Topic Q3C(R4). Impurities: guideline for residual solvents. http://www.ema.europa.eu /docs/en_GB/ document_library/Scientific_guideline/2009 /09 / WC500002674.pdf

Heiskanen, H., Denifl, P., Pitkänen, P., Hurme, M. Effect of preparation conditions on the properties of microspheres prepared using an emulsion-solvent extraction process. Chemical Engineering Research and Design 90 (2012) 1517–1526.

L'Annunziata, M.F. Handbook of radioactivity analysis. Academin Press, third edition, San Diego, United States (2013).

Lee, Y.L., Surfactant effects on mass transfer during the drop-formation and drop falling stages. American Institute of Chemical Engineers Journal 49 (2003) 1859-1869.

Rodríguez-Barquero, L., Grau-Carles, A. The influence of the primary solute on alpha/beta discrimination. Applied Radiation and Isotopes 49 (9–11) (1998) 1065–1068.

Tarancón, A., García, J.F., Rauret, G. First approach to radionuclide mixtures quantification by using plastic scintillators: Influence of the diameter of the plastic beads. Analytica Chimica Acta 590 (2007) 232–238

Chapter 5

Conclusions

5. CONCLUSIONS

The organic solvent extraction/evaporation methodology was implemented at the laboratory to produce PSm. The methodology proved simple and highly feasible, since PSm were produced in an easy way with a high yield (100%) and a high reproducibility between batches. Psm were produced at the laboratory showing optimal physical features and radiometric capacities, comparable to the commercial ones.

PSm of different sizes were produced through the organic solvent extraction/evaporation methodology by varying their formulation, the operational parameters and by establishing combined procedures in which the potential synergies between the operational and the formulation parameters were evaluated. The ability to produce PSm of different diameters and compositions allowed employing them in diverse applications for measuring radioactivity.

PSm with the ability to discriminate alpha and beta particles were produced first by the addition of naphthalene within their composition and then by adding DIN instead of napthahlene. The use of the PSm in a Triathler spectrometer together with an optimization of the integration areas resulted in misclassification values lower than 5%.

The Spray Drying methodology allowed the production of PSm using toluene as organic solvent. Although the obtained PSm showed similar radiometric performances to PSm produced by organic solvent extraction/evaporation and to those of commercial microspheres, the low yield of production obtained with Spray Drying would increase drastically the associated operational cost.

The supercritical antisolvent methodology allowed the production of polystyrene based submicron particles and the encapsulation of the fluorescent solutes and a second organic solvent within the polystyrene matrix. Radiometric capacities of the submicron scintillating particles were poor due to the optical quenching although the methodology may result useful in case that plastic scintillation particles in the nanometric scale are needed.

Detection efficiency when measuring with PSm depends mainly on two factors: the energy of the particle and the diameter of the microsphere, which defines the level of optical and particle quenching. Optical quenching is important when PSm of low

diameters are used, whereas particle quenching is important for PSm which possess a higher diameter. Optical and particle quenching show opposite behaviour and the final detection efficiency and spectra position is defined by the balance between these two types of quenching. Higher detection efficiencies are obtained for PSm with a median diameter of around 10 μm (depending on the energy of the beta particle).

Detection efficiency when measuring with PSm is also affected by substances that cause an increase of the solution density (particle quenching), colored compounds (color quenching) and compounds like the nitromethane, which causes chemical quenching. When using liquid or gel scintillation cocktails, the addition of substances like NaCl, $BaCl_2$ or glycerine may cause also particle quenching although the most relevant effect is related with changes in the size of the micelles, appearance of precipitates or phase separation. In these cases, detection efficiency decreases with the addition of increases amounts of the substance, although the changes in the optical properties of the scintillating sample lead to an increase of the SQP(E) and shift of the spectra to high energies due to decrease of the optical quenching of the solution.

The first attempts to produce PSm at an industrial scale were performed by employing the organic solvent extraction/evaporation methodology. Although PSm with optimal physical features and radiometric capacities were obtained, the operational parameters should be optimized in order to obtain a high yield of PSm with the desired size and size distribution.

ACKNOWLEDGEMENTS

My deepest gratitude goes to my thesis directors Dr. Alex Tarancón Sanz and Dr. José Francisco García Martínez for giving me the opportunity of working in their research team, of motivating me all this time, of teaching me not only about plastic scintillation but also about life, of their advice and support.

I would like to acknowledge the Spanish Ministry of Economy and Competitiveness for the FPI grant (BES-2009-028673 CTM2008-01147) which allowed us to perform this research.

Thanks for the colleagues of Qüestram-R and the Analitycal Chemistry Department with whom I had the opportunity to share time and experiences. I would like to express my gratitude also to Ricard Alvarez (citometry laboratory) for his goodwill and help.

I want to thank the laboratoy M2P2 in Aix-Marseille Universitè (France), especially Dra. Elisabeth Badens and Dra. Yasmine Masmoudi for allowing me to perform the research project in their laboratory, for teaching me about supercritical fluids and for all their dedication and patience.

A special gratitude for the family Möbius for their advices, for pushing me to be a better person and a better professional and also for their affection and support.

My warm thanks to professor Xavier Rius of the University Rovira i Virgili, who was the director of the master in Nanoscience and Nanotechnology, many thanks for giving me the chance to start my educational adventure on abroad.

And last but not least, I would like to thank my family which has been with me all the time even from distance; they are my biggest fountain of motivation and example of perseverance. Also many thanks for all those who have been part of my life during these past years, I owe you so much - for those who have been beside me from the very first day in Barcelona (Enrique Parra and Angélica Díaz) - friends and colleagues sharing this period of time of the doctorate - flatmates who have become my family here, my friends of Rotaract and Rotary, friends of M2P2 in France and FTU in Karlsruhe, my cousins from Terrasa and everyone who has been part of my days in a special way!